UNIVERSITY OF SOUTHAMPTON

FACULTY OF ENGINEERING AND THE ENVIRONMENT

Institute of Sound and Vibration Research

Shock isolation systems incorporating Coulomb friction

by

Mohd Ikmal bin Ismail

Thesis for the degree of Doctor of Philosophy

July 2012

Dedicated to my beloved parents,
Ismail Abd. Karim & Kasmah Haji Maidin
and my beloved fiancee
Fatin Nabila Sharyzat Abu Bakar.

Thank you for your endless support, love and prayers.

UNIVERSITY OF SOUTHAMPTON

ABSTRACT

FACULTY OF ENGINEERING AND THE ENVIRONMENT

INSTITUTE OF SOUND AND VIBRATION RESEARCH

Doctor of Philosophy

SHOCK ISOLATION SYSTEMS INCORPORATING COULOMB FRICTION

by Mohd Ikmal Bin Ismail

This study investigates a novel approach to the problem of shock isolation. The questions considered are whether friction produces a better performance in terms of reduced response during a shock compared to viscous damping and a lower residual response after the shock.

To gain physical insight, a single degree of freedom model with friction applied to the isolated mass is analysed. It serves as a benchmark to the performance of a two degree of freedom model where friction is applied to a secondary mass. The isolation system performance is then quantified. For the two degree of freedom system with an intermediate secondary spring which connects the primary and secondary mass, it is possible to obtain the reduction in the displacement response as good as the single degree of freedom system and at the same time smoother acceleration response compared to the single degree of freedom system. For the purpose of further improvement, a control strategy is introduced to switch on and off friction in both models depending on some response parameters and this is compared to the passive systems. This is the semi active control strategy where friction is changed within a cycle of vibration (discontinuous). The control strategy provides more displacement reduction to ensure the maximum displacement response is much smaller than the base input which cannot be obtained with the passive systems.

The practical implementation and experimental validation is presented only for the first stage of the response during the shock. For the practical implementation of the switchable friction, an electromagnet is applied to separate the friction surfaces. Good agreement with the simple theoretical models for both passive and switchable systems is obtained. The reduced displacement and smooth acceleration response were obtained from the experiments with the system used to represent the two degree of freedom model. The issues and limitations in the practical implementation are identified and discussed.

TABLE OF CONTENTS

LIST OF FIGURES

LIST OF TABLES

DECLARATION OF AUTHORSHIP

I, MOHD IKMAL BIN ISMAIL declare that this thesis entitled ‘Shock isolation systems incorporating Coulomb friction’ and the work presented in the thesis are both my own, and have been generated by me as the result of my own original research. I confirm that:

1. This work was done wholly or mainly while in candidature for a research degree at this university.
2. Where any part of this thesis has previously been submitted for a degree or any other qualification at this university or any other institution, this has been clearly stated.
3. Where I have consulted the published work of others, this is always clearly attributed.
4. Where I have quoted from the work of others, the source is always given. With the exception of such quotations, this thesis is entirely my own work.
5. I have acknowledged all main sources of help.
6. Where the thesis is based on work done by myself jointly with others, I have made clear exactly what was done by others and what I have contributed myself.
7. Parts of this work have been published as: [1].

Signed: ……

Date: ……

ACKNOWLEDGEMENTS

I would like to express my high gratitude to my supervisor, Dr Neil Ferguson and my previous co-supervisor Prof Michael Brennan because of their valuable academic guidance and understanding throughout the project. Their guidance has helped to facilitate and improve the quality of the project.

I would also like to thank Prof David Thompson and Dr Ben Lineton because of their useful suggestions after each review meeting. Their suggestions have improved this project very much. At the same time, I would also like to thank Prof Steve Daley because of his willingness to loan the D Space equipment to perform the validation experiment.

Many thanks also to my sponsor, Majlis Amanah Rakyat 'MARA' for providing the funding and scholarship for the development of this project. Also not least, grateful thanks also to the ISVR technicians for their help and support in developing the practical test rig.

Finally, I would like to thank my parents, my fiancée, my brothers, my family and my friends for their encouragement and support over all these years during the completion of this project.

LIST OF SYMBOLS

English lower case alphabetical order

f_{c1}	: fundamental natural frequency of a coupled system (Hz)
f_{c2}	: second natural frequency of a coupled system (Hz)
f_{beat}	: beat frequency
g	: gravity acceleration
k	: stiffness of spring
k_1	: stiffness of primary spring
k_2	: stiffness of secondary spring
m	: mass
m_1	: primary mass
m_2	: secondary mass
t	: time
t_v	: variable of integration in Duhamel's integral
$\breve{t}$	: time takes for the relative velocity to reach zero
$u, \dot{u}, \ddot{u}$	: displacement, velocity and acceleration of a base input
u_{mag}	: base input magnitude
$\breve{u}$	: displacement of the base input when relative velocity reaches zero
$u_1, \dot{u}_1, \ddot{u}_1$	: first uncoupled mode's displacement, velocity and acceleration
$u_{1i}, \dot{u}_{1i}$	: first uncoupled mode's initial displacement and velocity
$u_2, \dot{u}_2, \ddot{u}_2$	: second uncoupled mode's displacement, velocity and acceleration
$u_{2i}, \dot{u}_{2i}$	: second uncoupled mode's initial displacement and velocity
$x, \dot{x}, \ddot{x}$	: absolute displacement, velocity and acceleration of the mass
$x_i, \dot{x}_i$	: initial displacement and velocity of the mass
x_{max}	: maximum displacement
$\ddot{x}_{max}$	: maximum acceleration of a base input and the sticking mass
x_{st}	: static displacement of the mass for a system subjected to friction
$\breve{x}$	: absolute displacement of the mass when relative velocity reaches zero
x_{min}	: lowest maximum response for a SDOF system with the control strategy suggested
$x_1, \dot{x}_1, \ddot{x}_1$	: absolute displacement, velocity and acceleration of the primary mass
$x_2, \dot{x}_2, \ddot{x}_2$	: absolute displacement, velocity and acceleration of the secondary mass

English capitals alphabetical order

A_1, A_2, B_1, B_2	: constants
C_1	: new variable to represent friction value
E_1	: energy in the primary system
E_2	: energy in the secondary system
E_i	: initial energy for a coupled system
E_{total}	: total energy for a coupled system
F	: sliding friction force
F_{st}	: friction required for sticking to the moving surface
$P(t_v)$	: force function of time in Duhamel's integral
T	: undamped natural period
T_1	: fundamental natural period of a coupled system
T_P	: length of a pulse

Greek lower case

ω	: circular frequency (rad/s)
ω_n	: undamped natural frequency (rad/s)
ω_1	: primary system undamped natural frequency (rad/s)
ω_2	: secondary system undamped natural frequency (rad/s)
ω_{c1}	: fundamental natural frequency of a coupled system (rad/s)
ω_{c2}	: second natural frequency of a coupled system (rad/s)
ω_L	: locked frequency
η_1	: primary system structural damping
η_2	: secondary system structural damping

Greek capitals

Φ	: mode shape matrix

Non-dimensional parameters:

English lower case alphabetical order

$\hat{k}$	: stiffness ratio
$\hat{t}$	: time
y, y', y''	: absolute displacement, velocity and acceleration of the mass
y_i, y_i'	: initial displacement and velocity of the mass
y_1, y_1', y_1''	: absolute displacement, velocity and acceleration of the primary mass
y_2, y_2', y_2''	: absolute displacement, velocity and acceleration of the secondary mass
y_{max}	: maximum displacement
y_{rel} y'_{rel}	: relative displacement and velocity
y_{st}	: static displacement of the mass for a system subjected to friction

English capitals alphabetical order

$\hat{F}$	: sliding friction
$\hat{F}_{on}$	: value of sliding friction when friction is turned on
$\hat{F}_{opt}$	: friction that yields lowest maximum response
$\hat{F}_{st}$	: friction required for sticking to the moving surface
U	: displacement of a base input
U_{mag}	: base input magnitude

Greek lower case

μ	: mass ratio
τ	: time
$\hat{\omega}$	: frequency ratio

1. INTRODUCTION

1.1 Background

Vibration in its general sense is a dynamic response typically described in terms of physical quantities such as displacement, velocity or acceleration. In some cases it is beneficial when used in some applications, e.g. a clock, a vibration conveyor, music and others. However, for most of the time it could lead to damage, wear, noise or discomfort when a system is not properly designed and is subjected to high levels of vibration. For example, people travelling in vehicles with poor suspension will feel real discomfort because of high road roughness excitation, structures might collapse because of earthquakes or wind loading and machines might emit noise or experience fatigue. For these reasons, many engineers have sought solutions over more than 60 years to control and isolate vibration from the source to the receiving structure or person.
It is essential to understand the characteristics of the source of vibration and type of input, because the system can be designed accordingly to control vibration. There are three main types of input normally considered, namely harmonic input, transient or shock input and random input. A rotating machine such as a pump or turbine typically produces periodic inputs which can be harmonic at one frequency. On the other hand, transient input can be produced by a vehicle traversing a bump or electronic equipment dropped onto the floor. Finally, random input can represent wind loading, a car travelling over a rough road, etc.

In this thesis, the focus will be on the transient or shock input. The research scope in this thesis has been restricted to shock isolation rather than harmonic or random input for which other approaches can be considered. Transient input is a short duration input, usually occuring for an interval of time comparable with or less than the fundamental period of oscillation of the structure. It is often harmful because it typically involves high forces and subsequently can produce high stresses and damage. The solution for the mechanical system response due to the transient excitation normally requires the time history of a quantity that describes the motion, usually displacement, velocity or acceleration[2]. As it is harmful, a reliable mechanical system design which could sustain different levels of shock excitation and is fast enough to adapt, if necessary, should be designed.

This study is concerned with alternative methods to reduce the vibration suffered when a system is subjected to transient inputs. This chapter comprises the background of the research topic, description of the thesis content, a brief overview of the objectives of the study and the contributions of this thesis. The background will primarily cover passive isolation with some outline of relevant adaptive and active systems.

1.2 Vibration isolation for shock

1.2.1 Vibration control and isolation

A vibrating system can be represented by three main components, namely the vibration source, the transmission path and the receiver. The main objective is to reduce the vibration at the receiver. There are three main ways to implement this objective, i.e., control vibration at the source, modify the transmission path and control vibration at the receiver. Control of vibration at source is the best solution, but it is not always possible. Control of vibration at the receiver can be done by changing the mechanical properties of the receiver, namely the stiffness, damping and mass of the receiver. The final one which is often the easiest to implement and more commonly considered can be done by modifying the vibration transmission path. This method can be done by inserting a vibration isolator between the source and the receiver to reduce vibration transmission to the receiver without modifying the existing structure. The vibration isolator, typically an elastic element, normally is very small and its attachment to the existing structure can be implemented in a very simple way.

A suitable isolator could be designed dependent upon the source of the vibration, namely the type of input and the characteristics of the input. It is essential to know whether the input is harmonic, transient or random to consider different isolator designs. Not only that, it also depends upon the properties of the receiver; it also needs to be designed to be suitable with the existing characteristics of the receiver. If the isolator is properly designed, the response level of the receiver can be reduced significantly.

The simplest form of vibration isolator is a passive isolator. When the physical properties of the isolator, i.e. typically the stiffness, is fixed for a particular application, it is said to be passive. The passive vibration isolator is a simple, low cost and reliable solution but it only works for particular cases. The performance might deteriorate and produce worse response

under different loading situations. Therefore, it is not good for the system when it is exposed to different types of unpredictable excitation. It has been studied extensively and the research related to passive shock isolation is reviewed in the next section.

1.2.2 Passive shock isolation

One of the first applications of shock isolation was to protect the transportation of fragile items[3]. The monograph by Mindlin[4] is probably one of the first comprehensive studies related to shock dynamics and isolation. The study mostly is about the dynamics of objects subjected to free fall, which considers practical package cushioning techniques and supporting theoretical analysis. The isolator element is modelled with a combination of different types of linear and nonlinear elastic and damping elements.

Subsequently, Ayre *et al* [5] extended the shock response analysis by investigating the response of single degree-of-freedom undamped and damped models. This is one of the best texts into shock response until recent times. The results obtained by Ayre were subsequently compiled into the Shock and Vibration Handbook, edited by Harris and Crede [2]. The latter is generally now regarded as the key core textbook in this area. The study by Ayre is more diverse and useful under different types of excitation, whether it is a force excitation or any type of ground excitation. He also introduced the idea of using a versed sine, half sine and rectangular pulse to represent a shock input. Furthermore, shock response spectra (SRS) were produced [2] for these types of pulse to indicate the potential for damage when a system is subjected to different pulse durations. SRS is an important tool to evaluate the severity of the potential damage which might occur due to a particular shock and to design an isolator [6]. SRS is the normalized peak response (either absolute, relative or residual normalized with respect to the maximum amplitude of the shock input) produced by the shock on the isolated mass as a function of the natural frequency of the mass on its elastic support, or more commonly as a function of the ratio between the duration of the pulse and the natural period of the system [6].

Snowdon [7] then explored the topic by comparing the transient response to steplike ground displacement of nonlinear shock mountings with ideal linear mountings. The emphasis was on the influence of damping, the input rise time and nonlinearity of the system when subjected to the excitation. It was shown that a mount that softens upon compression and has low damping produces a lower response for a long rise time of the

input. Contrary to Ayre who presented the SRS as the indicator of the damage potential, Snowdon presented the shock acceleration ratio (SAR), shock displacement ratio (SDR) and relative displacement ratio (RDR) which are plotted as functions of a parameter which describes the rise time of the steplike pulse. In another paper [8], Snowdon discussed the identification of the parameter that indicates damage, whether it is the displacement or acceleration according to the length of the pulse. If the length of the pulse is long compared to the natural period of oscillation of the mass supported on the elastic support, the mounted mass closely follows the base input and the acceleration of the mass is a measure of the liability to damage. On the other hand, if the length of pulse is short, the mass remains substantially at rest until motion of the support has ceased and the maximum displacement of the support determines the likelihood of damage. Finally, if the pulse is neither long nor short, no simple damage criterion can be found. The conclusion was thus to propose a shock acceleration ratio versus a relative displacement ratio to compare the performance of different shock mounts. Following this, the analysis was extended to pulselike ground displacement[9] and three element isolation mounting[10], where a spring is in parallel with another spring and a damper, which is known as Zener model.

Recently there have been significant research studies into the effect of shock on electronic equipment such as circuit boards and hard disk drives. Suhir [11] studied shock protection for portable electronics by using a softening spring. The use of a softening spring in the analysis was because of its ability to reduce the maximum acceleration compared to a linear constant stiffness spring. Suhir then used a probabilistic approach to design a soft spring with a low probability of a rigid impact in the case when the drop height is usually unknown. Shu *et al* [12] used a half sine acceleration pulse to study the pulse width effect on the response of an actuator arm of hard disk drive using a combination of the finite element method and a simplified single degree of freedom system. Similarly, Tsai *et al* [13]and Zhou *et al* [14] also studied the response of electronic components by using a single degree of freedom model for half sine acceleration inputs.

A significant amount of work has considered shock in relation to machinery applications. The objective is typically to isolate the shock produced by machinery on the surrounding areas. Grootenhuis [15] in 1965 analysed a machine producing a shock which was resiliently mounted on an elastic foundation. It was found that good isolation can be achieved when the suspension frequency is less than one quarter of the foundation natural frequency. An experiment was conducted and good agreement was obtained with the

theoretical predictions. Later Novak *et al* [16] incorporated damping in the analysis for a hammer foundation. More recently, Chehab *et al*[17] analysed the response of one particular mass hammer foundation and provided a closed form solution for the dynamic response under different kinds of hammer load namely a rectangular pulse, half sine pulse and triangular pulse.

Comprehensive studies on vehicle dynamics were summarised by Gillespie in 1992[18]. This included a study of the suspension isolation from road excitation for a quarter car model. Recently, Waters *et al*[19] explored the influence of dual rate suspension damping on the shock response of a simple vehicle model. A simple approximation was made for the peak acceleration during an impulse of both short and long durations compared to the natural period to observe the role of the viscous damper component. Alternatively, Zong *et al*[20] investigated the biodynamic human response when subjected to ship shock motion by modelling a human body sitting on a chair as a lumped parameter system. A study for shock produced by high speed craft has also been made[21], where the relationship between various seat and operational conditions was considered on the response of a seated person. The seat was represented as a two degree of freedom system with base excitation and the occupant mass with suspension preload was varied and the change in the response quantities were analysed.

The study by Hyun, Waters *et al*[19, 22] became the initial inspiration to investigate the effect of damping on the response of the lumped parameter system subjected to base excitation. Based on their study, it was shown that a viscous damper could transmit a high force during a shock. Therefore, friction was considered as another alternative to damping to limit the force transmitted, because it is not dependent on the magnitude of the relative velocity between the mass and the base. A necessary initial phase is to investigate how much work has been done in analysing the application of friction for shock isolation. The next few sections will review the previous work on the effect of friction on the shock isolation for both passive and semi active systems.

1.2.3 Friction for vibration isolation and control

The friction mechanism and its nonlinear behaviour has been a subject of research for a significant period of time. Den Hartog [23], in early 1930's, introduced the idea of an equivalent linear viscous damper for Coulomb friction. He calculated the energy

dissipation due to Coulomb friction with the viscous damping in one cycle of motion for the forced vibration due to a harmonic force. In a paper, Den Hartog [24] gave the steady state analytical solution of a one degree of freedom system with either Coulomb friction or combination of Coulomb and viscous damping when a single degree of freedom system was subjected to a harmonic force. In a later study, Hundal [25] studied the response of a base excited system with Coulomb and viscous damping. Contrary to Den Hartog who applied the harmonic force direct to the mass, Hundal chose to apply harmonic base excitation.

Subsequently, there have been many studies using the lumped parameter models with Coulomb friction subjected to harmonic excitation [26-34]. Ferri [26], surveyed the literature on the use of dry friction in passive damping and vibration isolation. Several analytical techniques were presented with applications of dry friction from various areas and it was found that dry friction plays an important role in many mechanical systems. Later, Tan *et al* [27] analysed the energy dissipated by friction in each mode of a multi degree of freedom system, deriving several models for the equivalent friction modal damping. It worked very well when sliding motion dominated the response.

Hong *et al*[28, 29] estimated the maximum velocity and time lag for systems with no sticking (zero stop per cycle) and the categorization of the steady state motion with 0,1,2,4,6,8,10,12 and 14 stops per cycle in the parametric space of the ratio of the forces versus frequency. A recent study by Lopez *et al*[32, 34] determined the energy dissipated per cycle as a function of the system parameters and experimental validation was reported. There are numerous studies concerned with the response of a system with Coulomb friction subjected to a harmonic force and the application being to isolate the vibration for this type of excitation. However, to the author's knowledge, not many studies have considered a system with Coulomb friction subjected to a shock input. Furthermore, studies in this area are only interested in either the semi active or adaptive Coulomb friction. Only a brief section in a paper written by Choi *et al*[35] discussed shock isolation for a system incorporating passive friction. However, the focus of the paper was on a magnetorheological damper and the former served as a performance benchmark to the latter. Furthermore, the friction was applied directly to the primary mass and not to a secondary mass as will be shown later in this thesis. Moreover, to the author's knowledge, there are also not many studies which combine the overall response of a system subjected

to a shock input which consists of the forced response during the shock and free vibration after the shock. Most of the studies only concern the forced response during the shock.

For harmonic excitation, the main concern is the forced steady state vibration response. However, for shock excitation the interest is not only on the forced vibration of the system but also the residual vibration (the free vibration after the shock has stopped). This is because, the residual vibration needs to be rapidly suppressed. The free vibration analytical solution of a single degree of freedom system with friction was given by Timoshenko *et al* [36]. This solution serves as a main reference for this thesis to predict the behaviour of a lumped parameter system after a shock and to identify whether friction is a good alternative to dissipate the residual energy.

Among the first studies of a shock isolator configuration with Coulomb friction is the work by Mercer *et al*[37]. They realized that Coulomb friction has a quality in that it can limit the acceleration transmitted to a mounted mass which cannot be obtained using a viscous damper. The adaptive configuration for which the normal force is taken as a function of the displacement allows for the possibility of minimizing the maximum displacement, whilst still limiting the maximum acceleration. An optimum isolator is a single degree of freedom system where an elastic linear spring is in parallel with a variable Coulomb friction element and a linear viscous damping. When the motion is dominated by high frequency content, the viscous damper is rigid and the isolator behaves as a spring with the Coulomb friction acting in parallel. Then, when the input motion becomes less severe, Coulomb friction becomes less dominant and viscous damping takes over to dissipate energy and restore the isolator to its equilibrium position. There are more systems with Coulomb friction under semi active and adaptive control which are presented in the next section.

1.2.4 Active and semi active shock isolation

Control strategies are typically designed and implemented to make sure a mechanical system experiences the lowest response possible. Passive isolation systems have limitations because the choice of spring and damping properties, which are constant, could give good characteristics in certain situations but also could give worse behaviour for other conditions. For example, if the amplitude and frequency of the shock excitation are changed, the response of the system will be different so different spring and damping properties are needed in order to suppress the corresponding vibration response.

For a system with friction, it is even harder for the passive system to give a good response because the direction of friction force always changes, depending on the relative sliding velocity. Therefore, a good control strategy is needed to suppress vibration during and after the shock. There are numerous control methods that have been developed in the literature for variable friction devices and these can generally be classified as either discontinuous or continuous force control[38]. A discontinuous force control law is simple and easy to be implemented, but it is usually accompanied by abrupt changes in the friction force that can produce a high frequency response and increase the acceleration response level [38, 39]. In contrast, a continuous force control law normally produces a smoother change of the friction force resulting in a lower system acceleration response [38, 40-43].

Among the numerous control methods available, semi active and adaptive controls are widely used in various applications. They are used because there are great advantages in terms of low power consumption compared to active control and they are normally stable because no additional energy is supplied to the mechanical system. The difference between the semi active and adaptive configurations is that in the adaptive systems the properties are changed relatively slowly (continuous) while in the semi active systems the properties are changed within a cycle of vibration (discontinuous) [3, 44]. Because semi active control offers great advantages, there are a significant number of studies related to this type of control. Nader [45] summarized different types of semi active control ranging from variable rate dampers, variable spring elements, hybrid elements and on-off control. However, the input used was harmonic and the systems analysed were linear.
Although there are many studies on semi active and adaptive controls for harmonic input and linear systems, only a few papers exist on semi active and adaptive controls of a friction system to isolate shock [46-49]. Semi active control of the normal force has been used to control the friction force acting on the structure. For example, Ferri and Heck [47] presented three control strategies for a low bandwidth friction system to obtain excellent shock isolation properties. Dupond *et al* [46] proposed control laws for friction dampers which maximize the energy dissipation in an instantaneous sense by modulating the normal force at the friction interface. The forced vibration response was analyzed with harmonic input for a friction system with multiple friction elements. Moreover, the free vibration response due to initial displacements and initial velocity without external forcing was also analysed.

In this study, semi active friction will be considered. The study of sequential variations existed as early as 1974, when Karnopp *et al* [48] proposed a semi active vibration isolation system employing a force generator based on skyhook control. The name 'skyhook' is derived from the fact that it corresponds to a passive damper hooked to an imaginary inertial reference point[44]. Since then a significant number of studies have proposed semi active vibration isolation employing sequential on-off damping to create a system that looks almost the same as a skyhook system. The reason why on-off control was considered in this study is because the implementation of on-off control is very simple. The implementation is only based on the sign of the parameters and not their magnitude. On-off control also produces significant reduction in the maximum response of a system.

Yamaguchi *et al*[49] presented the strategy of on-off control for a friction force at a spring support. The system consists of a primary isolated mass supported by a primary spring connected to a secondary mass supported by a secondary spring via interfacial friction force. The numerical simulations were conducted to observe the response of the system when subjected to transient and harmonic force. It was shown that the energy of the primary system (primary mass and primary spring) was reduced even if the total energy was not dissipated, because energy was transferred to the secondary system (secondary mass and secondary spring).

Although a few studies exist on shock isolation with semi active friction as given above, most of these studies deal with single degree of freedom systems. This thesis also considers a two degree of freedom system to take benefit of a relaxation secondary spring, to avoid any acceleration discontinuity of the primary isolated mass. Only Yamaguchi *et al*[49] studied a two degree of freedom system, but the system configuration and control law proposed are different from that presented in this thesis. Furthermore, no experiment was conducted to validate the control strategies proposed. In this thesis, a novel control law is proposed. An experimental rig was also built to test and validate the response of both a passive system and a system with the proposed control strategies.

1.2.5 Friction models

In order to predict the behaviour of the systems with friction, a good friction model is required that can replicate the behaviour of real friction with sufficient accuracy. There are many friction models discussed in the literature, each of them suitable to particular applications.

Friction generally is highly stochastic in nature [50] . Friction between sliding surfaces occurs a result of stochastic interactions between rubbing asperities. In nearly all cases of friction there are significant variations in both amplitude and frequency, but most friction models do not take these variations into account and instead represent friction by a smooth mean value to simplify the computational process without sacrificing too much in the accuracy of the results.

Despite many years of research the mathematical description of this phenomenon is not yet fully developed [49-51]. The phenomenon is not always reproducible, as its extent depends on surface state, lubrication, asperities, temperature, magnitude of normal force, relative velocity, etc [51-53].

Various approaches to model the friction are presented in the literature, e.g. [53, 54]:

- The macro-approach often described as a static friction model. It assumes a single dissipative force acting at the interface between the sliding surfaces [53]:

The most popular, widely used and simple friction model to use is the Coulomb friction model, which can be formulated as

$$F = \begin{cases} F_c \operatorname{sgn}(v) & \text{if } v \neq 0 \\ F_{st} & \text{if } v = 0 \text{ and } F_{st} \leq F_c \end{cases} \tag{3.1}$$

where F_c is the sliding friction force defined as $F_c = \mu_c N$, μ_c is the coefficient of friction and N the normal load in contact. The sign function $\operatorname{sgn}(v)$ is often written as

$$\operatorname{sgn}(v) = \begin{cases} +1 & \text{for } v > 0 \\ -1 & \text{for } v < 0 \end{cases} \tag{3.2}$$

In some papers e.g. [53], in the sticking condition the friction force for velocity equal to zero $v = 0$ is allowed to be slightly higher than in the sliding case. This is because, in reality, the coefficient of friction is higher when the system sticks instead of sliding [36]. Since the equation of motion for the dynamic system is strongly non-linear with the Coulomb friction model, sometimes a viscous friction model is used. This model is easier to simulate but the representation of the friction is often poor. Sometimes, the combination of Coulomb and viscous friction is also used. Since the Coulomb friction model is problematic in the simulation and the viscous friction model does not give good results, a combination of those two models could be beneficial. Such a model will have the following forms

$$F = \begin{cases} F_c \min\left(k_{sat} v, 1\right) & if\ v \geq 0 \\ F_c \max\left(k_{sat} v, -1\right) & if\ v < 0 \end{cases} \tag{3.3}$$

where k_{sat} is a coefficient that determines the speed of the transition from – to +. There is a smooth linear transition when the velocity changes sign. There are also other models which have smooth transition when the velocity changes sign, for example the tanh and error functions (erf).

Finally, there is also the Stribeck friction model [50] which is introduced for systems with well-lubricated surfaces. In this case the friction force is also dependent on the magnitude of the relative velocity. The friction force changes when the motion running state changes in either boundary, mixed or full film lubrication [50].

- The micro-approach often described as a dynamic friction model takes into account detailed knowledge of characteristics of the sliding surfaces including roughness, asperities, adhesive phenomena, friction hysteresis, limit cycles, surface lubrication, other tribological parameters, etc [53]:

There are some models using a micro-approach, for example Dahl, Dankowicz, Canudas de Wit *et al* [50]. The models are more complicated than the macro-approach. The models are important for the case of small displacement which is important in many high precision applications [50]. At this point, it is not necessary to go into details about this kind of model because it is expected the systems analysed in this thesis should have sufficient displacement to prevent a need for such detailed analysis.

For this thesis, the Coulomb friction model is chosen. For the purpose of a simplified computation process, the erf function will be used and will be discussed in the next chapter. Also, in order to simplify the analysis, the coefficient of static friction is chosen to be equal to the dynamic friction. This decision could affect the behaviour at the transition point, when the motion starts or changes direction, especially when the friction force is small. There will also be a shorter sticking period if the static friction is equal to the dynamic friction and a system does not need higher velocity to overcome the high static friction force in order to start sliding.

However, there are some papers e.g. by Lopez *et al* [34] that use the Coulomb friction model with the coefficient of static friction equal to the dynamic friction and their validation experiments give a good agreement to the prediction within 10%. Based on the results, they conclude that this kind of model can be expected to give realistic predictions of the performance of friction dampers with stiff localized contacts and large relative displacement within the contacts.

1.3 Objectives and contributions

Based on the background in the shock isolation literature, this project was conceived. The objectives of the study were as follows

- To conduct review of passive and semi active shock isolation

- To perform an in-depth analysis of passive single and two degree of freedom system configurations with Coulomb friction, to see the advantages of these configurations for shock isolation considering the problem in two phases, namely the reduction of response during a base shock input and the suppression of the residual vibration after the shock.

- To implement control strategies for both single and two degree of freedom systems with Coulomb friction for the reduction of response during a base shock input.

- To compare the response of a single degree of freedom system with a two degree of freedom system with Coulomb friction.

- To determine the advantages of control strategies to the response of the systems compared to the passive systems.

- To investigate a practical realisation of a passive two degree of freedom system and implementation of control strategies, to compare with the theoretical predictions.

The contributions in this thesis are:

- Presentation and analysis of a shock isolation system with Coulomb friction, namely a two degree of freedom system where friction is applied to a small secondary mass which is attached to a primary mass by a secondary spring.

- Presentation and analysis of a control strategy to improve the response during a shock than for the respective passive system.

- Presentation of an in-depth analysis of the behaviour of passive two degree of freedom system after a shock by investigating the residual free vibration.

- Identification of the optimum configuration based on the choice of stiffness ratio, mass ratio and friction to obtain a reduced response to a shock and improved residual shock response.

- The development of an experimental rig to validate the theoretical prediction for the response of a two degree of freedom system with passive friction subjected to a base shock input.

- The implementation of the practical control of friction by switching on and off the normal forces, which are provided by an electromagnet to validate the theoretical prediction for the response of a two degree of freedom system with switchable friction subjected to a base shock input.

1.4 Thesis overview

The presentation of the thesis incorporating the modelling, simulation and experimental validation is given in details in the remaining chapters. Chapter 2 presents the analysis of the response of passive single and two degree of freedom systems with Coulomb friction during a base shock input. In this chapter, there is no variation in friction throughout the motion. It is important to establish the understanding of a passive single degree of freedom system before moving to more complicated systems such as a two degree of freedom and a semi active system. A single degree of freedom model acts as a reference model to help in understanding the basic behaviour of a system and assists in figuring out which key parameters take an important role in affecting the behaviour of the system. The comparison is made between the behaviour of passive single and two degree of freedom systems in terms of the response parameters. The advantages and disadvantages of both systems are determined in terms of minimizing the response during a shock.

Chapter 3 provides the control strategies for both the single and two degree of freedom systems to reduce the vibration during a shock. The control strategies outlined have the objective to improve the response of a passive system. The control strategies are developed from the concept of reducing the net force acting on the targeted mass. In this thesis an on-off control strategy is considered. The friction is turned on and off depending on the force acting on the system. Finally, a comparison is made between the response of the control and passive system to observe whether the control system could bring any improvement to the passive system as expected.

Then, chapter 4 provides the analysis of the residual free vibration response of the passive single and two degree of freedom systems with Coulomb friction after a base shock input. The comparison between the response and energy dissipation of the two configurations with Coulomb friction is made. The main objective is to identify the benefits and limitations of both configurations in terms of dissipating the residual energy. A control strategy is introduced for the residual vibration suppression by setting the value of friction based upon the initial conditions. The strategy is expected to bring the mass back to its equilibrium in the shortest possible time without further vibration.

The next two chapters cover the experimental design and validation. Chapter 5 is focused on the design of the experimental rig and the extensive experimental validation of the two degree of freedom system with passive friction. An experimental rig which behaves as a

two degree of freedom system for frequencies below 200 Hz has been designed. The experimental rig is a T beam configuration which was initially designed by building a Finite Element (FE) model. Initially, chapter 5 presents the validation of the FE model by measuring the response of the beam configuration under broadband random excitation. Then, the two degree of freedom model parameters are estimated from the transmissibility curve of the T beam configuration. Subsequently, the value of friction is also estimated by fitting the free vibration response of the T beam configuration to the piecewise free vibration response of a two degree of freedom model. Finally, based on the estimated parameters, the measured shock response of the T beam configuration is compared with the predicted two degree of freedom model response.

Chapter 6 presents the implementation and the validation of the two degree of freedom system with switchable friction. On-off friction is introduced by an electromagnet which is controlled by a D Space platform. The results are then compared with the theoretical prediction to validate it. Chapter 7 concludes the study presented in this thesis and provides some suggestions for future studies.

2. SHOCK ISOLATION WITH PASSIVE COULOMB FRICTION

2.1 Introduction

For the purpose of limiting the transmission of base motion, a model of a shock isolation system with friction has been developed. In this chapter only passive friction is considered; i.e. where there is no variation in the value of the friction throughout the motion. A Coulomb friction model is used. As Coulomb friction does not depend on the magnitude of the velocity, it could supply significant forces to the system throughout the subsequent motion.

Initially, several single degree of freedom models with friction have been studied. They are studied to get a better understanding of the system behaviour under friction before moving to a more complicated system such as a two degree of freedom system. Finally, a two degree of freedom system with friction applied to the secondary mass is introduced and the comparison between both systems is made.

2.2 Motivation

It is expected that a conventional shock isolation system, which is a single degree of freedom system comprising a mass, spring and viscous damper, could not sustain transient load. This is because, the system response will depend on the magnitude of the relative velocity across the viscous damper. Transient input, which is normally very short duration, could cause high relative velocity across the viscous damper and consequently transmit a high force and acceleration to the mass. The acceleration response for a viscously damped single degree of freedom system is made available in the Appendix A for a reference. Although a viscous damper could cause a large response during a shock, it has a good quality in reducing the vibration after the shock.

For this reason, it is good to find an alternative which could be a substitute for the viscous damper. The new substitute element has to be as good as the viscous damper in producing the decay of the residual vibration after the shock and at the same time produces a good response during the shock. Consequently, a friction element is a potential substitute since it has the quality in limiting the transmission of force to the isolated mass. From the Coulomb friction law, friction does not depend upon the magnitude of velocity but depends only on the direction of velocity. Therefore, the force transmitted to the mass only depends on how much friction is applied to the mass and does not depend on the nature of the shock. Subsequently, friction is also expected to perform after the shock in reducing the residual vibration.

Several configurations of shock isolation model with friction are considered, namely a single and a two degree of freedom system. For a single degree of freedom system, the friction is applied directly to the targeted mass. On the other hand, for a two degree of freedom system, the friction is applied to an auxiliary mass which is attached to the targeted mass by a secondary spring. The comparison between the systems will be made to identify both the benefits and the weaknesses of both configurations. At the same time, in the next chapter, the concept of semi active friction will be introduced where friction is turned on and off according to a proposed control law. Subsequently, a system with semi active friction will be compared with a system with passive friction. The objective is to reduce the response of the system as much as possible and, if achievable, the response should be smaller than the base input to achieve a good isolation.

2.3 Transient vibration stages and response evaluations

When a system is subject to a shock input, the system will undergo two phases of vibration [2]. The first phase will be forced vibration which will begin immediately when and during the time that the shock input is applied to the system. After the shock, the second phase will begin which is free or residual vibration.

For shock isolation, the most important values to consider are the maximum response of the system at any time and the residual response of the system. The maximum response might be equal to the maximum residual response depending on the length of pulse compared to the natural period of the system. If a short pulse is applied, typically the maximum response of the system occurs after the shock has ended, so it will also be equal to the maximum residual response. However, when a long duration pulse is applied, the maximum response can occur during the application of the shock with lower levels for the residual vibration[2]. The maximum overall and residual response of a single degree of freedom system with a half sine or a versed sine input are available through calculation and inspection of the Shock Response Spectrum (SRS)[2]. The SRS for an undamped single degree of freedom system is in Appendix B for a reference.

The most important response characteristics for vibration isolation, either in a single or two degree of freedom system, are the absolute displacement of the primary mass, the absolute acceleration of the primary mass and the relative displacement. Absolute displacement and acceleration are important response parameters as these can correspond to a measure of stress and possible damage of the system [3]. Only absolute displacement and acceleration of the primary mass are important, and not the secondary mass if the system has two degrees of freedom. The primary mass corresponds to the main structure for which the vibration level should be reduced. The relative displacement is important to consider how much sway space the system requires in order to ensure that the system has enough free space. Shekhar *et al* [55] evaluated the performance of shock isolator systems using the three following indices: relative displacement ratio (maximum relative displacement between the mass and the base normalized with the maximum displacement of the base), shock displacement ratio (maximum displacement of the mass normalized with maximum displacement of the base) and shock acceleration ratio (maximum acceleration of the mass normalized with maximum acceleration of the base).

2.4 Types of base input

There are two main types of shock input considered in articles, the step-like and pulse-like shock. Snowdon [7, 9], in some of his papers, studied the transient response of nonlinear isolation mountings to step-like and pulse-like shock. His model consists of isolation mountings with nonlinear stiffness. He also studied the steady state and transient behaviour of different types of isolation mountings using the step-like and pulse-like shock [10].

In this thesis, the base input applied to the end of the spring or friction interface is either a rectangular, half sine or versed sine which are given in the equations below, where $\hat{u}$ is the amplitude of the input and T_p is the base input duration. A rectangular pulse is a step-like pulse, whereas half sine and versed sine are pulse-like shock.

Rectangular pulse:

$$u(t) = u_{mag} \qquad \left[0 \le t \le T_p\right]$$

$$u(t) = 0 \qquad \left[T_p \le t\right]$$

Half sine pulse:

$$u(t) = u_{mag} \sin\left(\frac{\pi t}{T_p}\right) \qquad \left[0 \le t \le T_p\right]$$

$$u(t) = 0 \qquad \left[T_p \le t\right]$$

Versed sine pulse:

$$u(t) = \frac{u_{mag}}{2}\left(1 - \cos\left(\frac{2\pi t}{T_p}\right)\right) \qquad \left[0 \le t \le T_p\right]$$

$$u(t) = 0 \qquad \left[T_p \le t\right]$$

These three types of base input are shown in Figure 2.1. From Figure 2.1, it can be seen that transient input is applied at time equal to zero. Before zero, there is no input applied. The input starts to be applied at $t = 0$ and it ends at the time equal to the length of the pulse, $t = T_p$.

A half sine input is a simple and easy representation of shock excitation, used widely in textbooks and journal papers [12-14, 56]. Half sine displacement input is not practical though because its derivative or its velocity is in a cosine form. Therefore, there will be a positive velocity at time equal to zero. This requires infinite acceleration to get the velocity of a real system to that positive velocity. A rectangular pulse is also not practical, because the system needs infinite velocity at time equal to zero to get the displacement to the desired level.

As an alternative, a versed sine input is often used. This input has smooth first derivative. Therefore, its velocity will start from zero at the starting point of the input. Waters, Hyun and Brennan [19] used a versed sine input to approximate the peak acceleration during an impulse of both short and long durations compared to the natural period of a single degree of freedom model. For all of the analysis in this chapter, a versed sine pulse is used. Simulations for half sine and rectangular pulses are in the Appendix C and D for the purpose of reference and comparison.

There are three categories of shock input based on the length of the pulse compared to the natural period of the system[3]. If the length of pulse is very short compared to the natural period of the system, the mass stays substantially at rest until motion of the support has ceased. In contrast, when the length of the pulse is very close to the natural period of the system, the maximum response of the system is greater than the amplitude of the shock. This is known as the amplification region. Meanwhile, if the length of the pulse is very long compared to the natural period of the system, the response tends to be quasi static and it follows closely the shape of the base input. In this study, the input close to the natural period of the system and the shorter input will be used. The input close to the natural period of the system is used because friction is expected to give a significant reduction to the maximum displacement of the system over an undamped system. On the other hand, the short input is used because friction is expected to give significant reduction to the maximum acceleration of the system. The long input is not considered, because it is expected that there is little or no improvement by having the friction applied to the system. The response in this latter case will always closely follow the shape of the base input.

2.5 Shock response of a single degree of freedom system incorporating sliding friction

Two different models of a single degree of freedom system with passive friction, shown in Figure 2.2, are introduced to investigate the effect of friction in term of shock isolation. Both configurations are analysed when subjected to transient shock inputs.

The equation of motion of the system model 1 where the friction interface does not move in Figure 2.2(a) is given below in equation(2.1).

$$m\ddot{x} + kx + F\,\mathrm{sgn}(\dot{x}) = ku(t) \tag{2.1}$$

While, the equation of motion of the system model 2 where the friction interface moves with the base in Figure 2.2(b) is given below in equation (2.2)

$$m\ddot{x} + kx + F\,\mathrm{sgn}(\dot{x} - \dot{u}) = ku(t) \tag{2.2}$$

The base input displacement is denoted by u and the displacement response is denoted by x, while k is the stiffness of the system, m is the mass of the system, F is friction applied to the system and $\omega_n = \sqrt{\frac{k}{m}}$ is the undamped natural frequency of the system. Non-dimensional parameters can be defined in terms of the system parameters as non-dimensional displacement $y = \frac{\omega_n^2 x}{g}$, non-dimensional friction $\hat{F} = \frac{F}{mg}$, non-dimensional base input $U = \frac{\omega_n^2 u}{g}$, non-dimensional time $\tau = \omega_n t$ and differentiation with respect to non-dimensional time $\odot' = \frac{d\odot}{d\tau}$.

One of the reasons why the equations of motion of the systems are normalized with respect to the weight of the mass mg is because the solution of these non-dimensional equations allows one to examine for a given system with mass and stiffness, the effect of the level of friction and base input independently. Furthermore, it is suitable to normalize the equations both for the shock stage and the subsequent residual stage. Another alternative option is to

normalize the equations with respect to ku_{mag}, where u_{mag} is the magnitude of the base input.

The case when the friction interface does not move corresponds to an ideal case but in practical the friction interface always move with the base. That's why it is important to look at both cases. The equations of motion given in Eq. (2.1) and (2.2) can be subsequently written in non-dimensional form as Eq. (2.3) and (2.4) respectively.

$$y'' + y + \hat{F}\,\mathrm{sgn}(y') = U(\tau) \tag{2.3}$$

$$y'' + y + \hat{F}\,\mathrm{sgn}(y' - U') = U(\tau) \tag{2.4}$$

The only difference in the equations of motion for the two systems is the dependency in the direction of friction on either the absolute or relative velocity of the mass. The first model, in Figure 2.2(a), has friction determined by the sign of $\dot{x}$, which is the absolute velocity of the mass. The friction in model 2.2(a) always opposes the direction of motion. If the mass moves in the positive direction, the friction acts in the negative direction and vice versa. This is the case when the friction interface is isolated from the shock excitation.

However, the second model in Figure 2.2(b) has friction which acts in a direction which is determined by the sign of the relative velocity $\dot{x} - \dot{u}$ between the mass and the base input. In this case, if the mass moves with a positive velocity it does not necessarily mean the friction acts in a negative direction. The mass velocity can be smaller than the input velocity, so eventhough the mass moves with a positive velocity, the friction can also act in the positive direction. This is the case when the friction interface moves with the same velocity as the input excitation.

In general, the difference between the two models produces different responses to a given input. It is necessary to do a separate analysis for both models to see the behaviour when both models are subjected to transient excitation. However, the analysis is focused on the second model. This is because, in the real world, it is hard to isolate the friction interface from the base input. Therefore, the analysis will be more focused on the second model and there will be a brief analysis about the first model as a comparison. Also, the first model has been previously examined and reported for harmonic excitation[25].

2.6 Simulations and results

2.6.1 Introduction

The numerical simulation of the ordinary differential equations is an important technique in dynamics. Since many ordinary differential equations (ODE) are not soluble analytically, numerical integration is often the only way to obtain a solution [22]. Among all of the methods to solve ordinary differential equations, the Runge Kutta method has been considered. The simulations and results presented were calculated using ODE solvers in MATLAB. These ODE solvers use variable step numerical integration routines (Runge-Kutta method) to perform the numerical integration [3]. In the Runge-Kutta method, the second order differential equation is first reduced to two first-order equations. For example, by letting $y' = w$, equations (2.1) and (2.2) can be reduced to:

$$y'' = w' = U - y - \hat{F}\,\mathrm{sgn}(w) \tag{2.5}$$

$$y'' = w' = U - y - \hat{F}\,\mathrm{sgn}(w - U') \tag{2.6}$$

Throughout this thesis, the Coloumb friction model is used. In order to make computation faster and easier using MATLAB, a smooth function is used instead of the sign function in the numerical implementation and solution of the governing differential equations of motion. The smooth function used in this case is the error function, erf. It is the error function encountered in integrating the normal distribution (which is a normalized form of the Gaussian function). This function resembles the sign function closely, except that there is no discontinuity at $\dot{x} = 0$. How close the error function is to the sign function is governed by a constant 'a' which controls the smoothness of the error function curve.

If smaller 'a' is used, the error function is smoother at $\dot{x} = 0$. However, the results and the approximation would differ excessively from the sought non-smooth one [53, 57]. In the results, there will be a smooth transition every time friction changes its direction which is not quite close to how a system with Coulomb friction behaves. There is also less sticking period when the velocity passes through zero since at a small velocity, friction will also be small and not straightly jump to a higher value. If larger 'a' is used, the computation effort will be increased significantly [53, 57]. There exists some papers on what is the appropriate value for the constant 'a', for example [53, 58] . In the papers, it is mentioned that a value of $a \geq 1000$ suffices to fit within the analytical solution within 1% .Therefore,

in this thesis a=1000 is used. The comparison between $\mathrm{sgn}(\dot{x})$ and $\mathrm{erf}(a\dot{x})$ function is shown in Figure 2.3.

For some simplified cases, the analytical solutions are also presented. These solutions are presented to gain physical insight into the system response.

2.6.2 A single degree of freedom system under versed sine base input

In this section, the model in Figure 2.2(a) is considered in which the friction interface is isolated from the shock excitation. The pulse duration is chosen to be equal to the natural period of the system. For an undamped single degree of freedom system with no friction and input duration, $T_p = T$, the non-dimensional displacement response y of the system will be amplified to a value about 1.7 times the maximum amplitude of the versed sine base input. $T = \dfrac{2\pi}{\omega_n}$ is the natural period of the system. This is shown by the Shock Response Spectrum (SRS) in the Appendix B. The reduction of the response due to friction when the input duration is close or equal to the natural period of the system could be significant. Not much improvement can be made for a long pulse, which will follow the motion of the input. A short input corresponds to a case in the region of isolation [3].

Figure 2.4 shows the time response of the single degree of freedom with friction subject to versed sine base excitation. It is expected that if friction were to be applied to the system one can reduce the maximum response, because friction might provide dissipation to the system. From Figure 2.4, it can be seen that as friction increases, the maximum displacement response is smaller compared to the case when the friction is small or negligible.

To investigate the maximum displacement response as friction is varied, further simulations were performed. Figure 2.5 is plotted to show the maximum displacement response for different levels of friction. The maximum displacement of the mass decreases as the friction increases until the point where the mass does not move at all.

It can be seen that the system mass does not move at all when static friction is high, for example the corresponding value is $\hat{F} = 10$. The influence of the parameters which

produce no mass displacement can be derived from $F = ku_{mag}$ or $\hat{F} = \frac{\omega_n{}^2 u_{mag}}{g} = U_{mag}$. Using these relationships the friction required to make the mass fixed for all time depends upon the stiffness and the magnitude of the base input. It also shows that by varying the system properties (stiffness and mass subsequently the natural frequency) and the input magnitude, friction that needs to be applied to produce the same behaviour has to be changed accordingly. For example, if the input magnitude is two times larger than the current input, the system will start to stick at $\hat{F} = 20$ considering the same system is used. Also, when the system properties are changed such that the natural frequency of the system is two times the current natural frequency, the system will start to stick at $\hat{F} = 40$ considering the same input is used. On the other hand, if the natural frequency and the input magnitude are both changed such that the non-dimensional base input magnitude remains $U_{mag} = 10$, the system will still start to stick at $\hat{F} = 10$. This knowledge will assist in finding out the amount of friction needed to produce certain behaviours if the properties of the system and input are known.

In order to test how sensitive the changes in the results at the region of the pulse length close to the natural period of the system, further simulation was performed for pulse length equal to $0.8T$ $0.9T$ $1.1T$ and $1.2T$. The results are subsequently compared to the results for the pulse length equal to the natural period of the system in Figure 2.6. The results only vary slightly when friction is small, $\hat{F} < 10$. There is no variation when $\hat{F} \geq 10$ because the mass remains stationary above this value.

2.6.3 A single degree of freedom system under versed sine input at the base and on the supported mass

The second model, shown in Figure 2.2(b), behaves slightly differently compared to the first model shown in Figure 2.2(a). For this section and the next section, the analysis will focus only on the second model with different pulse length. As in the previous section, a versed sine input with pulse duration equal to the natural period of the system is chosen.

Figure 2.7 shows the displacement response of a single degree of freedom system under versed sine excitation at the base and on the supported mass. When the friction increases, it can be seen that the maximum displacement response reduces. Therefore, both models will have reductions in the maximum displacement response. However, what makes them

different is that the second model will have a high displacement with high friction at the beginning of the shock, while the first model experiences a lower displacement at the beginning of the shock as friction increases. However, after about half the period of the shock, the displacement reduces for higher friction. The reason for the higher displacement of the mass at the beginning of the shock is because the velocity of the mass is smaller than the base input velocity, so friction acts in the same direction of the motion and accelerates the mass. However, as time progresses, the velocity of the mass becomes larger than the base input velocity and friction begins to act to oppose the motion of the mass.

The other difference is that instead of remaining stationary, as in the case for large friction for the first model, the second model will follow the motion of the input when large friction is present. This is shown in Figure 2.8, a plot of the maximum displacement response of the second model as friction is varied. It can be seen that for large friction, the normalized response of the mass with respect to the versed sine base input is unity, where the mass follows exactly the motion of the input.

One possible response occurs due to the condition of the mass sticking onto the friction interface. Therefore, as long as the friction interface is moving the mass will follow exactly the motion of the friction interface. In order to derive this relationship, the equation of motion for the second model is used. The acceleration of the mass is set to be the same as the base input, in this case a versed sine input is used so the acceleration of the versed sine input is calculated.

$$\ddot{x} = \ddot{u} = \frac{u_{mag}}{2}\left(\frac{2\pi}{T_p}\right)^2 \cos\left(\frac{2\pi t}{T_p}\right) \tag{2.7}$$

So, the maximum acceleration of the mass is

$$\ddot{x}_{max} = \frac{u_{mag}}{2}\left(\frac{2\pi}{T_p}\right)^2 \tag{2.8}$$

Consider the value of friction necessary to accelerate the mass with the same base acceleration, i.e.

$$\begin{aligned} F_{st} &= m\ddot{x}_{max} = m\frac{u_{mag}}{2}\left(\frac{2\pi}{T_p}\right)^2 \\ \hat{F}_{st} &= \frac{m\ddot{x}_{max}}{mg} = \frac{2\pi^2 u_{mag}}{T_p{}^2 g} \end{aligned} \tag{2.9}$$

It can be seen that the friction required for sticking to the moving surface, F_{st}, will depend upon the input magnitude and the pulse duration, which is related to the excitation frequency. Increasing the input magnitude and increasing the excitation frequency or reducing the pulse length will require higher friction in order to make the mass stick.

However, the smallest maximum response is not obtained when the mass sticks. It is obtained when the mass still slides with respect to the friction interface. From Figure 2.8, it can be observed that when there is no friction, the maximum response is about 1.7 times the amplitude of the input. This corresponds to the case of an undamped system. When the friction increases, the maximum response decreases. The maximum response decreases up to the point when its value is just slightly below unity. Then, further increases in the amount of friction will cause a slight increment in the maximum response before the mass sticks. With the parameters used, the lowest maximum displacement occurs when $\hat{F}$ is approximately equal to 4 and the mass sticks when $\hat{F}$ is approximately equal to 5. This happens if $\frac{\omega_n{}^2 u_{mag}}{g} = U_{mag} = 10$. As explained in the previous section, the value of friction needed to produce the same behaviour will change according to the natural frequency of the system and the input magnitude. The lowest maximum displacement response with respect to the base input magnitude is about 0.99 when $\hat{F} = 4$.

A second order ordinary differential equation (ODE) of the form of equation (2.2) is easily solved by numerical integration when the sign function is approximated. However, in this case an analytical solution is possible which yields rather more physical insight into the system. Duhamel's Integral is used as shown in equation (2.10). It is a well known approach to the solution of transient vibration problems for linear systems[2]. However, a friction system is a piecewise linear system. The Duhamel Integral solution outlined below can be used only during the interval of the motion when the sign of the relative velocity is negative. Therefore, it can be used to find the solution at the beginning of the shock from $t = 0$ until $t = \bar{t}$ when the relative velocity reaches zero and starts to turn positive.

$$x = \left(x_i - \frac{1}{m\omega_n} \int_0^t P(t_v) \sin(\omega_n t_v)\, dt_v \right) \cos \omega_n t + \left(\frac{\dot{x}_i}{\omega_n} + \frac{1}{m\omega_n} \int_0^t P(t_v) \cos(\omega_n t_v)\, dt_v \right) \sin \omega_n t \quad (2.10)$$

where $x_i = 0, \dot{x}_i = 0, P(t_v) = \frac{ku_{mag}}{2}\left(1-\cos\left(\frac{2\pi t_v}{T_p}\right)\right) + F$ for $t \le T_p$ and $\dot{x} - \dot{u} < 0$. Since T_p is equal to T, then $P(t_v)$ is equal to $\frac{ku_{mag}}{2}(1-\cos(\omega t_v)) + F$ for $t \le T_p$ and $\dot{x} - \dot{u} < 0$.

Equation (2.10) can be solved to produce displacement of a single degree of freedom system with friction from $t = 0$ until the point where $\dot{x} - \dot{u} = 0$ at $t = \breve{t}$.

$$x = \frac{u_{mag}}{2} - \frac{u_{mag}}{2}\cos\omega_n t - \frac{\omega u_{mag}}{4} t \sin\omega_n t + \frac{F}{k}(1-\cos\omega_n t) \qquad (2.11)$$

$$\text{for } 0 \le t \le \breve{t}$$

Equation (2.11) can be differentiated twice to obtain the acceleration which is given by

$$\ddot{x} = \frac{\omega_n{}^3 u_{mag}}{4} t \sin\omega_n t + \frac{F}{m}\cos\omega_n t \qquad (2.12)$$

$$\text{for } 0 \le t \le \breve{t}$$

The relative velocity between the mass and input velocity can also be derived to solve for the time at which the relative velocity becomes greater than zero, at which point the friction changes its direction. This is important to know the time when the solution above is still valid. The relative velocity is set to be equal to zero:

$$\left(\frac{\omega_n u_{mag}}{2} - \frac{\omega_n u_{mag}}{4} - \frac{\pi u_{mag}}{T_p} + \frac{\omega_n F}{k}\right)\sin\omega_n \breve{t} - \frac{\omega_n{}^2 u_{mag}}{4}\breve{t}\cos\omega_n \breve{t} = 0 \qquad (2.13)$$

Equation (2.13) can be simplified for the case of $T_p = T$ to give

$$\frac{1}{\breve{t}}\tan\omega_n \breve{t} = \frac{\left(\frac{\omega_n{}^3 u_{mag}}{4g}\right)}{\left(\hat{F} - \frac{\omega_n{}^2 u_{mag}}{4g}\right)} \qquad (2.14)$$

For the case when friction is absent, ie $\hat{F} = 0$, equation (2.14) reduces to $\tan\omega_n \breve{t} = -\omega_n \breve{t}$, i.e. $\breve{t} = \frac{0.6459\pi}{\omega_n}$. With friction present, it is expected that $0 \le \breve{t} < \frac{0.6459\pi}{\omega_n}$ depending on the value of friction, which can be solved from equation(2.14). This can be seen in Figure

2.9. As friction increases the time taken for the relative velocity to reach zero $\breve{t}$ becomes shorter. There is also stick and slip motion when the friction increases.

By inspection, the acceleration reaches its first peak at the time when the relative velocity is equal to zero. Therefore, the first maximum in the acceleration can be determined by substituting $\breve{t}$ into equation (2.12). After reaching maximum acceleration, if there is friction, there will be an acceleration discontinuity; the acceleration will jump to a smaller value. The jump is equal to $2\hat{F}$ as seen in Figure 2.10.

Again, in order to test how sensitive the changes in the results at the region of the pulse length close to the natural period of the system, further simulation was performed for pulse length equal to $0.8T$ $0.9T$ $1.1T$ and $1.2T$. The results are subsequently compared to the results for the pulse length equal to the natural period of the system in Figure 2.11. The results only vary when friction is small. The variation with pulse length is larger than the previous case when the friction interface is isolated from the input. The reason for this may due to the change in the friction direction with respect to the relative displacement between the mass and the base instead of the absolute velocity of the mass. Therefore, friction might act in the same direction as the motion instead of always opposing it in the case of the isolated friction interface. For slightly higher friction, the mass sticks and moves with the base which does not make any difference with any pulse length used.

Table 2.1 lists the smallest maximum displacement achieved with the variation of the pulse length and how much friction is required to achieve this. From the table, the smallest maximum displacement does not vary much when the pulse length is very close to the natural period of the system. However, there is significant variation on how much friction is needed to achieve this situation. The amount of friction needed to obtain the smallest maximum displacement can change from $\hat{F} = 3$ to $\hat{F} = 6$ as the pulse length changes from $T_p = 1.2T$ to $T_p = 0.8T$.

2.6.4 A single degree of freedom system under short duration versed sine input at the base and on the supported mass

The complete solution of a single degree of freedom system with friction can be solved by combining the complementary solution of a single degree of freedom undamped system as in reference [2] and adding the effect of friction as long as the friction force is acting in the same direction. The solution is shown in equation(2.15). This equation is only valid when

the relative velocity is negative and it can be used to obtain the response of the system from $t = 0$ until $t = \breve{t}$, where $\breve{t}$ is the time when the relative velocity turns positive.

$$x = \left(\frac{\left(\frac{u_{mag}}{2} \right)}{1 - \left(\frac{T_p^2}{T^2} \right)} \right) \left(1 - \left(\frac{T_p^2}{T^2} \right) + \left(\frac{T_p^2}{T^2} \right) \cos\left(\frac{2\pi t}{T_p} \right) - \cos \omega_n t \right) + \frac{F}{k} \left(1 - \cos \omega_n t \right) \qquad (2.15)$$

$$\text{for } 0 \le t \le \breve{t}$$

For a short base input, $\frac{T_p}{T} \approx 0$ and $\cos \omega_n t \approx 1$.So equation (2.15) can be approximated as

$$x \approx \left(\frac{u_{mag}}{2} + \frac{F}{k} \right) \left(1 - \cos \omega_n t \right) \qquad (2.16)$$

Equation (2.16) shows that there is not much effect of friction on the displacement of a single degree of freedom system for a short base input. Since $\cos \omega_n t \approx 1$, the displacement of the mass x will be very small during the shock. However, there is a big effect due to friction on the acceleration of a single degree of freedom system for a short base input. Equation (2.15) can be differentiated twice to get the expression of acceleration of a single degree of freedom system with friction as follows

$$\ddot{x} = \left(\frac{\left(\frac{\omega_n{}^2 u_{mag}}{2} \right)}{1 - \left(\frac{T_p^2}{T^2} \right)} \right) \left(\cos \omega_n t - \cos\left(\frac{2\pi t}{T_p} \right) \right) + \frac{F}{m} \cos \omega_n t \qquad (2.17)$$

Therefore, when $\cos \omega_n t \approx 1$ equation (2.17) can be approximated as

$$\ddot{x} \approx \left(\frac{\omega_n{}^2 u_{mag}}{2} \right) \left(1 - \cos\left(\frac{2\pi t}{T_p} \right) \right) + \frac{F}{m} \qquad (2.18)$$

From equation (2.18), an increase in friction will cause an increase in the acceleration of the system. The maximum acceleration for a short base input occurs at approximately half of the pulse length, $t = 0.5T_p = \breve{t}$. It is equal to the time when the relative velocity turns positive. From the analytical solution, the friction causes a significant increase in the acceleration of a single degree of freedom system, although there is no significant increase

in the displacement of the system. See Figure 2.12 for the acceleration plot of a single degree of freedom system with friction under a short base input.
An increase in friction will cause an increase in the maximum acceleration which is a linear function of the level of the friction for this case. Based on equation (2.18), the maximum acceleration increases at a rate of $\frac{F}{m}$. In this case, the maximum non-dimensional acceleration increases at the rate of $\hat{F}$. The behaviour is shown in Figure 2.13. The numerical solution using ODE also validates this relationship.

2.7 Shock response of a two degree of freedom system incorporating sliding friction

2.7.1 Introduction

After the in depth investigation of a single degree of freedom system with friction applied directly to the mass, the next task is to investigate a two degree of freedom model with friction. For this purpose, a two degree of freedom system shown in Figure 2.14 is considered. x_1 and x_2 are the absolute displacement of the two masses and u is the base input. At this time, friction is applied to the secondary mass which is connected to the primary mass via a secondary spring. This system is expected to improve the acceleration response compared to the single degree of freedom model, which experiences unsmooth changes in the acceleration when friction changes its direction as shown in Figure 2.10.

The equations of motion of the system in Figure 2.12 are

$$\begin{aligned} m_1\ddot{x}_1 + k_1x_1 + k_2(x_1 - x_2) &= k_1u \\ m_2\ddot{x}_2 - k_2(x_1 - x_2) + F\,\mathrm{sgn}(\dot{x}_2 - \dot{u}) &= 0 \end{aligned} \tag{2.19}$$

where $\omega_1 = \sqrt{\frac{k_1}{m_1}}$ and $\omega_2 = \sqrt{\frac{k_2}{m_2}}$ are the natural frequency of the primary system and secondary mass respectively.

Non-dimensional parameters can be defined in terms of the system parameters as non-dimensional displacements $y_1 = \frac{\omega_1^2 x_1}{g}$, $y_2 = \frac{\omega_1^2 x_2}{g}$, frequency ratio $\hat{\omega} = \frac{\omega_2}{\omega_1}$, mass ratio $\mu = \frac{m_2}{m_1}$, stiffness ratio $\hat{k} = \frac{k_2}{k_1}$, non-dimensional friction force $\hat{F} = \frac{F}{m_1 g}$, non-dimensional

base input $U = \frac{\omega_1^2 u}{g}$, non-dimensional time $\tau = \omega_1 t$ and differentiation with respect to non-dimensional time $\odot' = \frac{d\odot}{d\tau}$.

The equations of motion given in equation(2.19) can subsequently be written in non-dimensional form as

$$\begin{aligned} y_1'' + y_1 + \hat{k}(y_1 - y_2) &= U \\ \mu y_2'' + \hat{k}(y_2 - y_1) + \hat{F}\,\mathrm{sgn}(y_2' - U') &= 0 \end{aligned} \tag{2.20}$$

The system is subjected to versed sine base input and the dynamic response is then analyzed. The influence of the system parameters such as stiffness ratio, mass ratio and friction on the response of the system is discussed to determine which combinations of the parameters give the best response. Finally, a comparison is made to the single degree of freedom system with friction in terms of the benefits and weaknesses of both systems.

2.7.2 The effect of friction on the maximum displacement response of the masses

For a fixed mass ratio, pulse duration and amplitude of the pulse, the effect of variation in the friction on the maximum displacement response of the masses under specific values of the frequency ratio $\hat{\omega}$ can be examined and plotted. The mass ratio μ is initially set to be equal to 0.1, which means that the secondary mass is ten times smaller than the primary mass. As the mass ratio is kept fixed, when $\hat{\omega}$ is varied the value of the stiffness ratio $\hat{k}$ is also varied. Four frequency ratios are selected, which correspond to a soft secondary spring ($k_2 = 0.4k_1$), medium stiffness ($k_2 = 2.5k_1$, $k_2 = 100k_1$) and a stiff secondary spring ($k_2 = 2500k_1$) compared to the primary spring.

The non-dimensional base input amplitude U_{mag} is set to be equal to 10, therefore $u_{mag} = \frac{U_{mag} g}{\omega_1^2} = \frac{10g}{\omega_1^2}$. The pulse duration is chosen to be equal to the first natural period of the system, which corresponds to the fundamental natural frequency of the combined system. The reason why the length of pulse is chosen to be equal to the fundamental period of the system is to investigate whether the presence of friction in the system can reduce the response which is large for the undamped system. In the analysis of the two degree of

freedom system, the short duration input is not considered. The reason is because from the earlier analysis on the single degree of freedom system, friction is expected to increase the acceleration of the mass. Therefore, it is predicted even by applying friction at the secondary mass, there is no improvement that could be made in this stage without further modifications.

Figure 2.15 shows the maximum displacement response of the masses for different levels of friction under a versed sine base input. As stated in the earlier sections on the single degree of freedom model, that by varying the system properties and the input magnitude, the amount of friction that needs to be applied to produce the same behaviour has to be changed accordingly, in the case of a two degree of freedom model it is dependent on the input magnitude and the fundamental natural frequency of the coupled system.

It is interesting to see that from Figure 2.15(d), the maximum displacement response of the masses for a two degree of freedom system when friction is varied looks almost identical to the response of the mass for a single degree of freedom system. This corresponds to the case when the secondary stiffness is very large compared to the primary stiffness. In this case, the two masses move together and behave in a way almost identical to a single degree of freedom system.

Generally, from Figure 2.15, it can be seen that the maximum displacement response of the primary mass decreases as friction increases from zero to a friction value which yields a maximum reduction, which is defined as $\hat{F}_{opt}$ for further reference. The value of $\hat{F}_{opt}$ is different depending on the secondary stiffness (stiffness ratio). The value of $\hat{F}_{opt}$ as stiffness ratio is varied and the normalized displacement response for the primary mass, $\left(\frac{y_1}{U}\right)_{min}$ produced at $\hat{F}_{opt}$ is listed in Table 2.2. When the stiffness ratio is small, the reduction of the primary mass response compared to an undamped system is small. The value of $\left(\frac{y_1}{U}\right)_{min}$ is 1.56. As stiffness ratio increases, there is more reduction on the displacement response of the primary mass. The largest reduction is produced when stiffness ratio $\hat{k}$ is equal to 250. For this case, $\left(\frac{y_1}{U}\right)_{min}$ is equal to 0.98.

However, if the friction is further increased to be larger than $\hat{F}_{opt}$, there is no further reduction of the maximum response of the primary mass. The maximum response of the primary mass will increase until it reaches the point at which the secondary mass sticks to the friction interface. Then, further increases in the friction will not cause any change in the maximum response of the primary mass. When the secondary mass sticks, the primary mass will become an undamped single degree of freedom. It can be seen that the smallest maximum displacement can be obtained while the secondary mass slides on the friction interface instead of fully sticking.

Figures 2.16 and 2.17 show the time history and phase plane plots of the primary and secondary mass of a two degree of freedom system. Two different secondary stiffnesses are used, corresponding to a low stiffness ratio $\hat{k} = 0.4$ and a medium stiffness ratio $\hat{k} = 2.5$. A high stiffness ratio will produce the same response as a single degree of freedom system; see Figures 2.7 to 2.10. Three different friction values are used which correspond to no friction, friction which yields the smallest maximum response and large friction which makes the secondary mass fully stick or almost fully stick to the friction interface during the shock.

From Figures 2.15 to 2.17 it can be seen that the secondary mass of the system with a softer secondary spring needs lower friction to fully stick to the friction interface and move with it compared to the system with a stiff secondary spring. Blue lines in Figure 2.15(a), for the case of $\hat{k} = 0.4$, show that the secondary mass sticks when the friction is about $\hat{F} = 3.5$ compared to other systems which used larger secondary stiffness. This is as the force from the secondary spring is not large enough to overcome the friction. However, when the secondary stiffness increases, the friction needed to make the secondary mass stick to the friction interface becomes larger. A system with medium stiffness, Figure 2.15(b) with $\hat{k} = 2.5$, sticks when $\hat{F}$ is about 9. The same value is found when the stiffness ratio $\hat{k}$ is increased to $\hat{k} = 10$ and $\hat{k} = 250$, where the system still sticks when $\hat{F}$ is about 9. The system fully sticks when there is no further change in the maximum relative displacement between the masses and the maximum absolute displacement of both masses as friction is increased.

If lower friction than that which could make the secondary mass fully stick to the friction interface is used, the secondary mass may experience full sliding motion or stick-slip

during the shock depending upon the level of friction. For low friction, the system fully slides with respect to the friction interface. As friction increases, the system starts to experience stick-slip motion before it fully sticks at high friction.

From Figure 2.15, the maximum relative displacement increases as friction increases until the point when the secondary mass fully sticks or almost fully sticks to the friction interface. The reason for this is that for low friction the base input comes mainly through the primary spring. Therefore, there is not much compression or extension in the secondary spring. However, for higher friction, the base input will produce movement of the friction interface as well. However, after the secondary mass sticks on the friction interface, increased friction levels will not cause any significant difference to the maximum relative displacement of the masses. The maximum relative displacement of the masses decreases as the secondary stiffness increases. As it increases, the primary and secondary masses tend to move together with a very small relative displacement.

When the secondary mass fully sticks, it will follow exactly the same motion as the base input, described by

$$x_2 = u = \frac{\hat{u}}{2}\left(1-\cos\left(\frac{2\pi t}{T_p}\right)\right) \tag{2.21}$$

When equation (2.21) is applied to the first part of equation (2.19), this gives

$$m_1\ddot{x}_1 + (k_1+k_2)x_1 = (k_1+k_2)u \tag{2.22}$$

This is the equation of a one degree of freedom undamped system with natural frequency $\omega_n = \sqrt{\frac{k_1+k_2}{m_1}}$. This equation of motion will describe the motion of the primary mass. The maximum response of the primary mass when friction is large enough to hold the secondary mass from sliding with respect to the friction interface can be solved using equation (2.22), as in the single degree of freedom model.

2.7.3 The acceleration response of the primary mass

Another important response quantity to look at the acceleration response of the primary mass. In this section, the acceleration response of a two degree of freedom model is discussed particularly the acceleration response of the primary mass. From section 2.6, which discussed a single degree of freedom system with friction, there is an instantaneous change in the acceleration response of the mass every time the friction force changes its direction and at the start of the motion. The change is equal to $2\hat{F}$. This is because, friction is applied directly to the primary mass for the case of a single degree of freedom system and based on the Coulomb friction law, the friction force instantaneously changes its value every time the velocity direction of the mass changes. By attaching a secondary system to the primary mass and letting friction be applied to the secondary mass, it is expected that this instantaneous change to the acceleration response of the primary mass could be avoided and a smoother response could be produced.

The acceleration response of the primary mass for different stiffness ratios is plotted in Figure 2.18. Figure 2.18 shows the acceleration response of a two degree of freedom model under a versed sine base input when $\hat{F} = \hat{F}_{opt}$. From the previous section, it is known that $\hat{F}_{opt}$ produces the smallest maximum displacement for the primary mass at each stiffness ratio. In this section, it is beneficial to see whether $\hat{F}_{opt}$ also could produce a good acceleration response for the primary mass.

From Figure 2.18(a), it can be observed that when stiffness ratio is small, the acceleration response of the primary mass is smooth. When the stiffness ratio is increased, the acceleration response changes more sharply at the start of the motion and every time the friction force changes its directions; see Figures 2.18(b) and (c). This is because of a stronger coupling between the primary mass and the secondary mass on which the friction is applied. In this case, the friction has a stronger influence on the behaviour of the primary mass. However, for all of the cases the response is better than the case of a single degree of freedom system presented in Figure 2.10.

2.7.4 The effect of mass ratio on the maximum displacement response of the masses

In the previous section, the mass ratio is kept fixed using a small secondary mass, $m_2 = 0.1m_1$. It is desirable that the secondary mass is small so that the addition of a secondary system does not cause a large change in the overall weight of the system. However, it is important to see whether increasing the secondary mass could give a better response during the shock. Therefore, the variation in the mass ratio will be investigated. For this purpose, two more mass ratio values are chosen, $\mu = 0.32$ and $\mu = 1$. For these two values of mass ratio, the maximum displacement response of the masses as friction is varied are plotted in Figure 2.15, on the same plot as for the mass ratio $\mu = 0.1$. All of the blue lines in the plot correspond to the case of mass ratio $\mu = 0.1$. On the other hand, all of the black lines in the plot correspond to the case of the mass ratio $\mu = 0.32$ and all of the red lines in the plot correspond to the case of the mass ratio $\mu = 1$.

The time response and phase plane plots for the case of the mass ratio $\mu = 0.32$ and $\mu = 1$ are plotted in Figures 2.19 to 2.22. Figures 2.19 and 2.20 are plotted for the case of $\mu = 0.32$ with the stiffness ratio $\hat{k} = 0.4$ and $\hat{k} = 2.5$ respectively. On the other hand, Figures 2.21 and 2.22 are plotted for the case of $\mu = 1$ with the stiffness ratio $\hat{k} = 0.4$ and $\hat{k} = 2.5$ respectively. As for the case of a small mass ratio $\mu = 0.1$ discussed in section 2.7.2, three different friction values are used which correspond to no friction, friction which yields the smallest maximum response and large friction which makes the secondary mass fully stick or almost fully stick to the friction interface during the shock.

From inspection of Figure 2.15, as the stiffness ratio is increased, the influence of the mass ratio on the maximum displacement response of the masses becomes less significant. There is a large difference in the maximum displacement response of the masses at each friction value for different mass ratios when the stiffness ratio is small. On the other hand, when the stiffness ratio is high enough as in Figure 2.15(d), there is no difference in the maximum displacement response of the masses for different mass ratios. The big difference for the case of a small stiffness ratio is caused by the existence of two significant modes that dominate the response of the system. As the mass ratio is varied for a given stiffness ratio, the frequency ratio changes. The change in the frequency ratio produces a big change in the displacement response of the masses for a small stiffness ratio because it changes how the two modes interact to produce the response of the system. On

the other hand, when the stiffness ratio is larger, the second mode is shifted to a higher frequency and its contribution to the response of the system is quite small. As the length of the input is chosen to be equal to the fundamental period of the system, the change in mass ratio by changing the secondary mass only causes a small difference in the response of the masses.

For the case of medium stiffness ratio, $\hat{k} = 2.5$ and $\hat{k} = 10$ with low friction, there is not much difference in the maximum response of the masses as the mass ratio is varied. However, at high friction, the maximum response of the primary mass is smaller for the case of a larger mass ratio. When the secondary mass (mass ratio) is large, the primary mass oscillates at a lower amplitude when the secondary mass fully sticks because of high friction. The example can be seen by comparing Figures 2.17(c), 2.20(c) and 2.22(c).

The value of friction that causes the secondary mass to fully stick is dependent on the mass ratio. As mass ratio becomes larger, which means increasing the size of the secondary mass, less friction is needed to cause the secondary mass to fully stick. For example, in Figure 2.15(a), the secondary mass fully sticks at $\hat{F} = 2.1$ when the mass ratio $\mu = 1$, at $\hat{F} = 2.3$ when the mass ratio $\mu = 0.32$ and at $\hat{F} = 3.5$ when the mass ratio $\mu = 0.1$. This is expected since a small mass needs higher friction to stop sliding relative to the friction interface.

2.8 Comparison between a single and a two degree of freedom system incorporating sliding friction

At this point, it is appropriate to make a comparison between the systems. The comparison outlines the advantages and disadvantages found in both systems in terms of the response during the base shock input. For this reason, the comparison has been made in terms of the displacement and the acceleration response during the shock. The comparison is summarised in Table 2.3.

From the investigation, a single degree of freedom system is better in terms of the displacement response under versed sine base input. If this system is used, for the pulse length equal to the natural period of the system, $T_p = T$, the best displacement response is achieved when $\hat{F}$ is equal to 4. For this case, the normalized response with respect to the base input magnitude is equal to 0.99. On the other hand, the undamped system using the same parameters produced a normalized response of about 1.7. The reduction produced

compared to an undamped system is about 42 percent. On the other hand, the reduction in the displacement response of the primary mass of a two degree of freedom model is small if a soft secondary spring is used. The normalized displacement response of the primary mass when $\hat{k} = 0.4$ is equal to 1.58. The reduction produced for this case compared to an undamped single degree of freedom system is only about 7 percent. As the stiffness of the secondary spring is increased, more reduction could be produced and, as the stiffness of the secondary spring becomes very large, the response of the system becomes close to the response of a single degree of freedom system.

In terms of the acceleration response, a two degree of freedom system produces a better response. By using this system, the instantaneous change during the start of the motion and friction changing direction could be improved. The response is very smooth if a soft secondary spring is used, for example $\hat{k} = 0.4$. This contrants with to the case of a single degree of freedom system where there is an instantaneous change every time motion starts or friction changes direction. However, again as the stiffness of the secondary spring is increased, the changes in response become less smooth compared to the case of a softer secondary spring. As the stiffness of the secondary spring becomes very large, the response of the system becomes close to the response of a single degree of freedom system with instantaneous changes in the acceleration.

2.9 Conclusions

This chapter has introduced two shock isolation configurations, namely a single and a two degree of freedom system with Coulomb friction. In this chapter passive friction is considered, where there is no variation in friction throughout the motion. An in-depth analysis has been done for the two configurations in terms of the displacement and acceleration responses of the primary targeted mass during the shock. The objective is to reduce and improve both the displacement and acceleration responses of the primary targeted mass. The benefits and the disadvantages of both configurations have been identified and compared to each other.

In overall terms, applying the friction does reduce the maximum displacement response of the system compared to an undamped system. For a single degree of freedom system, the smallest displacement response achieved is 0.99 compared to the base input magnitude, which is 42% smaller than for the undamped system, for pulse length equal to the natural period. There is however concern about the instantaneous acceleration change every time the friction changes its direction.

For this reason, a two degree of freedom system with friction applied to a secondary mass has been proposed to improve the acceleration response. For the proposed system, there is a smooth acceleration change when the stiffness ratio $\hat{k}$ is not high. However, the displacement reduction is lower than for the case of a single degree of freedom system. It is desirable to have a two degree of freedom system with an intermediate stiffness ratio $\hat{k}$ to obtain medium reduction in the displacement response and at the same time retain the good acceleration response of the primary isolated mass.

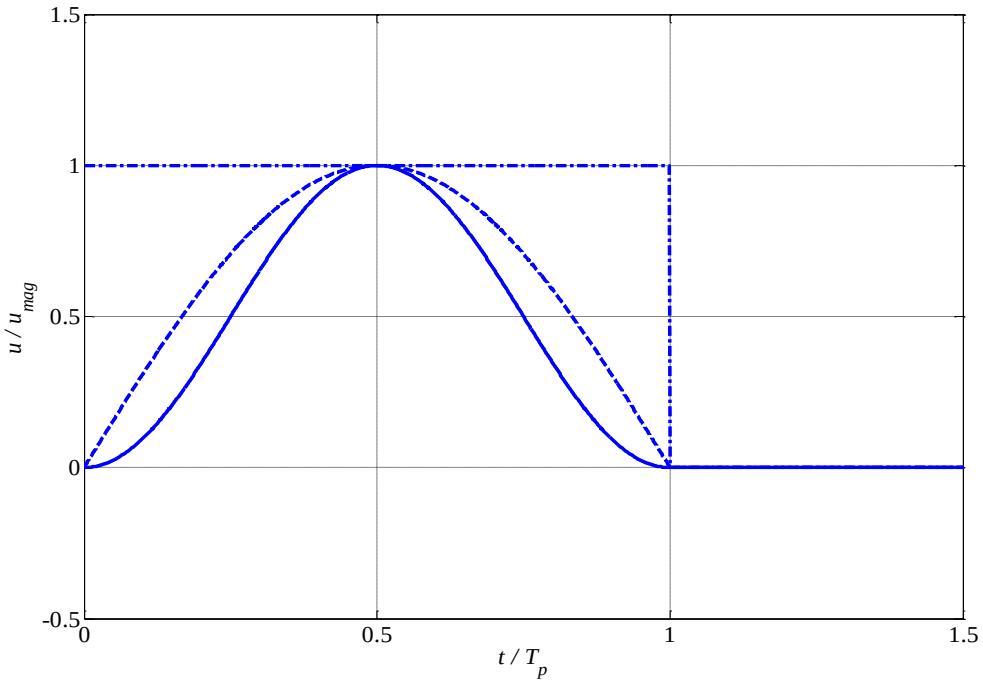

Figure 2.1: Three different inputs applied to the base of the system. Solid line: versed sine input, dash line: half sine input, dash dot line: rectangular input. Normalized input magnitude versus normalized time t/T_p. T_p is the length of the pulse.

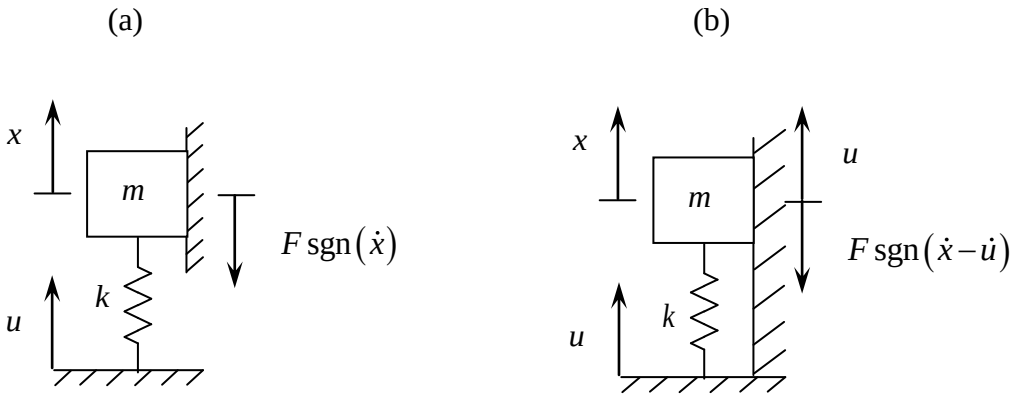

Figure 2.2: A one degree of freedom system configuration with Coulomb friction subjected to a base input. (a) Friction interface does not move. (b) Friction interface moves with the same input as the base motion.

(a)

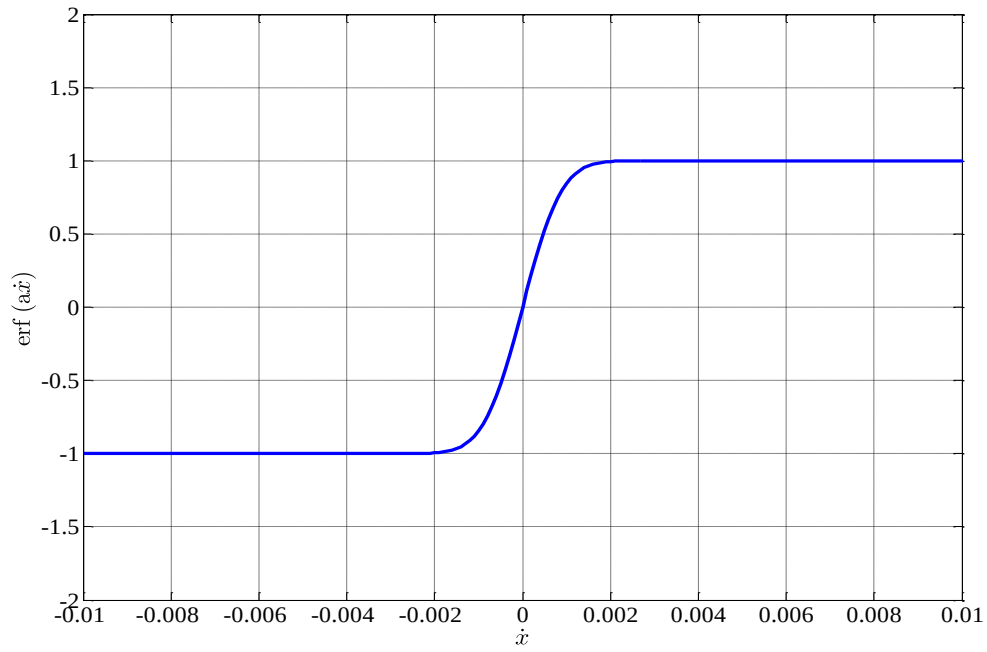

(b)

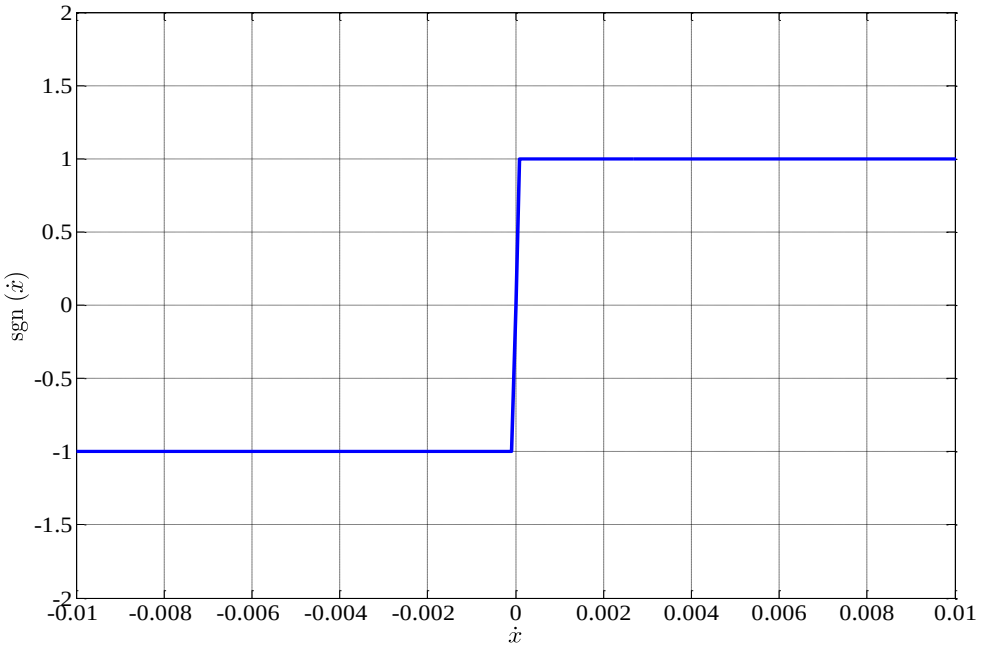

Figure 2.3: Comparison between the error function (erf) and sign function (sgn), (a) error function with the error function parameter *a*=1000, (b) sign function.

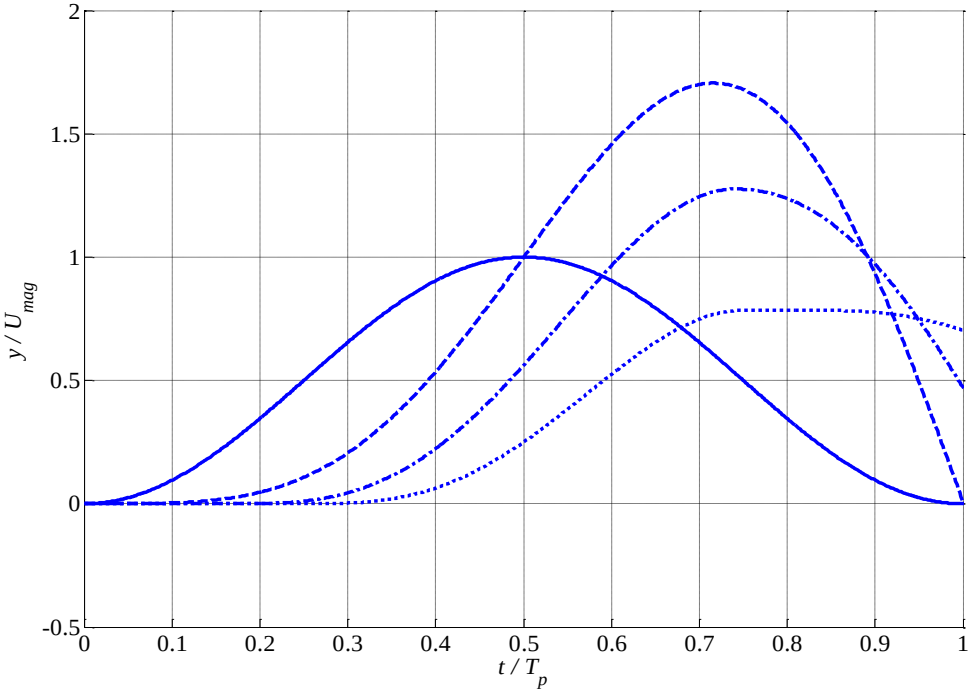

Figure 2.4: Displacement response of a single degree of freedom model under a versed sine base input. Non-dimensional base input magnitude $U_{mag} = 10$ and pulse length $T_p = T$.
Solid line: base input. Dash line: no friction $\hat{F} = 0$. Dash dot line: $\hat{F} = 2.5$. Dot line: $\hat{F} = 5$.

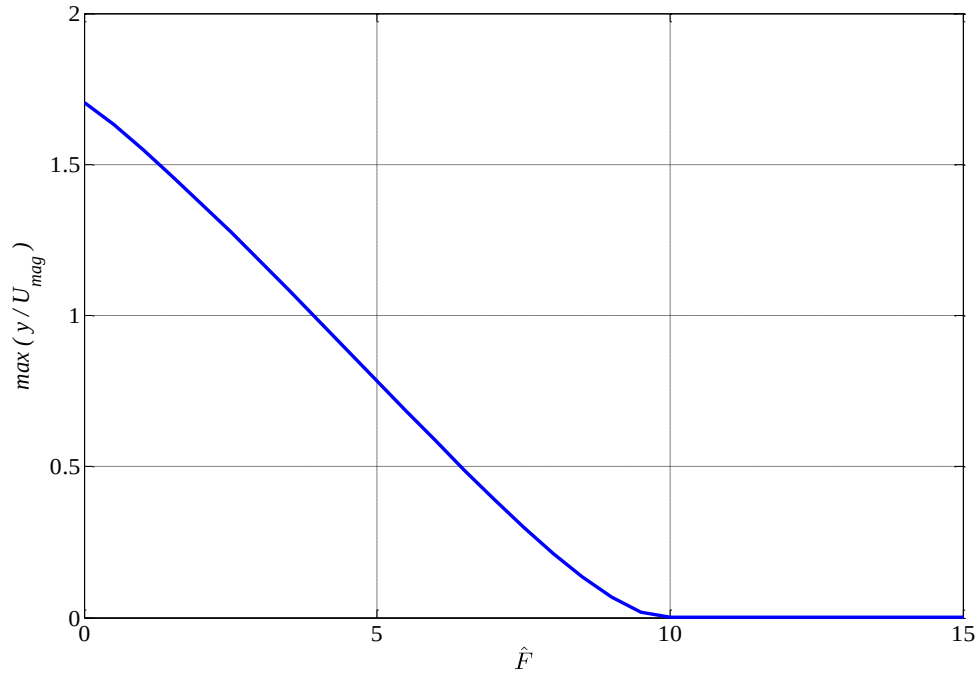

Figure 2.5: Maximum displacement response of a single degree of freedom model under a versed sine base input when the friction is varied. Non-dimensional base input magnitude $U_{mag} = 10$ and pulse length $T_p = T$.

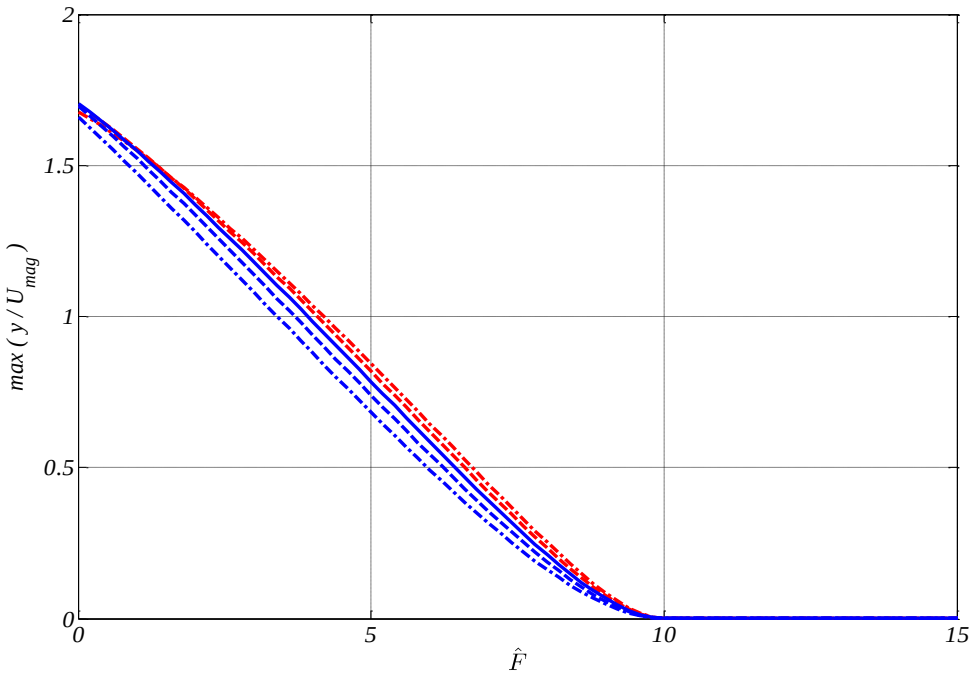

Figure 2.6: The maximum displacement of a single degree of freedom model under versed sine base input when the friction is varied for different pulse lengths. Non-dimensional base input magnitude $U_{mag} = 10$. Solid line: pulse length $T_p = T$. Dash blue line: $T_p = 0.9T$. Dash dot blue line: $T_p = 0.8T$. Dash red line: $T_p = 1.1T$. Dash dot red line: $T_p = 1.2T$.

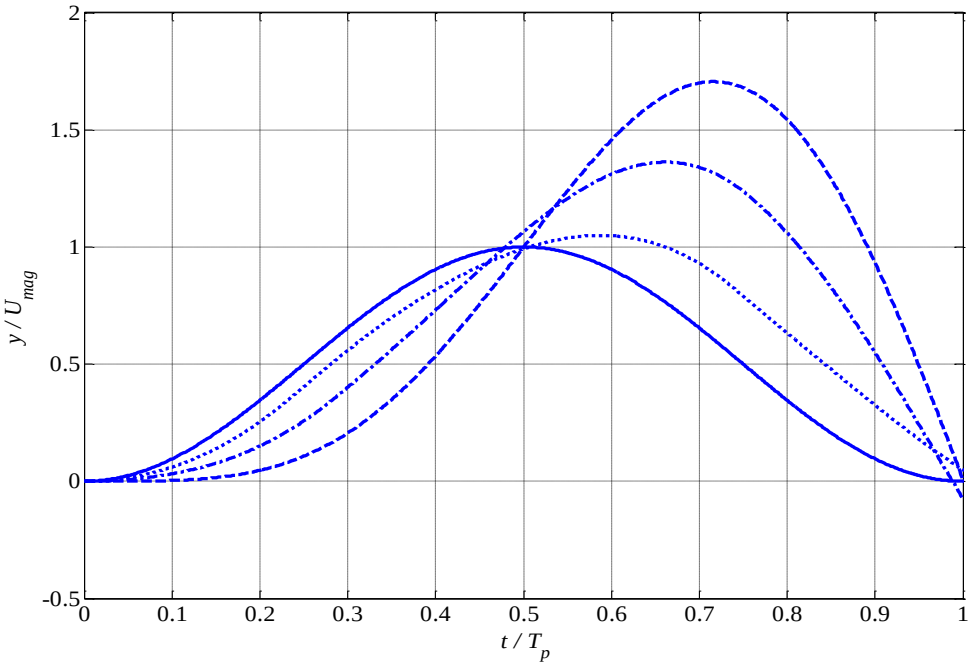

Figure 2.7: Displacement response of a single degree of freedom model under a versed sine base input. Non-dimensional base input magnitude $U_{mag} = 10$ and pulse length $T_p = T$. Solid line: base input. Dash line: $\hat{F} = 0$. Dash dot line: $\hat{F} = 1.5$. Dot line: $\hat{F} = 3$.

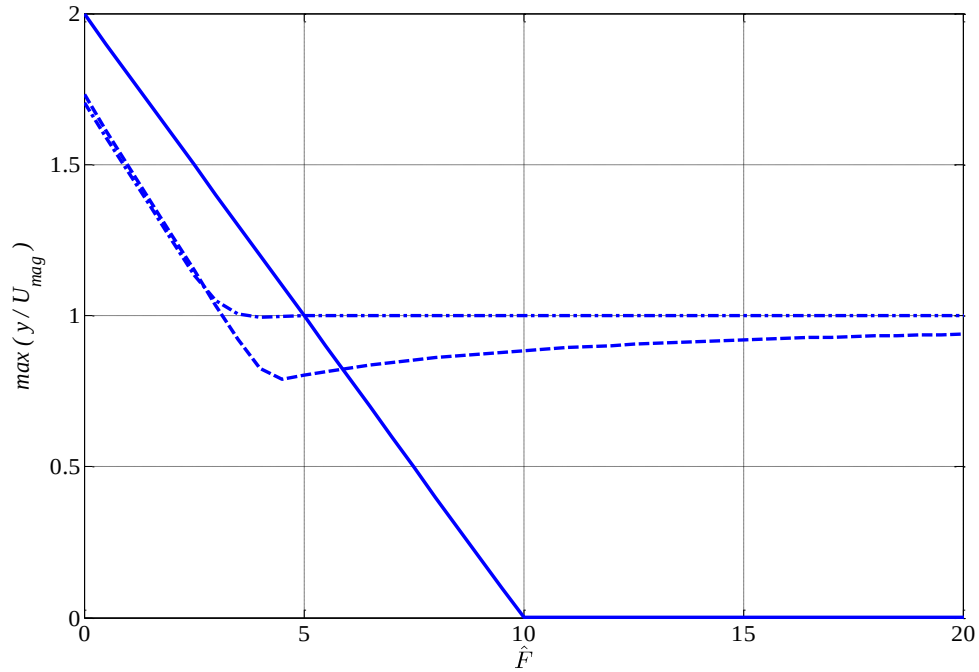

Figure 2.8: Comparison of the maximum displacement of a single degree of freedom model under different types of base input when the friction is varied. Non-dimensional base input magnitude $U_{mag} = 10$ and pulse length $T_p = T$. Solid line: Rectangular base input. Dash line: Half sine base input. Dash dot line: Versed sine base input.

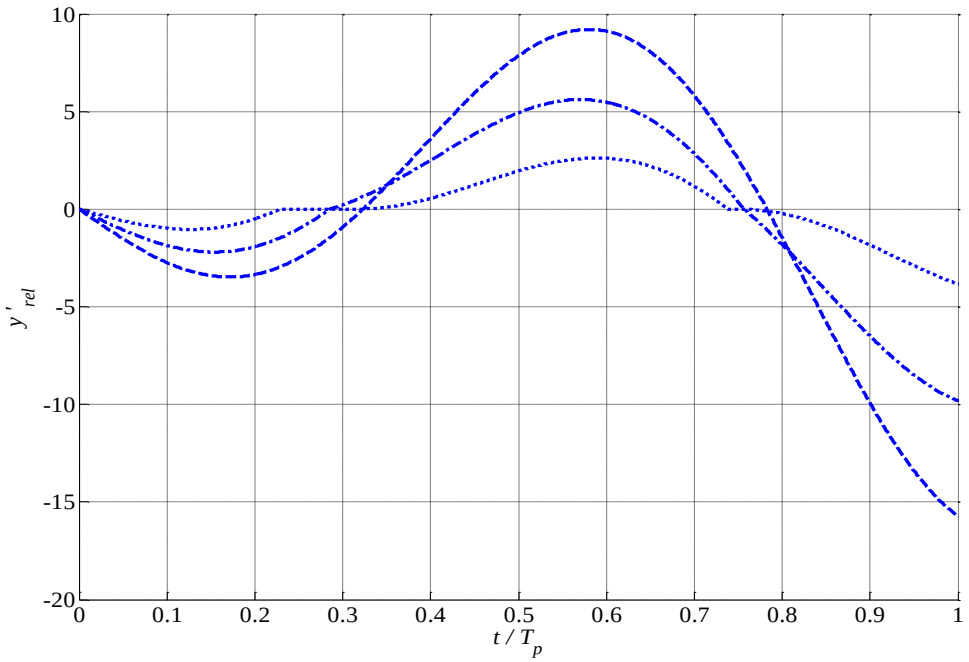

Figure 2.9: Relative velocity of a single degree of freedom system under a versed sine base input. $y'_{rel} = y' - U', y' = \frac{dy}{d\tau}, U' = \frac{dU}{d\tau}, \tau = \omega t$. Non-dimensional base input magnitude $U_{mag} = 10$ and pulse length $T_p = T$. Dash line: $\hat{F} = 0$. Dash dot line: $\hat{F} = 1.5$. Dot line: $\hat{F} = 3$.

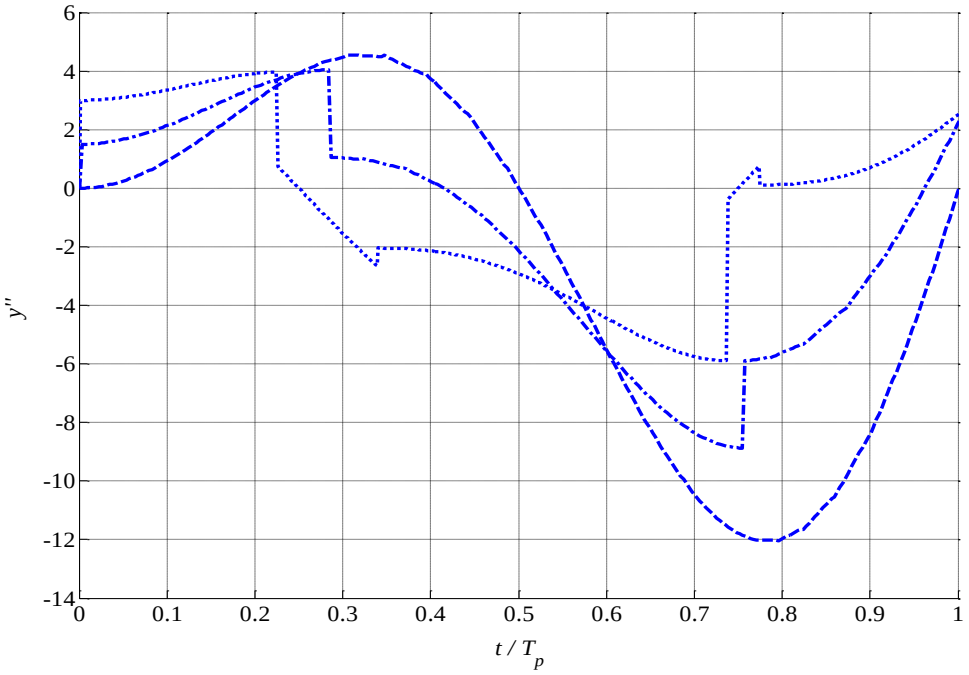

Figure 2.10: Acceleration response of a single degree of freedom model under a versed sine base input. Dash line: $\hat{F} = 0$. Dash dot line: $\hat{F} = 1.5$. Dot line: $\hat{F} = 3$. Non-dimensional base input magnitude $U_{mag} = 10$ and pulse length $T_p = T$.

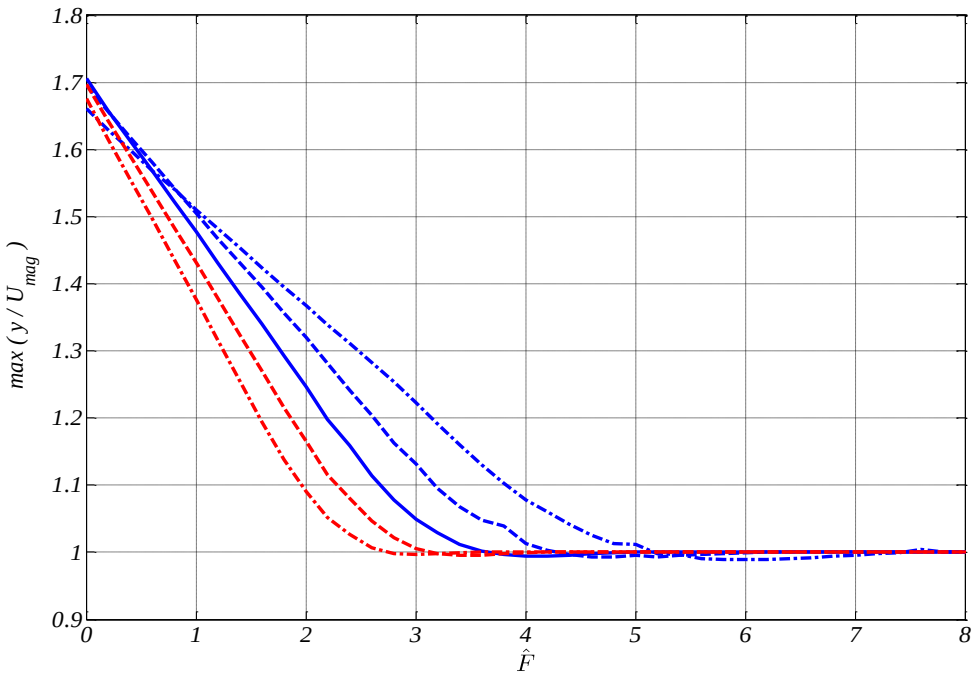

Figure 2.11: The maximum displacement of a single degree of freedom model under versed sine base input when the friction is varied for different pulse lengths. Non-dimensional base input magnitude $U_{mag} = 10$. Solid line: pulse length $T_p = T$. Dash blue line: $T_p = 0.9T$. Dash dot blue line: $T_p = 0.8T$. Dash red line: $T_p = 1.1T$. Dash dot red line: $T_p = 1.2T$.

Pulse length, T_p	Non-dimensional friction, $\hat{F}$ at which the smallest maximum displacement occurs	The smallest maximum displacement, $\left(max\left(\frac{y}{U_{mag}} \right) \right)_{min}$
$T_p = 1.2T$	$\hat{F} = 3$	0.9964
$T_p = 1.1T$	$\hat{F} = 3.4$	0.9954
$T_p = 1T$	$\hat{F} = 4$	0.9939
$T_p = 0.9T$	$\hat{F} = 5.2$	0.9932
$T_p = 0.8T$	$\hat{F} = 6$	0.9889

Table 2.1: The smallest maximum displacement achieved for different pulse lengths and the amount of friction needed to achieve them.

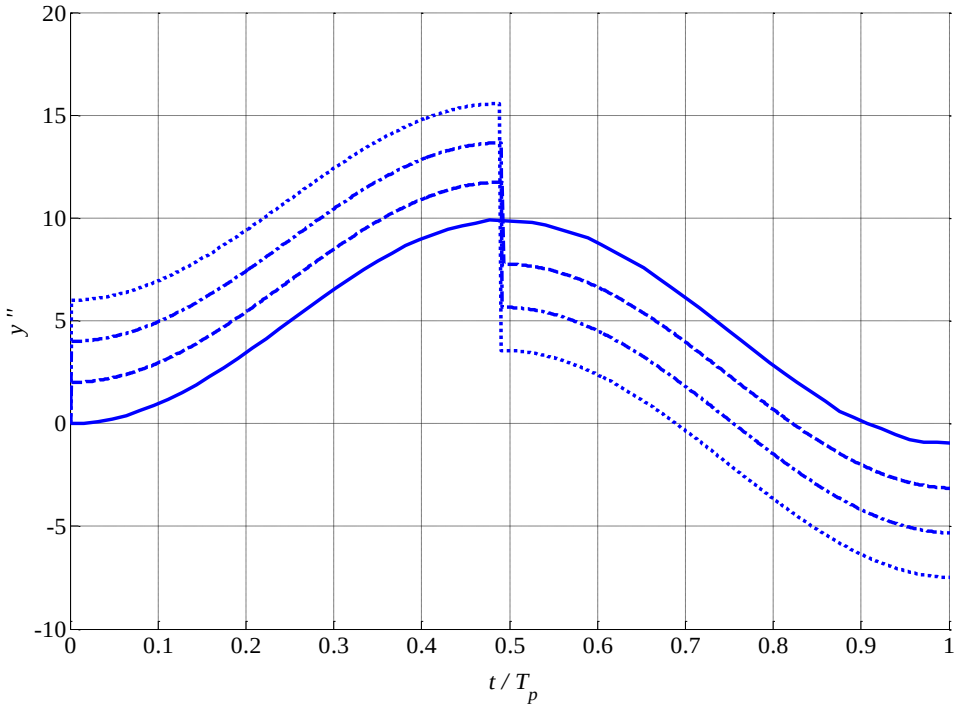

Figure 2.12: Acceleration response of a single degree of freedom system under short duration versed sine base input. Non-dimensional base input magnitude $U_{mag} = 10$ and pulse length $T_p = 0.1T$. Solid line: $\hat{F} = 0$. Dash line: $\hat{F} = 2$. Dash dot line: $\hat{F} = 4$. Dot line: $\hat{F} = 6$.

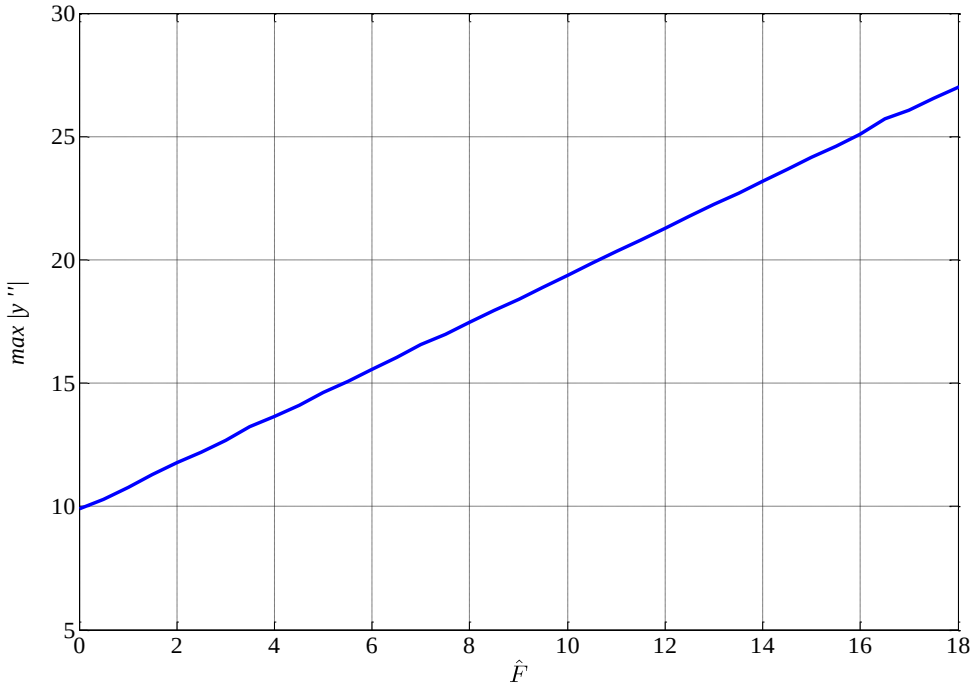

Figure 2.13: Maximum acceleration of a single degree of freedom system under short duration versed sine base input when the friction is varied. Non-dimensional base input magnitude $U_{mag} = 10$ and pulse length $T_p = 0.1T$.

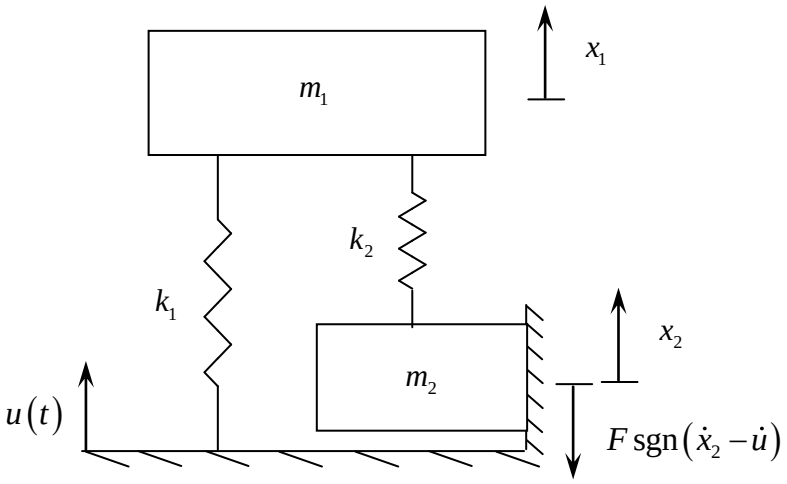

Figure 2.14: A two degree of freedom system configuration with Coulomb friction subjected to a base input.

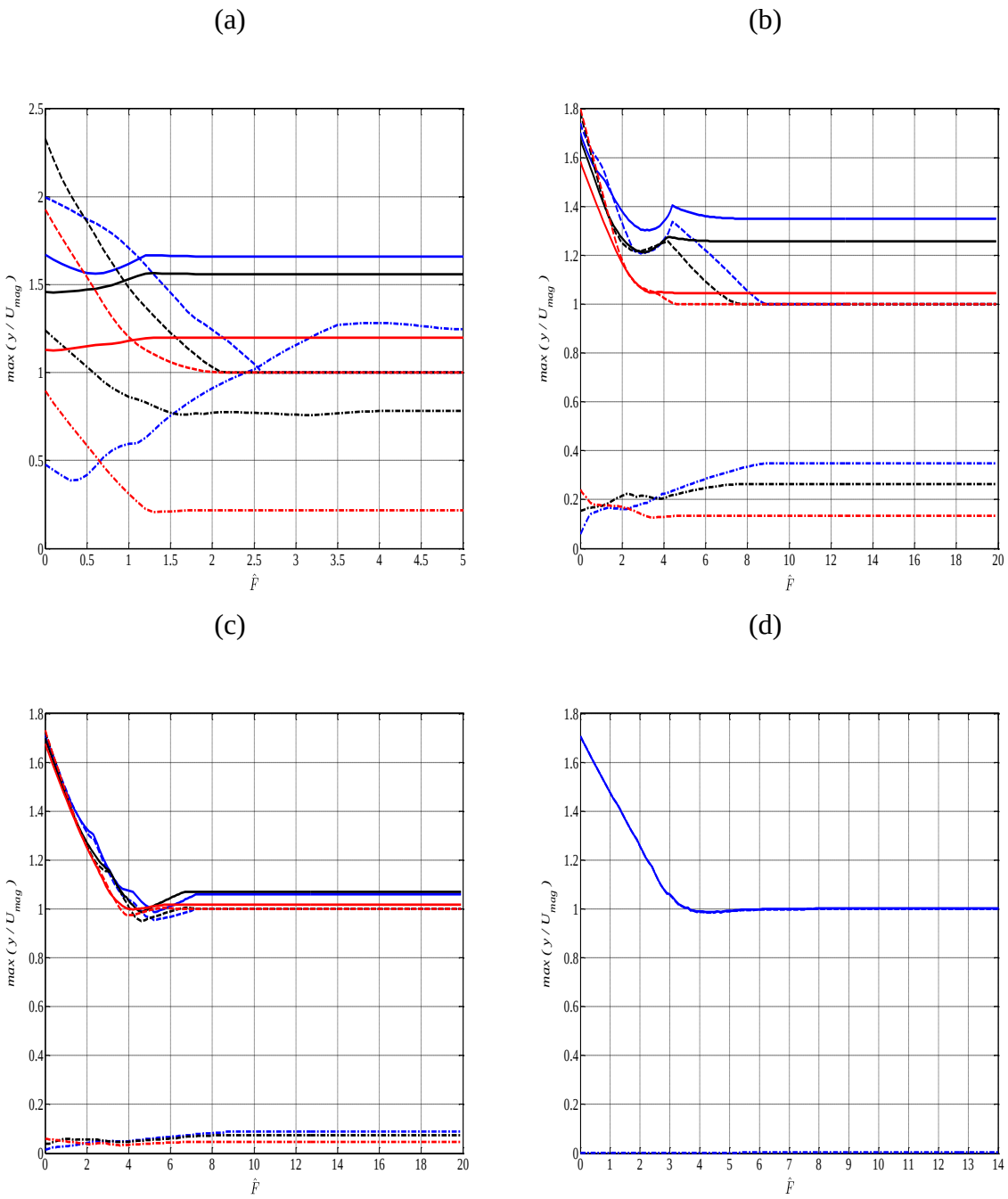

Figure 2.15: The maximum displacement response of masses under a versed sine base input for different levels of friction. Solid line: Primary mass displacement, dash line: Secondary mass displacement,dash dot line Relative displacement, blue line: $\mu = 0.1$, black line: $\mu = 0.32$, red line: $\mu = 1$. Pulse length $T_p = T_1$, non-dimensional base input magnitude $U_{mag} = 10$, stiffness ratio $\hat{k}$. (a) $\hat{k} = 0.4$, (b) $\hat{k} = 2.5$, (c) $\hat{k} = 10$,(d) $\hat{k} = 250$.

Stiffness ratio, $\hat{k}$	$\hat{F}_{opt}$	Normalized displacement response of the primary mass, $\left(max\left(\frac{y_1}{U_{mag}} \right) \right)_{min}$
0.4	0.6	1.56
2.5	3.1	1.3
10	5.3	0.99
250	4.2	0.98

Table 2.2: The value of friction which produces the smallest maximum displacement response of the primary mass as the stiffness ratio is varied and the corresponding displacement response.

Type of response	SDOF	2DOF
Displacement	Reduction in the displacement response for the pulse length equal to the natural period of the system, $T_p = T$. With the parameter used $U_{mag} = 10$, the best response is achieved when $\hat{F}$ is equal to 4. If the system natural frequency and the input magnitude are changed, this value will shift following the relationship $U_{mag} = \frac{\omega_n^2 u_{mag}}{g}$. For example, if the base input magnitude is doubled, the best response is achieved when $\hat{F}$ is equal to 8.	Reduction in the displacement response for the pulse length equal to the natural period of the system $T_p = T_1$. The best reduction is achieved when stiffness ratio $\hat{k}$ is high and the amount of reduction for this case is the same as a SDOF system. If $\hat{k}$ is not sufficiently high, the reduction in displacement response is less than a SDOF system.
Acceleration	Acceleration of the mass experiences instantaneous change when the relative velocity between mass and base input changes sign. Acceleration does not change smoothly.	Acceleration of the primary mass changes smoothly when the relative velocity between the secondary mass and base input changes sign for intermediate and low stiffness ratio $\hat{k}$. If $\hat{k}$ is sufficiently high, the behaviour of this system follows a SDOF system.

Table 2.3: The comparison between the response of a single degree of freedom system and a two degree of freedom.

(a) $\hat{F} = 0$

(b) $\hat{F} = 0.6$

(c) $\hat{F} = 3.5$

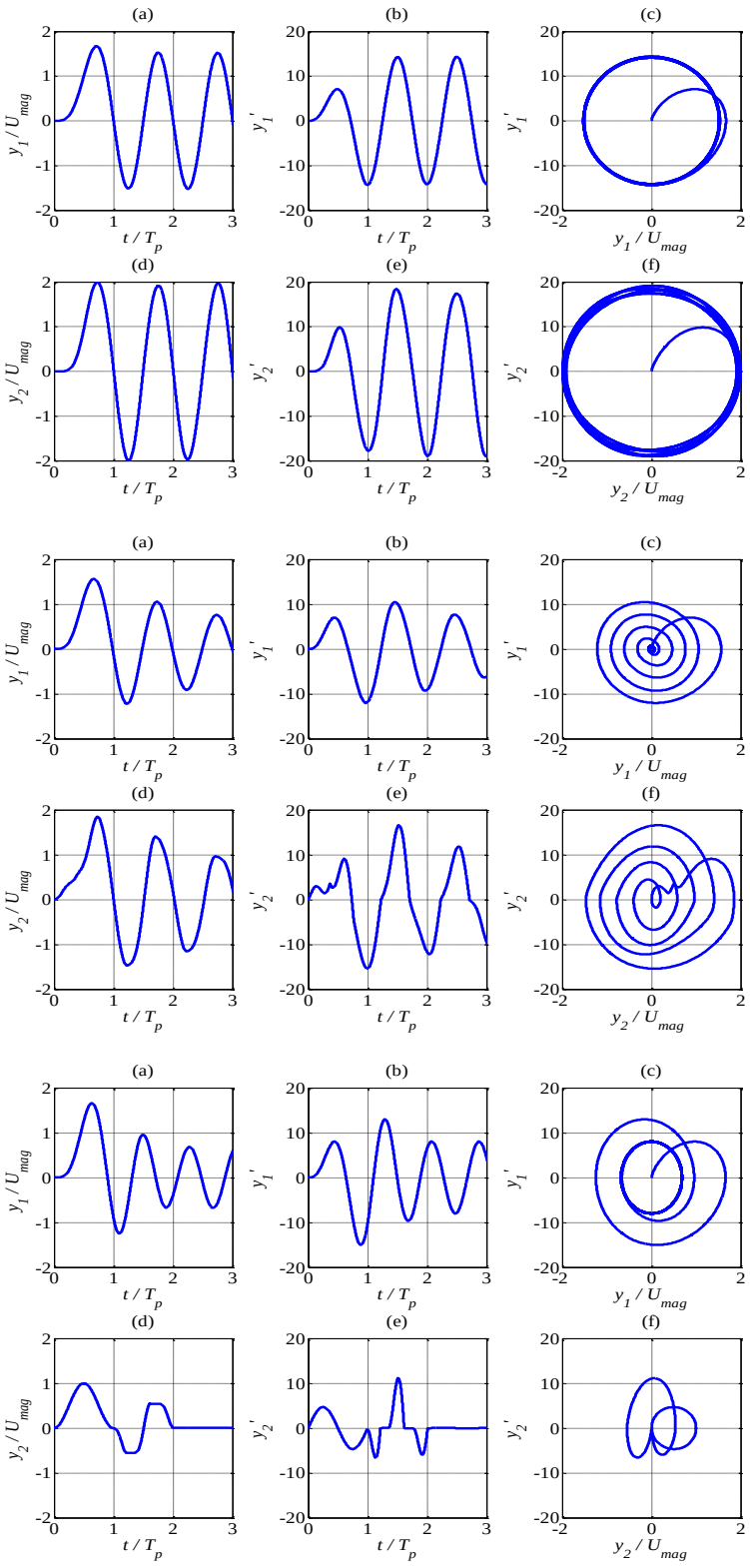

Figure 2.16: Time histories and phase plane plots for the case of a soft secondary spring stiffness compared to the primary spring under a versed sine base input, frequency ratio $\hat{\omega} = 2$, stiffness ratio $\hat{k} = 0.4$. (a) Primary mass displacement. (b) Primary mass velocity. (c) Primary mass phase plane plot. (d) Secondary mass displacement. (e) Secondary mass velocity. (f) Secondary mass phase plane plot.

(a) $\hat{F} = 0$

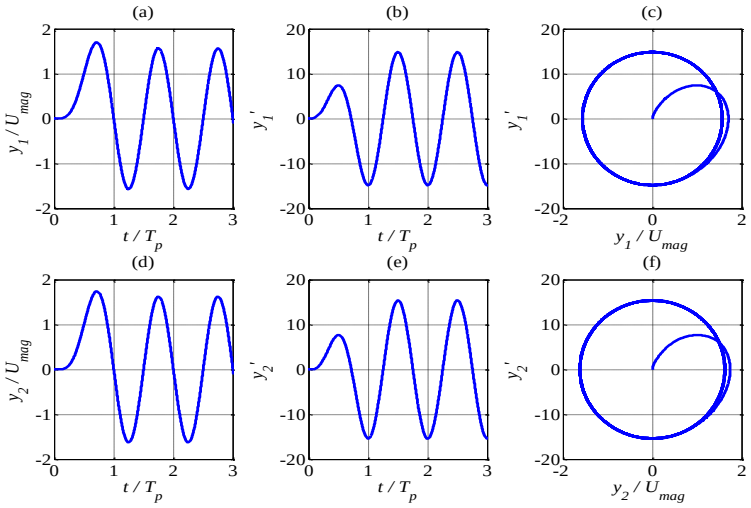

(b) $\hat{F} = 3.1$

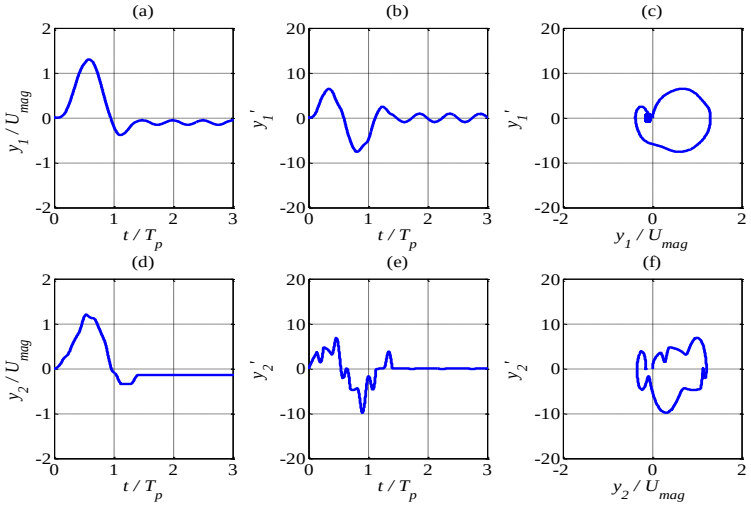

(c) $\hat{F} = 9$

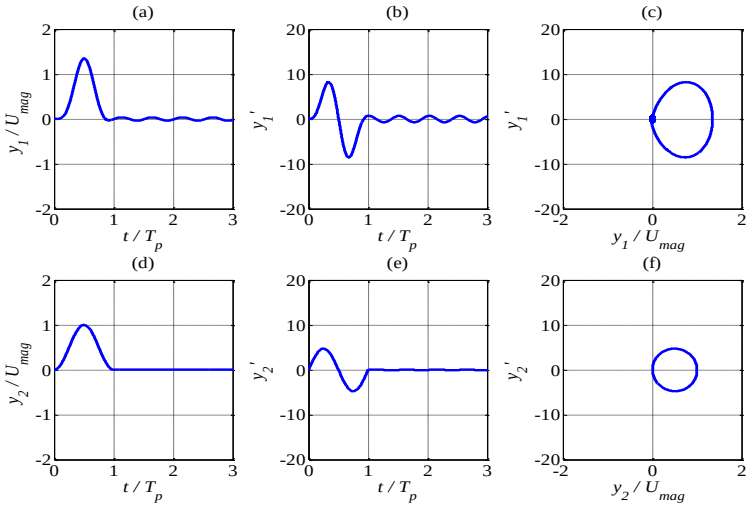

Figure 2.17: Time histories and phase plane plots for the case of a soft secondary spring stiffness compared to the primary spring under a versed sine base input, frequency ratio $\hat{\omega} = 5$, stiffness ratio $\hat{k} = 2.5$. (a) Primary mass displacement. (b) Primary mass velocity. (c) Primary mass phase plane plot. (d) Secondary mass displacement. (e) Secondary mass velocity. (f) Secondary mass phase plane plot.

(a)

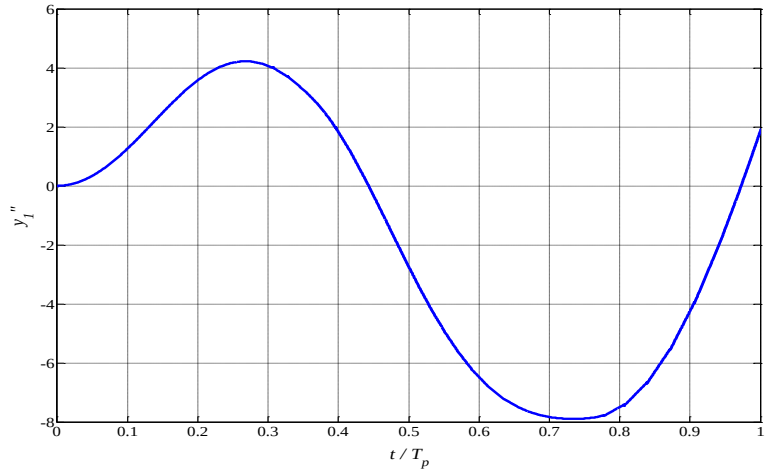

(b)

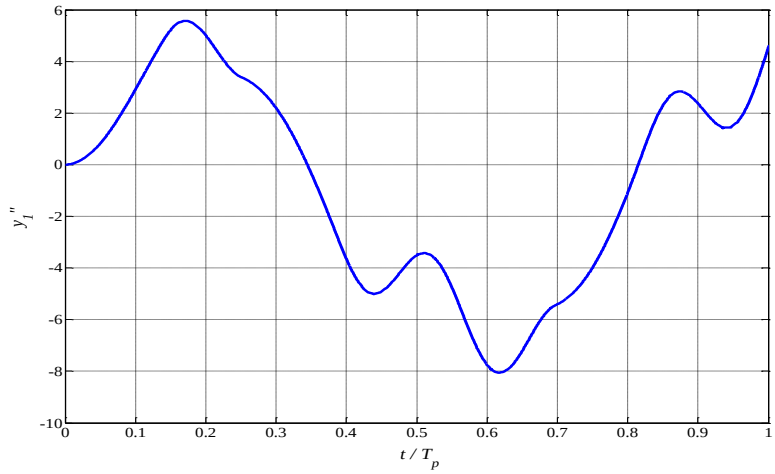

(c)

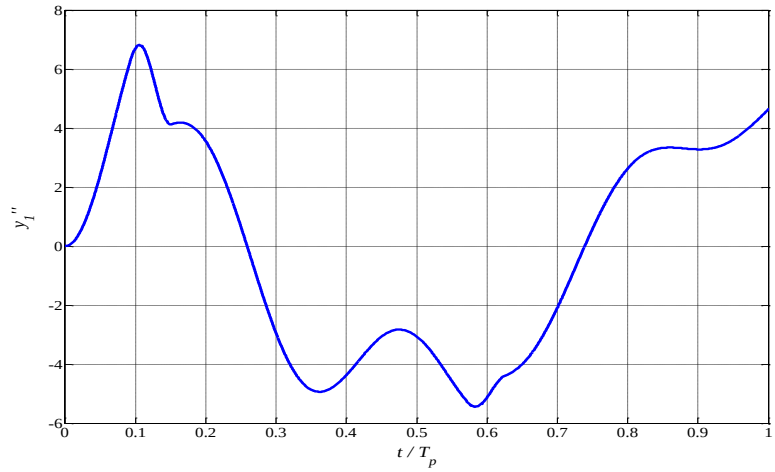

Figure 2.18: Acceleration response of the primary mass of the two degree of freedom model under a versed sine base input when $\hat{F} = \hat{F}_{opt}$. (a) stiffness ratio $\hat{k} = 0.4$, $\hat{F}_{opt} = 0.6$. (b) stiffness ratio $\hat{k} = 2.5$, $\hat{F}_{opt} = 3.1$. (c) stiffness ratio $\hat{k} = 10$, $\hat{F}_{opt} = 5.3$.

(a) $\hat{F} = 0$

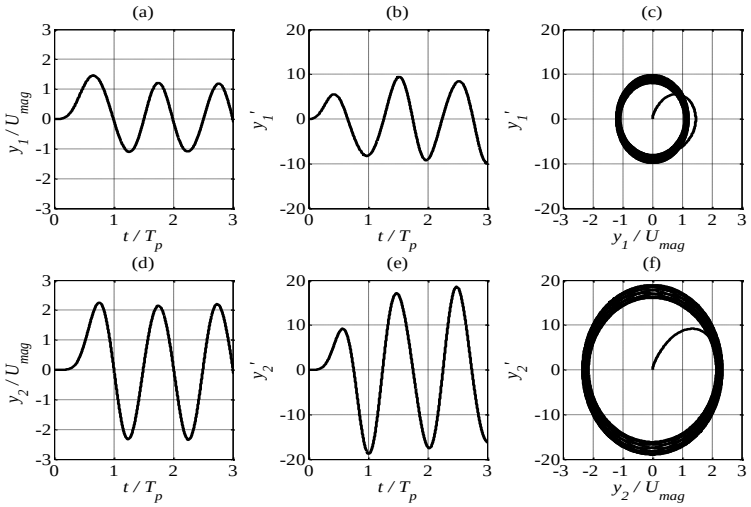

(b) $\hat{F} = 0.1$

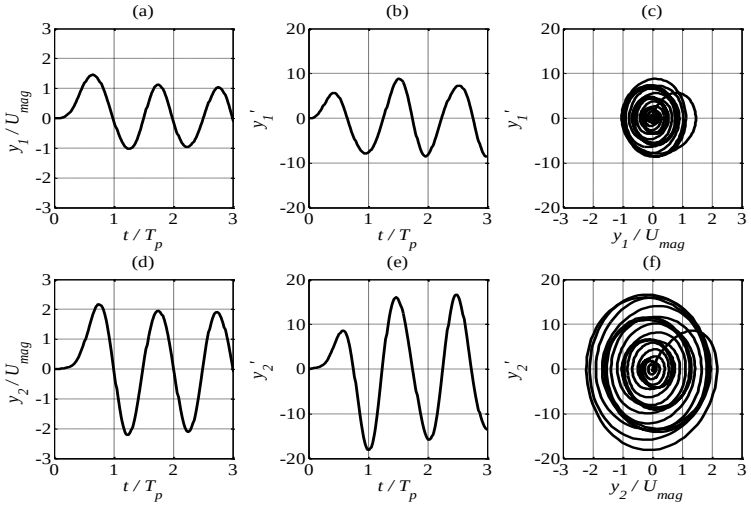

(c) $\hat{F} = 2.3$

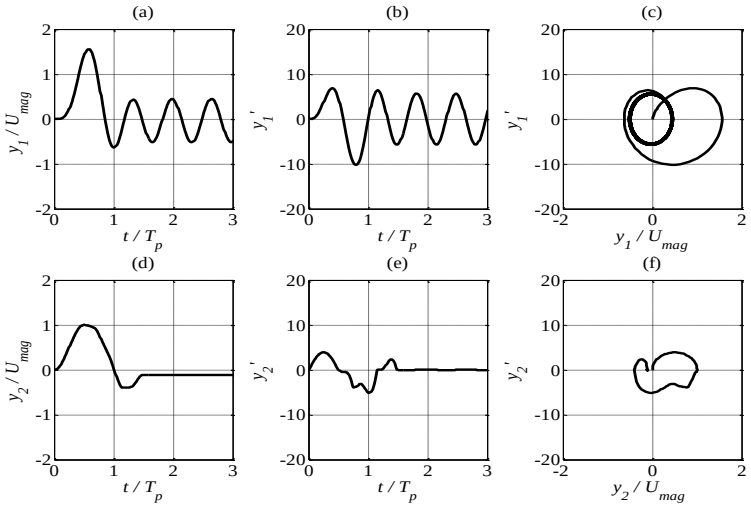

Figure 2.19: Time histories and phase plane plots for the case of a soft secondary spring stiffness compared to the primary spring under a versed sine base input, frequency ratio $\hat{\omega} = 1.12$, stiffness ratio $\hat{k} = 0.4$, mass ratio $\mu = 0.32$. (a) Primary mass displacement. (b) Primary mass velocity. (c) Primary mass phase plane plot. (d) Secondary mass displacement. (e) Secondary mass velocity. (f) Secondary mass phase plane plot.

(a) $\hat{F} = 0$

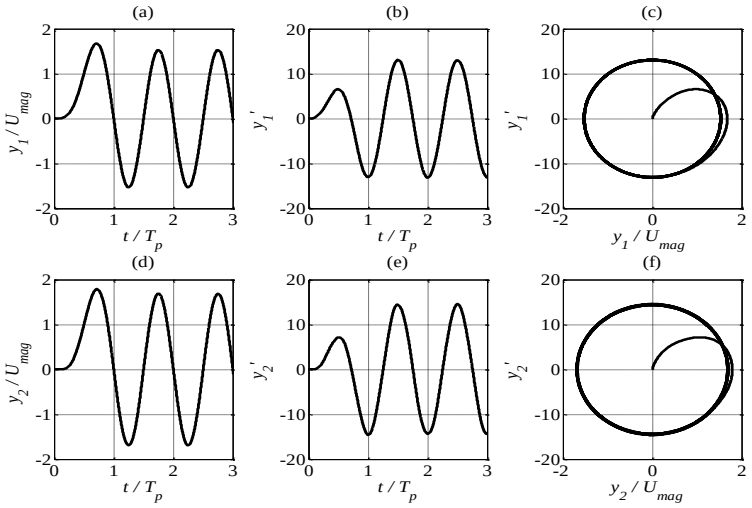

(b) $\hat{F} = 3$

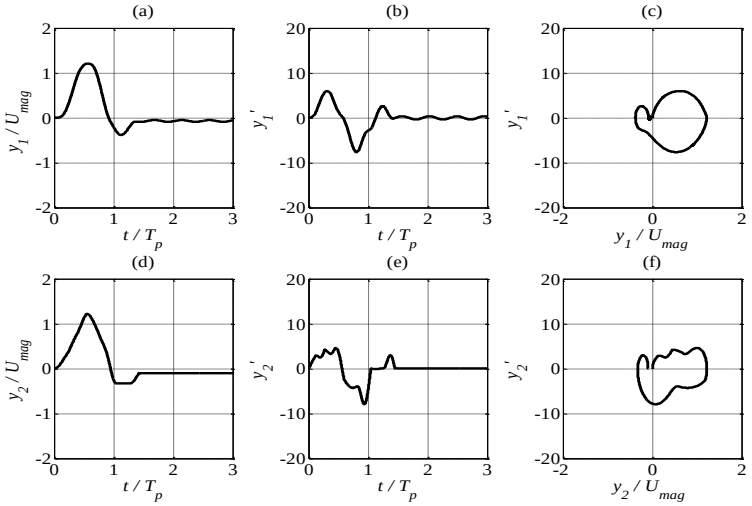

(c) $\hat{F} = 7.7$

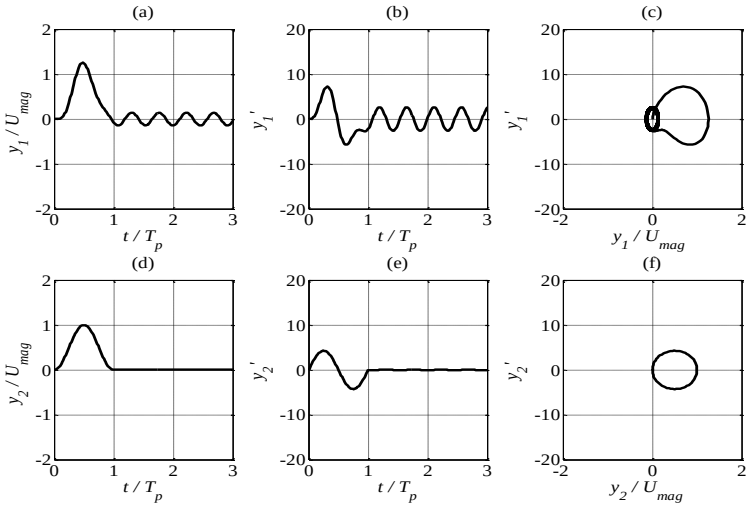

Figure 2.20: Time histories and phase plane plots for the case of a soft secondary spring stiffness compared to the primary spring under a versed sine base input, frequency ratio $\hat{\omega} = 2.8$, stiffness ratio $\hat{k} = 2.5$, mass ratio $\mu = 0.32$. (a) Primary mass displacement. (b) Primary mass velocity. (c) Primary mass phase plane plot. (d) Secondary mass displacement. (e) Secondary mass velocity. (f) Secondary mass phase plane plot.

(a) $\hat{F} = 0$

(b) $\hat{F} = 0.1$

(c) $\hat{F} = 2.1$

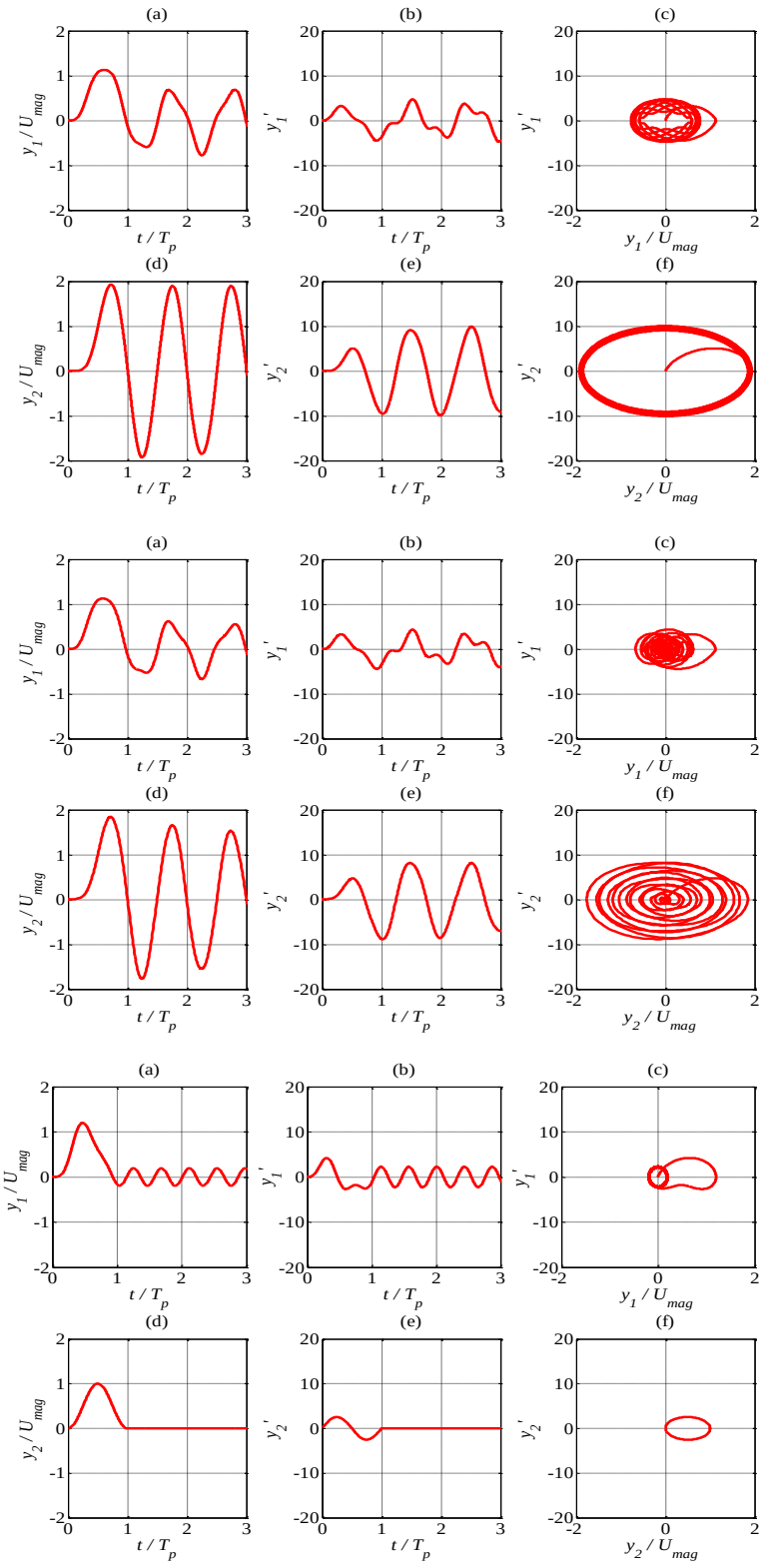

Figure 2.21: Time histories and phase plane plots for the case of a soft secondary spring stiffness compared to the primary spring under a versed sine base input, frequency ratio $\hat{\omega} = 0.63$, stiffness ratio $\hat{k} = 0.4$, mass ratio $\mu = 1$. (a) Primary mass displacement. (b) Primary mass velocity. (c) Primary mass phase plane plot. (d) Secondary mass displacement. (e) Secondary mass velocity. (f) Secondary mass phase plane plot.

(a) $\hat{F} = 0$

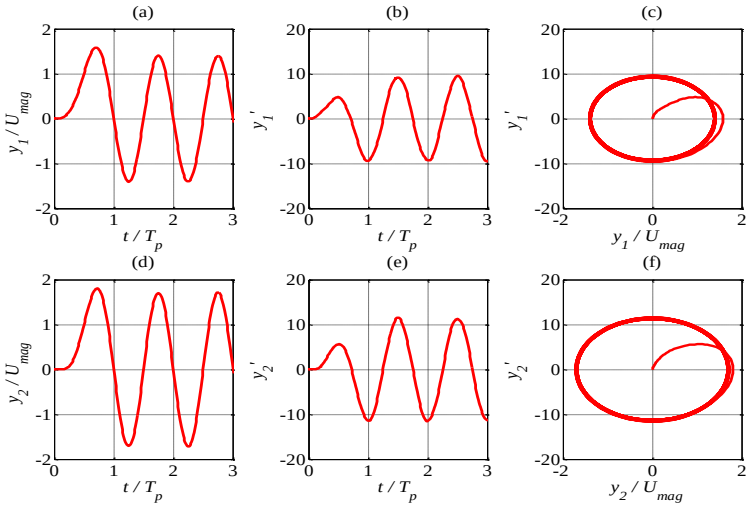

(b) $\hat{F} = 3.3$

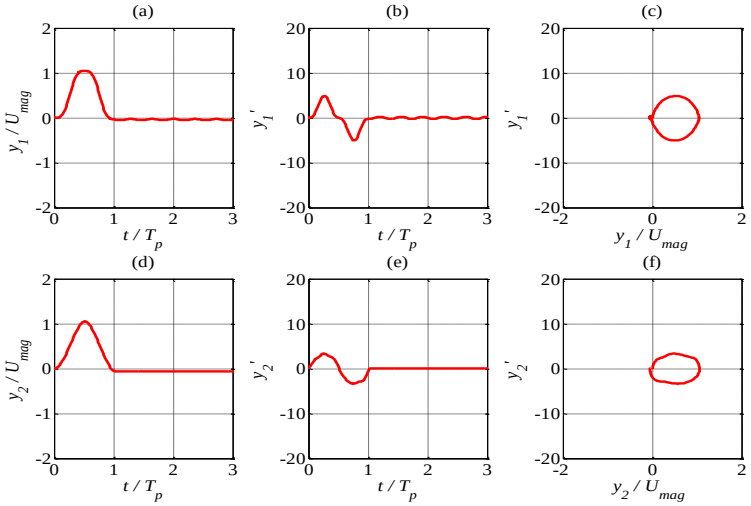

(c) $\hat{F} = 4.8$

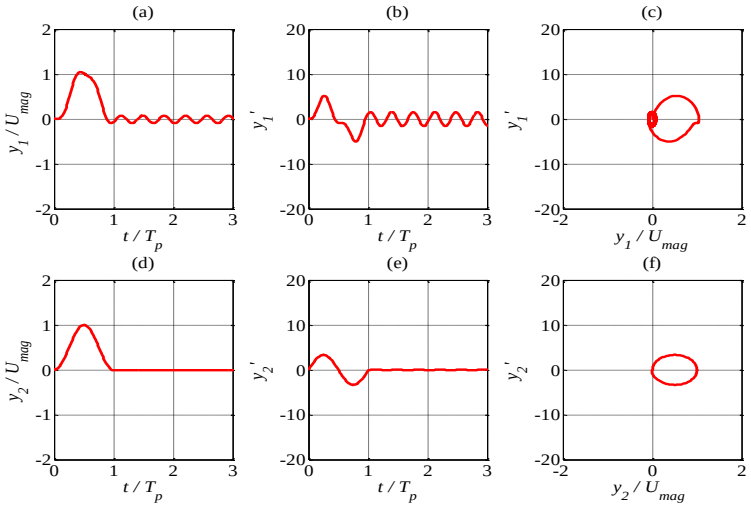

Figure 2.22: Time histories and phase plane plots for the case of a soft secondary spring stiffness compared to the primary spring under a versed sine base input, frequency ratio $\hat{\omega} = 1.58$, stiffness ratio $\hat{k} = 2.5$, mass ratio $\mu = 1$. (a) Primary mass displacement. (b) Primary mass velocity. (c) Primary mass phase plane plot. (d) Secondary mass displacement. (e) Secondary mass velocity. (f) Secondary mass phase plane plot.

3. SHOCK ISOLATION WITH SEMI ACTIVE COULOMB FRICTION

3.1 Introduction

In this chapter, semi active control strategies are introduced for single and two degree of freedom models. It is expected that the control strategies could further improve the response and produce further response reduction for improved isolation. The following control strategies are developed from the idea of reducing the net force acting on the targeted mass. Approximation of Coulomb friction with an error function is still used throughout this chapter.

The response of the system with the control strategy is analysed for the case of the input length equal to the natural period of the system and for a very short input compared to the natural period for a single degree of freedom model. For a two degree of freedom model, the analysis is performed only for the case of the input length equal to the fundamental natural period of the system. Subsequently, the response for both models is compared to the response of the respective passive system.

3.2 A single degree of freedom system with semi active friction

3.2.1 Introduction and control strategy

Figure 3.1 shows there are two forces acting on the mass of a single degree of freedom system which are the stiffness force from the spring and the friction force. These two forces will contribute to the net force which accelerates the mass. It is good to know if these two forces act in opposite directions; then they will partially cancel each other and reduce the acceleration of the mass. However, if the two forces act in the same direction, the condition will be worse because it will increase the magnitude of the acceleration of the mass. The nature of the friction force, which changes its direction depending on the relative sliding velocity, will not ensure in general that these forces will cancel each other.

Therefore, a good control strategy can be to switch on and off the friction dependent upon the condition and direction of the friction force. When the friction acts in the same direction as the spring force and the absolute velocity of the mass it is better to switch off the friction or set the friction to a minimum value because the presence of friction will make the situation worse. However, when the friction acts in the opposite direction to the spring force or the mass velocity, the friction should be turned on because the presence of friction will reduce the acceleration. In some papers, [59, 60] a similar type of control strategy is used. Stammers *et al* [59] used on-off control for a friction system. They used different strategies for forced vibration and free vibration of the system. However, the system is slightly different than the system considered in this thesis because the friction interface in their papers is isolated from the input. Another difference is that the system considered in this thesis has no viscous damping element. Furthermore, they also did not consider the mass velocity as another important parameter to be used for the decision logic of their control strategies. They only consider the direction of the friction compared to the spring force to switch on and off the friction.

The strategy appears to be a good strategy because the direction of the spring force and the friction can always be determined at every instant of time by measuring both the relative displacement and relative velocity. So, the process of switching the friction on and off can be done accurately. However, on-off control causes discontinuity in the acceleration of the mass and subjects it to chatter. Chattering occurs in the region of a switching point [46]. Because of that, some papers construct control strategies to avoid chatter [44, 46, 61]. In order to avoid chatter, in later sections of this study, the friction is not applied directly to

the primary mass. The friction is applied to a small secondary mass which is attached to the primary mass by a secondary stiffness as in the previous chapter. This solution is proposed to improve the discontinuity in the acceleration of the primary mass.

A shock input normally occurs over a very short duration and it is necessary to examine whether a friction system with the outlined control strategy could act fast enough to isolate the shock. The outlined control strategy is described mathematically as follows:

$$\begin{aligned} &\hat{F} = 0 \\ &\text{if } \dot{x} \geq 0,\ x - u < 0 \text{ and } \dot{x} - \dot{u} < 0 \\ &\text{or } \dot{x} < 0 \text{ and } x - u \geq 0 \text{ and } \dot{x} - \dot{u} \geq 0 \end{aligned} \qquad \text{for } 0 \leq t \leq T_p$$

$$\hat{F} = \hat{F}_{on} \text{ for other cases}$$

$\hat{F}_{on}$ is the value of friction when the friction is turned on. It will be varied to see which value will give the best response for a controlled system. The best feature of a controlled friction system is in reality the fact that the friction can be turned off completely, which is not the case for a controlled viscous damper system [44].

3.2.2 The response for the case of a pulse length equal to the natural period of the system

The length of pulse used is $T_p = T$, where T is the natural period. The length of the pulse is chosen to be equal to the natural period of the system because the passive system response will be very large if the length of pulse is equal to or close to the natural period of the system as discussed in Chapter 2. The system where the friction interface moves with the base is considered since it is more practical.

For comparison, it is best to know the value of friction which produces the lowest response for a passive system. This step was executed for comparison with the response of the controlled system and to ensure that the controlled system produces a better result. Therefore, the friction value which yields the minimum displacement response of a simple passive system is chosen to represent the best situation. From the previous chapter, the lowest maximum response is achieved when the non-dimensional friction $\hat{F} = \dfrac{F}{mg}$ is approximately equal to 4. The normalized displacement response with respect to the base input magnitude for this case is about 0.99. The analysis in this chapter also uses the same

system properties and base input magnitude as in the previous chapter to yield non-dimensional base input $U_{mag} = \frac{\omega_n{}^2 u_{mag}}{g} = 10$. Bear in mind that, the amount of friction needed to produce the same behaviour will shift according to the relationship $\frac{\omega_n{}^2 u_{mag}}{g}$ as explained in the previous chapter.

As stated before, the control strategy is a modification to the original concept widely published in the literature by including another parameter to perform the logic. Figure 3.2 shows a comparison between the maximum displacement response of a system with the control strategy suggested, the control strategy widely used in the literature and a passive system. This shows that the proposed strategy is in fact better than the system published in the literature, as seen from an improvement at small friction. However, there is no difference in the response at higher friction because the mass sticks at the friction interface.

It can be seen that the maximum displacement response of a system with the control strategy will only have a smaller displacement response than a passive system for non-dimensional friction larger than 4.3; i.e. $\hat{F} > 4.3$. For lower friction, a passive system has a smaller maximum displacement response than the controlled system. Figures 3.3 and 3.4 show a comparison of the displacement and acceleration response for low friction, a value $\hat{F} = 3$. A control system with the control strategy suggested does not provide improvements for low friction. This happens because the relative velocity of a passive system reaches zero faster than with the control strategy. After the passive system reaches zero relative velocity, an acceleration jump to a negative acceleration occurs which decelerates the mass. Figure 3.5 shows the comparison between the relative displacement and relative velocity for both systems. Figure 3.6 shows how friction switches during the application of the shock on a switchable system. There are three switching points, at about $\frac{t}{T_p} =$ 0.32, 0.68 and 0.8. Friction is switched off from 0 to 0.32 and 0.68 to 0.8 because within these time intervals friction acts in the same direction as both the spring force and the absolute velocity of the mass.

When the friction force is increased, the passive system will fully stick but the control system will have a smaller maximum response. In Figure 3.2, with the parameters chosen, the lowest maximum response of the system with control is achieved when the non-

dimensional friction $\hat{F} \geq 10$ which produced a normalized displacement response, $\frac{y}{U} = 0.55$. Figures 3.7 and 3.8 show the displacement and acceleration response for both systems for non-dimensional friction $\hat{F} = 10$. $\hat{F} = 10$ is a case when the system with control fully sticks to the friction interface after switching on the friction. This is the best that the control system can produce. Figure 3.9 shows the relative displacement and relative velocity of the system with control when $\hat{F} = 10$. Figure 3.10 shows how friction switches as the shock is applied for a switchable system. From Figures 3.9 and 3.10, when the relative velocity reaches zero the friction is turned on, then the relative velocity remains at zero. On the other hand, the relative displacement stays constant until the shock ends. This behaviour shows that the mass sticks completely to the friction interface after switching on the friction.

The lowest maximum response of the control system can be estimated by using two solutions, the solution before relative velocity reaches zero, $t < \breve{t}$, and the solution after the mass sticks. The solution before the relative velocity reaches zero can be computed from the complete solution of an undamped single degree of freedom system from reference [2]. By substituting $t = \breve{t}$, the displacement at the time when the relative velocity reaches zero $\breve{x}$ can be calculated using

$$\breve{x} = \left(\frac{\left(\frac{u_{mag}}{2} \right)}{1 - \left(\frac{T_p^2}{T^2} \right)} \right) \left(1 - \left(\frac{T_p^2}{T^2} \right) + \left(\frac{T_p^2}{T^2} \right) \cos\left(\frac{2\pi \breve{t}}{T_p} \right) - \cos \omega_n \breve{t} \right) \tag{3.1}$$

The input displacement at time $t = \breve{t}$ can also be calculated using

$$\breve{u} = \frac{u_{mag}}{2} \left(1 - \cos\left(\frac{2\pi \breve{t}}{T_p} \right) \right) \tag{3.2}$$

Then, these two values can be easily used to calculate the maximum displacement response of the system as shown by $x_{min} = \breve{x} + \left(\hat{u} - \breve{u} \right)$, because the mass fully sticks to the friction interface and follows the base input. In this case, the lowest value of the normalized maximum response $\frac{x_{min}}{u_{mag}}$ is estimated to be equal to 0.55 which is equal to the value from the plot.

3.2.3 The response for the case of a short duration input compared to the natural period of the system

For a base input of duration equal or close to the natural period of the single degree of freedom system, both the maximum displacement and acceleration are important measures of the severity of the shock. However, the situation is different when the duration of the base input is short compared to the natural period. In this case, typically only the maximum acceleration is important. As explained in chapter 2, there is a significant increase in the maximum acceleration of a single degree of freedom system as friction increases. On the other hand, there is no significant increase in the maximum displacement. Therefore, in this section the analysis will only focus on the maximum acceleration of the system.

Figure 3.11 shows the maximum acceleration as friction is varied. There are two curves, the solid line represents a passive system and the dash line represents a controlled system. As shown in the plot, the maximum acceleration for a controlled system is better than a passive system for all values of friction. From the figure, the maximum acceleration of a controlled system stays constant until the non-dimensional friction $\hat{F}$ is approximately equal to 10. Then, the maximum acceleration increases linearly with friction at the same rate as a passive system. In order to investigate the behaviour of the system for non-dimensional friction $\hat{F}$ less than 10 and greater than 10, two values were chosen which are $\hat{F} = 5$ and $\hat{F} = 15$. The time responses of the system for these cases were plotted in Figures 3.12 to 3.19.

Figure 3.12 to 3.14 show the comparison between the time response of a passive system and a controlled system for non-dimensional friction $\hat{F} = 5$. As stated previously, the acceleration of a passive system has an instantaneous change at the start of the motion equal to the amount of friction applied to the system. Then, when the acceleration reaches its maximum and the relative velocity reaches zero at around $t = 0.5T_p$, friction changes its direction which causes another instantaneous change, see Figure 3.12. However, for a controlled system, the friction is off until around $t = 0.5T_p$. If friction is turned on before this point, the system will behave like a passive system with high response during the first half of the shock. For this case, after friction is turned on, it always acts in the opposite direction to either the spring force or the direction of motion. Therefore, there is no need to

turn off the friction again until the shock ends. Figure 3.15 shows the friction force applied to the system as the motion progresses.

For the acceleration and velocity response of the system, it can be seen that the acceleration of the passive system during the first half of the shock is higher than for a controlled system. The high level of acceleration increases the velocity of the passive system mass by a larger amount than for the controlled system during the first half of the shock, see Figure 3.13. By using the control strategy, the maximum acceleration of the system occurs at the point of switching on the friction at about $t = 0.5T_p$. A second peak in the acceleration occurs at the end of the shock period which is always smaller than the first acceleration peak which occurs at half the shock period for the case of $\hat{F}$ less than 10. Therefore, any friction value less than 10 does not change the maximum acceleration response, because the maximum acceleration response occurs before friction is turned on. This is the reason why for $\hat{F}$ less than 10, the maximum acceleration response from Figure 3.11 is constant.

The next case to investigate is the behaviour of the system when $\hat{F}$ is greater than 10, $\hat{F} = 15$ was used as an example. Figures 3.16 to 3.18 show the comparison between the time response of a passive system and a controlled system for this case. It is interesting to observe that when $\hat{F}$ is greater than 10, the second acceleration peak becomes larger than the first acceleration peak. The second acceleration peak increases as friction increases. This is because the instantaneous change at the point of switching on the friction is equal to the amount of friction applied to the mass. Therefore, when $\hat{F}$ is greater than 10, the second acceleration peak will become the maximum acceleration of the system instead of the first acceleration peak and it increases linearly with increases in friction. Figure 3.19 shows the friction force applied to the system as the motion progresses. As in the previous case, the friction is turned on at around $t = 0.5T_p$. The only slight difference is at nearly the end of the shock, the friction is turned off and then turned on again slightly after that. This is because a change in the direction of the relative displacement and the relative velocity takes place during that time.

Figure 3.18 compares the relative displacement and relative velocity for a passive and a controlled system for $\hat{F} = 15$. The relative velocity of the passive system reaches zero faster than the controlled system. This is the reason why the acceleration of the passive system

jumps to a negative acceleration before the controlled system. As friction is further increased for the passive system it will completely stick to the friction interface from the beginning of the shock.

3.3 A two degree of freedom system with semi active friction

3.3.1 Introduction and control strategy

Initially, a control strategy has been introduced to improve the response of a single degree of freedom system. However, from the acceleration response of a single degree of freedom system with friction there are some transition points as motion progresses where the acceleration response of the primary mass changes instantaneously. For a passive system, the instantaneous change occurs at the start of the motion and every time friction changes its direction. On the other hand, a controlled system experiences the instantaneous change at the point of switching on and off the friction. As stated before, this is because friction is applied directly to the primary mass. It is expected that by applying the friction to a secondary mass, which is attached to the primary mass by a secondary spring, it could provide a smooth change at the transition points. From Chapter 2, it was found that the maximum displacement response of a passive two degree of freedom system is always equal to or larger than the magnitude of the base input dependent upon the choice of the secondary stiffness and stiffness ratio. It is beneficial to investigate whether the control strategy implemented on a single degree of freedom system could be modified to work on a two degree of freedom system as well to improve its response. To the author's knowledge no such strategy has been introduced before to improve the response of this kind of system.

The idea to generate a suitable and good control strategy for a two degree of freedom system still comes from the concept to reduce the net force acting on the primary targeted mass by switching on and off the friction. Therefore, the initial step in getting the right parameters to perform the control decision logic is to draw the free body diagram of a two degree of freedom system with friction applied to the secondary mass and determine which forces act on the system. The free body diagram is shown in Figure 3.20. From the free body diagram, there are two forces which act on the primary mass. These are the force from the primary spring and the force from the secondary spring. On the other hand, the friction does have some influence on the force in the secondary spring because both forces act on the secondary mass. It is expected that friction could be controlled to cause the force

across the secondary spring to act to oppose the force across the primary spring which subsequently minimizes the net force acting on the primary isolated mass.

A basic investigation has been made to observe the expected force direction in the two springs and friction as the motion progresses. This step has been done in order to see whether switching on and off friction could be used. Subsequently, the parameters to perform the decision logic for control are determined. The investigation starts by observing what happens to the force direction in the two springs and the friction as the motion starts. When a versed sine base input is applied to the system, the primary spring is initially compressed. Both masses move in the positive direction. Therefore, the secondary spring should be stretched to minimize the net force acting on the primary mass. This is only possible when there is no friction during this interval of time. The presence of friction during this state will only cause the compression of the secondary spring and an increase in the acceleration of the primary mass. The friction force depends on the sign of relative velocity between the secondary mass velocity and the base input velocity. During the initial stage of shock, the secondary mass velocity unless the friction interface is locked, is smaller than the base input velocity. Therefore if friction is present it will compress the secondary spring.

Then, after some time, the relative velocity starts to turn positive. When the relative velocity turns positive, the friction will stretch the secondary spring if it is present in the system. Because the primary spring is still in compression and the primary mass still moves in the positive direction, the presence of friction during this phase of the motion could help to reduce the net force acting on the primary mass. Therefore, the friction should be turned on. As the motion progresses, it is expected that by turning on and off friction depending on the primary spring force, the direction of friction and the primary mass velocity then one could improve the response of a two degree of freedom system. Therefore, the parameters which are needed to perform the decision logic for control are the sign of the relative displacement across the primary spring, the sign of relative velocity between the secondary mass and the base input and the primary mass velocity. The sign of the relative displacement across the primary spring defines the direction of primary spring force and the sign of relative velocity between the secondary mass and the base input defines the direction of friction. The friction is turned on only when both quantities have the opposite sign or when friction acts to oppose the direction of motion. The sign of the relative displacement across the secondary spring is not considered since the outlined control strategy appears to be sufficient to cause the force across the secondary spring

(relative displacement across the secondary spring) to act to oppose the force across the primary spring (relative displacement across the primary spring) for most of the time. This situation will minimize the net force acting on the primary isolated mass.

The control strategy for a two degree of freedom with friction applied directly to the secondary mass is as follows

$$\hat{F} = 0$$
$$\text{if } \dot{x}_1 \geq 0,\ x_1 - u < 0 \text{ and } \dot{x}_2 - \dot{u} < 0$$
$$\text{or } \dot{x}_1 < 0,\ x_1 - u \geq 0 \text{ and } \dot{x}_2 - \dot{u} \geq 0 \qquad \text{for } 0 \leq t \leq T_p$$

$$\hat{F} = \hat{F}_{on} \text{ for other cases}$$

$\hat{F}_{on}$ is the value of friction when the friction is turned on.

3.3.2 Effect of varying the stiffness ratio to the maximum displacement of the primary mass

For this section, only the case where the pulse length is equal to the fundamental period of the system is considered. Previously, extreme cases for a secondary spring stiffness with either the stiffness too soft or too stiff did not produce good overall response for the primary mass. If it is too soft, a smooth acceleration response at the switching points can be produced. However, its displacement response is not as good as a single degree of freedom system. On the other hand, if it is too stiff, it will behave like a single degree of freedom system. From section 3.2.2, a single degree of freedom system with the control strategy suggested obtains the smallest displacement response when non dimensional friction $\hat{F} \geq 10$. However, at the same time it experiences instantaneous acceleration changes at friction switching points.

Instead of having either of these two extremes which do not produce an overall good response, it is expected that if an intermediate stiffness ratio is chosen the smallest displacement response such as for a single degree of freedom system could be achieved and at the same time a smooth acceleration response could be produced. Here, the objective is to see how large a stiffness ratio is needed to obtain the displacement response for the primary mass such that it as small as for a single degree of freedom system when $\hat{F}$ is at least equal to 10. The first step is to plot the maximum response of the primary mass of a two degree of freedom system with the suggested control strategy when the

stiffness ratio $\hat{k}$ is varied for four different friction values, namely $\hat{F} = 2.5$, $\hat{F} = 5, \hat{F} = 7.5$ and $\hat{F} = 10$. By conducting this investigation, a system that has both good displacement and acceleration responses could be identified.

Figure 3.21 shows the maximum response of the primary mass of a two degree of freedom system under a versed sine base input with the suggested control strategy when the stiffness ratio $\hat{k}$ is varied. From the plot, the maximum displacement response of the primary mass decreases as the stiffness ratio increases until the point where the stiffness ratio is high enough. After this point, further increment in the value of $\hat{k}$ does not change the maximum displacement response of the primary mass. Therefore, there is no point to set the value of $\hat{k}$ to be very large in order to obtain the smallest maximum displacement response since it could be achieved by setting $\hat{k}$ at an intermediate value. Another advantage of setting $\hat{k}$ to an intermediate value is to produce a smooth acceleration response at switching points.

From the plot, as friction increases from $\hat{F} = 2.5$ to $\hat{F} = 10$, the maximum displacement response of the primary mass decreases except for the case when the stiffness ratio is very small, $\hat{k} < 0.6$. When the stiffness ratio is very small, there is no obvious difference in the maximum displacement response of the primary mass as friction increases because friction does not have a significant effect on the response of the primary mass. Friction does not have a significant effect in this case since it is applied to the secondary mass and the secondary spring stiffness is quite soft. However, if the stiffness ratio is set to a larger value, the friction begins to affect the response of the primary mass. From the plot, the case of $\hat{F} = 5, \hat{F} = 7.5$ and $\hat{F} = 10$ produce a maximum normalized displacement response smaller than unity when the stiffness ratio is sufficiently large. When $\hat{F} = 5$, the maximum normalized displacement response is smaller than unity when $\hat{k}$ is larger than 7.7. On the other hand, for the case of $\hat{F} = 7.5$ and $\hat{F} = 10$, the maximum normalized displacement response is smaller than unity when $\hat{k}$ is larger than 2.2. For the case of $\hat{F} = 10$, the value of $\hat{k} > 37.2$ is required to produce a normalized response smaller than 0.6 which is close to the smallest response produced by a single degree of freedom system which is 0.55.

For a better understanding of these cases, the time response of the primary mass is plotted for three cases, $\hat{k} = 2$, the case of a small stiffness ratio, $\hat{k} = 10$, the case of an

intermediate stiffness ratio and $\hat{k} = 80$, the case of a large stiffness ratio. The response for the three cases are plotted in Figures 3.22 to 3.30. Figures 3.22 to 3.24, 3.25 to 3.27 and 3.28 to 3.30 are the response time histories for $\hat{k} = 2$, 10 and 80 respectively. The discussion of the findings is given in the following sections.

3.3.3 The case of a soft secondary spring (small stiffness ratio)

From Figure 3.22, the reduction in the maximum displacement of the system is not much compared to the case of passive friction for a small friction value, $\hat{F} = 2.5$. When friction is increased, more reduction is achieved, for example when $\hat{F} = 10$, the normalized maximum displacement is about equal to unity. See Table 3.1 (a) for a comparison between the maximum displacement of the primary mass for the case of a small stiffness ratio $\hat{k} = 2$. When $\hat{F} = 2.5$, the maximum displacement of the primary mass with the control strategy is only 2.22 percent smaller than the respective passive system. However, when $\hat{F}$ is increased to 5, 7.5 and 10; the maximum displacement of the primary mass with the control strategy shows more reduction compared to the respective passive system. When $\hat{F} = 10$ the system with the control strategy has the maximum displacement which is 28.17 percent smaller than the respective passive system.

Because the secondary spring is quite soft in this case, the reduction is expected to be smaller than the case when the secondary spring is much stiffer than the primary spring. For the next case, it is expected by increasing the stiffness of the secondary spring, more reduction could be achieved in terms of the displacement response so that the normalized maximum displacement is much smaller than unity. The displacement reduction of 28.2 percent compared to the respective passive system confirms the expectation that the control strategy can improve the response of a passive system quite significantly. On the other hand, in terms of velocity and acceleration, its response is smooth without discontinuities unlike the case of a single degree of freedom system. However, after switching on the friction for the first time, the primary mass starts to oscillate at a higher frequency. From the velocity and acceleration plots in Figure 3.23, it looks like the system oscillates at about 3 times the original frequency which is essentially the natural frequency of the primary mass on both the primary and secondary springs acting in parallel.

In terms of the relative response from Figure 3.24, the second mass will stick after the relative velocity reaches zero right after the friction is turned on for the first time. Then, the system starts to experience a stick-slip motion. The system with a higher friction value sticks for longer than the other systems as the shock is applied. After the friction is turned on for the first time, the system with a higher friction value also sticks for longer than the other systems. For example, for the case of $\hat{F} = 2.5$, the system starts to slip when the normalized time $\frac{t}{T_p}$ is about 0.4. However, for higher friction values the system starts to slip again when the normalized time is 0.45, 0.5 and 0.55 for the case of $\hat{F} = 5$, $\hat{F} = 7.5$ and $\hat{F} = 10$ respectively.

3.3.4 The case of an intermediate secondary spring (intermediate stiffness ratio)

From Figure 3.25, it can be seen that for small friction, for example $\hat{F} = 2.5$, the displacement of the system with control is larger than the respective passive system. It is understood from earlier in this chapter for the case of a single degree of freedom system, that for small friction values the displacement response of the system with the control strategy is larger than the respective passive system. This is also the case for a two degree of freedom system, where the displacement of the system with the control strategy is 2.38 percent larger compared to the respective passive system, see Table 3.1 (b).

As friction increases, the displacement response of the primary mass with control starts to become better than the respective passive system. When $\hat{F} = 10$, the displacement of the primary mass with the control strategy is 32.1 percent smaller than the respective passive system. By using an intermediate $\hat{k}$, in this case $\hat{k} = 10$, it is possible to achieve isolation where $\frac{y_1}{U} < 1$ and at the same time have a smooth transition at the point of switching on the friction. From Figure 3.25(a) and Table 3.1 (b), the maximum displacement of the primary mass is less than the magnitude of the base input for the case of high friction values, for example, $\hat{F} = 5$, $\hat{F} = 7.5$ and $\hat{F} = 10$.

Figure 3.26 shows the velocity and acceleration response of the primary mass with control. As for the case of a soft secondary spring, after switching on the friction for the first time the primary mass starts to oscillate at a higher frequency. From comparison of Figure 3.23

to Figure 3.26, the primary mass oscillates at a higher frequency in the case of an intermediate secondary spring than for the case of a soft secondary spring. As before, the primary mass oscillates on both the primary and the secondary combined stiffness which is much stiffer than in the previous case.

As in the case of a soft secondary spring, the second mass will stick after the relative velocity reaches zero right after the friction is turned on for the first time, see Figure 3.27. However, as $\hat{k}$ increases, the time taken for the secondary mass to stick after the friction is switched on for the first time becomes less. Then, as usual the system experiences stick-slip motion. The system with a small friction value slides more than the other system rather than sticking to the friction interface.

3.3.5 The case of a stiff secondary spring (large stiffness ratio)

If one refers back to Figure 3.21, increasing the value of $\hat{k}$ above $\hat{k} = 80$ does not change the maximum displacement of the primary mass of a two degree of freedom system for the four friction values used, namely $\hat{F} = 2.5$, $\hat{F} = 5$, $\hat{F} = 7.5$ and $\hat{F} = 10$. Therefore, increasing the value of $\hat{k}$ does not bring any benefit in term of reducing the displacement response of the primary mass. Here, the objective is to investigate what happens to the time response of the system when $\hat{k} = 80$, at the point where no further reduction could be made if the stiffness ratio is increased.

Figure 3.28 shows the displacement of the primary mass under a versed sine base input with control and the comparison with the respective passive system. From the figure, it can be seen that the displacement of the primary mass with control is larger than the respective passive system for a small friction value, e.g. $\hat{F} = 2.5$. From inspection of Table 3.1(c), the maximum displacement of the primary mass is 9.4 percent larger than the respective passive system. This is the same as the case of an intermediate stiffness ratio and the case of a single degree of freedom system with the control strategy suggested. However, as friction increases the system with the control strategy is much better than the respective passive system. By increasing the non-dimensional friction the displacement of the primary mass with control becomes much smaller than the respective system with up to 43% reduction for $\hat{F} = 10$. For higher friction values, the maximum normalized displacement

$\frac{y_1}{U}$ is smaller than unity. This is comparable to the smallest maximum response achieved by a single degree of freedom system, e.g. for $\hat{F} = 10$ and $\frac{y_1}{U} = 0.57$.

Figure 3.29 shows the velocity and acceleration response of the primary mass with control. As in the two previous cases, after switching on the friction for the first time, the primary mass starts to oscillate at a higher frequency. In comparison to the acceleration and velocity plots of the previous two cases, the primary mass oscillates at a higher frequency in the case of a large secondary spring than in the previous cases.

Finally, Figure 3.30 shows the relative response of the system. In this case, the system still experiences stick slip motion. When friction is large, for example $\hat{F} = 10$, the secondary mass sticks to the friction interface for most of the time after the friction is turned on until the shock ends. On the other hand when friction is small, for example $\hat{F} = 2.5$, the secondary mass slides for most of the time after the friction is turned on until the shock ends. In this case, the behaviour of the system is close to a single degree of freedom system but with a little improvement to the velocity and acceleration response in terms of discontinuities at the point of switching on the friction. The smallest displacement response is comparable to the case of a single degree of freedom system.

3.4 Conclusions

In this chapter, control strategies have been introduced for single and two degree of freedom systems with Coulomb friction. The control strategies are implemented by switching on and off the friction according to the direction of the spring force, friction and mass velocity. The objective is to further improve the response in comparison to the respective passive system for base shock input. The response is evaluated for two types of pulse lengths namely a pulse length equal to the natural period of the system and a short pulse compared to the natural period of the system.

For the case of a single degree of freedom system and a pulse length equal to the natural period, the displacement response is smaller than the respective passive system only when friction is significantly large. If not, the displacement response will be larger than for the respective passive system. With control, the smallest maximum displacement achieved is reduced by about 44% compared to the smallest maximum displacement achieved for a passive system. For the case of a short pulse compared to the natural period, the acceleration response is always smaller than for the respective passive system. Therefore, the control strategy can be used to improve the acceleration response of a passive system for any value of friction.

A control strategy has also been introduced for a two degree of freedom system configuration to further improve the response relative to the respective passive and single degree of freedom systems. In this case, the control strategy is implemented by switching on and off the friction according to the direction of the primary spring force, friction and secondary mass velocity. Generally, as in the case of a single degree of freedom system, the displacement response is smaller than the respective passive system only when friction is high. For an intermediate stiffness ratio, for example $\hat{k} = 10$, it is enough to provide a maximum displacement smaller than the magnitude of the base input and at the same time provide a smooth acceleration response especially at the point of switching on-off the friction.

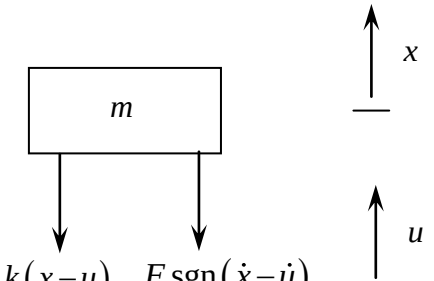

Figure 3.1: Free body diagram of a single degree of freedom system with friction, $u =$ base input displacement, $F =$ sliding friction force.

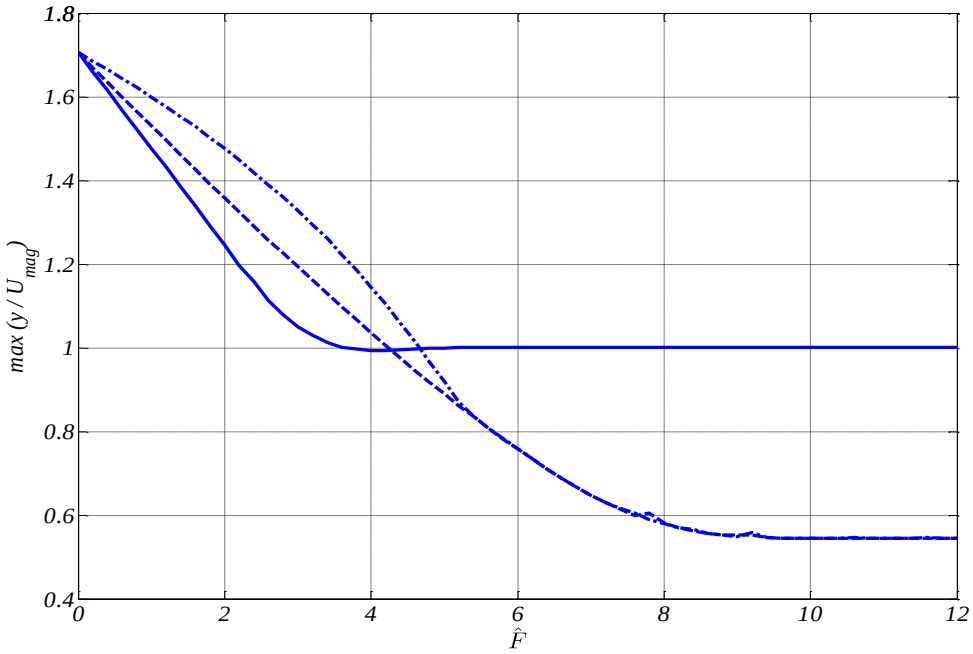

Figure 3.2: Comparison between the maximum response of a passive single degree of freedom system and a system with control under a versed sine base input when the friction is varied. Solid line: passive system. Dash line: controlled system introduced in this thesis. Dash dot line: controlled system widely published in the literatures. Non-dimensional base input magnitude $U_{mag} = 10$, pulse length $T_p = T$ and non-dimensional friction $\hat{F} = \dfrac{F}{mg}$.

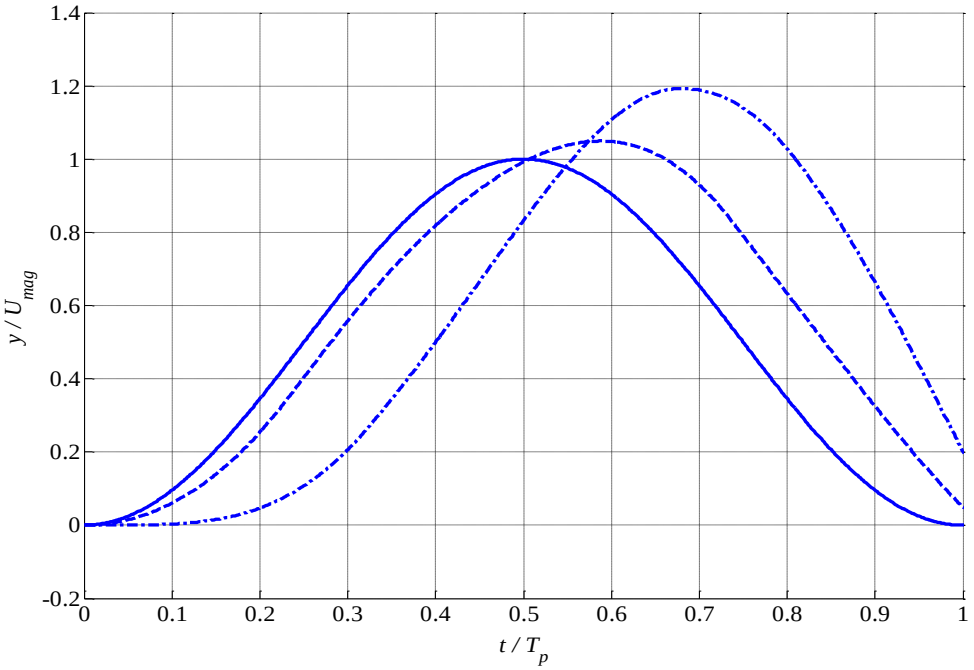

Figure 3.3: Comparison between the displacement response of a passive single degree of freedom system and a system with control. Solid line: base input, Dash line: passive system, Dash dot line: controlled system. Non-dimensional base input magnitude $U_{mag} = 10$, pulse length $T_p = T$, non-dimensional friction $\hat{F} = 3$.

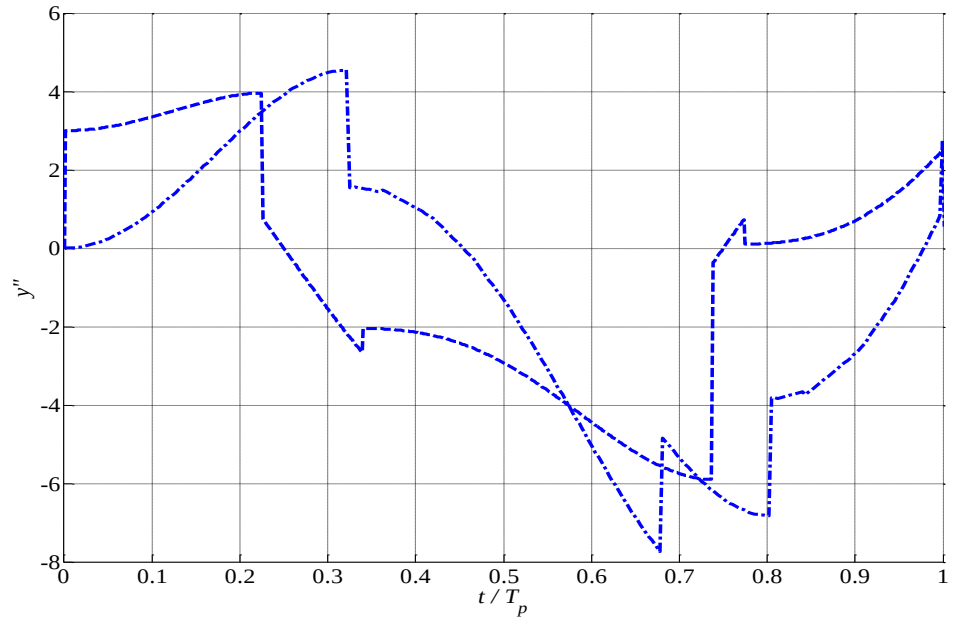

Figure 3.4: Comparison between the acceleration response of a passive single degree of freedom system and a system with control. Dash line: passive system, Dash dot line: controlled system. Non-dimensional base input magnitude $U_{mag} = 10$, pulse length $T_p = T$, non-dimensional friction $\hat{F} = 3$.

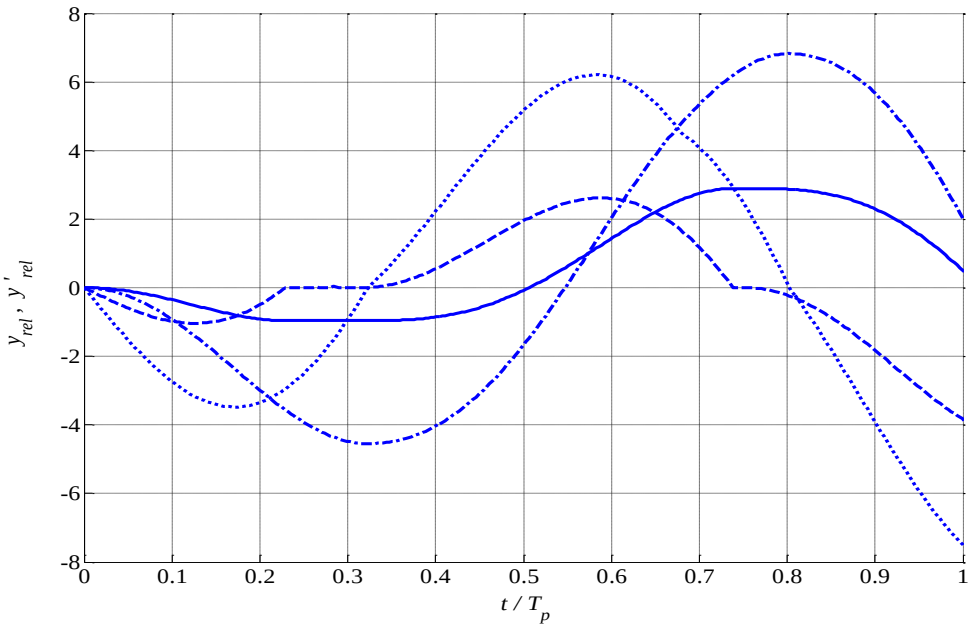

Figure 3.5: Comparison between the relative displacement and relative velocity of a passive single degree of freedom system and a system with control. Solid line: passive system relative displacement, Dash line: passive system relative velocity,
Dash dot line: controlled system relative displacement, Dot line: controlled system relative velocity. $y_{rel} = y - u, y'_{rel} = y' - U', y' = \frac{dy}{d\tau}, U' = \frac{dU}{d\tau}, \tau = \omega_n t$. Non-dimensional base input magnitude $U_{mag} = 10$, pulse length $T_p = T$, non-dimensional friction $\hat{F} = 3$.

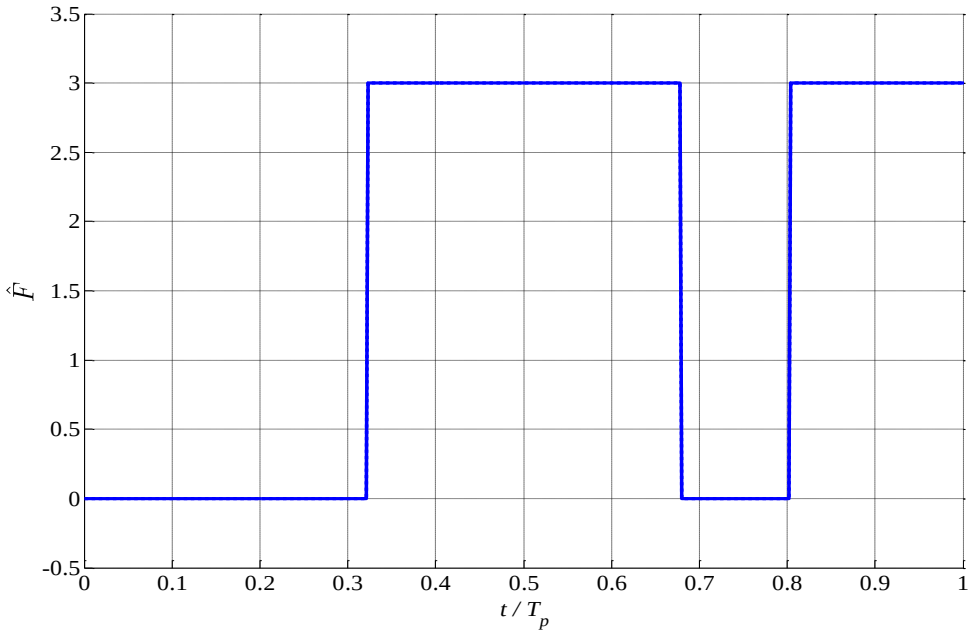

Figure 3.6: Friction force versus time for a system with control. Non-dimensional base input magnitude $U_{mag} = 10$, pulse length $T_p = T$, non-dimensional friction $\hat{F} = 3$.

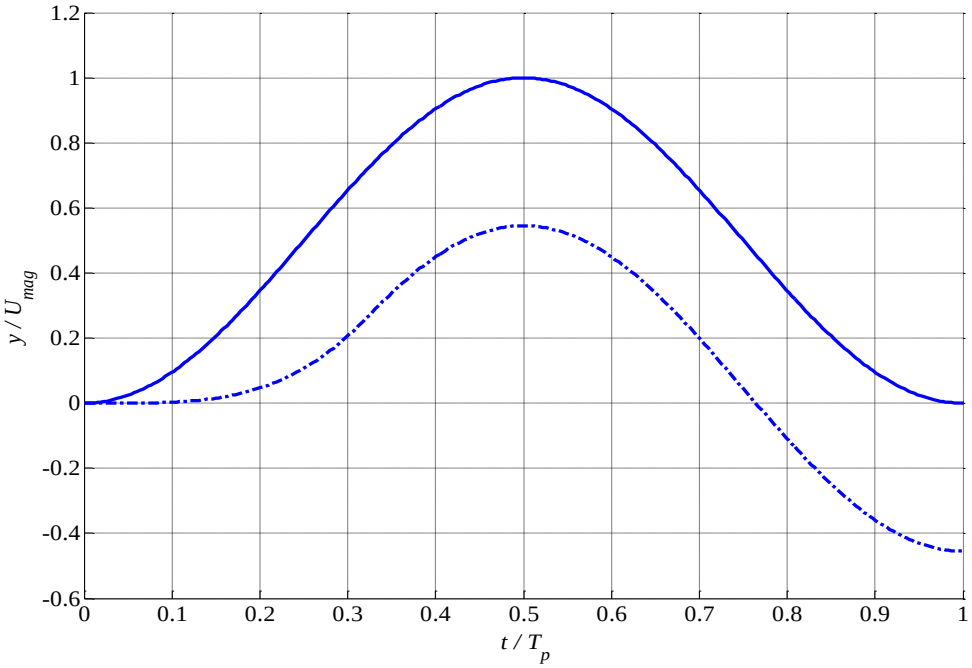

Figure 3.7: Comparison between the displacement response of a passive single degree of freedom system and a system with control (high friction case). Solid line: base input and passive system (passive system follows the base input since it fully sticks),
Dash line: controlled system. Non-dimensional base input magnitude $U_{mag} = 10$, pulse length $T_p = T$, non-dimensional friction $\hat{F} = 10$.

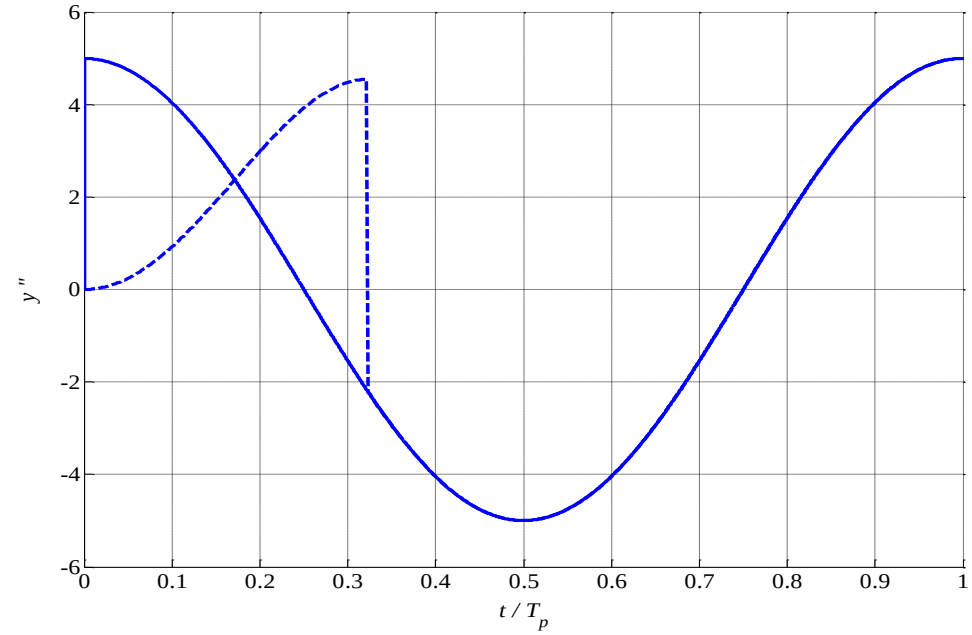

Figure 3.8: Comparison between the acceleration response of a passive single degree of freedom system and a system with control (high friction case). Solid line: Base input and passive system (passive system follows the base input since it fully sticks),
Dash line: controlled system. Non-dimensional base input magnitude $U_{mag} = 10$, pulse length $T_p = T$, non-dimensional friction $\hat{F} = 10$.

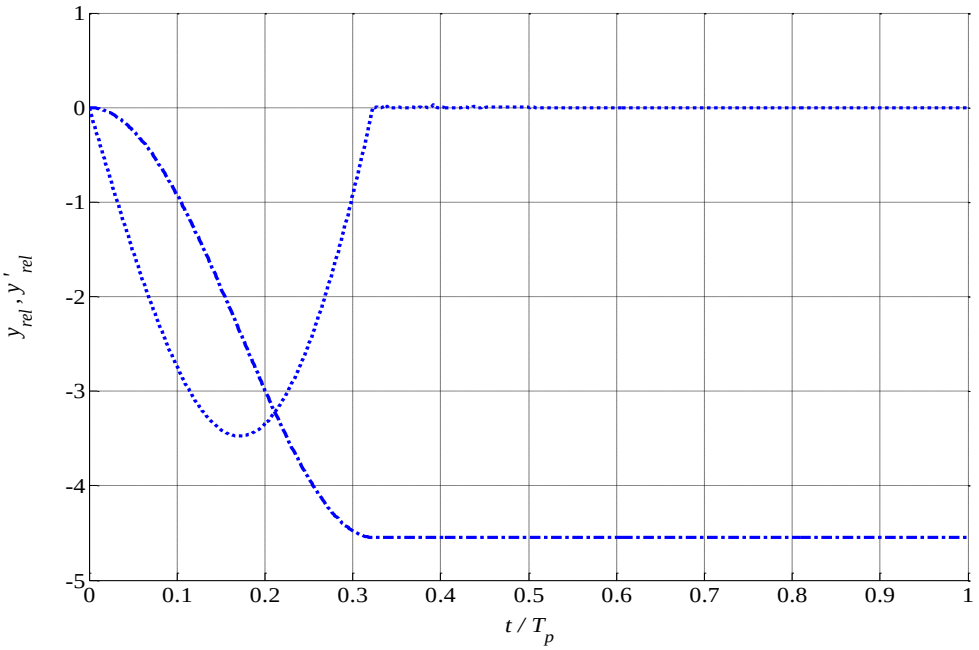

Figure 3.9: The relative displacement and the relative velocity of a system with control (high friction case). Dash dot line: controlled system relative displacement, Dot line: controlled system relative velocity. The relative displacement and the relative velocity of a passive system is zero until the end of the shock base input.

$y_{rel} = y - U, y'_{rel} = y' - U', y' = \frac{dy}{d\tau}, U' = \frac{dU}{d\tau}, \tau = \omega_n t$. Non-dimensional base input magnitude $U_{mag} = 10$, pulse length $T_p = T$, non-dimensional friction $\hat{F} = 10$.

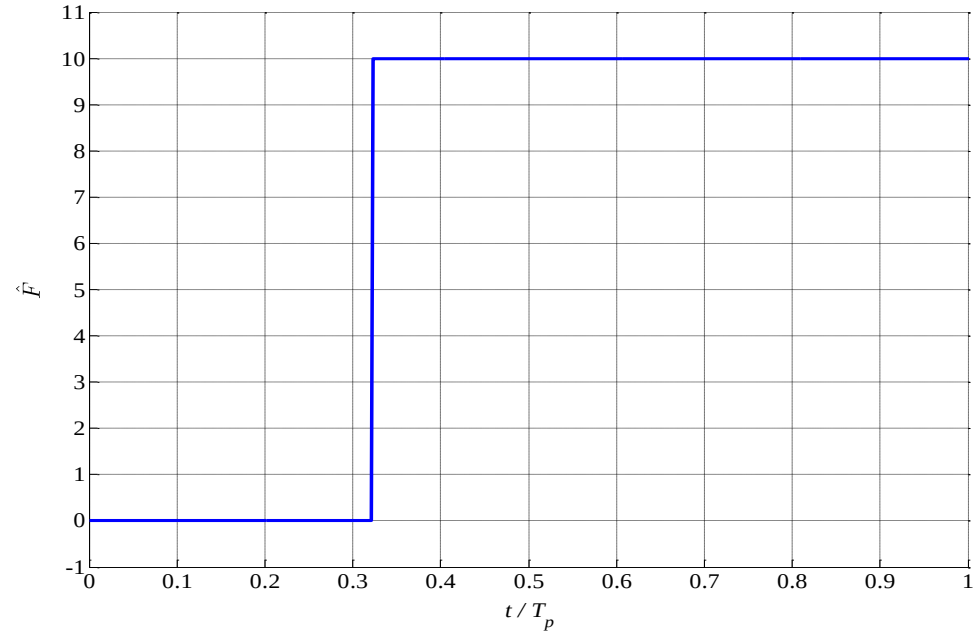

Figure 3.10: Friction force versus time for a system with control (high friction case). Non-dimensional base input magnitude $U_{mag} = 10$, pulse length $T_p = T$, non-dimensional friction $\hat{F} = 10$.

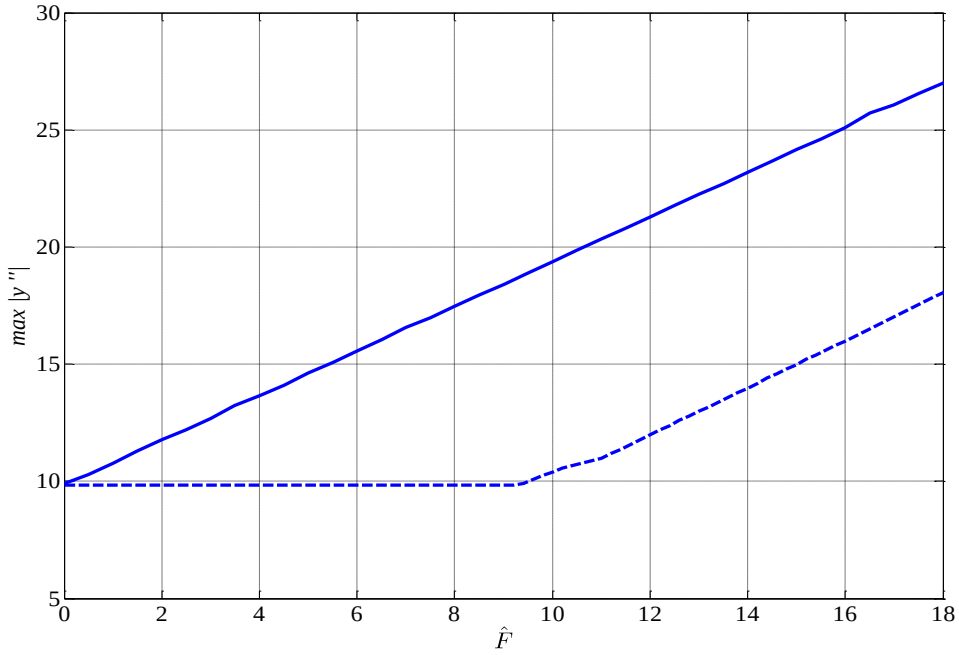

Figure 3.11: Comparison between the maximum acceleration of a passive single degree of freedom system and a system with control under a versed sine base input when the friction is varied. Solid line: passive system, dash line: controlled system. Non-dimensional base input magnitude $U_{mag} = 10$, pulse length $T_p = 0.1T$.

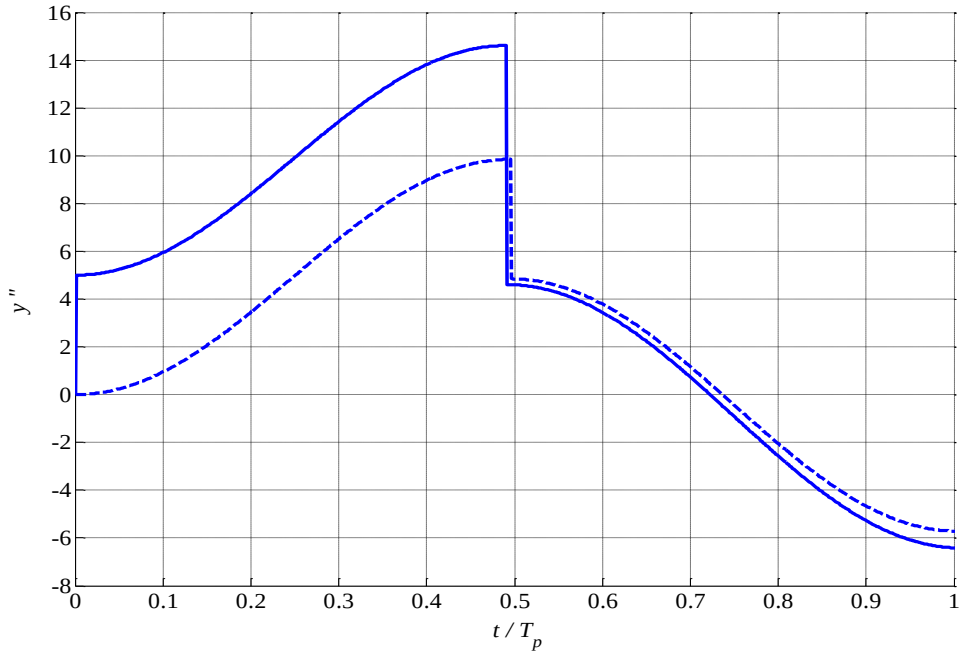

Figure 3.12: Comparison between the acceleration responses of a passive single degree of freedom system and a system with control under a versed sine base input.
Solid line: passive system, Dash line: controlled system. Non-dimensional base input magnitude $U_{mag} = 10$, pulse length $T_p = 0.1T$, non-dimensional friction $\hat{F} = 5$.

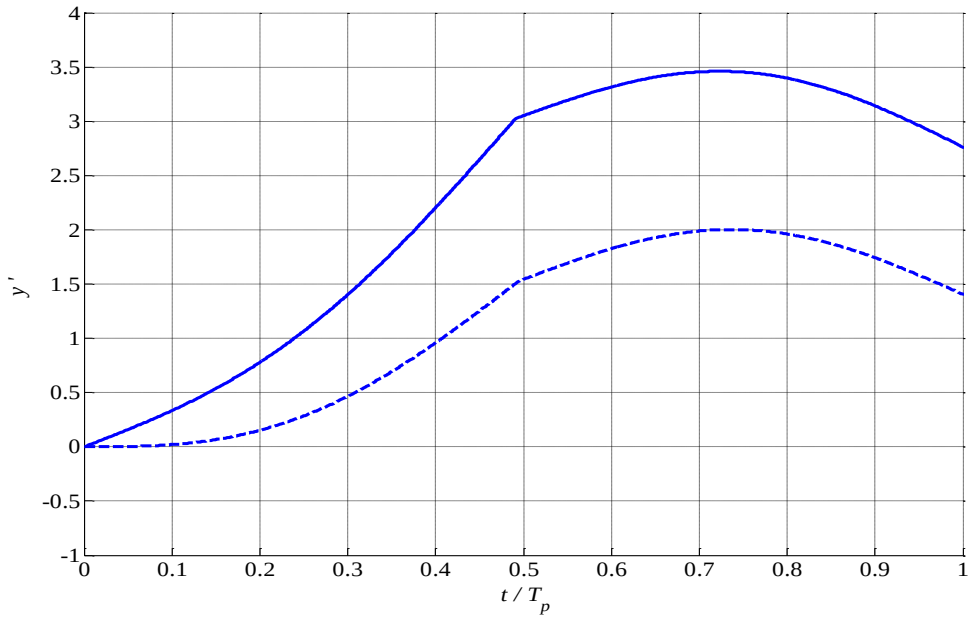

Figure 3.13: Comparison between the velocity responses of a passive single degree of freedom system and a system with control under a versed sine base input. Solid line: passive system, Dash line: controlled system. Non-dimensional base input magnitude $U_{mag} = 10$, pulse length $T_p = 0.1T$, non-dimensional friction $\hat{F} = 5$. y' = non--dimensional velocity of the mass.

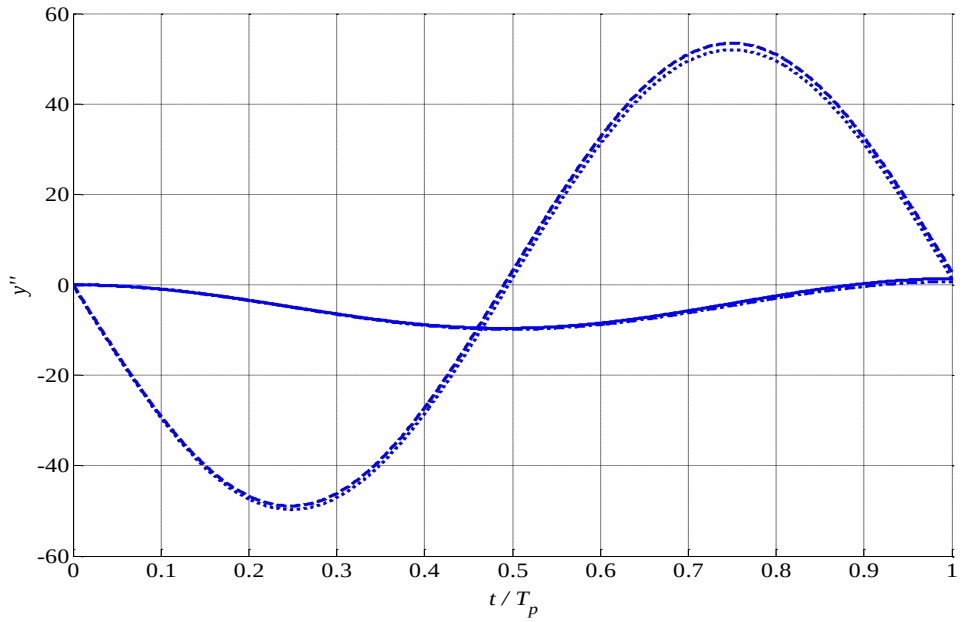

Figure 3.14: Comparison between the relative displacement and the relative velocity of a passive single degree of freedom system and a system with control under a versed sine base input. Solid line: passive system relative displacement, Dash line: passive system relative velocity, Dash dot line: controlled system relative displacement, Dot line: controlled system relative velocity. Non-dimensional base input magnitude $U_{mag} = 10$, pulse length $T_p = 0.1T$, non-dimensional friction $\hat{F} = 5$.

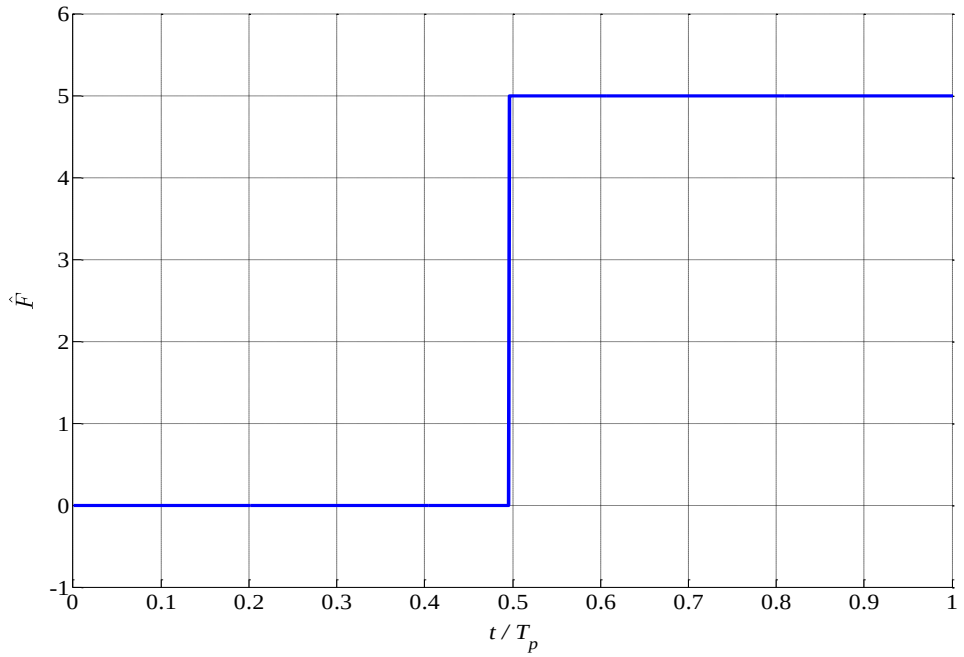

Figure 3.15: Friction force versus time for a system with control. Non-dimensional base input magnitude $U_{mag} = 10$, pulse length $T_p = 0.1T$, non-dimensional friction $\hat{F} = 5$.

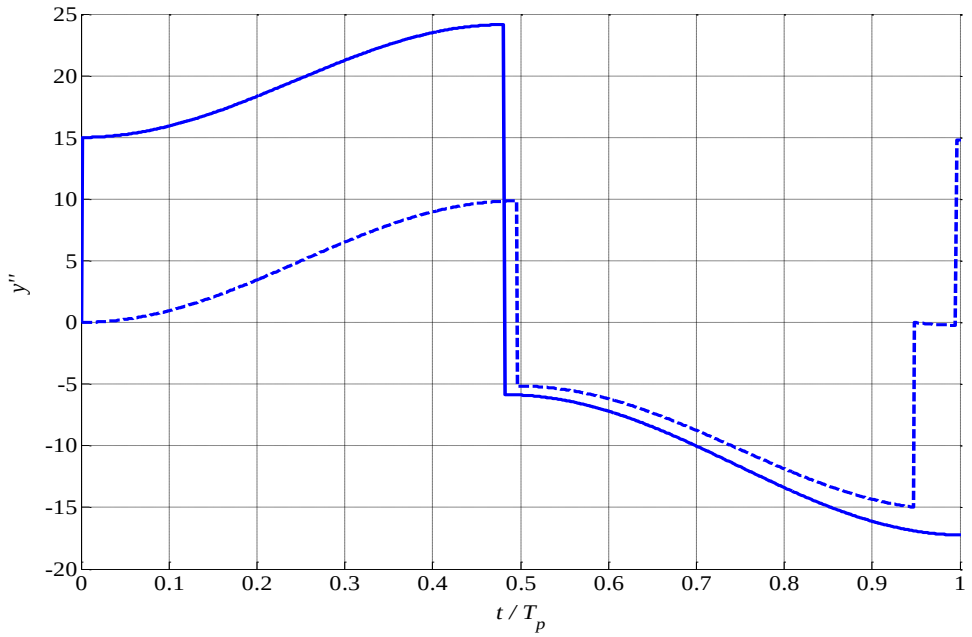

Figure 3.16: Comparison between the acceleration responses of a passive single degree of freedom system and a system with control under a versed sine base input. Solid line: passive system, Dash line: controlled system. Non-dimensional base input magnitude $U_{mag} = 10$, pulse length $T_p = 0.1T$, non-dimensional friction $\hat{F} = 15$. y'' = non-dimensional acceleration of the mass.

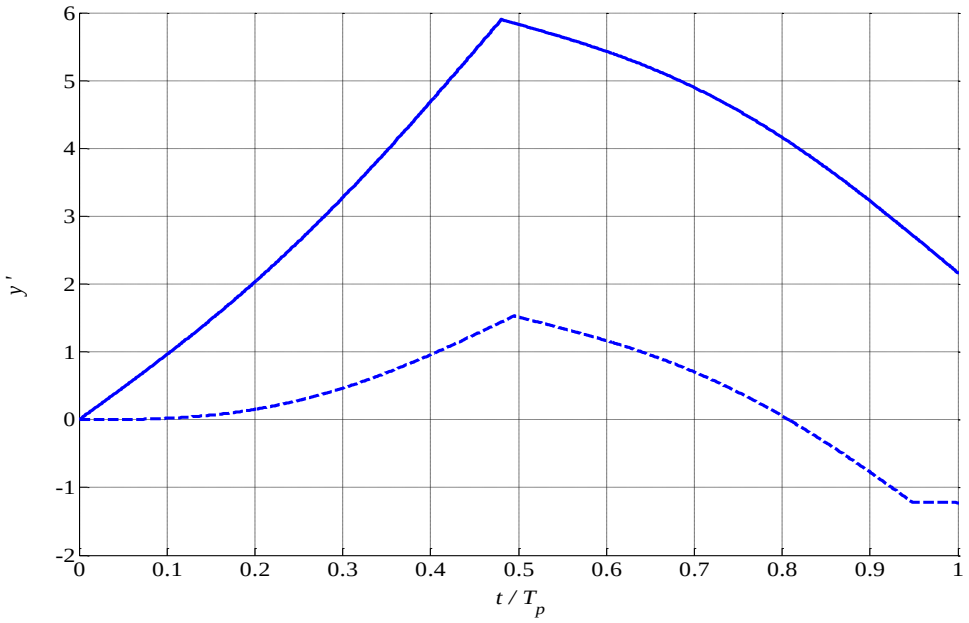

Figure 3.17: Comparison between the velocity responses of a passive single degree of freedom system and a system with control under a versed sine base input. Solid line: passive system, Dash line: controlled system. Non-dimensional base input magnitude $U_{mag} = 10$, pulse length $T_p = 0.1T$, non-dimensional friction $\hat{F} = 15$. y' = non-dimensional velocity of the mass.

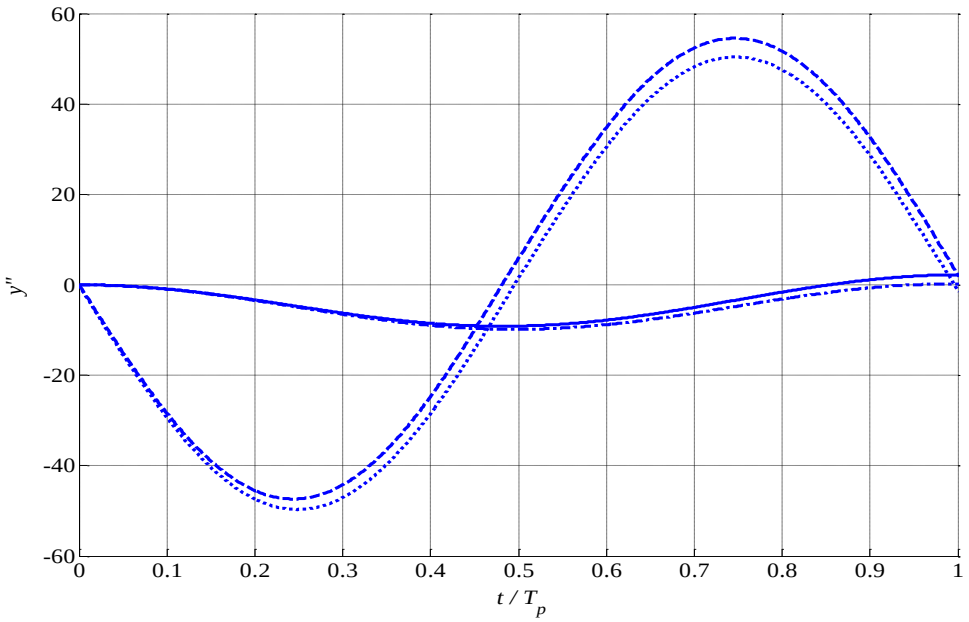

Figure 3.18: Comparison between the relative displacement and the relative velocity of a passive single degree of freedom system and a system with control under a versed sine base input. Solid line: passive system relative displacement, Dash line: passive system relative velocity, Dash dot line: controlled system relative displacement, Dot line: controlled system relative velocity. Non-dimensional base input magnitude $U_{mag} = 10$, pulse length $T_p = 0.1T$, non-dimensional friction $\hat{F} = 15$.

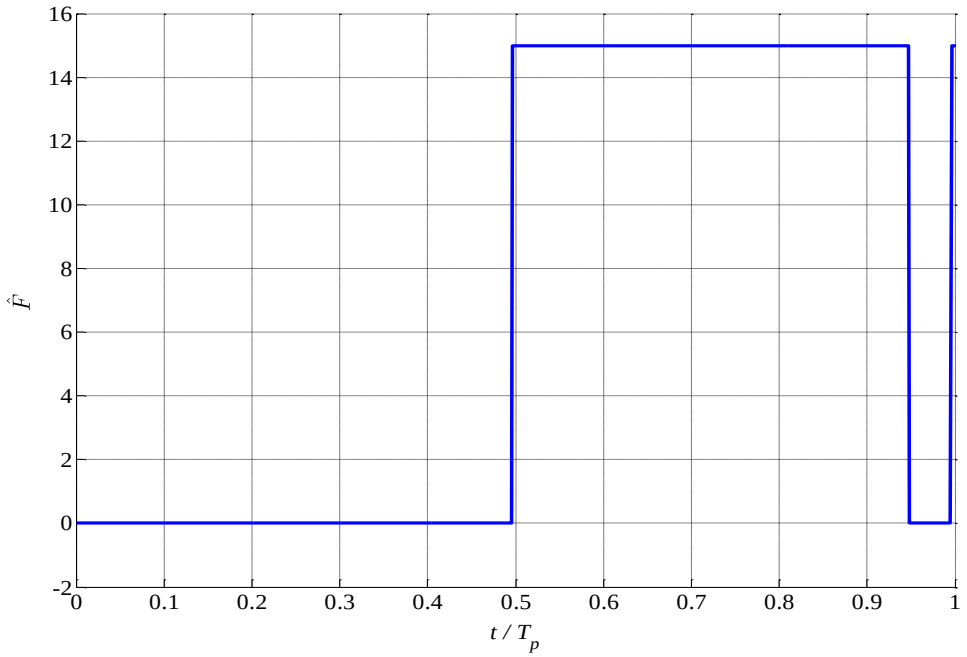

Figure 3.19: Friction force versus time for a system with control. Non-dimensional base input magnitude $U_{mag} = 10$, pulse length $T_p = 0.1T$, non-dimensional friction $\hat{F} = 15$.

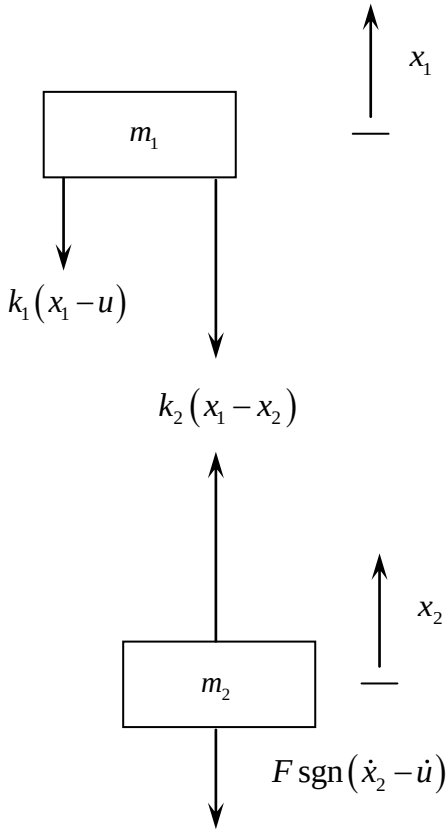

Figure 3.20: Free body diagram of a two degree of freedom system with friction.

(a)

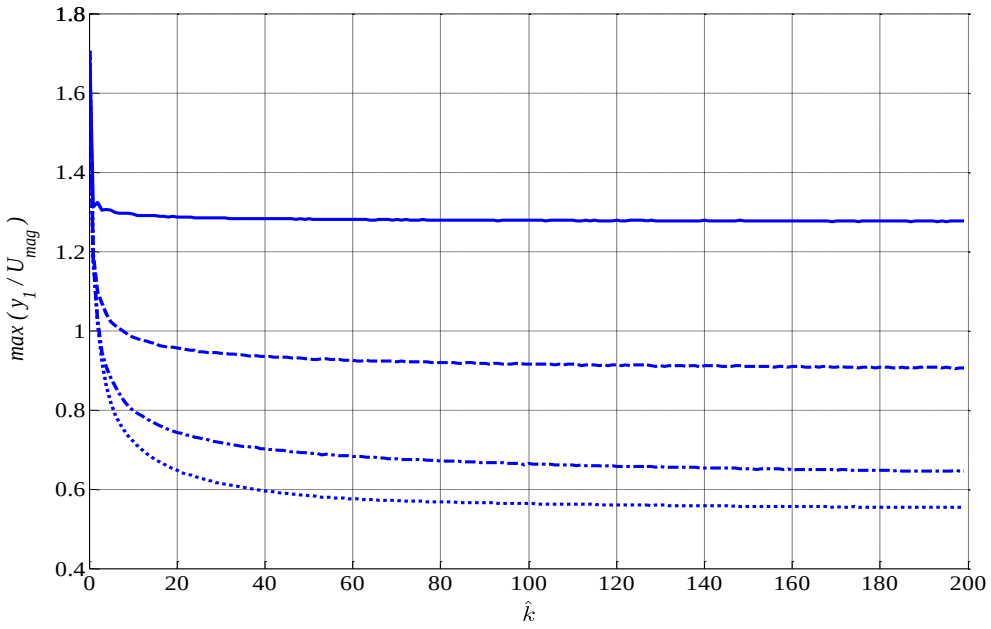

(b)

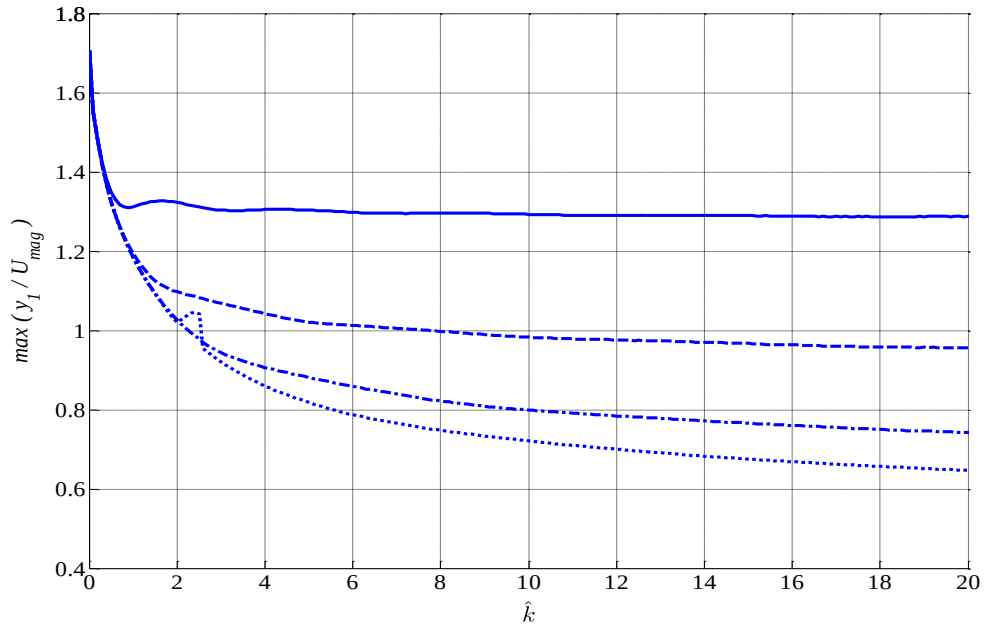

Figure 3.21: The maximum displacement response of the primary mass of a two degree of freedom system under a versed sine base input with control when the stiffness ratio $\hat{k}$ is varied. Solid line: $\hat{F} = 2.5$, Dash line: $\hat{F} = 5$, Dash dot line: $\hat{F} = 7.5$, Dot line: $\hat{F} = 10$. Non-dimensional base input magnitude $U_{mag} = 10$, pulse length $T_p = T_1$. Figure 5.15(b) is produced for a clear view of the region for small stiffness ratio.

(a)

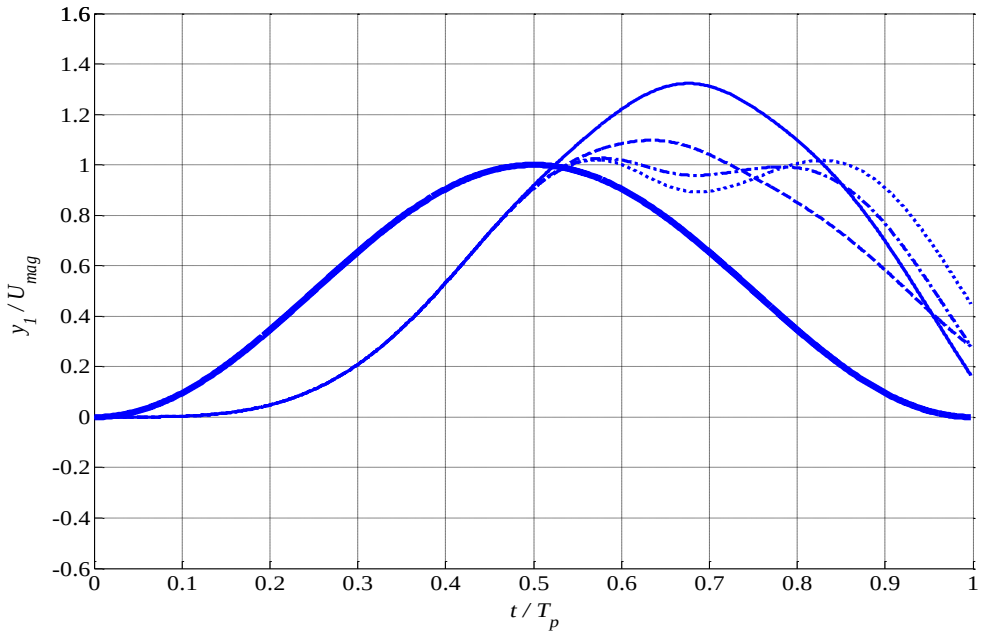

(b)

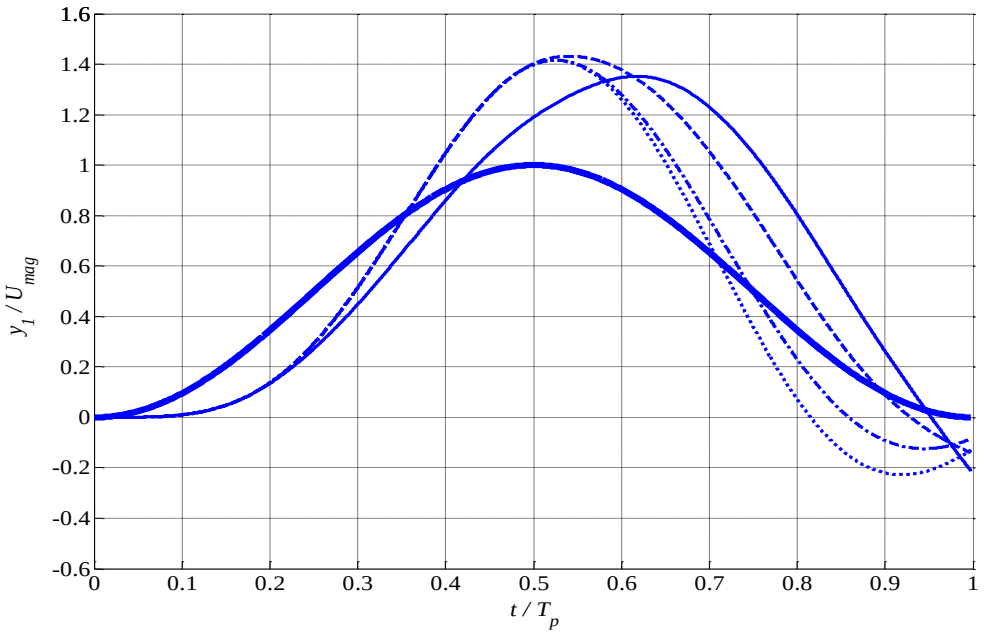

Figure 3.22: Displacement response of a two degree of freedom system under a versed sine base input with control and the comparison with its respective passive system. Bold line: base input, Solid line: $\hat{F} = 2.5$, Dash line: $\hat{F} = 5$, Dash dot line: $\hat{F} = 7.5$, Dot line: $\hat{F} = 10$. Non-dimensional base input magnitude $U_{mag} = 10$, pulse length $T_p = T_1$, low stiffness ratio $\hat{k} = 2$. (a) Displacement of the primary mass with the control strategy suggested. (b) Displacement of the primary mass for a passive system.

(a)

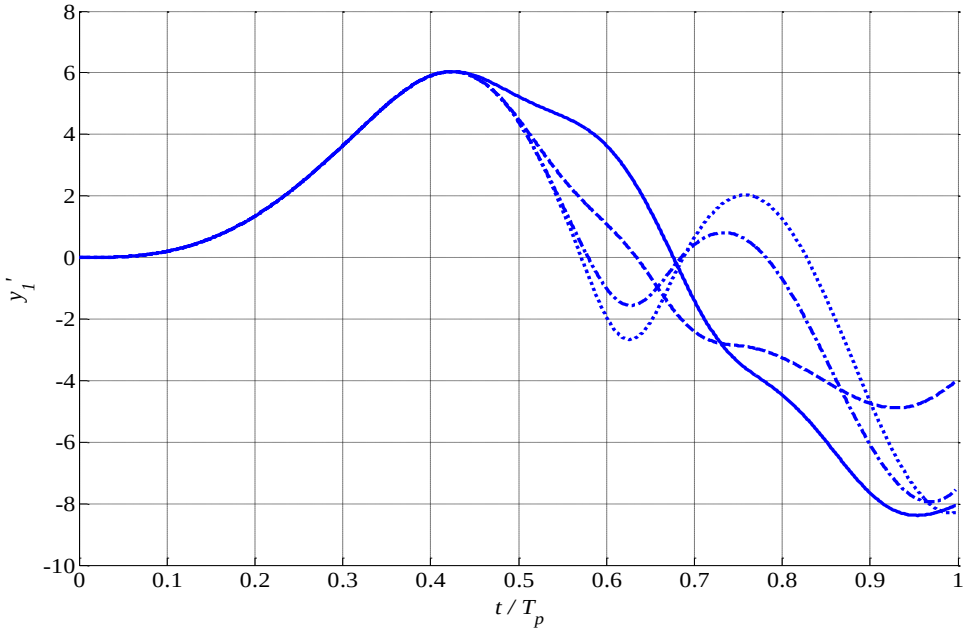

(b)

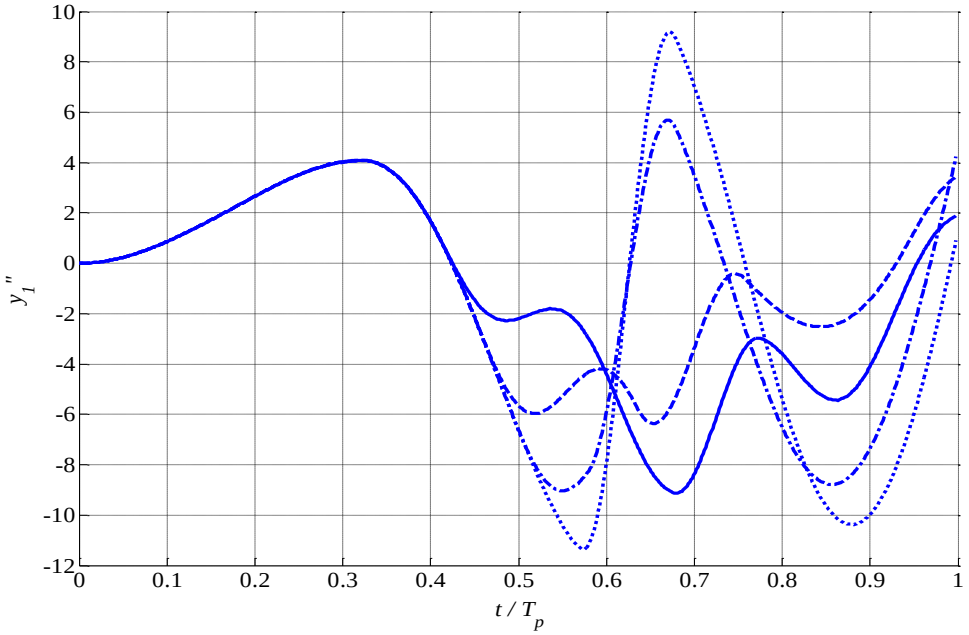

Figure 3.23: Response of a two degree of freedom system under a versed sine base input with control. Solid line: $\hat{F} = 2.5$, Dash line: $\hat{F} = 5$, Dash dot line: $\hat{F} = 7.5$, Dot line: $\hat{F} = 10$. Non-dimensional base input magnitude $U_{mag} = 10$, pulse length $T_p = T_1$, low stiffness ratio $\hat{k} = 2$. (a) Velocity of the primary mass. (b) Acceleration of the primary mass.

(a)

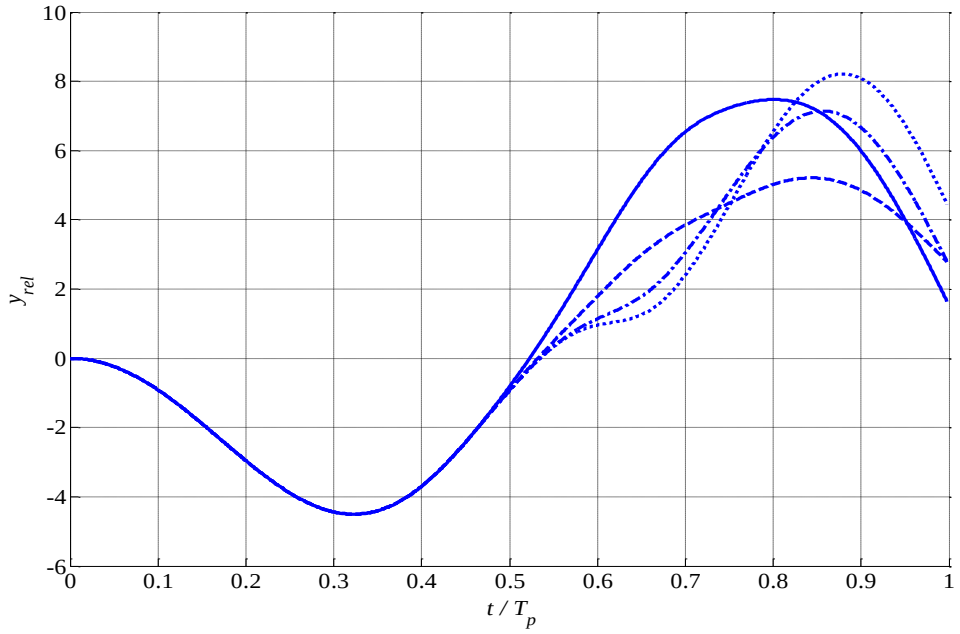

(b)

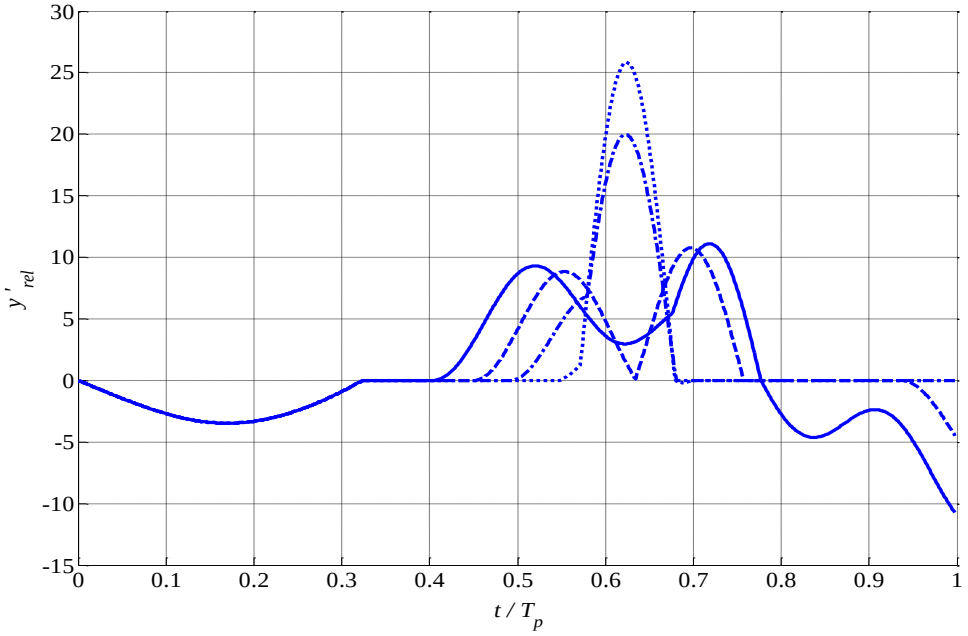

Figure 3.24: Response of a two degree of freedom system under a versed sine base input with control. Solid line: $\hat{F} = 2.5$, Dash line: $\hat{F} = 5$, Dash dot line: $\hat{F} = 7.5$, Dot line: $\hat{F} = 10$. Non-dimensional base input magnitude $U_{mag} = 10$, pulse length $T_p = T_1$, low stiffness ratio $\hat{k} = 2$.(a) Relative displacement of the primary mass, $y_{rel} = y_1 - U$. (b) Relative velocity of the secondary mass, $y'_{rel} = y_2 - U'$.

(a)

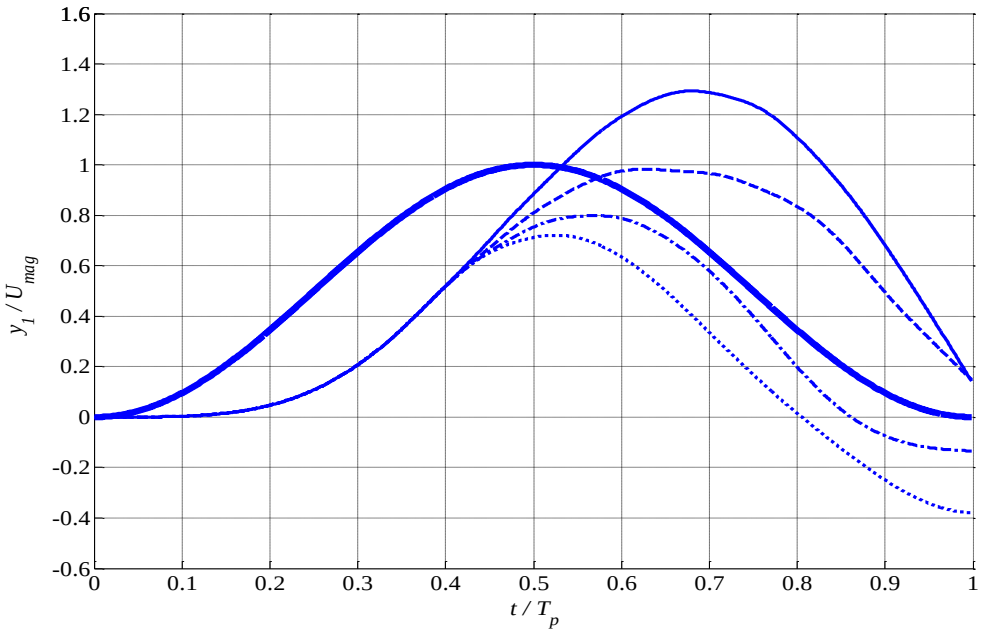

(b)

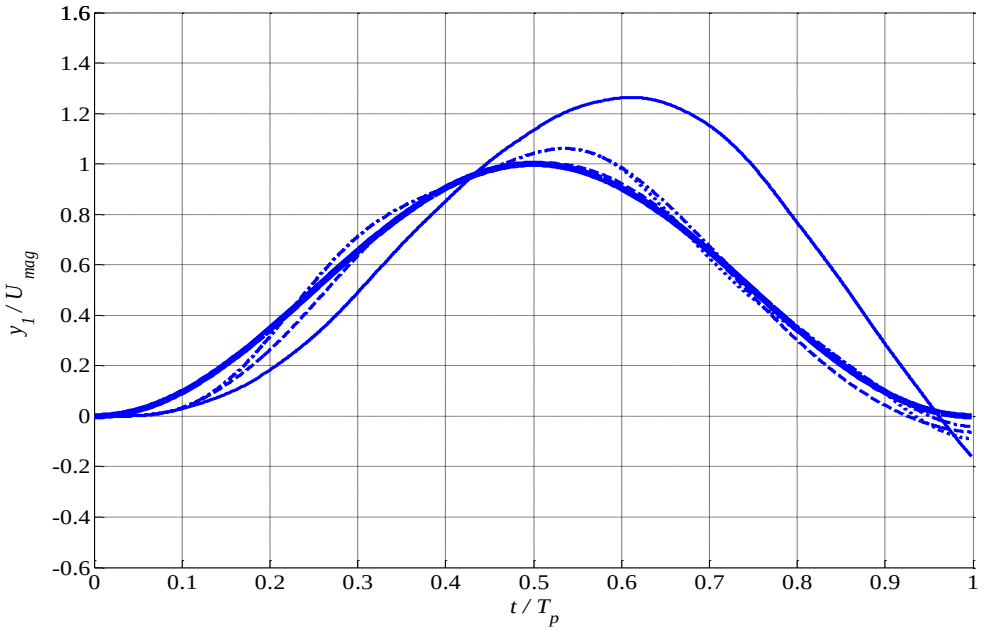

Figure 3.25: Displacement response of a two degree of freedom system under a versed sine base input with control and the comparison with its respective passive system.
Bold line: base input, Solid line: $\hat{F} = 2.5$, Dash line: $\hat{F} = 5$, Dash dot line: $\hat{F} = 7.5$,
Dot line: $\hat{F} = 10$. Non-dimensional base input magnitude $U_{mag} = 10$, pulse length $T_p = T_1$,
intermediate stiffness ratio $\hat{k} = 10$. (a) Displacement of the primary mass with the control strategy suggested. (b) Displacement of the primary mass for a passive system.

(a)

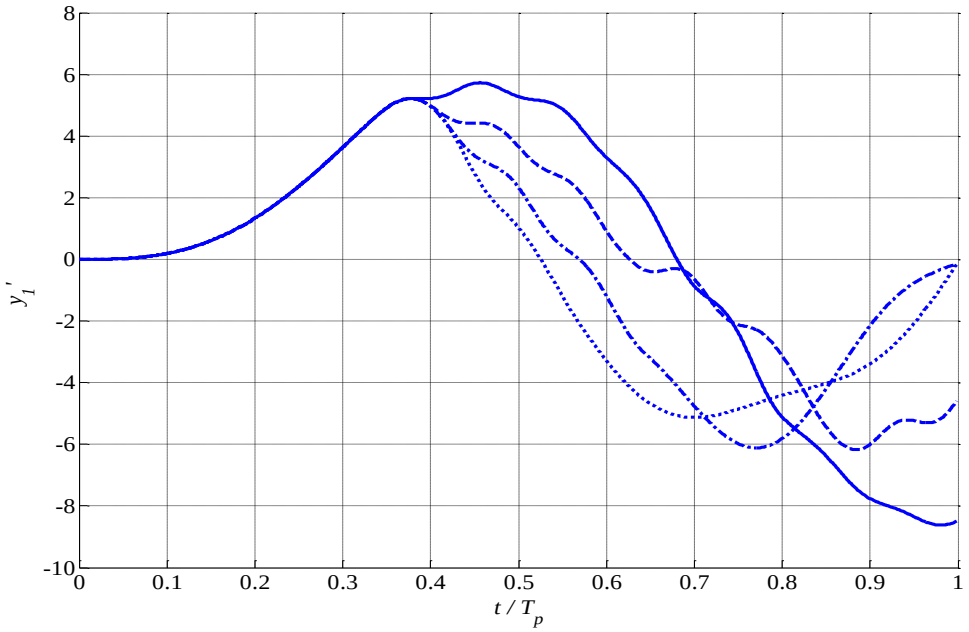

(b)

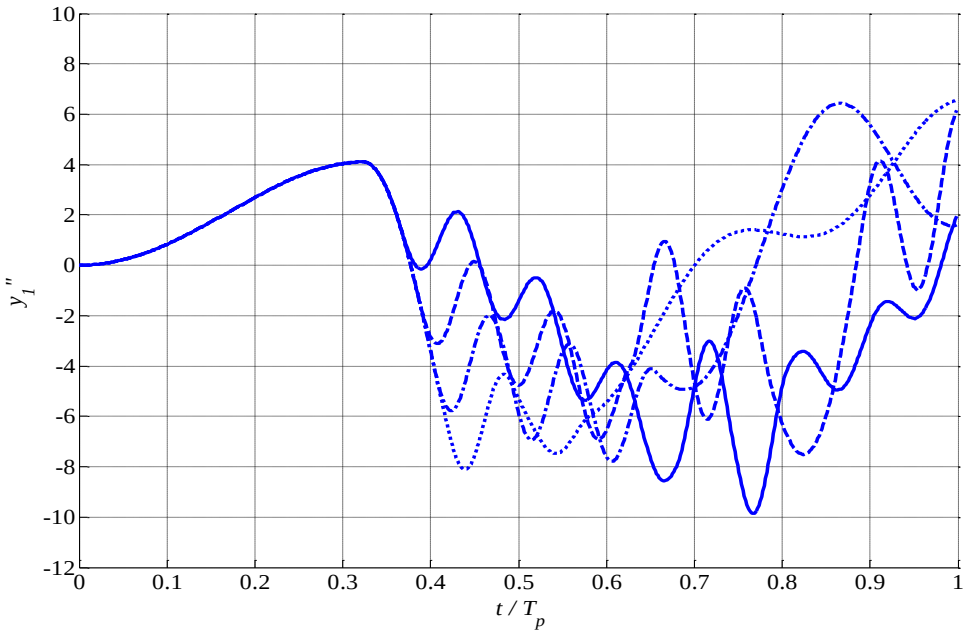

Figure 3.26: Response of a two degree of freedom system under a versed sine base input with control. Solid line: $\hat{F} = 2.5$, Dash line: $\hat{F} = 5$, Dash dot line: $\hat{F} = 7.5$, Dot line: $\hat{F} = 10$. Non-dimensional base input magnitude $U_{mag} = 10$, pulse length $T_p = T_1$, intermediate stiffness ratio $\hat{k} = 10$. (a) Velocity of the primary mass.(b) Acceleration of the primary mass.

(a)

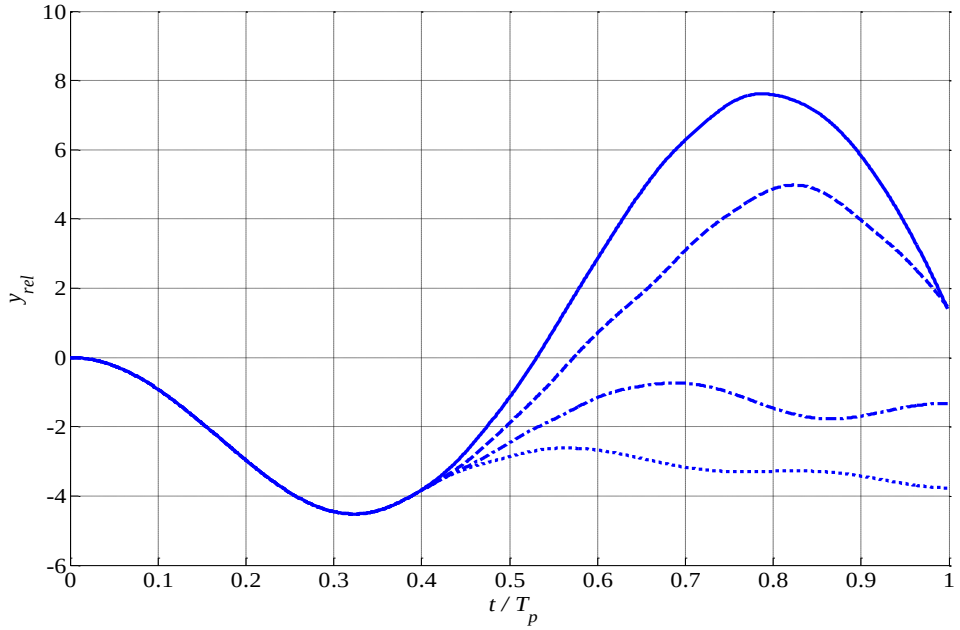

(b)

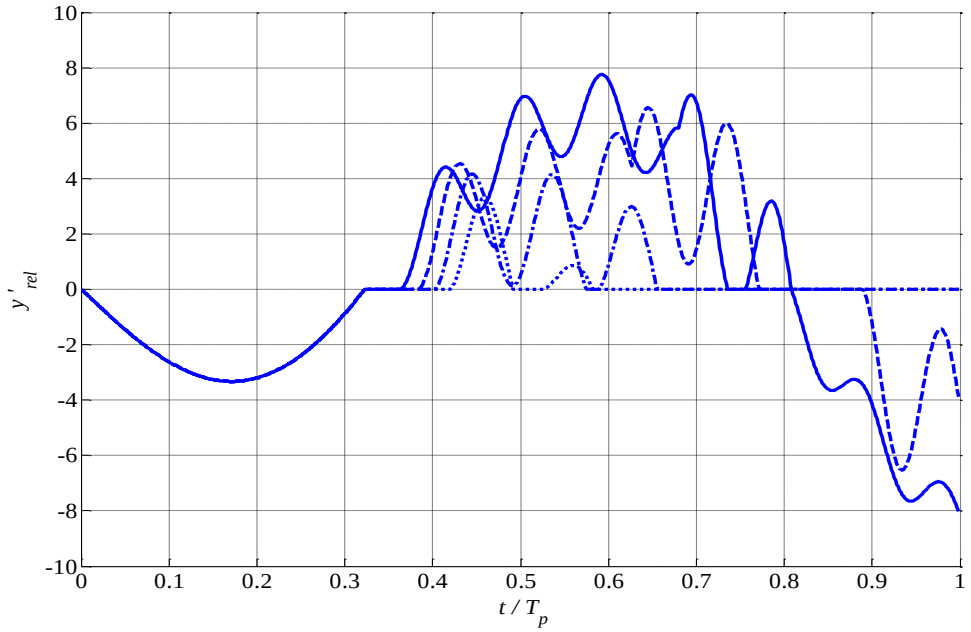

Figure 3.27: Response of a two degree of freedom system under a versed sine base input with control. Solid line: $\hat{F} = 2.5$, Dash line: $\hat{F} = 5$, Dash dot line: $\hat{F} = 7.5$, Dot line: $\hat{F} = 10$. Non-dimensional base input magnitude $U_{mag} = 10$, pulse length $T_p = T_1$, intermediate stiffness ratio $\hat{k} = 10$.(a) Relative displacement of the primary mass, $y_{rel} = y_1 - U$. (b) Relative velocity of the secondary mass, $y'_{rel} = y_2 - U'$.

(a)

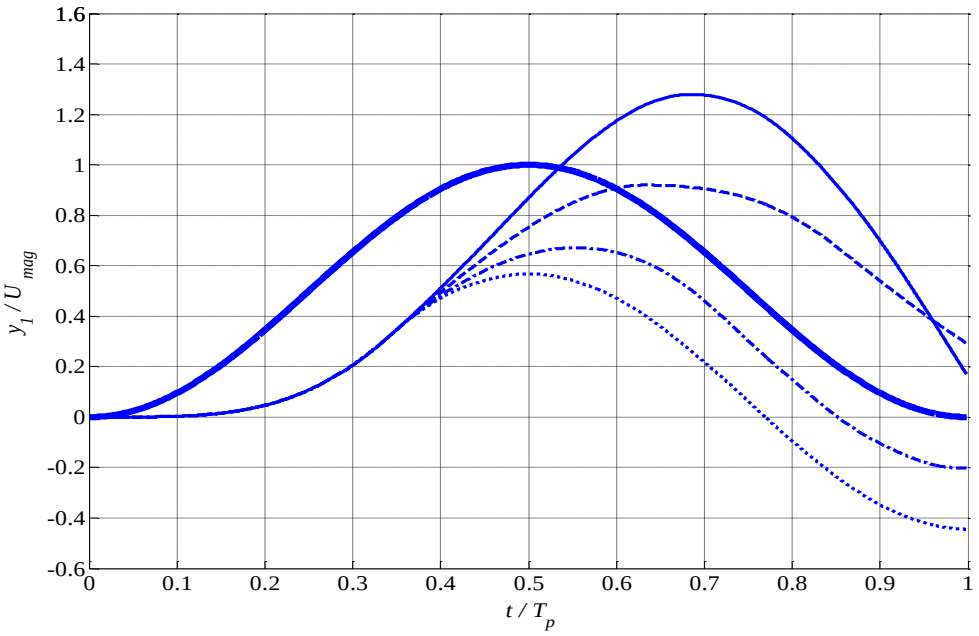

(b)

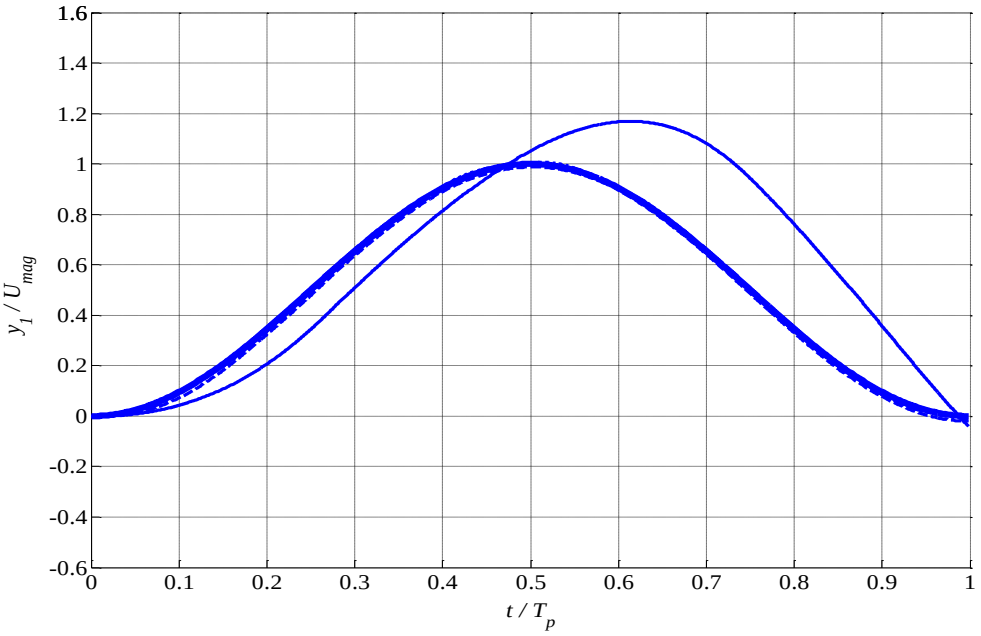

Figure 3.28: Displacement response of a two degree of freedom system under a versed sine base input with control and the comparison with its respective passive system. Bold line: base input, Solid line: $\hat{F} = 2.5$, Dash line: $\hat{F} = 5$, Dash dot line: $\hat{F} = 7.5$, Dot line: $\hat{F} = 10$. Non-dimensional base input magnitude $U_{mag} = 10$, pulse length $T_p = T_1$, high stiffness ratio $\hat{k} = 80$. (a) Displacement of the primary mass with the control strategy suggested. (b) Displacement of the primary mass for a passive system.

(a)

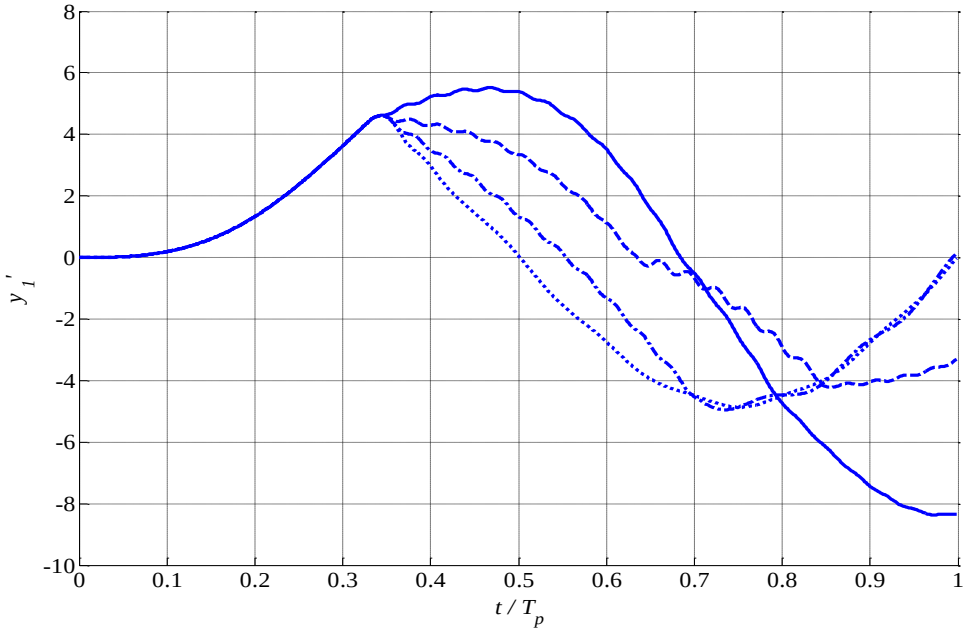

(b)

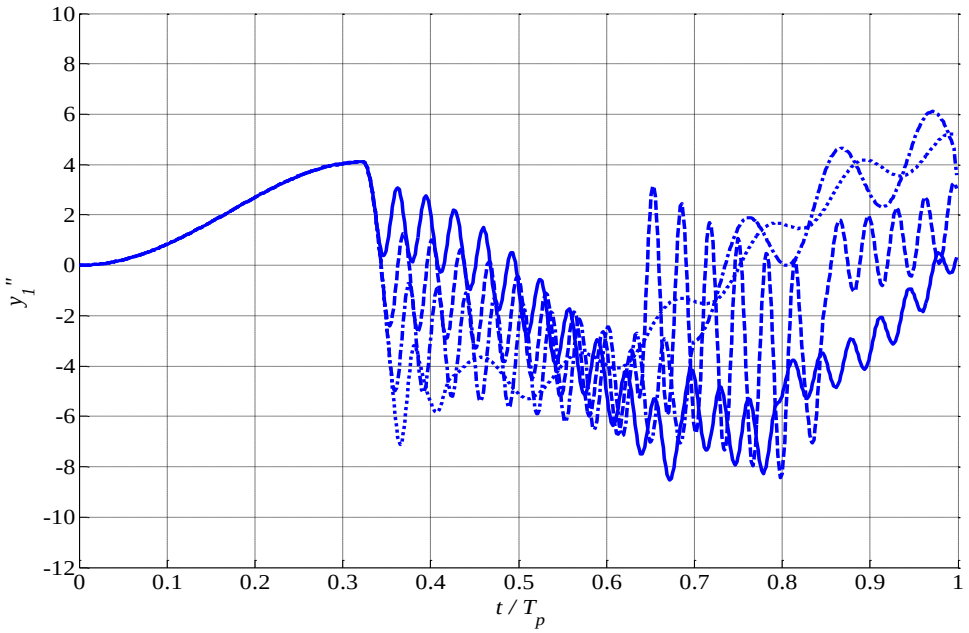

Figure 3.29: Response of a two degree of freedom system under a versed sine base input with control. Solid line: $\hat{F} = 2.5$, Dash line: $\hat{F} = 5$, Dash dot line: $\hat{F} = 7.5$, Dot line: $\hat{F} = 10$. Non-dimensional base input magnitude $U_{mag} = 10$, pulse length $T_p = T_1$, high stiffness ratio $\hat{k} = 80$. (a) Velocity of the primary mass. (b) Acceleration of the primary mass.

(a)

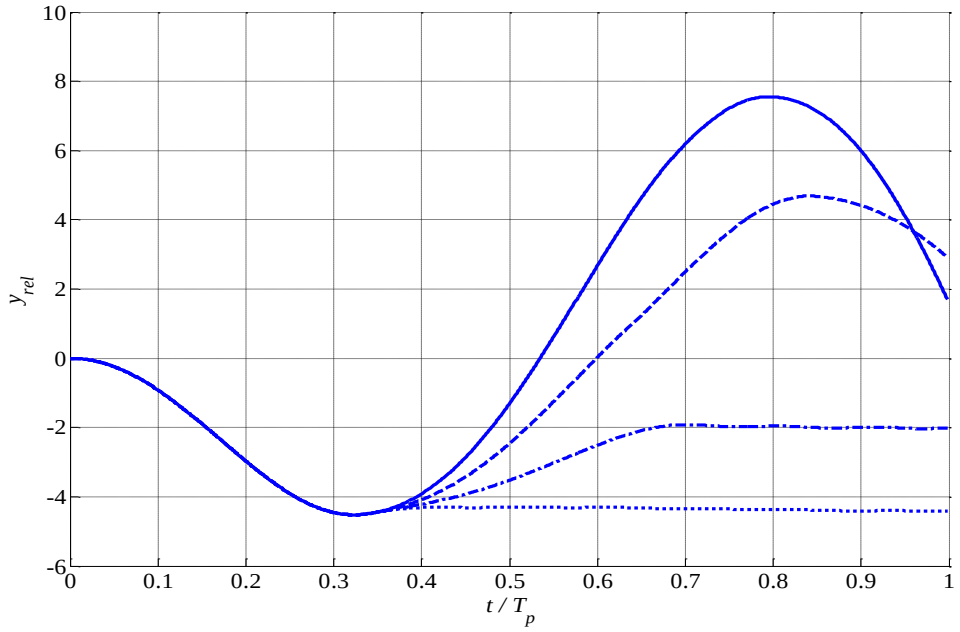

(b)

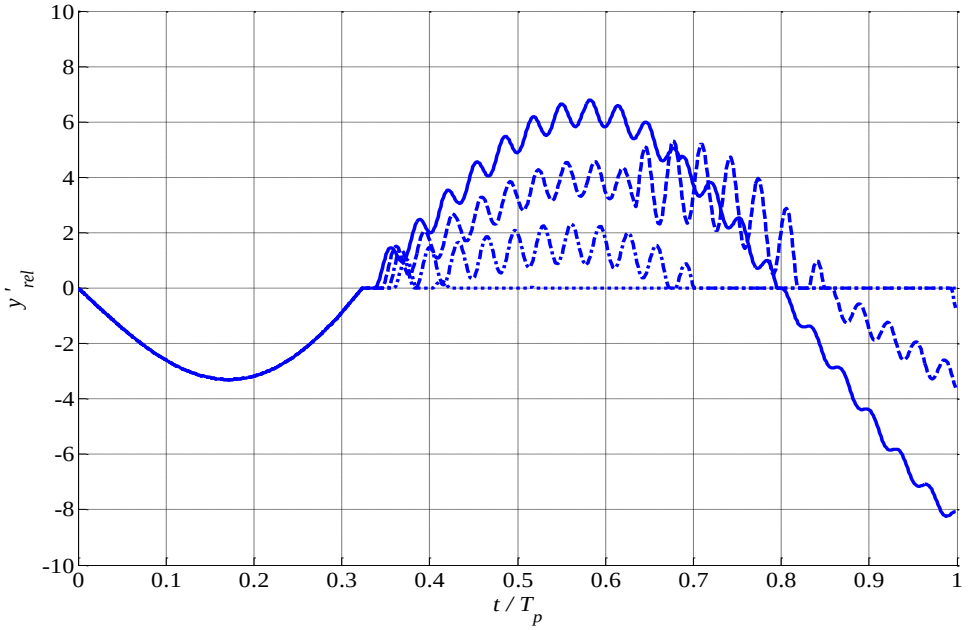

Figure 3.30: Response of a two degree of freedom system under a versed sine base input with control. Solid line: $\hat{F} = 2.5$, Dash line: $\hat{F} = 5$, Dash dot line: $\hat{F} = 7.5$, Dot line: $\hat{F} = 10$. Non-dimensional base input magnitude $U_{mag} = 10$, pulse length $T_p = T_1$, high stiffness ratio $\hat{k} = 80$.(a) Relative displacement of the primary mass, $y_{rel} = y_1 - U$. (b) Relative velocity of the secondary mass, $y'_{rel} = y_2 - U'$.

(a)

Non dimensional friction	Maximum normalized displacement of the primary mass, $\left(\frac{y_1}{U}\right)_{max}$		
	With control strategy	Passive system	Percentage reduction
$\hat{F}=2.5$	1.32	1.35	2.22
$\hat{F}=5$	1.10	1.43	23.08
$\hat{F}=7.5$	1.03	1.42	27.46
$\hat{F}=10$	1.02	1.42	28.17

(b)

Non dimensional friction	Maximum normalized displacement of the primary mass, $\left(\frac{y_1}{U}\right)_{max}$		
	With control strategy	Passive system	Percentage reduction
$\hat{F}=2.5$	1.29	1.26	-2.38
$\hat{F}=5$	0.98	1	0.02
$\hat{F}=7.5$	0.8	1.06	24.53
$\hat{F}=10$	0.72	1.06	32.08

(c)

Non dimensional friction	Maximum normalized displacement of the primary mass, $\left(\frac{y_1}{U}\right)_{max}$		
	With control strategy	Passive system	Percentage reduction
$\hat{F}=2.5$	1.28	1.17	-9.4
$\hat{F}=5$	0.92	1	8
$\hat{F}=7.5$	0.67	1	33
$\hat{F}=10$	0.57	1	43

Table 3.1: Comparison between the maximum normalized displacement of the primary mass for the system with control and the respective passive system. (a) $\hat{k}=2$, (b) $\hat{k}=10$, (c) $\hat{k}=80$.

4. RESIDUAL VIBRATION SUPPRESSION WITH COULOMB FRICTION

4.1 Introduction

The objective of this chapter is to investigate the residual response after the shock for both configurations, a single and a two degree of freedom system with Coulomb friction. As seen in the previous two chapters, the objective was to minimize the shock response during a base shock input but there are residual effects after the shock that need to be rapidly suppressed. Since the direction of friction is only dependent upon the mass velocity for this case, friction is expected to always act to oppose the motion. Therefore, it is expected that the friction could help in reducing the residual free vibration. How effective friction is in assisting with the residual decay is dependent on the amount of friction and also the stiffness ratio or the mass ratio in the case of a two degree of freedom system configuration. For this reason, an investigation is conducted to identify the parameters and their effect on the residual vibration. Throughout the analysis, passive friction is used where friction is unchanged throughout the motion. A control strategy is introduced for the residual vibration suppression by setting the value of friction based upon the initial conditions.

Finally, a comparison is made between both configurations. The benefits and limitations of both configurations are identified in terms of the effective residual vibration suppression. The amount of friction that will bring the mass back to the equilibrium position in the shortest possible of time without further vibration is identified for both configurations.

4.2 Residual response of a single degree of freedom system incorporating friction

4.2.1 Introduction and analytical solution

A single degree of freedom model configuration with Coulomb friction as shown in Figure 4.1 is analysed to investigate the effect of Coulomb friction. The equation of motion of the system shown in the figure is

$$m\ddot{x} + kx + F\,\mathrm{sgn}(\dot{x}) = 0 \tag{4.1}$$

In the literature, there is an analytical solution to this system for free vibration [36] and forced vibration under harmonic loading [23]. Therefore, it will be easier to compare any later numerical solutions of the system with the available analytical solutions and understand the behaviour of the free vibration of a system with friction.

To understand the behaviour of the system under free vibration, the analysis starts with the simplest case of the system with an initial displacement, x_i, and no initial velocity, $\dot{x}_i = 0$. Subsequently, the analysis is continued to the system with initial displacement, x_i and velocity, $\dot{x}_i$, where $\dot{x}_i$ is chosen to be either positive or negative. Finally, a control strategy for residual vibration control is introduced to calculate the amount of friction which could return the mass to equilibrium in the shortest possible time for any combination of the initial conditions.

Suppose the mass in Figure 4.1 is displaced in the positive *x* direction by an amount $x_i >> x_{st}$ and then released from rest, where $x_{st} = \dfrac{F}{k}$ is the static displacement of the mass. There is solution of a piecewise linear system [36]. When the mass is released, it will move in the negative *x* direction and the solution to response is:

$$\begin{aligned} x &= x_0 \cos\omega_n t + \frac{F}{k}(1-\cos\omega_n t) = x_{st} + (x_0 - x_{st})\cos\omega_n t \\ \dot{x} &= -\omega_n (x_0 - x_{st})\sin\omega_n t \end{aligned} \tag{4.2}$$

where $x_0 = x_i$ in equation (4.2) for the first half of the cycle.

This motion is valid within time range of $0 \le t \le \frac{\pi}{\omega_n}$. A harmonic component of the motion is added to the static component with frequency $\omega_n = \sqrt{\frac{k}{m}}$. At time, $t = \frac{\pi}{\omega_n}$, the maximum negative displacement is $-(x_i - 2x_{st})$ and the velocity changes sign from negative to positive.

In the next time interval, $\frac{\pi}{\omega_n} \le t \le \frac{2\pi}{\omega_n}$, the mass moves in the positive *x* direction and the solution for the response is:

$$\begin{aligned} x &= -x_0 \cos \omega_n t - \frac{F}{k}(1 - \cos \omega_n t) = -x_{st} - (x_0 - x_{st}) \cos \omega_n t \\ \dot{x} &= \omega_n (x_0 - x_{st}) \sin \omega_n t \end{aligned} \tag{4.3}$$

where $x_0 = x_i - 2x_{st}$ in equation (4.3) for the second half of the cycle.

The motion in this time interval comprises a harmonic component superimposed on a static component and the former has the same angular frequency ω_n as before. Then, for the next time interval, the solution goes back to equation (4.2) but using different value of x_0 which decreases by an amount $2x_{st}$ every half cycle. Every half cycle, the solution changes between equation (4.2) and (4.3) ; and it will repeat until the mass stops in the displacement range $-x_{st} \le x \le x_{st}$.

4.2.2 Non dimensional parameters and solutions.

The equations of motion given in (4.1) can be subsequently written in non-dimensional form as

$$y'' + y + \hat{F} \operatorname{sgn}(y') = 0 \tag{4.4}$$

The numerical solution using ODE solvers in MATLAB gives exactly the same plot as the analytical solution. The normalised displacement response is shown in Figure 4.2. It is normalised with respect to the non-dimensional static displacement of the mass,

$y_{st} = \frac{\omega_n^2 x_{st}}{g}$ which is equal to $\hat{F}$. In the plot, the mass is displaced by an amount equal to $y_i = 2y_{st}$, $y_i = 3y_{st}$, $y_i = 4y_{st}$ and $y_i = 5y_{st}$ respectively before it is released. As can be seen from the plot, the amplitude of the response decreases linearly with time by an amount $2y_{st}$ for every half cycle which results in a decrement of $4y_{st}$ for every cycle of oscillation. The system finally stops in the displacement range $-y_{st} \le y \le y_{st}$.

There exists an upper limit for the applied friction force which determines whether the mass is moving at least by a small amount or not. If the friction force is equal to or larger than this value, there is no initial velocity of the system and the mass will not move at all and will stick at its initial displaced position. However, if the friction force is less than this value, the mass will move at least by a small amount. The upper limit is given by $\hat{F} = y_i$. When the non-dimensional friction equals this value, y_i will be equal to y_{st} and it is already known that if $\hat{F} \ge y_i$, the value of y_i will be in the range of $-y_{st} \le y_i \le y_{st}$ which causes the mass to remain stationary. On the other hand, if the system is displaced less than $2\,y_{st}$, the mass will stop before it reaches the equilibrium position. In the next two sections, the value of friction that could bring the mass back to its equilibrium position in the shortest possible of time will be calculated based on the initial conditions of the free vibration phase. The main focus to bring the mass back to its equilibrium position before subsequent shock is because the static friction will affect the motion of the mass. If the mass stops away from its equilibrium, when a subsequent shock is applied, the static friction is expected to influence the dynamic response of the system by contributing to the net force acting on the mass.

4.2.3 Energy dissipation with Coulomb friction

If the mass is displaced by an amount x_i in the positive direction and released, there should be an amount of friction that is needed to make it return to its equilibrium position in the least amount of time without further oscillation. The initial conditions are

$$\begin{aligned} x(0) &= x_i \\ \dot{x}(0) &= 0 \end{aligned} \tag{4.5}$$

One can calculate the necessary friction force by equating the work done by the friction force with the initial potential energy stored in the elastic spring as shown below

$$\left|Fx_i\right| = \frac{1}{2}kx_i^{\,2} \tag{4.6}$$

This is because, before the mass is released, the energy in the system consists only of potential energy in the spring. This value of friction is only valid for the initial condition outlined above. On the other hand, if the system is given an initial velocity this value is not valid, because now there is a contribution of kinetic energy to the total initial energy in the system. If the friction is greater than the friction needed to bring the mass back to its equilibrium, the mass will stick somewhere along the way. However, if the friction is lower than that value, the mass will pass the equilibrium position and, dependent on how much friction has been applied, it will continue oscillating or stick when *x* is in the range of $-x_{st} \le x \le x_{st}$ after completing its first half cycle.

From equation (4.6), the friction necessary to return the mass to the equilibrium position (x=0) at the end of the first interval of time is

$$F = \left|\frac{1}{2}kx_i\right| \tag{4.7}$$

In terms of the non-dimensional parameters, equation (4.7) can be written as $\hat{F} = \left|\frac{1}{2}y_i\right|$.

This can be seen from Figure 4.2, when $x_i = \frac{2F}{k} = 2x_{st}$ or $y_i = 2\hat{F} = 2y_{st}$ is used, the mass returns to its equilibrium position at the end of the first interval of time.

If there is an initial velocity imposed on the system in addition to the initial displacement, the equation has to be modified. For a positive velocity, the mass will move in the positive *x* direction first before reaching its maximum displacement and reversing back in the negative *x* direction. Therefore, the work-energy relationship can be constructed to equate the total initial energy (potential and kinetic energy) and total energy at the maximum displacement (potential energy and work done by friction to move the mass from x_i to x_{max}).

$$\frac{1}{2}kx_i^2 + \frac{1}{2}m\dot{x}_i^2 = \frac{1}{2}kx_{max}^2 + F\left|(x_{max} - x_i)\right| \tag{4.8}$$

After reaching x_{max}, it behaves in the same way as the problem with imposed initial displacement and zero initial velocity. Now, x_{max} is considered as an initial displacement and the friction needed to bring the mass back to the equilibrium position is

$$F = \left|\frac{1}{2}kx_{max}\right| \tag{4.9}$$

Substituting the value of friction needed to bring the mass back to equilibrium position back into equation(4.9), the maximum displacement of the mass can be calculated.

$$x_{max} = \left|\frac{1}{4}x_i\right| + \frac{\left(\sqrt{\frac{9}{4}x_i^2 + 2\frac{m}{k}\dot{x}_i^2}\right)}{2} \tag{4.10}$$

This value of x_{max} can be substituted back into equation (4.9) to find the value of friction needed to bring the mass back to its original position.

$$F = \left|\frac{1}{2}kx_{max}\right| = \left|\frac{1}{8}kx_i\right| + \frac{1}{4}k\left(\sqrt{\frac{9}{4}x_i^2 + 2\frac{m}{k}\dot{x}_i^2}\right) \tag{4.11}$$

However, again this value can only be used for the initial conditions outlined above with initial positive displacement and initial positive velocity, $x_i > 0$ and $\dot{x}_i > 0$. In terms of the non-dimensional parameters, equation (4.11) can be written as

$$\hat{F} = \left|\frac{1}{2}y_{max}\right| = \left|\frac{1}{8}y_i\right| + \frac{1}{4}\left(\sqrt{\frac{9}{4}(y_i)^2 + 2\left(y_i'\right)^2}\right) \tag{4.12}$$

Figure 4.3 shows the residual response of the mass subjected to a positive initial velocity and displacement. The initial displacement and velocity were chosen as $y_i = 1$ and $y_i' = 1$ respectively. If this initial condition is used, the non-dimensional friction $\hat{F}$ that could bring the mass back to its equilibrium position calculated from equation (4.12) is equal to 0.64 and the maximum non-dimensional displacement achieved is $y_{max} = 2\hat{F} = 1.28$.

From the plot, $\hat{F} = \frac{1}{2} y_{max} = 0.64$ brings the mass back to its equilibrium position which supports equation(4.12). The mass reaches a maximum displacement of y_{max} before it turns back to move in the opposite direction. After the maximum displacement, dependent upon the value of friction, the amplitude decreases by an amount $2y_{st}$ for every subsequent half cycle until the mass stops within the displacement range $-y_{st} \le y \le y_{st}$.

If there is an initial negative velocity applied to the system, a different energy relationship can be constructed to find the friction needed to bring the mass back to its equilibrium position.

$$\begin{aligned} |Fx_i| &= \frac{1}{2} k x_i^2 + \frac{1}{2} m \dot{x}_i^2 \\ F &= \left| \frac{1}{2} k x_i + \frac{1}{2} m \frac{\dot{x}_i^2}{x_i} \right| \end{aligned} \tag{4.13}$$

The initial conditions are $x_i > 0$ and $\dot{x}_i < 0$. In terms of the non-dimensional parameters, equation (4.13) can be written as

$$\hat{F} = \left| \frac{1}{2} y_i + \frac{1}{2} \frac{(y_i')^2}{y_i} \right| \tag{4.14}$$

Introducing a new variable

$$C_1 = \left| y_i + \frac{(y_i')^2}{y_i} \right| \tag{4.15}$$

Now, friction can be represented by the variable C_1. It is expected that if $\hat{F} = \frac{1}{2} C_1$ is used, the mass will return to its equilibrium position in the first interval of time.

In order to validate this, Figure 4.4 shows the response of a single degree freedom system subjected to a positive initial displacement and negative initial velocity, $y_i = 1$ and $y_i' = -1$ respectively. Based on this choice of initial conditions, the non-dimensional friction $\hat{F}$ needed to bring the mass back to its equilibrium position calculated from equation (4.14) is equal to 1. It is seen from the plot that $\hat{F} = \frac{1}{2}C_1$ brings the mass back to its equilibrium position and supports equation(4.14).

Because of the negative velocity, the mass might displace to a maximum displacement value at the end of the first half cycle of motion. After the first half cycle, then the amplitude of vibration of the mass will decrease by an amount $2y_{st}$ for every subsequent half cycle until the mass stops in the displacement range $-y_{st} \le y \le y_{st}$.

4.2.4 A control strategy for the level of friction for residual vibration control

At the end of a base shock input, the system may have some response at time T_p, where T_p is the length of the pulse. The response of the system at time T_p will become the initial conditions for the next phase of free vibration. It is desirable that after the shock ends, the mass returns to equilibrium in the shortest possible of time without further vibration. Based on the previous section, it is possible to ensure that the mass behaves like this by applying the appropriate friction based on the initial conditions. In this section, the analysis from the earlier part of the chapter is continued with a strategy to choose the value of friction at the start of the residual vibration for any value of the initial displacement and velocity.

There are two different ways to calculate the appropriate friction value. The choice of method depends upon the phase of the motion at the end of the shock, ie, whether $x_i\dot{x}_i < 0$, $x_i\dot{x}_i > 0$ or $x_i\dot{x}_i = 0$ where x_i and $\dot{x}_i$ are the displacement and the velocity at time T_p respectively. Figure 4.5 shows the phase plane plot for the initial conditions.

If $x_i\dot{x}_i < 0$, the energy in the system at time T_p, where T_p is the length of the pulse is equal to energy dissipated by friction was shown previously in equation (4.13). x_i and $\dot{x}_i$ are the displacement and velocity at time T_p respectively. This energy relationship can be used to calculate the amount of friction to bring the mass back to the equilibrium position.

In order to validate this, two simulations are presented with combinations of initial displacement and velocity which produce $x_i \dot{x}_i < 0$. For the first simulation, the initial condition chosen is $y_i = 1$ and $y_i' = -1$. For the second simulation, the initial condition chosen is $y_i = -1$ and $y_i' = 1$. For both cases, the non-dimensional friction calculated is $\hat{F} = 1$. The result from the simulations is shown in Figure 4.6. For both cases, the mass return to its equilibrium in the shortest possible of time without further vibration by using $\hat{F} = 1$. If higher friction is used, the mass stops before reaching its equilibrium position and if less friction is used the mass continues to oscillate after reaching its equilibrium for the first time. For simplicity, the result shown in Figure 4.6 is only for the case of $\hat{F} = 1$.

On the other hand, if $x_i \dot{x}_i > 0$, the energy in the system at time T_p equal to the energy dissipated by friction was shown previously in equation (4.8). This energy relationship can be used to calculate the amount of friction to bring the mass back to the equilibrium position as shown by equation (4.9) to equation (4.12).

In order to validate this, two simulations are presented with combinations of initial displacement and velocity which produce $x_i \dot{x}_i > 0$. For the first simulation, the initial condition chosen is $y_i = 1$ and $y_i' = 1$. For the second simulation, the initial condition chosen is $y_i = -1$ and $y_i' = -1$. For both cases, the non-dimensional friction determined is $\hat{F} = 0.64$. The result from the simulations is shown in Figure 4.7. For both cases, the mass returns to its equilibrium in the shortest possible of time by using $\hat{F} = 0.64$. As in the previous case, if a higher friction is used, the mass stops before reaching its equilibrium position and if less friction is used the mass continues to oscillate after reaching its equilibrium for the first time. For simplicity, the result shown in Figure 4.7 is only for the case of $\hat{F} = 0.64$.

Finally, if $x_i \dot{x}_i = 0$, the calculation depends on which parameter is zero at time T_p, either x_i, $\dot{x}_i$ or both of them. If both of them are zero, no further action is needed because the mass has already stopped at the equilibrium. If $\dot{x}_i$ is zero, equation (4.13) is reduced to

$$F = \left| \frac{1}{2} k x_i \right| \tag{4.16}$$

Non-dimensional friction can be written in the form

$$\hat{F} = \frac{F}{mg} = \left| \frac{1}{2} y_i \right| \tag{4.17}$$

On the other hand, if x_i is equal to zero, equation (4.8) can be simplified to

$$\frac{1}{2} m\dot{x}_i^2 = \frac{1}{2} kx_{max}^2 + \left| Fx_{max} \right| \tag{4.18}$$

Setting $x_{max} = \frac{2F}{k}$ in equation (4.18) yields

$$F = \left| \sqrt{\frac{km}{8}} \dot{x}_i \right| \tag{4.19}$$

This can be written in terms of the non-dimensional friction as

$$\hat{F} = \frac{F}{mg} = \left| \sqrt{\frac{1}{8}} y_i' \right| \tag{4.20}$$

In order to validate the case $x_i \dot{x}_i = 0$, four simulations are presented. For the first and second simulation, the initial velocity is set to zero and the initial displacement is set to be positive and negative, $y_i = 1$ and $y_i = -1$. The calculated non-dimensional friction for both cases is $\hat{F} = 0.5$. For the third and fourth simulation, the initial displacement is set to zero and the initial velocity is set to be positive and negative, $y_i' = 1$ and $y_i' = -1$. The calculated non-dimensional friction for both cases is $\hat{F} = \sqrt{\frac{1}{8}}$. The result from the simulations is shown in Figure 4.8. For all of the cases, the mass returns to its equilibrium in the shortest possible time without further vibration and the mass does not stop before reaching its equilibrium position.

4.3 Friction applied to the secondary mass

After understanding the single degree freedom system behaviour, with the mass in direct contact with the friction interface, the study moves towards understanding a system where the primary targeted mass is not in direct contact with the sliding friction interface. The model chosen is shown in Figure 4.9, where the mass is connected to a second spring and then the other end of the second spring is in contact with a friction interface. This model is the starting point before introducing a second mass at the location of the sliding interface, which is the actual model of the proposed shock isolation system.

The equations of motion are given by

$$\begin{aligned} m_1\ddot{x}_1 + k_1 x_1 + k_2(x_1 - x_2) &= 0 \\ k_2(x_1 - x_2) - F\,\mathrm{sgn}(\dot{x}_2) &= 0 \end{aligned} \tag{4.21}$$

The equations of motion can be combined and reduced to

$$\begin{aligned} x_2 &= \frac{(m_1\ddot{x}_1 + k_1 x_1 + k_2 x_1)}{k_2} \\ m_1\ddot{x}_1 + k_1 x_1 + F\,\mathrm{sgn}&\left(\frac{m_1\dddot{x}_1 + (k_1 + k_2)\dot{x}_1}{k_2}\right) = 0 \end{aligned} \tag{4.22}$$

It is complicated to put this equation of motion into a state space representation for a numerical solution. This is because the third derivative of x_1 exists inside the sign function. The solution to this problem is to introduce a very small mass at the location of the sliding interface. In this case, the mass ratio μ is chosen equal to 0.001 or the secondary mass is just one thousandth of the primary mass. The result should be similar in behaviour to the result without any mass.

The purpose of this model is to see the effect of friction when it is not in direct contact with the primary mass. Moreover, it is easier to study because the parameters needed reduce to only the stiffness ratio and friction. Therefore, few parameters need to be varied to see the effect. The results of the simulation are given in Figure 4.10 for the mass response for the case of a soft secondary spring $\hat{k} = 0.4$ subjected to low friction, $\hat{F} = 0.1$ and high friction, $\hat{F} = 10$. For the purpose of the simulations, both the mass and point of contact have been displaced with an initial displacement $y_i = 1$ before being released.

Based on the parameters chosen, $\mu = 0.001$ and $\hat{k} = 0.4$, the frequency ratio $\hat{\omega}$ is equal to 20. This can be observed from Figure 4.10 (i) where the contact point with the friction interface oscillates at about 20 times of the primary mass oscillation. By decreasing the mass ratio μ or the size of the secondary mass, the frequency ratio will be increased. The action will cause the contact point with the friction interface oscillating at a higher frequency.

For low friction, the point of contact with the friction interface mainly slides as the motion progresses and only sometimes sticks to the friction interface. During this stick-slip motion,

the amplitude of vibration reduces for both the point of contact and the mass. Then, when the point of contact stops moving, the mass still moves with a small amplitude without damping. A quite similar behaviour can be seen in the case when the friction is high. It can be observed that the point of contact does not move at all from the beginning of the free vibration phase and the mass moves with an amplitude based on the initial conditions without damping. It can be concluded that for the case of a soft secondary spring, the point of contact with the friction interface stops moving before all of the energy in the system is dissipated. As a result, there is still energy remaining in the system and the mass oscillates with a small amplitude.

This serves to illustrate extreme cases to be taken as the benchmark for the system behaviour corresponding to the case of high friction. There are two extreme cases. They are the case when there is no friction and the case when there is high friction. These are the only two cases when this nonlinear system acts and behaves like a linear system. When there is no friction, the system behaves like a linear undamped single degree of freedom system that oscillates on the primary spring if there is no attached mass at the end of the secondary spring. The equation of motion of the mass when friction is zero is

$$m_1\ddot{x}_1 + k_1 x_1 = 0 \tag{4.23}$$

If there is a secondary mass at the end of the secondary spring, the system behaves like a linear undamped two degree of freedom system, see Figure 4.11.

When the friction is very high, the point of contact is locked due to the friction interface and the primary targeted mass oscillates on a combined stiffness of $k_1 + k_2$. In this latter case, the primary targeted mass behaves like a linear undamped single degree of freedom system, see Figure 4.11(c). The equation of motion for this system is

$$\begin{aligned} &m_1\ddot{x}_1 + (k_1 + k_2)x_1 = 0 \\ &\ddot{x}_1 = \omega_L{}^2 x_1 \end{aligned} \tag{4.24}$$

In this case, the system will oscillate harmonically with a natural frequency due to the combined stiffness of $k_1 + k_2$.It is called the locked frequency, because in this case the second mass is held stationary due to the friction and is given by

$$\omega_L{}^2 = \sqrt{\frac{k_1 + k_2}{m_1}} \tag{4.25}$$

This locked frequency will also become the frequency of oscillation for the primary targeted mass when the point of contact is locked and stops moving before the mass stops. This could happen for the case when the secondary spring is comparable in stiffness to the first spring. What happens after the point of contact is locked is that the primary mass will oscillate forever at the locked frequency, because there is no further dissipation.

These are limiting situations. On the other hand, when the friction is in the middle of the range between no friction and very high friction, the behaviour of the system will generally be nonlinear. The dynamic behaviour will depend on the other parameters as well, such as the stiffness ratio, or if a secondary mass is introduced at the point of contact it is also dependent upon the frequency ratio or equivalently the mass ratio.

Figure 4.12 shows the response of a single degree of freedom system incorporating friction which is not directly applied to the mass for the case of a stiff secondary spring $\hat{k} = 4000$ subjected to low friction $\hat{F} = 0.1$ and high friction $\hat{F} = 10$. As in the case of a soft secondary spring, the mass and point of contact had been displaced with initial displacement $y_i = 1$ before being released. For the case of high secondary spring stiffness with applied friction, the system behaves in a similar manner as a single degree freedom system subjected to friction. As stated before, there is a linear decrement of $2x_{st}$ for every half cycle which results in a decrement of $4x_{st}$ for every cycle of oscillation. The mass finally stops in the displacement range $-x_{st} \le x \le x_{st}$. In this case, the mass follow the same motion as the point of contact and the mass stops at the same time as the point of contact with the friction interface.

4.4 Residual response of a two degree of freedom system incorporating friction

4.4.1 Introducing a secondary mass at the end of the secondary spring

In this section, a small secondary mass is applied at the end of the secondary spring where the friction is applied. Consider such a system with two masses as shown in Figure 4.13. In the case of free vibration, the equations of motion of the two masses are

$$
\begin{aligned}
m_1\ddot{x}_1 + k_1x_1 + k_2(x_1 - x_2) &= 0 \\
m_2\ddot{x}_2 - k_2(x_1 - x_2) + F\,\mathrm{sgn}(\dot{x}_2) &= 0
\end{aligned}
\tag{4.26}
$$

where $\omega_1 = \sqrt{\frac{k_1}{m_1}}$ and $\omega_2 = \sqrt{\frac{k_2}{m_2}}$ are the natural frequencies of the uncoupled primary system and secondary system respectively. Non-dimensional parameters can be defined in terms of the system parameters as non-dimensional displacements, $y_1 = \frac{\omega_1^2 x_1}{g}$, $y_2 = \frac{\omega_1^2 x_2}{g}$, frequency ratio, $\hat{\omega} = \frac{\omega_2}{\omega_1}$, mass ratio $\mu = \frac{m_2}{m_1}$, stiffness ratio $\hat{k} = \frac{k_2}{k_1}$, non-dimensional friction $\hat{F} = \frac{F}{m_1 g}$, non-dimensional time $\tau = \omega_1 t$ and differentiation with respect to non-dimensional time $\odot' = \frac{d\odot}{d\tau}$.

The equations of motion given in equation (4.26) can subsequently be written in non-dimensional form as

$$
\begin{aligned}
y_1'' + y_1 + \hat{k}(y_1 - y_2) &= 0 \\
\mu y_2'' + \hat{k}(y_2 - y_1) + \hat{F}\,\mathrm{sgn}(y_2') &= 0
\end{aligned}
\tag{4.27}
$$

As in the previous simulations, the equations are solved using ODE solvers in MATLAB. Four cases are investigated to understand the behaviour of a two degree of freedom system configuration with Coulomb friction under free vibration, namely the case of a soft secondary spring with low frequency ratio $\hat{k} = 0.001$, $\hat{\omega} = 0.1$ and $\mu = 0.1$, the case when the frequency ratio is equal to unity with a small secondary mass $\hat{k} = 0.01$, $\hat{\omega} = 1$ and $\mu = 0.01$, the case when the frequency ratio is equal to unity with a large secondary mass $\hat{k} = 1$, $\hat{\omega} = 1$ and $\mu = 1$ and the case of a high secondary spring stiffness with a high frequency ratio $\hat{k} = 1000$, $\hat{\omega} = 100$ and $\mu = 0.1$.

4.4.2 The case of a soft secondary spring with a low frequency ratio

For the case of a soft secondary spring $\hat{k} = 0.001$ with a low frequency ratio $\hat{\omega} = 0.1$, Figure 4.14 is plotted for the case of no friction. Figure 4.15 is plotted for increasing values of friction $\hat{F} = 0.0002$ and $\hat{F} = 0.1$.

Generally, from all of these figures it can be observed that when the stiffness of the secondary spring is significantly lower than that of the first spring, the masses oscillate almost independently of each other. The primary mass primarily oscillates at its natural frequency and the secondary mass oscillates at its own natural frequency. For example, as presented in Figure 4.14 for the case of no friction, the primary and secondary masses oscillate with different frequencies. In this simulation, the secondary mass oscillates at its uncoupled frequency, which is ten times smaller than the primary mass uncoupled frequency.

There is a weak secondary spring between the primary and secondary masses. Although the primary mass is displaced, the secondary mass will not move at all if there is no imposed displacement on the second mass. The same thing occurs to the primary mass if it has no imposed displacement. It will not move when the secondary mass is initially displaced. Furthermore, when each mass is displaced it will not significantly affect the motion of the other mass. Because of the weak connection between the masses, only the secondary mass amplitude decreases with time as a result of the friction as shown in Figure 4.15(i). As the friction increases, there is only large attenuation of the second mass until at some point the second mass does not move at all. Subsequently, the primary mass will still oscillate at its natural frequency without attenuation. See Figure 4.15 (ii) for such an example.

4.4.3 The case of unity frequency ratio and a small secondary mass

A small secondary mass compared to the primary mass is chosen, i.e. $\mu = 0.01$. The size of mass is not varied for the case of a low and high stiffness of the secondary spring, because there is no significant difference associated with a variation in the mass ratio.

When the frequency ratio is unity and the secondary mass is small a beating phenomenon occurs. Beating is an interference of two signals of slightly different frequencies. In the case when the frequency ratio is unity, the two natural frequencies of the coupled system

are very close together. For a small mass ratio, for example 0.01, this phenomenon occurs. It is a periodic variation of a sine wave whose amplitude is modulated.

$$\sin\left(\omega_{c1}t\right)+\sin\left(\omega_{c2}t\right)=2\cos\left(\frac{\omega_{c1}-\omega_{c2}}{2}t\right)\sin\left(\frac{\omega_{c1}+\omega_{c2}}{2}t\right) \tag{4.28}$$

When the two natural frequencies of the combined system are very close together, $\omega_{c1}\approx\omega_{c2}$ the system response has the form of a modulated sinusoidal signal where there are maxima and minima as a function of time. The modulation is governed by the beat frequency $f_{beat}=\frac{f_{c1}-f_{c2}}{2}$ where $f_{c1}=\frac{\omega_{c1}}{2\pi}$ and $f_{c2}=\frac{\omega_{c2}}{2\pi}$ are the natural frequencies of the system in cycles per second (Hz). This phenomenon can be observed in Figure 4.16 for the case of no friction.

For further analysis, instead of only looking at the response of the system in terms of the displacement and velocity response, the energy in the system is also considered. The energy calculation is very important to determine the energy flow in the system and understand the dynamic behaviour of this system. The energy quantity calculated is normalized with respect to the initial energy in the system. The expectation is to obtain energy reduction by friction dissipation. The equations for the energy ratios are

$$\begin{aligned}
\frac{E_1}{E_{initial}}&=\frac{\frac{1}{2}\dot{x}_1^{\,2}+\frac{1}{2}\omega_1^{\,2}x_1^{\,2}}{\frac{1}{2}\omega_1^{\,2}x_i^{\,2}}\\
\frac{E_2}{E_{initial}}&=\frac{\frac{1}{2}\mu\dot{x}_2^{\,2}+\frac{1}{2}\omega_2^{\,2}\mu(x_1-x_2)^2}{\frac{1}{2}\omega_1^{\,2}x_i^{\,2}}\\
\frac{E_{total}}{E_{initial}}&=\frac{E_1+E_2}{E_{initial}}
\end{aligned} \tag{4.29}$$

For the simulations, both masses are given the same initial displacement before they are released. Therefore, the initial energy $E_{initial}$ only comes from the contribution of the potential energy in the primary spring. There is no kinetic energy from both masses since they are not given an initial velocity and there is no potential energy from the secondary spring.

Figure 4.17 shows the total energy in the system as the motion progresses for the case of no friction. In terms of energy, there will be oscillation of energy from the primary system to the secondary system and back to the primary system. There is an enveloped oscillation of both systems in Figure 4.16. The enveloping displacement and velocity is at its peak at the moment when the energy is at its peak in either the primary or secondary system. This can be observed from comparison of Figures 4.16 and 4.17. Moreover when the energy is at its peak in the primary system, the energy in the secondary system is zero and when the energy is at its peak in the secondary system the energy in the primary system is zero. The total energy for the whole system is constant and the same as the initial energy in the case of no friction as shown in Figure 4.17. This is because no energy is dissipated since there is no friction applied.

However, when friction is in place, the amplitude of the total energy of the system decreases as time progresses. Figure 4.18 shows the displacement, velocity and phase plane plots of the system for the case of $\hat{F} = 0.0025$. Figure 4.19 shows the total energy in the system for this case as the motion progresses. Based on the figures, it can be seen that the amplitude of the envelope of the displacement and velocity decreases with time. When the total energy of both systems is plotted, it is observed that the total energy decreases with time. However, the total energy is not reduced to zero for the whole system. The primary mass still oscillates with a small amplitude after the secondary mass comes to rest. Therefore, the primary system again behaves like a single degree of freedom undamped system and there is no further dissipation of the remaining energy in the system after the secondary mass is locked. In this case, the first mass will be attached to the combined stiffness of $k_1 + k_2$ and will continue oscillating at the locked frequency given by equation(4.25).

4.4.4 The case of unity frequency ratio and a large secondary mass

In this case, a mass ratio $\mu = 1$ is used where the secondary mass is as large as the primary mass. In changing the mass ratio, the stiffness ratio is also changed to $\hat{k} = 1$.

For this case, when the secondary mass is large, there will be no enveloped signal as in the previous case. As the difference between the two natural frequencies becomes large, the modulation frequency becomes large compared to the oscillation frequency. When this happens, the interference of the two waves will not cause a periodic variation of the sine

wave as before. Moreover, it will cause a distortion of the combined response of the system. The response in this case is not periodic. It happens for a mass ratio equal to 0.1 and 1 for a frequency ratio equal to 1; see Figure 4.20. The motion is caused by the addition of two incommensurate natural frequencies of the system. It is called quasi-periodic motion [62]. Fourier analysis (MATLAB code given in [63]) demonstrates that the response signal is composed of two frequencies as shown in Figure 4.21. After analyzing the frequency content using a Fourier Transform, the complicated output signal from the response of a system with unity frequency ratio and a large secondary mass, in this case mass ratio $\mu = 1$, is composed of two distinct frequencies. These frequencies can be analyzed into two independent periodic motions [64].

Although the response is not periodic, there is still an interchange of energy between the primary and secondary masses as in the previous case. When the energy is maximum in the primary system, the secondary system will have minimum energy and vice versa. For the case of no friction, the amplitude of the total energy is constant and the same as the initial energy and Figure 4.22 displays this case.

When there is friction, and as it gets larger, it provides significant dissipation to the whole system. Figures 4.23 and 4.24 provide numerical results of the displacement, velocity and energy plots for such a case. The total energy reduces rapidly but the energy in the whole system is not reduced to zero. As in the previous cases, when the secondary mass stops moving, because the restoring force in the secondary spring does not have sufficient magnitude to overcome friction, the primary system will still continue to oscillate with a small amplitude. Subsequently there is no dissipation provided to the primary mass since the secondary mass is locked.

4.4.5 The case of a high secondary spring stiffness

The last case studied is the case when the secondary spring is significantly stiffer than the primary spring. When the frequency ratio and stiffness ratio are high, the two masses are almost connected by a rigid link and most likely to move as a single body. The frequency can be calculated using

$$\omega_1 = \sqrt{\frac{k_1}{m_1 + m_2}} = \sqrt{\frac{k_1}{m_1(1+\mu)}} \tag{4.30}$$

Both masses have almost the same motion, especially for the case when the frequency ratio is high and the second spring is very stiff. Figures 4.25 and 4.26 display this behaviour. Figure 4.24 corresponds to the case of no friction and Figure 4.25 is plotted to see the effect of increasing the friction. In both cases, the secondary mass used is 0.1 or 10% of the size of the primary mass.

In the case of a stiff second spring, the two masses are well coupled. Increasing the second spring stiffness and therefore the coupling causes more rapid energy transfer between the oscillators [65]. Then, this energy that is transferred to the second oscillator is dissipated by the friction. The dissipation imposed on the secondary mass works very well in attenuating the response of the primary mass. Therefore, the primary mass stops at almost the same time as the secondary mass. This differs from the case where the secondary spring is quite soft or comparable to the primary spring stiffness. In these cases, the secondary mass is weakly coupled to the primary mass and the dissipation imposed on the secondary mass will cause the secondary mass to stop moving earlier than the primary mass, as the force on the secondary spring is smaller than the friction force. As stated before, after the second mass is locked, the first mass keeps moving on a combined stiffness of $k_1 + k_2$.

For the case of a stiff secondary spring, it can be observed that the size of the secondary mass does not have any effect on the response of the system. For a given secondary spring stiffness and friction force, the system will behave in an identical way. Therefore, it will be better to use a small secondary mass.

4.5 Comparison between a single and a two degree of freedom system

After a separate in-depth analysis of the two systems, it is appropriate to make a comparison between the systems. The comparison outlines the advantages and disadvantages found in terms of the residual energy dissipation.

A single degree of freedom system is simpler and the rate of energy dissipation is based directly upon the choice of friction. There is a possibility that the mass could stick before it comes back to its equilibrium position if a large value of friction is used. However, it is not a significant problem since the friction value which could bring the mass back to its

equilibrium in the shortest possible of time can be calculated based on the phase of the motion at the end of the shock.

On the other hand, the two degree of freedom system behaviour is somewhat more complicated. As the parameter combinations are varied, the system behaves differently as shown earlier. For the case of a soft secondary spring and low frequency ratio, friction does not give any benefit in terms of dissipating energy. The friction only dissipates part of the total energy and locks the secondary mass while the primary mass still retains much more energy. Also, for the case of a frequency ratio equal to unity the situation is not much better. There is still remaining energy which causes the primary mass to oscillate with a small amplitude after the secondary mass is locked.

The best case is when the secondary spring stiffness is significantly higher than the primary spring. In this case, the two masses are almost connected by a rigid link and are likely to move as a single mass. The system behaves more or less like a single degree of freedom system and the primary mass stops moving at the same time as the secondary mass. It might be best to have a two degree of freedom system with an intermediate secondary spring stiffness as outlined in the previous chapters. An intermediate secondary spring stiffness is sufficient to possess the behaviour outlined above, but at the same time avoiding the discontinuities in the acceleration response as friction changes its direction.

4.6 Conclusions

The effectiveness of friction in improving the decay of the free vibration after the shock is dependent on the level of friction and also stiffness ratio for a two degree of freedom system configuration. For a single degree of freedom system, the rate of the energy dissipation is based upon the level of friction. The only problem of this configuration is that the mass might stop away from its equilibrium position. However, a strategy could be implemented to calculate the friction value that can bring the mass back to its equilibrium position in the shortest possible of time after the shock depending upon the phase of the motion at the beginning of the free vibration phase.

However, for a two degree of freedom configuration the behaviour is more complicated. It depends on the choice of parameters such as stiffness ratio, frequency ratio and mass ratio as well as friction. However, the general basic behaviour can be identified which exists for any parameter combination used. For example, the behaviour of the system after the secondary mass stops moving. From the simulations, the primary mass either continues to oscillate without further energy dissipation or completely stops at the same time as the secondary mass. The primary mass completely stops at the same time as the secondary mass only when the secondary spring is significantly stiffer than the primary spring. It does not have to be very stiff or totally rigid. An intermediate secondary spring is sufficient to closely follow this behaviour.

On the other hand, inclusion of a soft secondary spring does not work well in providing dissipation to the primary mass. A very soft spring causes the motion of the two masses to be independent, with little dissipation of the energy of the system. A small increment in the secondary stiffness is not enough. It will improve the response reduction a small amount by producing dissipation to the system. However, the secondary mass stops moving before the primary mass. From this point onwards, the primary mass continues to oscillate with a constant amplitude. The value of the secondary mass that slides is not important. If a sufficiently stiff secondary spring is used, whatever the value for the secondary mass it will not make any significant difference to the response. Therefore, a smaller secondary mass is preferred since it does not take so much space and it is easier to incorporate.

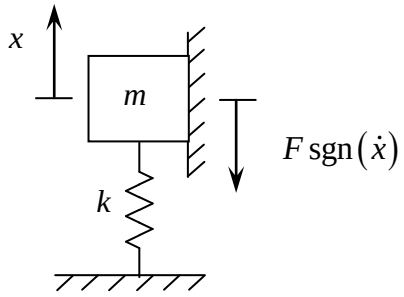

Figure 4.1: Model for the free vibration of a single degree of freedom system configuration with Coulomb friction.

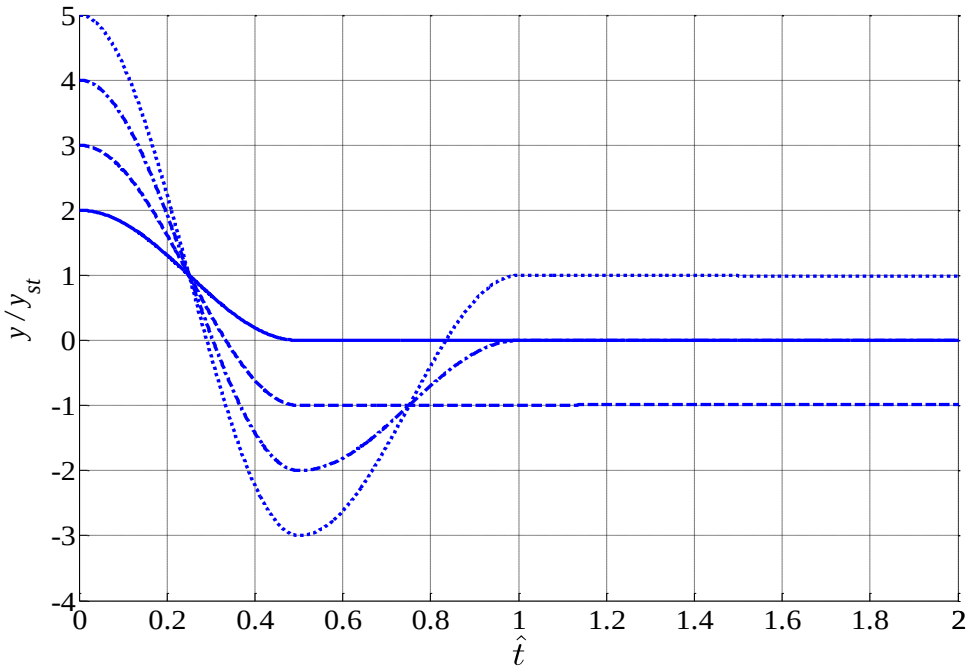

Figure 4.2: The normalized displacement response of a single degree freedom system subjected to sliding friction with different initial displacement and with zero initial velocity. Solid line: $y_i = 2y_{st}$, Dash line: $y_i = 3y_{st}$, Dash dot line: $y_i = 4y_{st}$, Dot line: $y_i = 5y_{st}$.Non dimensional time, $\hat{t} = \frac{\omega_n t}{2\pi} = \frac{\tau}{2\pi}$.

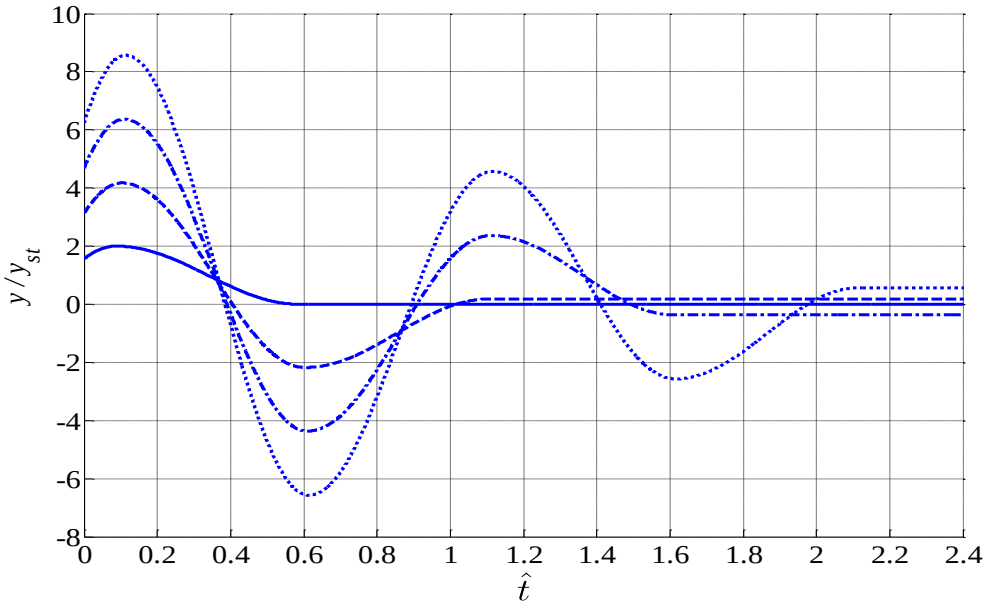

Figure 4.3: The normalized displacement response of a single degree freedom system subjected to sliding friction with positive initial displacement and velocity.

Solid line: $\hat{F}=\frac{1}{2}y_{max}$, Dash line: $\hat{F}=\frac{1}{4}y_{max}$, Dash dot line: $\hat{F}=\frac{1}{6}y_{max}$, Dot line: $y_i=\frac{1}{8}y_{max}$.Non-dimensional time, $\hat{t}=\frac{\omega_n t}{2\pi}=\frac{\tau}{2\pi}$. Initial conditions: $y_i=1, y_i'=1$.

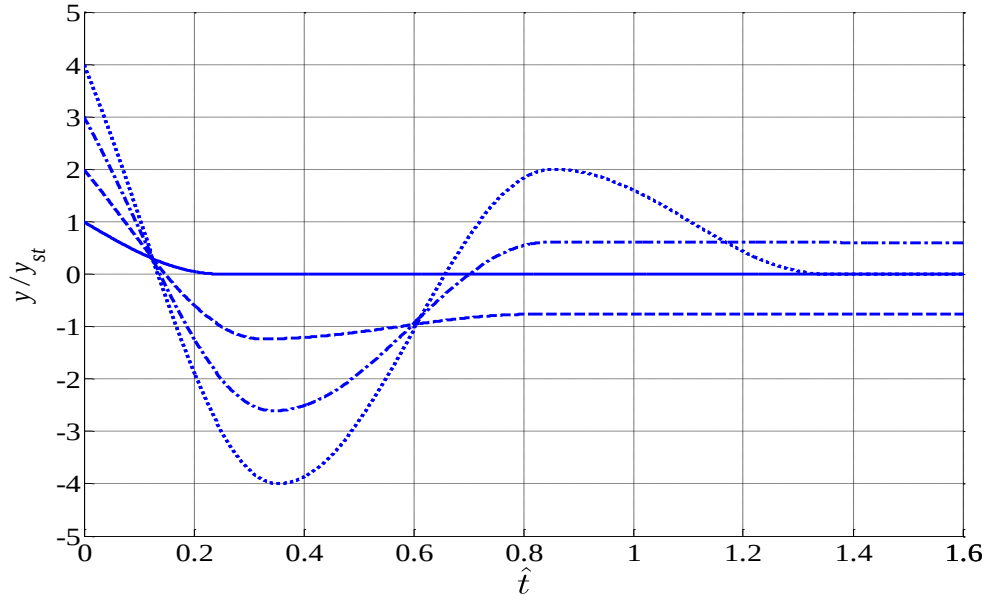

Figure 4.4 The normalized displacement response of a single degree freedom system subjected to sliding friction with positive initial displacement and negative initial velocity.

Solid line: $\hat{F}=\frac{1}{2}C_1$,Dash line: $\hat{F}=\frac{1}{4}C_1$, Dash dot line: $\hat{F}=\frac{1}{6}C_1$, Dot line: $\hat{F}=\frac{1}{8}C_1$, where $C_1=y_i+\frac{(y_i')^2}{y_i}$. Non-dimensional time, $\hat{t}=\frac{\omega_n t}{2\pi}=\frac{\tau}{2\pi}$. Initial conditions: $y_i=1$, $y_i'=-1$.

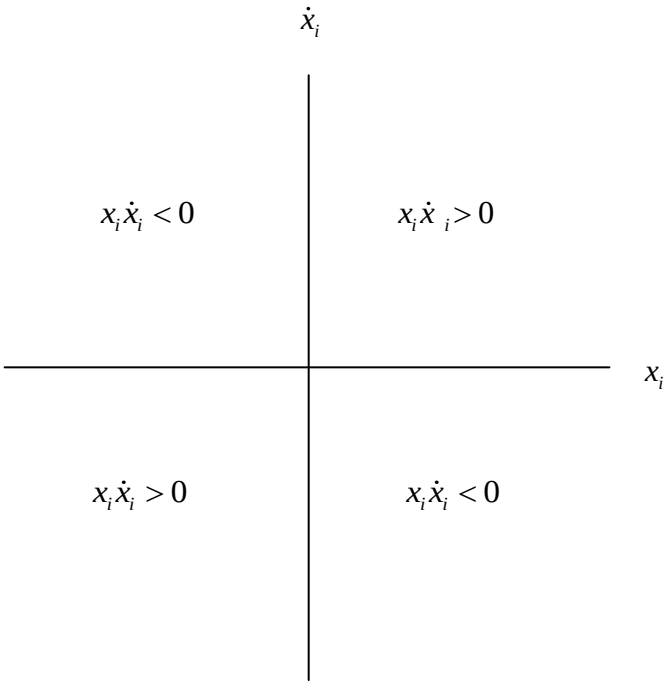

Figure 4.5: Phase plane for the regions covering the different initial conditions of the system.

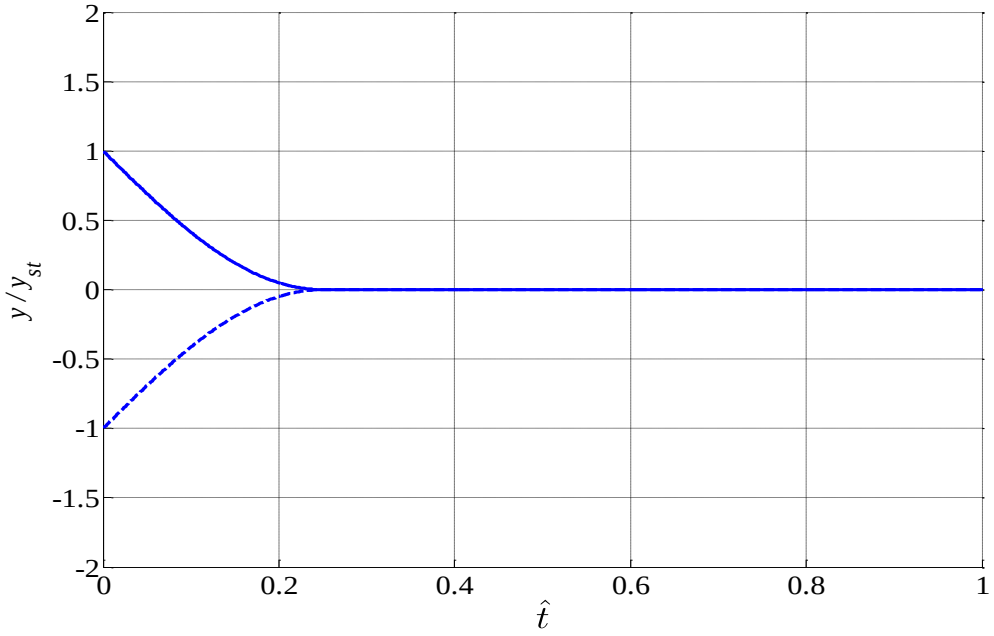

Figure 4.6: The normalized displacement response of a single degree freedom system subjected to sliding friction which is set to return the mass to its equilibrium in the shortest possible time without further vibration. Solid line: $y_i = 1, y_i' = -1$ and $\hat{F} = 1$.
Dash line: $y_i = -1, y_i' = 1$ and $\hat{F} = 1$.

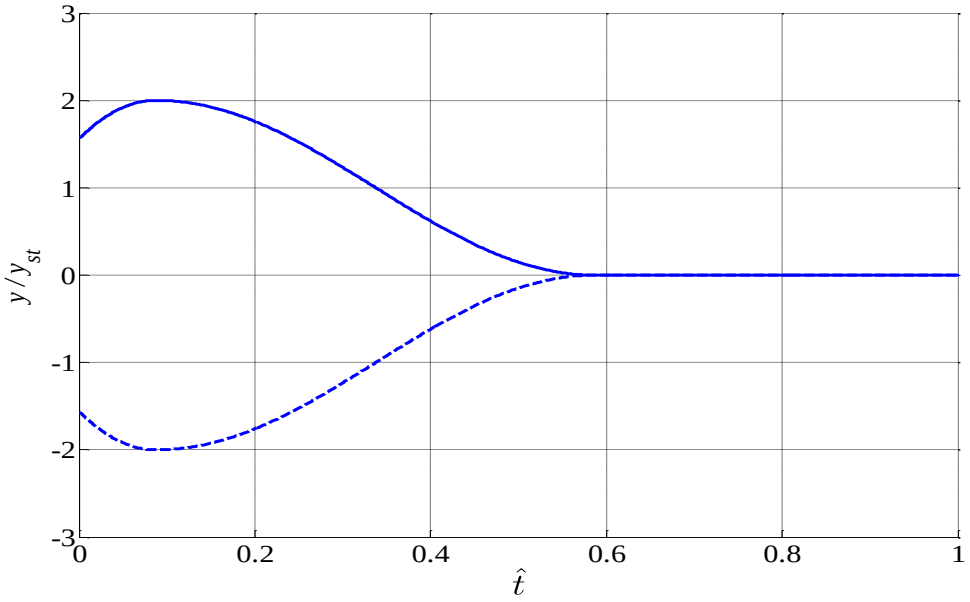

Figure 4.7: The normalized displacement response of a single degree freedom system subjected to sliding friction which is set to return the mass to its equilibrium in the shortest possible time without further vibration. Solid line: $y_i = 1, y_i' = 1$ and $\hat{F} = 0.64$. Dash line: $y_i = -1, y_i' = -1$ and $\hat{F} = 0.64$.

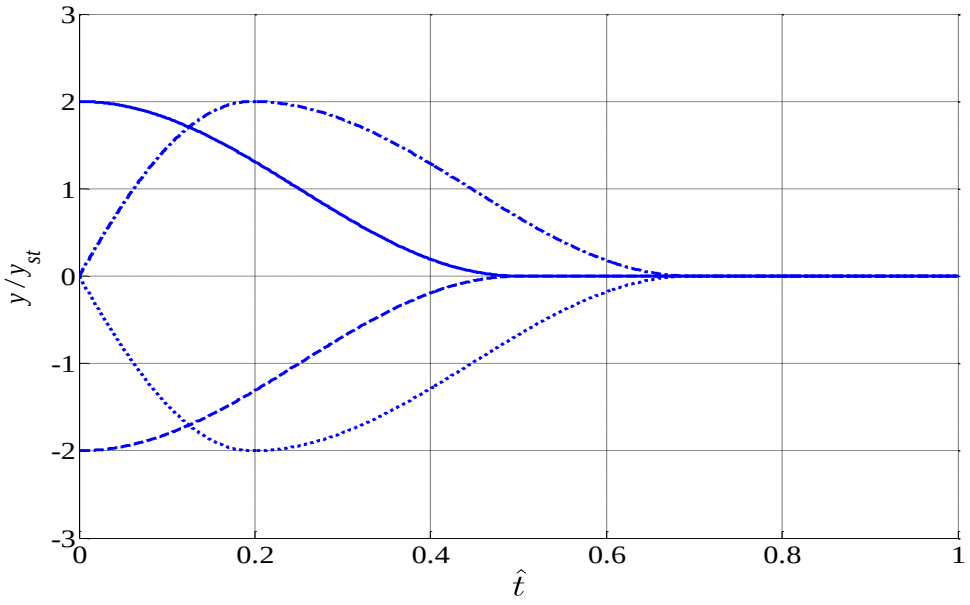

Figure 4.8: The normalized displacement response of a single degree freedom system subjected to sliding friction which is set to return the mass to its equilibrium in the shortest possible time without further vibration. Solid line: $y_i = 1, y_i' = 0$ and $\hat{F} = 0.5$. Dash line: $y_i = -1, y_i' = 0$ and $\hat{F} = 0.5$.Dash dot line: $y_i = 0, y_i' = 1$ and $\hat{F} = \sqrt{\frac{1}{8}}$. Dot line: $y_i = 0, y_i' = -1$ and $\hat{F} = \sqrt{\frac{1}{8}}$.

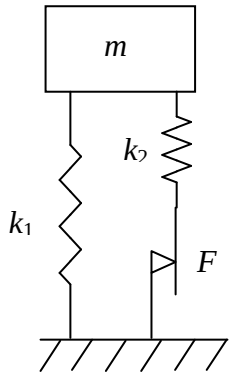

Figure 4.9: Model for the free vibration of a single degree of freedom system configuration with Coulomb friction where friction is not applied directly to the primary targeted mass.

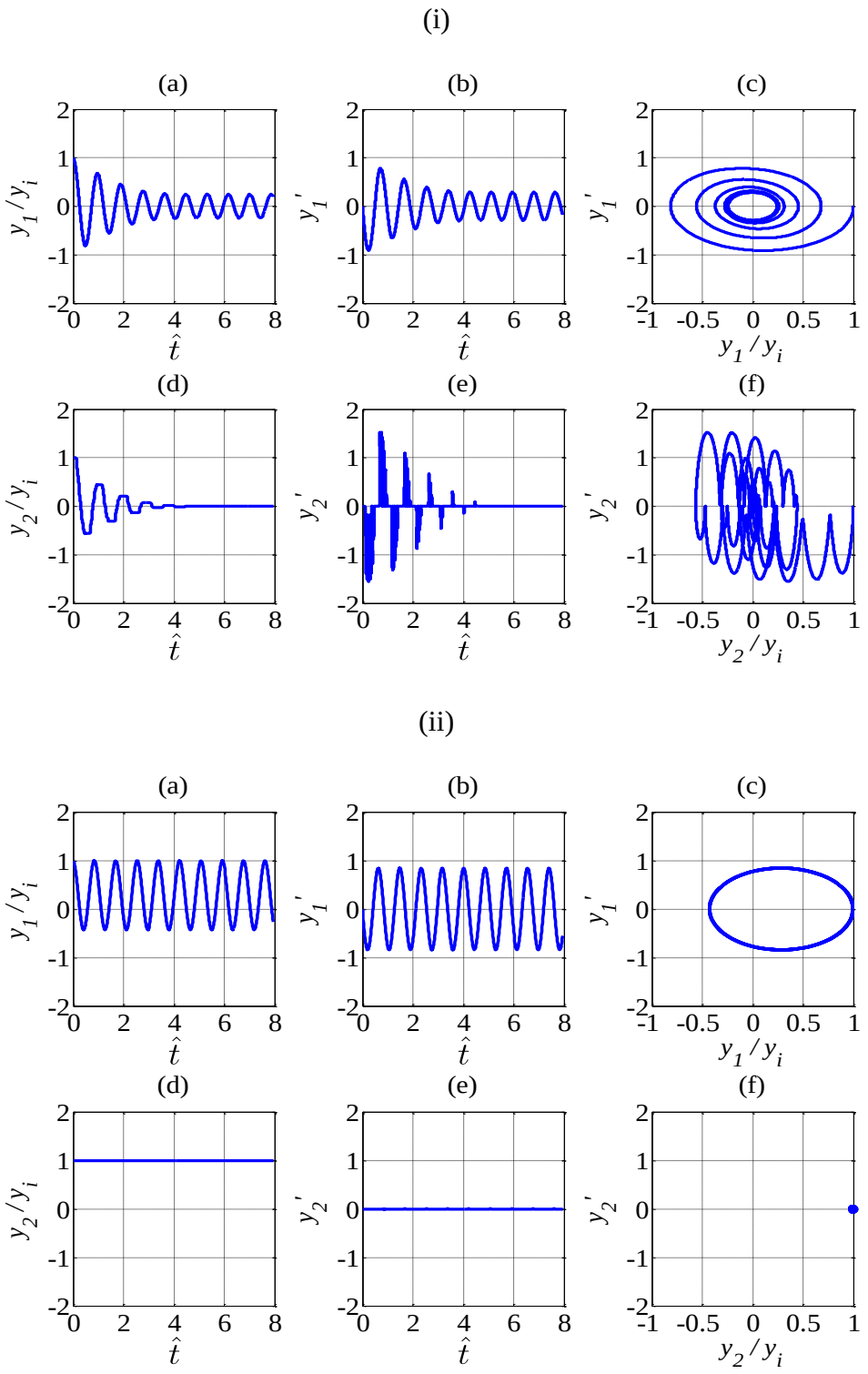

Figure 4.10: Response of a single degree of freedom system incorporating friction which is not directly applied to the mass for the case of a soft secondary spring. Stiffness ratio, $\hat{k} = 0.4$. Initial conditions: initial displacement, $y_i = 1$, initial velocity, $y_i' = 0$. (i) Low friction, $\hat{F} = 0.1$. (ii) High friction, $\hat{F} = 10$. (a) Mass displacement.(b) Mass velocity. (c) Mass response phase plane plot. (d) Friction contact point displacement. (e) Friction contact point velocity.(f) Friction contact point phase plane plot.

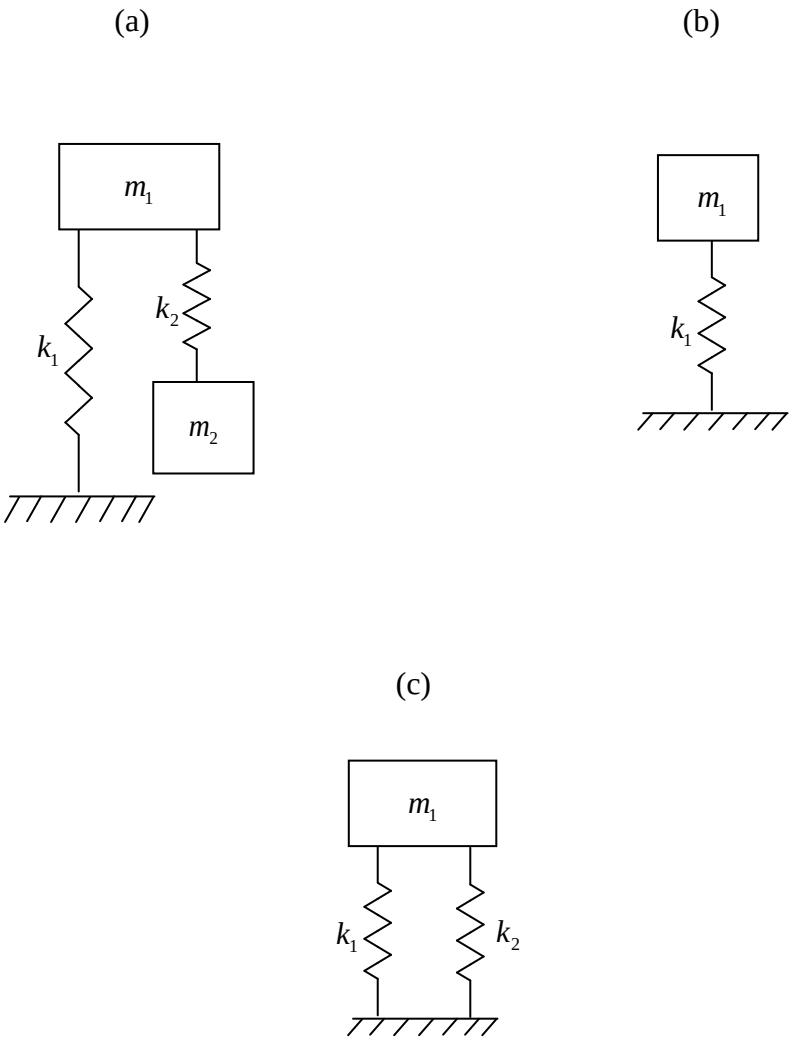

Figure 4.11: Benchmark cases for the case of no friction and high friction. (a) No friction with an attached secondary mass at the end of the secondary spring. (b) No friction with no attached secondary mass at the end of secondary spring. (c) High friction.

(i)

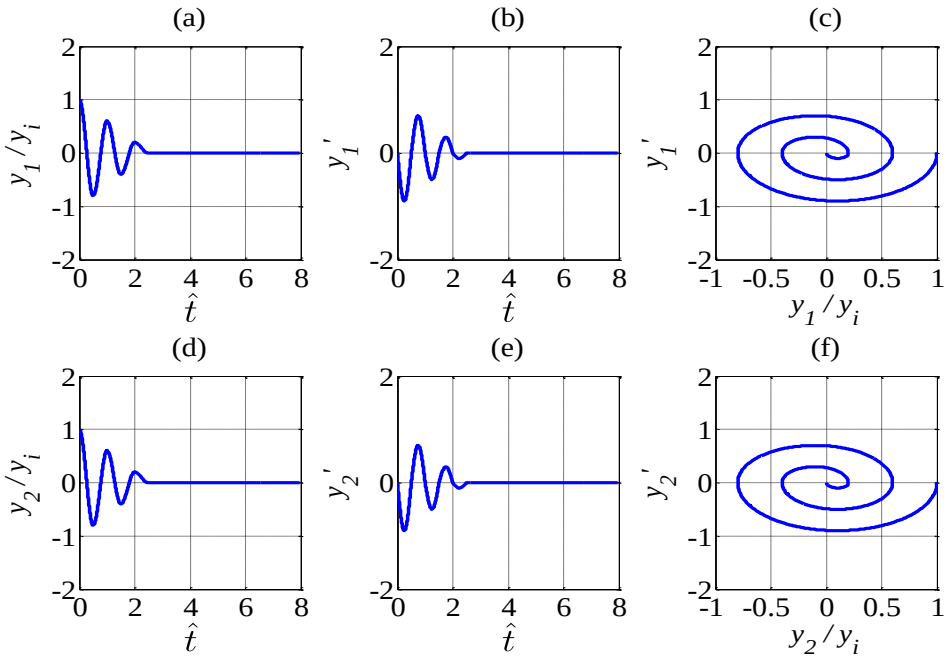

(ii)

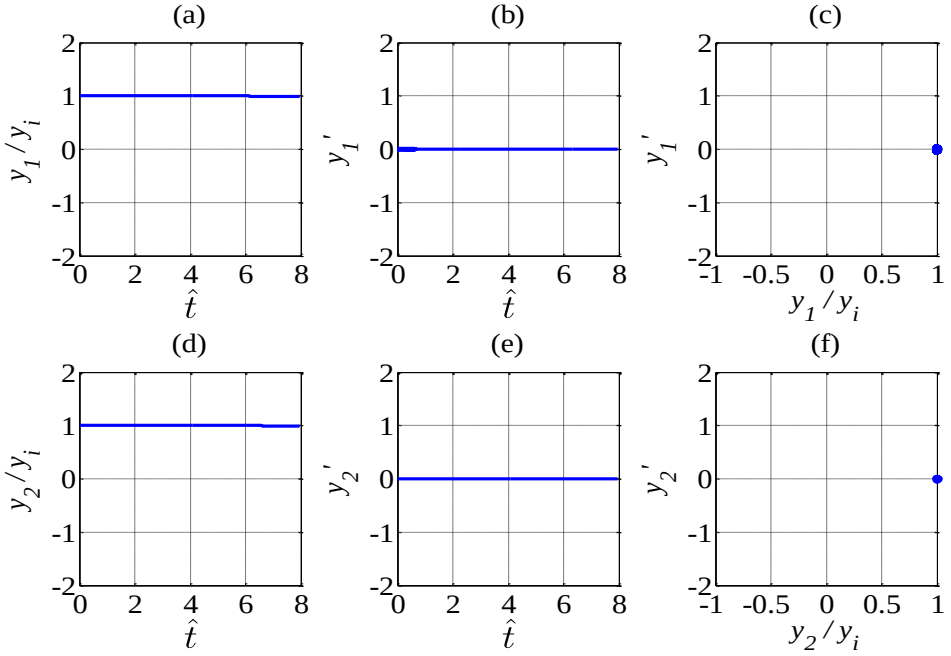

Figure 4.12: Response of a single degree of freedom system incorporating friction which is not directly applied to the mass for the case of a stiff secondary spring. Stiffness ratio, $\hat{k} = 4000$. Initial conditions: initial displacement, $y_i = 1$, initial velocity, $y_i' = 0$. (i) Low friction, $\hat{F} = 0.1$. (ii) High friction, $\hat{F} = 10$. (a) Mass displacement. (b) Mass velocity. (c) Mass phase plane plot. (d) Friction contact point displacement. (e) Friction contact point velocity. (f) Friction contact point phase plane plot.

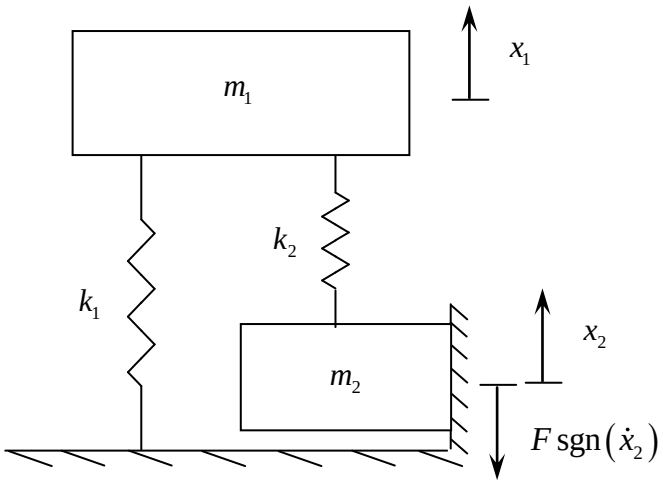

Figure 4.13: Model for the free vibration of a two degree of freedom system configuration with Coulomb friction.

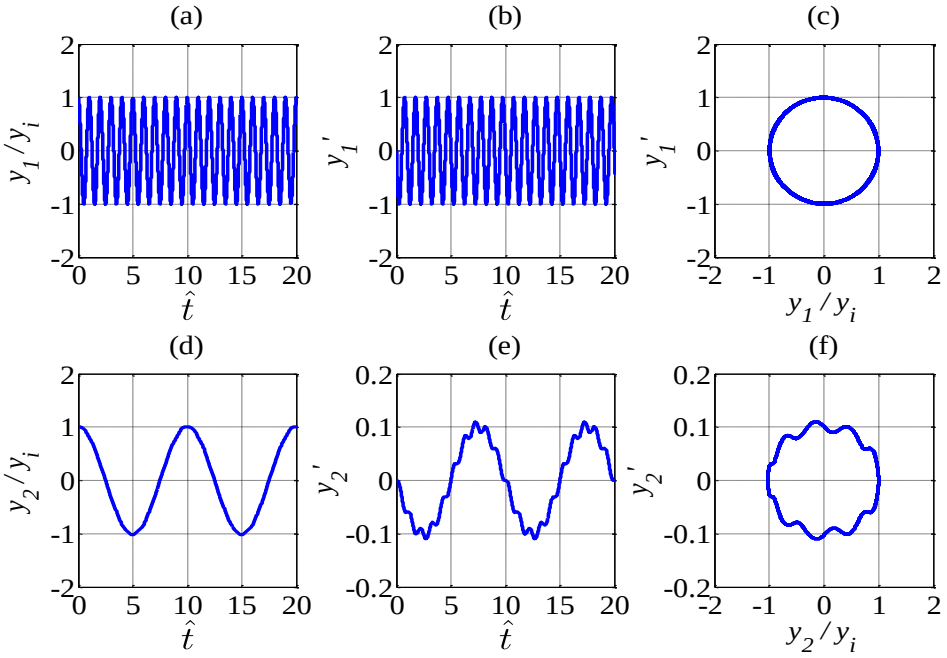

Figure 4.14: Response of a two degree of freedom system incorporating friction for the case of a soft secondary spring with low frequency ratio $\hat{\omega} = 0.1$ and no friction $\hat{F} = 0$. (a) Primary mass displacement. (b) Primary mass velocity (c) Primary mass phase plane plot. (d) Secondary mass displacement. (e) Secondary mass velocity. (f) Secondary mass phase plane plot. Stiffness ratio $\hat{k} = 0.001$, mass ratio $\mu = 0.1$.

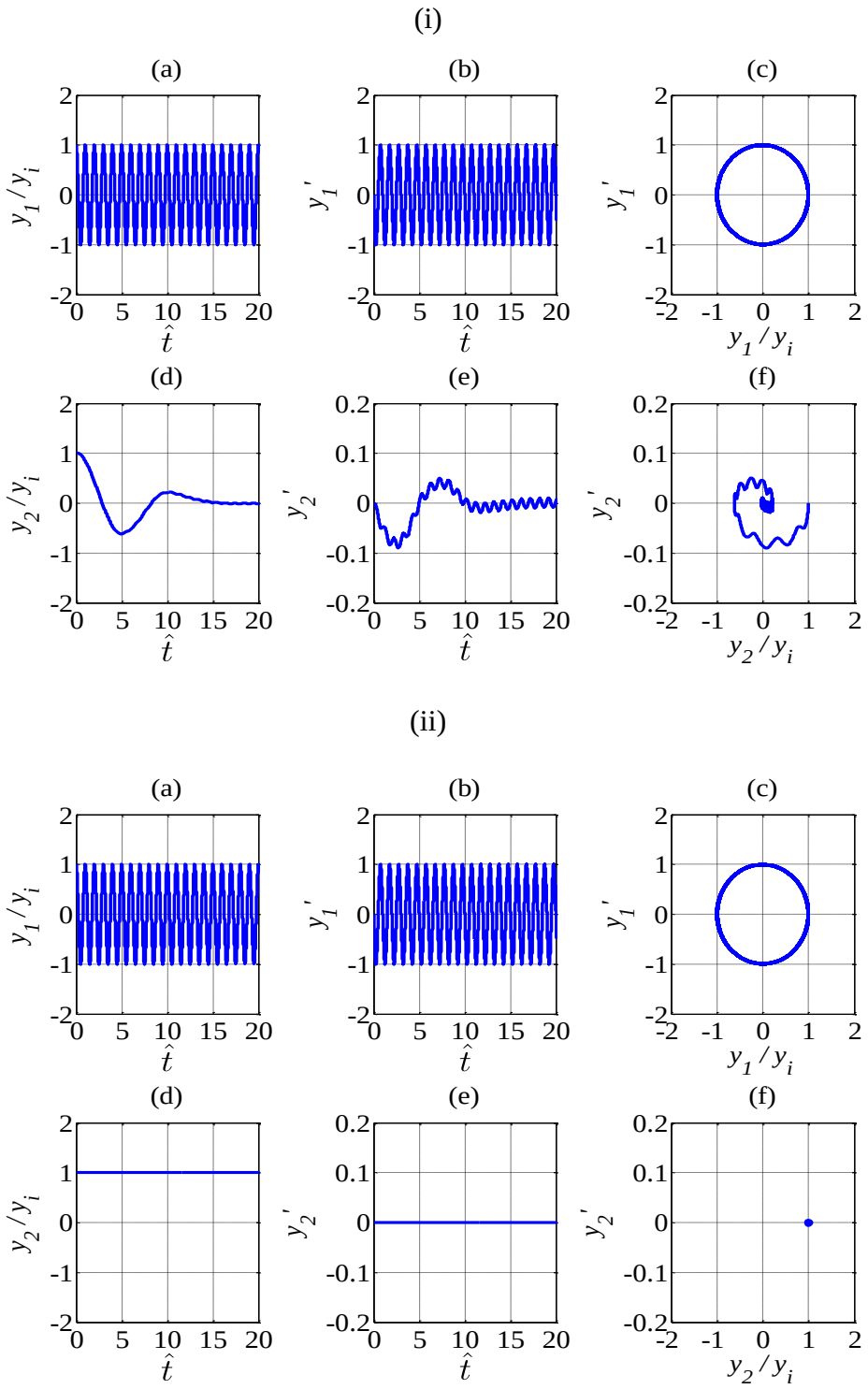

Figure 4.15: Response of a two degree of freedom system incorporating friction for the case of a soft second spring with low frequency ratio $\hat{\omega} = 0.1$ and increasing value of friction. (a) Primary mass displacement. (b) Primary mass velocity (c) Primary mass phase plane plot. (d) Secondary mass displacement. (e) Secondary mass velocity. (f) Secondary mass phase plane plot. Stiffness ratio $\hat{k} = 0.001$, mass ratio $\mu = 0.1$. (i) Non-dimensional friction $\hat{F} = 0.0002$. (ii) Non-dimensional friction $\hat{F} = 0.1$.

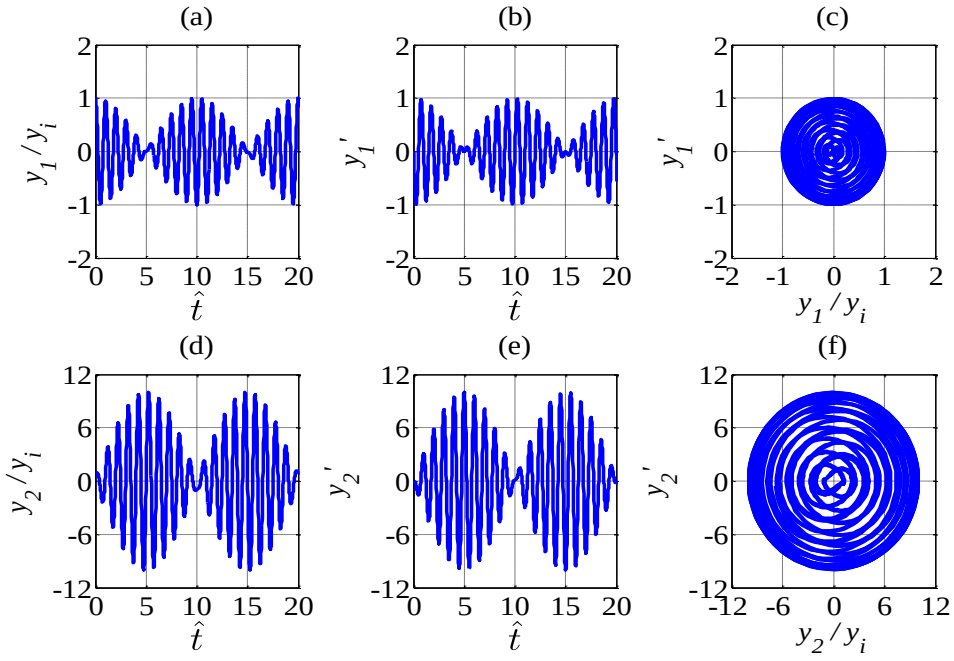

Figure 4.16: Response of a two degree of freedom system incorporating friction for the case of unity frequency ratio $\hat{\omega}=1$, a small secondary mass $\mu=0.01$ and no friction $\hat{F}=0$. (a) Primary mass displacement. (b) Primary mass velocity (c) Primary mass phase plane plot. (d) Secondary mass displacement. (e) Secondary mass velocity. (f) Secondary mass phase plane plot. Stiffness ratio $\hat{k}=0.01$.

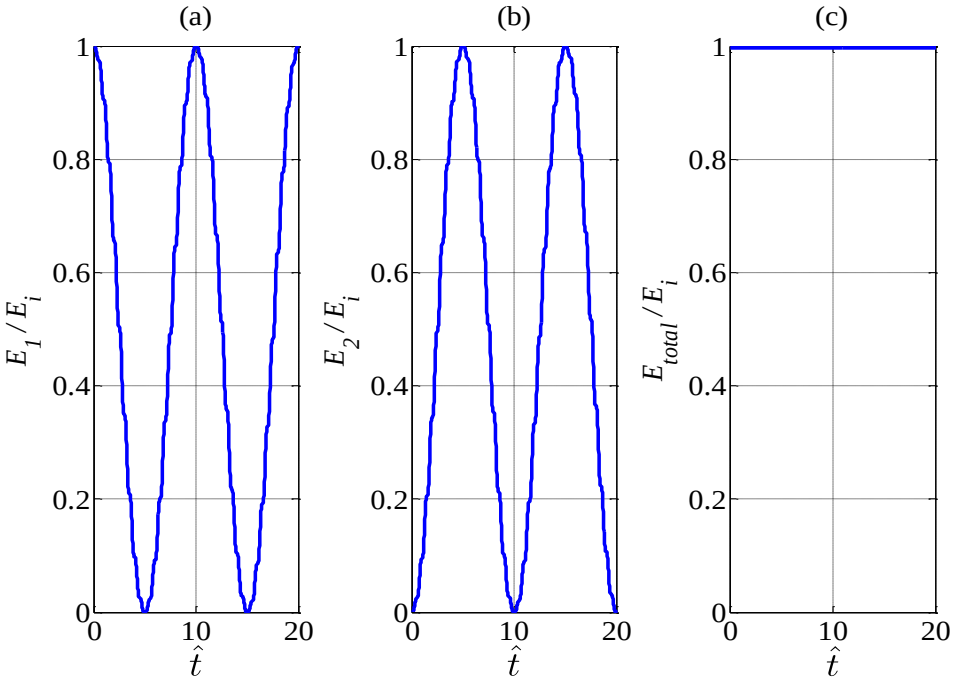

Figure 4.17: Total energy of a two degree of freedom system incorporating friction for the case of unity frequency ratio $\hat{\omega}=1$, a small secondary mass $\mu=0.01$ and no friction $\hat{F}=0$. (a) Total energy in the primary system. (b) Total energy in the secondary system. (c) Total energy in the whole coupled system. Stiffness ratio $\hat{k}=0.01$.

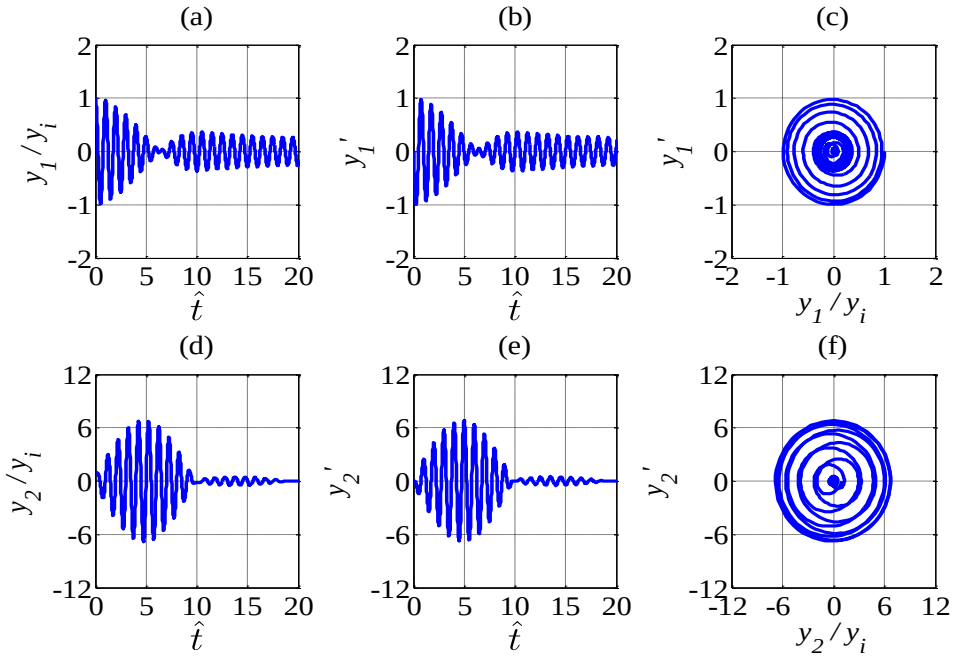

Figure 4.18: Response of a two degree of freedom system incorporating friction for the case of unity frequency ratio $\hat{\omega}=1$, a small secondary mass $\mu=0.01$ and small friction $\hat{F}=0.0025$. (a) Primary mass displacement. (b) Primary mass velocity (c) Primary mass phase plane plot. (d) Secondary mass displacement. (e) Secondary mass velocity. (f) Secondary mass phase plane plot. Stiffness ratio $\hat{k}=0.01$.

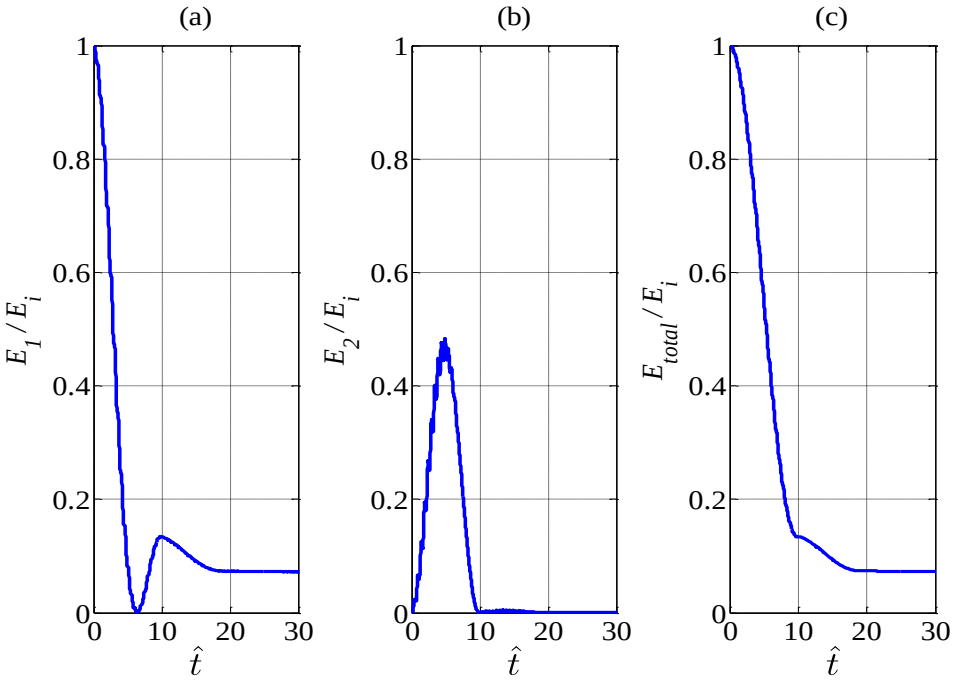

Figure 4.19: Total energy of a two degree of freedom system incorporating friction for the case of unity frequency $\hat{\omega}=1$, a small secondary mass $\mu=0.01$ and small friction $\hat{F}=0.0025$. (a) Total energy in the primary system. (b) Total energy in the secondary system. (c) Total energy in the whole coupled system. Stiffness ratio $\hat{k}=0.01$.

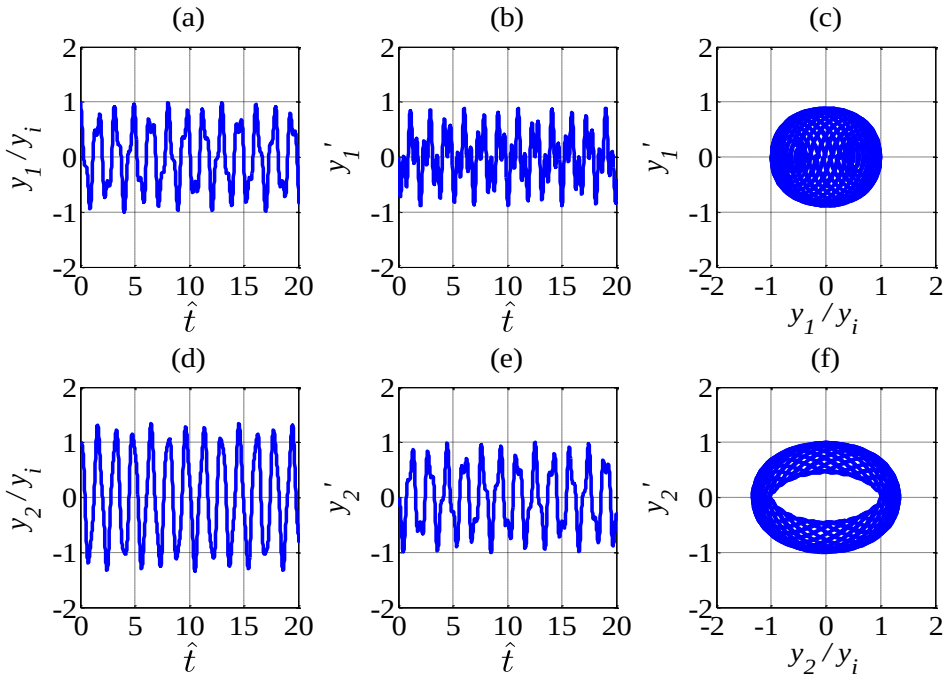

Figure 4.20: Response of a two degree of freedom system incorporating friction for the case of unity frequency ratio $\hat{\omega}=1$, a large secondary mass $\mu=1$ and no friction $\hat{F}=0$. (a) Primary mass displacement. (b) Primary mass velocity (c) Primary mass phase plane plot. (d) Secondary mass displacement. (e) Secondary mass velocity. (f) Secondary mass phase plane plot. Stiffness ratio $\hat{k}=1$.

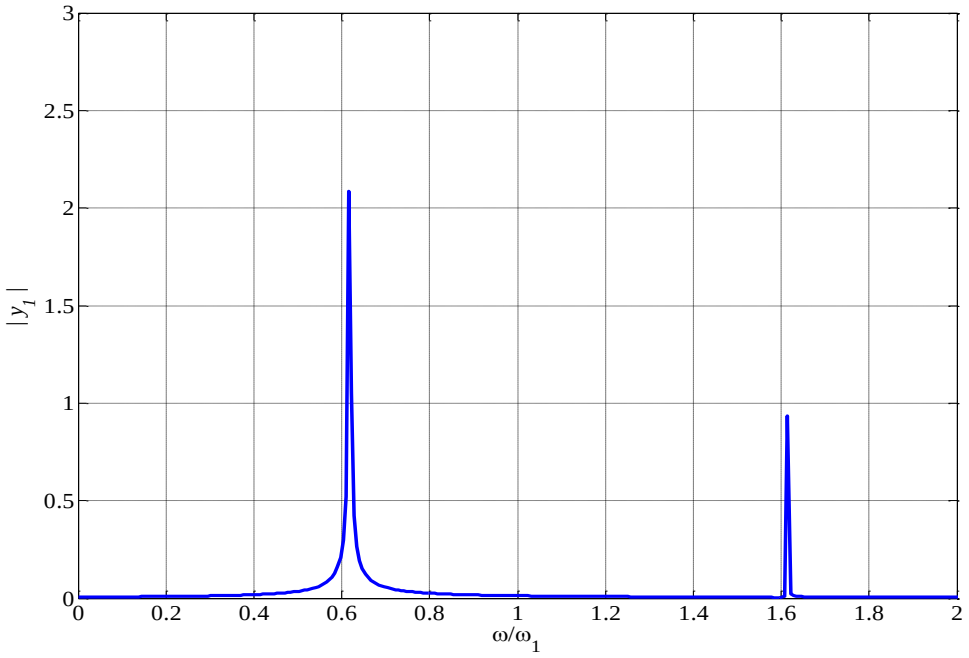

Figure 4.21: Fourier transform of the free vibration displacement signal for the system with unity frequency ratio $\hat{\omega}=1$, a large secondary mass $\mu=1$ and no friction.

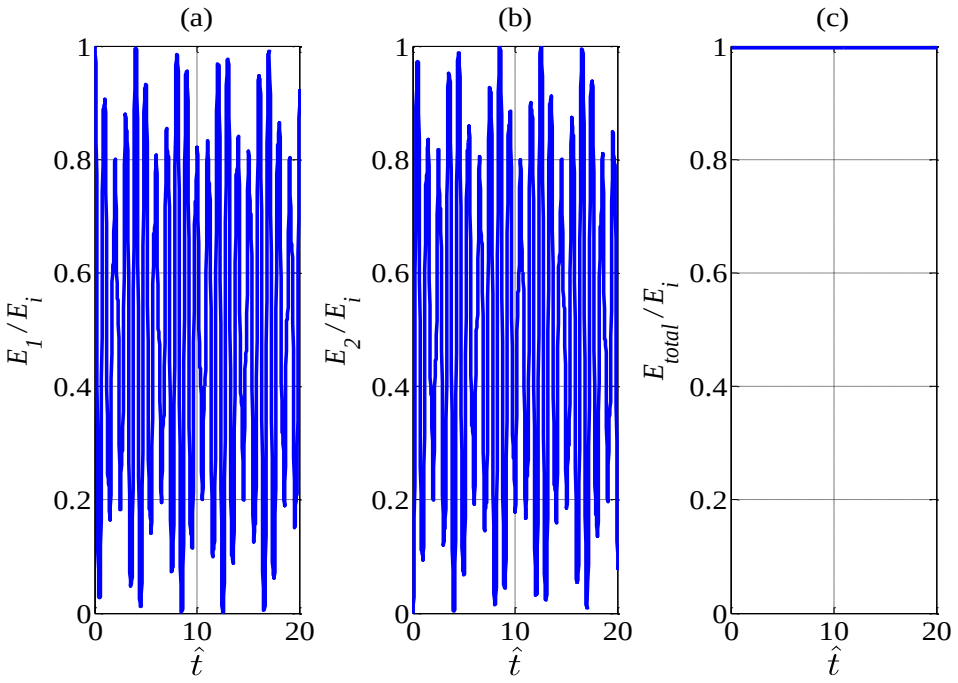

Figure 4.22: Total energy of a two degree of freedom system incorporating friction for the case of unity frequency ratio $\hat{\omega}=1$, a large secondary mass $\mu=0.1$ and no friction $\hat{F}=0$. (a) Total energy in the primary system. (b) Total energy in the secondary system. (c) Total energy in the whole coupled system. Stiffness ratio $\hat{k}=1$.

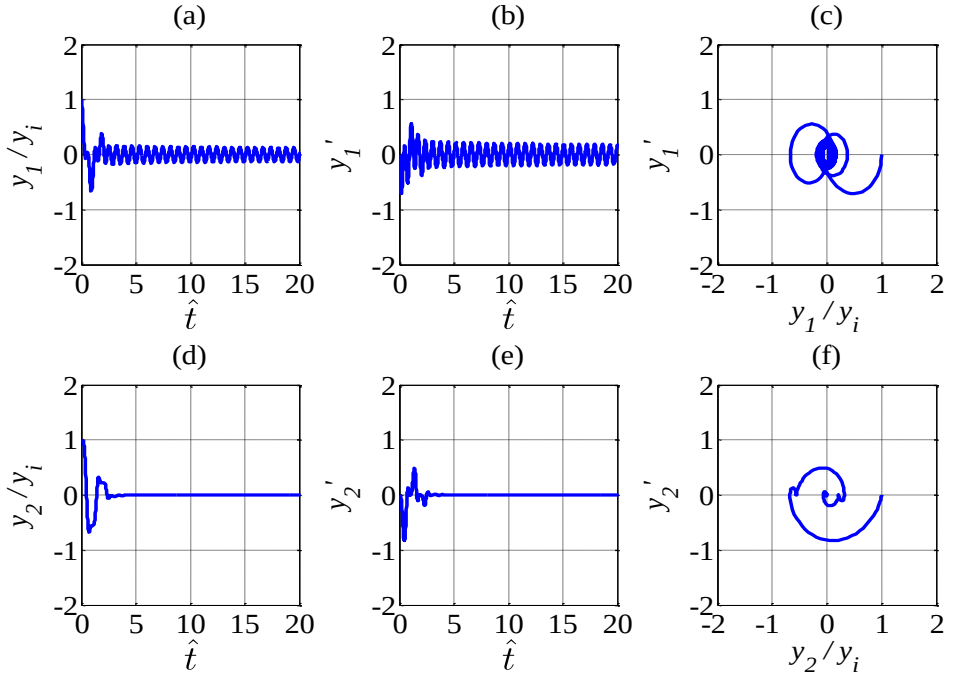

Figure 4.23: Response of a two degree of freedom system incorporating friction for the case of unity frequency ratio $\hat{\omega}=1$, a large secondary mass $\mu=1$ and small friction $\hat{F}=0.15$. (a) Primary mass displacement. (b) Primary mass velocity (c) Primary mass phase plane plot. (d) Secondary mass displacement. (e) Secondary mass velocity. (f) Secondary mass phase plane plot. Stiffness ratio $\hat{k}=1$.

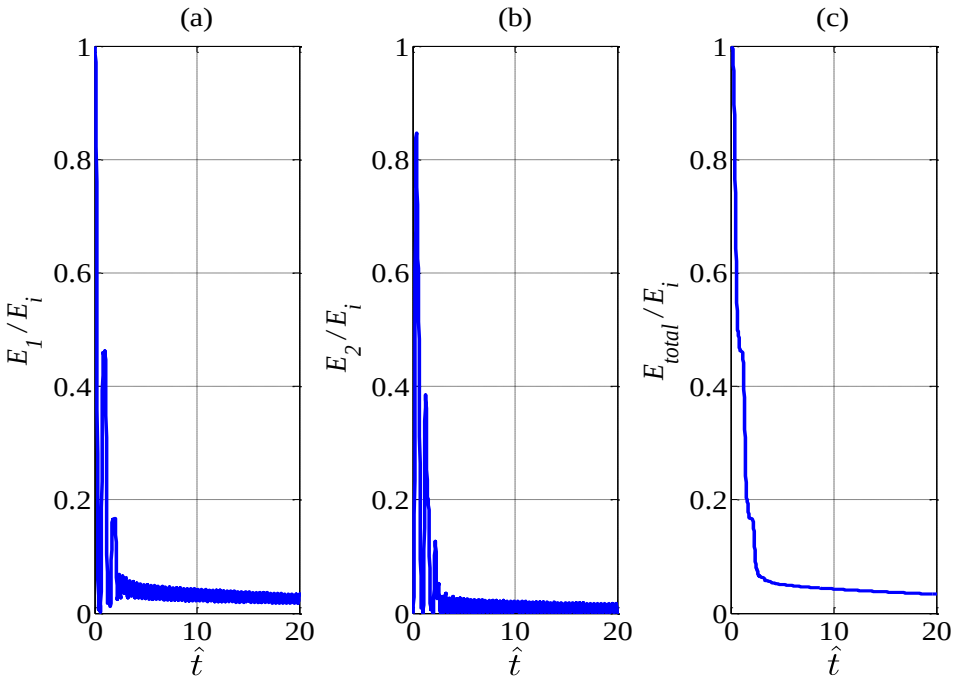

Figure 4.24: Total energy of a two degree of freedom system incorporating friction for the case of unity frequency ratio $\hat{\omega}=1$, a large secondary mass $\mu=0.1$ and small friction $\hat{F}=0.15$. (a) Total energy in the primary system. (b) Total energy in the secondary system. (c) Total energy in the whole coupled system. Stiffness ratio $\hat{k}=1$.

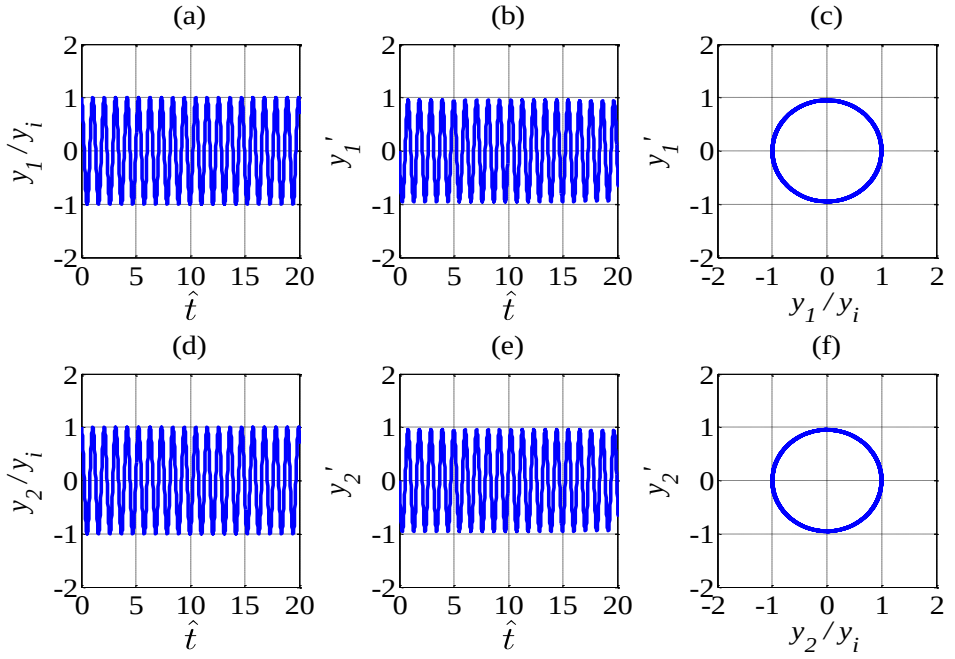

Figure 4.25: Response of a two degree of freedom system incorporating friction for the case of stiff secondary spring with high frequency ratio $\hat{\omega}=100$ and no friction $\hat{F}=0$. (a) Primary mass displacement. (b) Primary mass velocity (c) Primary mass phase plane plot.
(d) Secondary mass displacement. (e) Secondary mass velocity. (f) Secondary mass phase plane plot. Stiffness ratio $\hat{k}=1000$, mass ratio $\mu=0.1$.

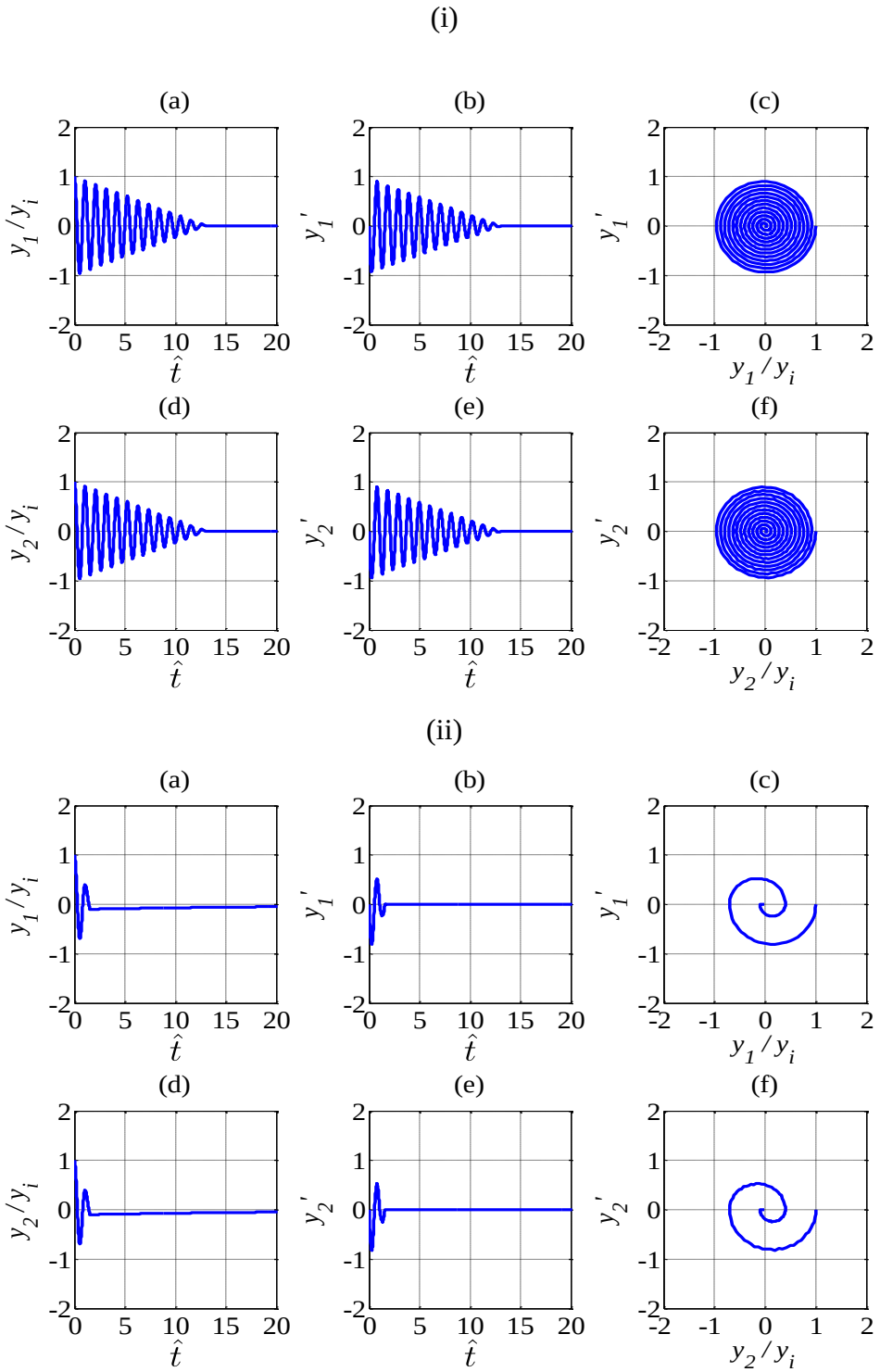

Figure 4.26: Response of a two degree of freedom system incorporating friction for the case of stiff secondary spring with high frequency ratio $\hat{\omega} = 100$ and increasing value of friction. (a) Primary mass displacement. (b) Primary mass velocity (c) Primary mass phase plane plot. (d) Secondary mass displacement. (e) Secondary mass velocity. (f) Secondary mass phase plane plot. Stiffness ratio $\hat{k} = 1000$, mass ratio $\mu = 0.1$. (i) Non-dimensional friction $\hat{F} = 0.02$. (ii) Non-dimensional friction $\hat{F} = 0.15$.

5. DESIGN AND EXPERIMENTAL VALIDATION OF A PASSIVE TWO DEGREE OF FREEDOM SYSTEM WITH FRICTION

5.1 Introduction

The main objective of this chapter is to describe the design of a test rig and its use to validate the response of a two degree of freedom system with passive friction. A T beam configuration is chosen and subsequently used during the experiment, as it can reproduce the behaviour of a two degree of freedom system at low frequencies. Initially, the rig design and the finite element (FE) model are described. Then, the beam system response is compared with a finite element (FE) model using ANSYS to ensure that for the stated frequency range, the beam configuration behaves like a two degree of freedom system which vibrates in two main modes, namely a flexural mode of the primary beam and flexural mode of the secondary beam. Furthermore, the physical properties of the two degree of freedom system, namely stiffness, damping and mass, are estimated by fitting the measured beam response to the two degree of freedom model results. Then, the friction value is also estimated by fitting the measured free vibration response with the analytical solution of the two degree of freedom system free vibration. Susbequently, the shock response of the beam system is compared to a two degree of freedom system for the model validation. Finally, a comparison is made between the beam system with a thin secondary beam and a thick secondary beam.

5.2 Description of the rig

The T beam consists of two aluminium beams, namely a primary and a secondary beam, as shown in Figure 5.1 which are connected with a bolted connection. Two different secondary beams were used during the experiment, namely a thin and thick secondary beam. The dimensions of the beam system are listed in Table 5.1. The coupled system with the thin secondary beam is expected to vibrate in two dominant modes at low frequencies and behave like a two degree of freedom system. On the other hand, the system with the thick secondary beam is expected to vibrate in one dominant mode at low frequencies and behave like a single degree of freedom system. The system with the thick secondary beam is used just for the sake of comparison.

Before any experiment with the beam system was conducted, a finite element (FE) model was built in ANSYS. The purpose of this is to predict the first few modes of the beam system and to investigate whether the beam system is suitable for comparison with a two degree of freedom system at low frequencies. The model was meshed and solved using a modal solver in ANSYS to extract the modes of the coupled beam system.

The effect of mass loading from the accelerometers and the bolted connection were modelled as point masses at the end of the primary beam and both ends of the secondary beam. A PCB accelerometer has an approximate mass of about 0.5 g according to the manufacturer's specification. The bolts that connect the primary beam with the secondary beam have a mass about 5 g. An additional mass of 0.1 g each are included in the model at the end of the primary beam and both ends of the secondary beam as a mass contribution from the wax that was used to attach each accelerometer to the beam structure. The mass of the wax is uncertain and its value might influence the difference between the FE model and the subsequent validation experiments. Other sources of discrepancy between FE and measurement include the boundary condition of the beam system and how the two beams are connected. In the FE model, the beam has a fixed support but in the experiment, the support may allow small movements and possibly there is energy dissipation at the support. Moreover, in the FE model, the beam system is treated as a single body but in the experiment, the beam system consists of two beams connected with a bolted connection. There might be energy dissipation in the bolted region as well, as a result from sliding between the primary and secondary beam at the region of contact. Figure 5.1 shows the finite element model for the T beam configuration with the thin secondary beam.

From the finite element model, the system with the thin secondary beam has two natural frequencies below 120 Hz. The two coupled modes are mainly a flexural mode of the primary beam predicted at 59.8 Hz and a flexural mode of the secondary beam predicted at 113.7 Hz. There is another mode which exists between these two modes, which is a torsional mode of the primary beam at 81.2 Hz. However, when an experiment was performed to test the transmissibility of the beam system, this mode had a very low amplitude and was insignificant compared to the other two modes. The transmissibility in this experiment is a measure of how much beam acceleration obtained from the applied acceleration at the base.

Therefore, it can be concluded that only two modes dominate the response of the system for the frequency range from 0 to 120 Hz. On the other hand, from the model, the system with the thick secondary beam has a torsional mode of the primary beam and flexural mode of the secondary beam, which are significantly higher in frequency than the system with the thin secondary beam. The flexural mode of the secondary beam increases significantly to 430.9 Hz. There is also an increase in the torsional mode of the primary beam to 106.1 Hz. The flexural mode of the primary beam is slightly lower than the case of the thin secondary beam which at around 48.8 Hz. The comparison of the three first natural frequencies of the beam system with the thin and thick secondary beam is shown in Table 5.2. Figures 5.2 and 5.3 show the predicted mode shapes of the first three modes of the T beam system for these two cases respectively.

In order to apply friction, a steel beam is used as a friction interface. This steel beam is bolted to the base, so that the friction interface could move with the base input as described in the model. The steel beam applies a normal force to both ends of the secondary beam which is perpendicular to the direction of motion. There is a small screw on each end of the secondary beam for the purpose of adjusting the normal force. The reason for introducing the steel beam is in order to use it for later switching on and off the friction. For this purpose, an electromagnet is used to attract the steel beam and modify the normal force and hence the friction force. This configuration is shown in Figure 5.4.

5.3 Finite element model validation

The initial experiment was performed to validate the finite element model. For this purpose, a laser vibrometer was used to confirm that the first three modes correspond to the flexural mode of the primary beam, the torsional mode of the primary beam and the flexural mode

of the secondary beam. The experimental rig was hung with four cords and a shaker was attached beneath the base to apply a base input to the rig, as shown in Figure 5.5. Broadband random excitation from the vibrometer system was used to drive the shaker (Derritron VP4) and the results were then compared with the finite element model.

The laser vibrometer (Polytec PSV400) was used to measure the response, whilst PCB accelerometers (type 35C22) were attached to the structure. The reason why the accelerometers were attached, without being used for any measurement, was that for the later experiments the accelerometers would be in place and might affect the response of the system. As the beam system is a lightweight structure, the mass loading from the accelerometers is quite significant, especially for the thin secondary beam.

Table 5.3 gives a comparison between the FE predicted and measured natural frequencies for the first three modes of the T beam system for the case of the thin secondary beam; the frequencies are very close to each other. The first and third natural frequencies have a difference of less than 3 percent, while the second natural frequency has a slightly larger difference of 6.9 percent. However, bearing in mind that the beam system is a very lightweight structure then any small difference in mass will cause a large change in the natural frequency. Therefore, up to 7 percent difference in the natural frequency is considered acceptable.

Figure 5.6 shows the first three measured operational deflection shapes (ODS) of the T beam system when the thin secondary beam was used. In order to validate the finite element model, the Modal Assurance Criterion [66] was used. It is a widely used technique to estimate the degree of correlation between mode shape vectors [67] . Eleven measurement points and three modes were used for this calculation using

$$MAC(i,j)=\frac{\left|\left\{\Phi_{measured}\right\}_i^T\left\{\Phi_{FE}\right\}_j\right|^2}{\left|\left\{\Phi_{measured}\right\}_i^T\left\{\Phi_{measured}\right\}_i\right|\cdot\left|\left\{\Phi_{FE}\right\}_j^T\left\{\Phi_{FE}\right\}_j\right|} \tag{5.1}$$

The result from the MAC calculation is

$$MAC(3,3)=\begin{pmatrix}0.9914 & 0.0070 & 0.1649\\ 0.0177 & 0.9780 & 0.0007\\ 0.1035 & 0.0009 & 0.9834\end{pmatrix} \tag{5.2}$$

Each predicted mode shape from the finite element model is within 3 percent error with its respective measured ODS. From the results, the mode shapes from the FE model are very close and in very good agreement with the measurements.

Therefore, the next step to be implemented is to measure the frequency response functions from the base to the end of the primary beam and both ends of the secondary beam. If the torsional mode of the primary beam has very low amplitude compared to the flexural modes, the system can be represented by a two degree of freedom model.

5.4 System model parameter estimation

A second experiment was performed to estimate the physical properties of the two degree of freedom system by fitting the measured acceleration transmissibility to the two degree of freedom model equations. This test was performed only for the beam system with the thin secondary beam. For the beam system with the thick secondary beam, it was not appropriate to fit it to the two degree of freedom model equations, because both second and third modes have been shifted to a higher frequency. For this case, at low frequencies, there is only one dominant mode corresponding to a flexural mode of the primary beam. Therefore, for the purpose of validation in the next two sections, the beam system with the thick secondary beam is considered to be acting as a single degree of freedom system.

A diagram showing the setup of the equipment is shown in Figure 5.7. The shaker was used to produce an impulse base input. Four accelerometers were used, one at the base of the rig, one at the end of the primary beam and two at opposite ends of the secondary beam. The response at the end of the primary beam was compared with the response of the primary mass in the theoretical model and the response at the end of the secondary beam was compared with the response of the secondary mass. A Data Physics analyzer was used to calculate the frequency response functions using the acceleration signals. The frequency response functions measured were between the base and the end of the primary beam and both ends of the secondary beam. The frequency response functions were acquired using a rectangular window, 3200 lines of resolution, a frequency span of 0 to 1000 Hz and 10 averages.

Furthermore, the measured frequency response curve of the T beam can be fitted to the two degree of freedom model equations to estimate all of the two degree of freedom system parameters namely the stiffness, damping and mass. The two degree of freedom

system with Coulomb friction is again shown in Figure 5.8, but for this section friction is set to zero. Subsequently, based on the two degree of freedom system parameters, the measurement results were compared with the the theoretical results. These are given by the following expressions for the acceleration transmissibility.

$$\frac{\ddot{x}_1}{\ddot{u}} = \frac{\left(k_1\left(1+j\eta_1\right)\right)\left(k_2\left(1+j\eta_2\right)-m_2\omega^2\right)}{\left(k_1(1+j\eta_1)+k_2\left(1+j\eta_2\right)-m_1\omega^2\right)\left(k_2\left(1+j\eta_2\right)-m_2\omega^2\right)-k_2{}^2\left(1+j\eta_2\right)-jk_2{}^2\eta_2\left(1+j\eta_2\right)} \quad (5.3)$$

$$\frac{\ddot{x}_2}{\ddot{u}} = \frac{k_2\left(1+j\eta_2\right)}{\left(k_2\left(1+j\eta_2\right)-m_2\omega^2\right)}\left(\frac{\ddot{x}_1}{\ddot{u}}\right) \quad (5.4)$$

Figure 5.9 shows the acceleration transmissibility of the T beam at low frequencies between 0 to 130 Hz for the case of a thin secondary beam. From inspection of the figure two frequencies are dominant, which are around 55 Hz and 108 Hz corresponding to the flexural modes of the primary beam and the secondary beam respectively. There is another resonance between these two frequencies, around 75 to 80 Hz, corresponding to a torsional mode of the primary beam. However, it has quite a small response in comparison to the resonances at the other two frequencies and can be considered to be negligible. To make a comparison with a two degree of freedom system, a MATLAB fitting function was used to find a combination of parameters that fit the acceleration transmissibility obtained from the experiment. The least squares error fit between the measured transmissibility and two degree of freedom model transmissibility was performed such that the following summation over the frequency range of available data is minimised

$$\sum_{\omega}\left|\left(\mathrm{Re}\left(\frac{\ddot{x}_1}{\ddot{u}}\right)_{measured}-\mathrm{Re}\left(\frac{\ddot{x}_1}{\ddot{u}}\right)_{model}\right)^2+\left(\mathrm{Re}\left(\frac{\ddot{x}_2}{\ddot{u}}\right)_{measured}-\mathrm{Re}\left(\frac{\ddot{x}_2}{\ddot{u}}\right)_{model}\right)^2 + \left(\mathrm{Im}\left(\frac{\ddot{x}_1}{\ddot{u}}\right)_{measured}-\mathrm{Im}\left(\frac{\ddot{x}_1}{\ddot{u}}\right)_{model}\right)^2+\left(\mathrm{Im}\left(\frac{\ddot{x}_2}{\ddot{u}}\right)_{measured}-\mathrm{Im}\left(\frac{\ddot{x}_2}{\ddot{u}}\right)_{model}\right)^2\right| \quad (5.5)$$

For the fitting process, only the transmissibility data from sensor 2 and sensor 3 are used. Sensor 2 and sensor 3 were mounted at the end of the primary beam and the secondary beam respectively during the experiment. The data from sensor 4 which was mounted at another end of the secondary beam is just used as a comparison to sensor 3 whether they are in very close agreement with each other.

The estimated parameters are listed in the Table 5.4. The transmissibility based on the fitted parameters is plotted on the same figure as the measured transmissibility (Figure 5.9) for comparison. The measured transmissibility from the experiment is in very close agreement with the predicted transmissibility of a two degree of freedom system with the parameters obtained. Coherence of the system is very good up to 200 Hz as shown in Figure 5.10.

For the case of the thick secondary beam, the measured transmissibility is plotted in Figure 5.11. It can be observed that the first mode, corresponding to the flexural mode of the primary beam at 45 Hz, dominates the response for low frequencies as stated before. The torsional mode of the primary beam and the flexural mode of the secondary beam have shifted to a higher frequency and are very low in amplitude. In this case, the system closely behaves as a single degree of freedom system with dominant frequency of 45 Hz. From Figure 5.12, the coherence is poor at high frequencies possibly caused by a low signal to noise ratio. The coherence is very good in the region of 45 Hz where the dominant contribution is located. Therefore, in this case the best choice for experimental validation is to compare the beam system with thick secondary beam to a single degree of freedom response.

5.5 Validation for the case of no friction

5.5.1 Generation of a versed sine pulse

Shock response simulations presented in chapter 2 and 3 use a versed sine pulse. This pulse is symmetrical, mathematically simple and convenient to use in the theoretical simulations. It also replicates the behaviour of real shock pulses with sufficient accuracy and was used in the experiment to validate the response of two degree of freedom system with friction.

Versed sine base input was generated using MATLAB and exported as a waveform audio format (WAV) file. This file can be played through a PC sound card connected via an amplifier to drive an electrodynamic shaker. This technique was used by Ramirez [3] to create a versed sine base input with an electrodynamic shaker with minimum residual vibration of the base. Please refer to the Appendix E for further information about this technique.

It is preferable to have a pulse with as small residual response as possible, so it approaches a theoretical versed sine especially if the residual response of a two degree of freedom system is something of interest. However, if only a shock response is considered, the residual vibration of the rig-shaker system is not important. For the analysis in this and next chapters, only the shock response is considered.

5.5.2 Shock response when no friction is applied: predicted versus measured

The measured acceleration is filtered with a high pass filter (cut off frequency around 5-15 Hz) and subsequently integrated to obtain velocity. Subsequently, the velocity is filtered again and integrated to obtain displacement. The reason to filter the low frequencies is to avoid output drift. If there is no filter, the low frequencies will dominate the displacement response which will cause a significant difference between the measured and the predicted results. Figure 5.13 shows the measured and ODE simulation displacement response of the beam system with the thin secondary beam and no friction. The displacement of both the beam and two degree of freedom system are normalised with respect to the maximum base input displacement. The time axis is normalised with respect to the length of the pulse.

The measured and ODE simulation displacement response are in very good agreement with each other until about a time corresponding to half of the pulse length. After this time, there is a slight difference between the measured and ODE simulation since the base input in the experiment is not a perfectly symmetric versed sine input. The length of the pulse measured in the experiment is about 0.02 s, which is very near to the first natural period of the beam system which is 0.018 s. The length of the pulse was kept the same for later experiments as well. If the pulse length is equal to the first natural period of the beam system, the beam will produce the highest response in the case of no friction.

Figure 5.14 shows the measured and ODE simulation displacement response of the beam system with the thick secondary beam and no friction. From the figure, the response at the end of the primary beam and the secondary beam do not have any significant difference. The reason for this is that the pulse length used only excites the first mode, at the lower frequency, and the contribution to the response of the system from the second mode is minimal.

In Figure 5.14, the measured and ODE simulation displacement response have slight differences because the experimental base input does not exactly follow the versed sine

curve. From normalised time equal to 0 until about 0.75, the simulation response is larger than the experimental response because the versed sine base input is larger than the experimental base input for the first half of the pulse length. Then, after half of the pulse length, the modelled versed sine base input becomes smaller than the experimental base input. This causes the simulation response to be smaller than the experimental response after a normalized time of 0.75. Otherwise, the experiment and simulation are in very good agreement with each other.

5.6 Validation for a system with a thin secondary beam and friction

5.6.1 Background information

From chapter 2, theoretically, a system with passive friction should produce a smaller response than a system without friction. Therefore, the use of friction is expected to produce a smaller response during the shock. In this section, friction was applied to the system and a measurement was made. The results are then compared to the theoretical results to validate them.

Two levels of friction are used in the experiment for validation. The first value of friction is chosen to be not so large, consequently the end of the secondary beam fully slides with respect to the friction interface. The value of friction used in this case is estimated by a free vibration response experiment which will be explained in the next subsection. Secondly, the value of friction is chosen to be sufficiently large so that the end of the secondary beam fully sticks with respect to the friction interface. The idea of performing the experiment with large friction is to see the behaviour of the system corresponding to an extreme case.

5.6.2 Friction estimate

The initial idea to estimate the value of friction is by performing a free vibration test on the two degree of freedom system with friction. The range of possible friction values can be determined by fitting the result from the experiment with the analytical solution for any cycle of vibration to determine the value of friction that minimizes the least square error, i.e.

$$\sum_{t}\left(x_{1measured}-x_{1model}\right)^2+\left(x_{2measured}-x_{2model}\right)^2+\left(\dot{x}_{1measured}-\dot{x}_{1model}\right)^2+\left(\dot{x}_{2measured}-\dot{x}_{2model}\right)^2 \quad (5.6)$$

Several cycles from the experimental data are used to observe whether the estimated friction value is nearly constant, unchanged and repeatable. Finally, this value of friction can be combined with the system parameters calculated from the previous section to perform ODE simulations for the shock response of the system with friction.

The initial step is to recall the analytical solution for this case. The equation of motion for the free vibration of the two degree of freedom system with Coulomb friction is

$$\begin{aligned} m_1\ddot{x}_1 + k_1 x_1 + k_2\left(x_1 - x_2\right) &= 0 \\ m_2\ddot{x}_2 - k_2\left(x_1 - x_2\right) + F\,\mathrm{sgn}\left(\dot{x}_2\right) &= 0 \end{aligned} \tag{5.7}$$

For the case, when friction is not too large to cause the secondary mass to stick, the equation of motion (5.7) can be transformed into equations of motion in the two distinct modes depending on the sign of the secondary mass velocity $\dot{x}_2$. The solution is valid only up to the point when $\dot{x}_2$ changes its sign. Then, the next solution in time can be computed based on the final condition of the previous phase.

If $\dot{x}_2$ is positive, equation (5.8) is considered. On the other hand, if $\dot{x}_2$ is negative, equation (5.9) is considered.

$$\begin{aligned} \ddot{u}_1 + \omega_1^2 u_1 + \Phi_{21} F &= 0 \\ \ddot{u}_2 + \omega_2^2 u_2 + \Phi_{22} F &= 0 \end{aligned} \tag{5.8}$$

$$\begin{aligned} \ddot{u}_1 + \omega_1^2 u_1 - \Phi_{21} F &= 0 \\ \ddot{u}_2 + \omega_2^2 u_2 - \Phi_{22} F &= 0 \end{aligned} \tag{5.9}$$

where $\Phi = \begin{pmatrix} \Phi_{11} & \Phi_{12} \\ \Phi_{21} & \Phi_{22} \end{pmatrix}$ is the mode shape matrix whose columns represent the undamped modes and $\omega_n = \begin{pmatrix} \omega_1 & 0 \\ 0 & \omega_2 \end{pmatrix}$ is the natural frequency matrix of the two degree of freedom system.

The solution of the equations (5.8) and (5.9) are as follows

$$u_1(t) = A_1 \cos \omega_1 t + B_1 \sin \omega_1 t - \frac{\Phi_{21} F}{\omega_1^2}$$
$$u_2(t) = A_2 \cos \omega_2 t + B_2 \sin \omega_2 t - \frac{\Phi_{22} F}{\omega_2^2} \quad (5.10)$$

$$u_1(t) = A_1 \cos \omega_1 t + B_1 \sin \omega_1 t + \frac{\Phi_{21} F}{\omega_1^2}$$
$$u_2(t) = A_2 \cos \omega_2 t + B_2 \sin \omega_2 t + \frac{\Phi_{22} F}{\omega_2^2} \quad (5.11)$$

A_1, A_2, B_1 and B_2 can be determined by considering the initial conditions. If $\dot{x}_2$ is positive,

$$u_1(0) = u_{1i} = A_1 - \frac{\Phi_{21} F}{\omega_1^2}$$
$$u_2(0) = u_{2i} = A_2 - \frac{\Phi_{22} F}{\omega_2^2}$$
$$\dot{u}_1(0) = \dot{u}_{1i} = B_1 \omega_1$$
$$\dot{u}_2(0) = \dot{u}_{2i} = B_2 \omega_2$$

If $\dot{x}_2$ is negative,

$$u_1(0) = u_{1i} = A_1 + \frac{\Phi_{21} F}{\omega_1^2}$$
$$u_2(0) = u_{2i} = A_2 + \frac{\Phi_{22} F}{\omega_2^2}$$
$$\dot{u}_1(0) = \dot{u}_{1i} = B_1 \omega_1$$
$$\dot{u}_2(0) = \dot{u}_{2i} = B_2 \omega_2$$

u_{1i}, u_{2i}, $\dot{u}_{1i}$ and $\dot{u}_{2i}$ are the initial conditions which are based on the final condition of the previous phase of the motion.

Then, the displacement of the primary and secondary mass can be determined by combining the solution of u_1 and u_2 i.e.

$$\begin{pmatrix} x_1 \\ x_2 \end{pmatrix} = \begin{pmatrix} \Phi_{11} & \Phi_{12} \\ \Phi_{21} & \Phi_{22} \end{pmatrix} \begin{pmatrix} u_1 \\ u_2 \end{pmatrix} \quad (5.12)$$

Depending on the sign of $\dot{x}_2$ and the initial condition, the correct solution can be chosen as the motion progresses and can be substituted into the MATLAB routine to estimate the value of friction.

Figure 5.15 shows some examples of comparison between the free vibration experimental results and the analytical solution using the friction estimated from the fitting process. The values of friction determined from the fitting process are listed next to the figure. It can be observed that there is variation in the estimated friction values,which is about $\pm 20\%$ relative to 0.5. From the simulations, it is expected the secondary mass will fully stick when non-dimensional friction $\hat{F}$ is about equal to 1. All of the estimated values for non-dimensional friction $\hat{F}$ are between 0 and 1, which is still in the sliding region.

These values of the estimated friction can be used together with the estimated two degree of freedom model parameters determined from the previous section to validate the time response of the system with Coulomb friction subjected to a versed sine base input.

5.6.3 Results and discussions

For low levels of friction applied to the system, the end of the secondary beam slides with respect to the friction interface and the system becomes non-linear or piecewise linear. Coherence in the response for cases with intermediate friction, shown by Figure 5.16, is not as good as the coherence of the system with no friction, as shown in Figure 5.10. This shows that there is potentially non-linearity involved in the system behaviour. It is expected that there is a reduction in the displacement response of the system when friction is applied. The measured displacement responses when friction is applied to the system are shown in Figure 5.17 (a).

From Figure 5.17 (a), it can be observed that the responses of the two ends of the secondary beam are slightly different. This is reasonable since it is quite hard to produce friction that is exactly equal on both ends of the beam. From Figure 5.17, the difference in the responses until a normalised time of 0.5 is small, and it subsequently increases slightly. This shows that friction is most likely changing as the beam moves, as a result of friction surface changes, and the bending of the steel beam friction interface.

Another possible reason for discrepancy from Figure 5.17 (a) is the existence of a pre-sliding region when the motion starts. Normally, if the range of displacement is large

enough, the pre-sliding motion is not significant and can be ignored in the analysis. However, during this experiment, the displacement range generated from the base input is quite small, roughly less than 1 mm. Therefore, the pre-sliding region is important in describing the behaviour of the system. This behaviour is clearly seen from normalized time t / T_p equal to 0 until about 0.25. This corresponds to a pre-sliding region since the displacement is very small, often between 1 and 10 μm [50]. The explanation of this behaviour is that before gross slip occurs, there is local sliding in the contact. This microscopic behaviour can be explained by the interaction between the contact asperities which behave as welded junctions and the shearing that tends to break them [68].

The size of this region depends on the surface roughness [69]. The Coulomb friction model is not very good in describing the behaviour of the system in this region [50]. Andersson *et al* in their paper explain that for small displacements there are other friction models which should be used to replace the Coulomb friction model. These models describe, for small displacements, that friction increases with displacement until it reaches the maximum friction which can be considered the Coulomb sliding friction force. This case is also discussed in other publications [68, 70, 71]. These publications state that during stationary contact and before gross slip, friction increases depends upon the stationary contact time. This finding will assist in explaining the difference between the experimental results and ODE simulation to be provided later.

Another possible reason for discrepancy is because the secondary stiffness is only about half of the primary stiffness from the parameter estimation. When the secondary stiffness is smaller than the primary stiffness, the secondary mass might stick for slightly higher levels of friction. Therefore, slight changes in the level of friction will cause a big difference in the secondary mass response.

The measured response shown in Figure 5.17(a) is compared with the ODE simulation in Figure 5.17(b). To create the response in Figure 5.17(b), the non-dimensional friction was set as $\hat{F} = 0.39$ and $\hat{F} = 0.48$, which are the examples of the estimated friction values determined from the previous section.

It can be seen that the system reaches its peak displacement in the experimental results after it does so in the simulation results. This means that the Coulomb friction model only appears to be appropriate after t / T_p of about 0.25, where the displacement of the end of

the secondary beam is significantly greater than 10 μm. Generally, however, the experimental results and simulations are in good agreement with each other. The overall behaviour of the system with friction can still be predicted with reasonable accuracy using ODE simulation.

When friction is high, it is expected that the secondary mass will stick and move with the base. It is also predicted that the primary mass will oscillate as a single degree of freedom system supported by both springs. In the experiment with the beam system for high friction, the transmissibility shows only one dominant peak for the response at the end of the primary beam. On the other hand, at the end of the secondary beam, the frequency response function which corresponds to the acceleration transmissibility is almost unity over the frequency range from 0 to 120 Hz as shown in Figure 5.18. From the estimated parameters in Table 5.4, the primary mass natural frequency can be calculated using

$$\omega_n = \sqrt{\frac{k_1 + k_2}{m_1}} \tag{5.13}$$

The estimated natural frequency using equation (5.13) is 83.6 Hz, which is close to the measured natural frequency, 81.25 Hz. The coherence function of the system is also very close to unity up to 200 Hz, see Figure 5.19.

Figure 5.20 compares the measured and the ODE simulation displacement response of the beam system with high friction. In this case, both ends of the secondary beam move almost with the same displacement as the base as expected and the primary mass oscillates as a single degree of freedom system at a slightly higher frequency than previously. The measured response is also in good agreement with the ODE simulation.

Finally, a comparison has been made for the system displacement with different levels of friction as shown in Figures 5.21 and 5.22. This comparison was made to see the effect of friction in reducing the displacement and velocity response during the shock, as theoretical findings showed in previous chapters. It can be seen that the system response with friction is smaller than without. For intermediate friction, the end of the secondary beam slides with respect to the friction interface and produces a smaller response. From chapter 2, it is expected that the smallest response is always produced when the secondary mass slides with respect to the friction interface instead of fully sticking. This result validates the theoretical conclusions in chapter 2. However, from the measurements the reduction is

small because of the choice of the T beam which produced a secondary spring that is softer compared to the primary spring in the two degree of freedom model. If the secondary spring is increased to a much larger value, more reduction in the response should be possible as discussed in Chapter 2.

Table 5.5 lists the maximum displacement for the system with different levels of friction. From the table, the agreement between experiment and simulation for the case of no friction and large friction is within 10%. They are generally in good agreement. On the other hand, the difference between experiment and simulation for the case with intermediate friction is up to 18%. This is mainly because of the pre-sliding region, when the motion starts, as discussed before. However, the large difference produced is only in the secondary mass responses. All of the primary mass responses have differences of less than 5% between measurement and predictions.

5.7 Validation for a system with a thick secondary beam and friction

For the system with the thick secondary beam, the displacement response of the beam system is presented in Figure 5.23 for the case of intermediate levels of friction, so that the end of the secondary beam slides. For comparison, the displacement response of a single degree of freedom model is also plotted in the same figure. Figure 5.24 presents the displacement response of the beam for the case when friction is high, so that the end of the secondary beam fully sticks. For comparison, the displacement response of a single degree of freedom model using high friction is presented in the same figure.

For the case of intermediate friction, the simulation was performed with two estimated friction values, $\hat{F} = 0.2$ and $\hat{F} = 0.3$. The simulation was performed using the measured base input, rather than the original versed sine base input, to obtain more accuracy in the comparison. From Figure 5.23, it can be seen that the displacement simulations using the estimated friction values are very close to the measurements. As the friction is increased to a higher level, the end of the primary beam and the secondary beam move together with the base input as expected.

As in the case of the thin secondary beam, when friction is applied, there is a reduction in the displacement response of the system. Moreover, for the case of the thick secondary beam, more reduction is expected for the response at the end of the primary beam. When

friction is applied during the experiment, the response at the end of the primary beam is smaller than the case of no friction. This can be seen clearly from Figure 5.25 which shows the displacement response of the system for different levels of friction and in Table 5.6 which lists the maximum displacement for the system with different levels of friction for the experiments and simulations. The experiments show a reduction of 21.8% in the displacement response at the end of the primary beam for intermediate friction. The normalized displacement response is reduced from 1.7 to 1.33. As the friction is further increased in the experiment, the normalized displacement is reduced to 1.13. This is a reduction of 33.5% compared to the case of no friction.

Finally, Table 5.7 compares the results with those of the thin secondary beam response. As displayed in Table 5.7, it is clear to see that more reduction is achieved when the thick secondary beam is used. As the end of the secondary beam sticks at the friction interface for high friction for the system with a thin secondary beam, the end of the primary beam still experiences a high response. However, for the case of the thick secondary beam, when the friction is increased, both ends of the primary and secondary beam experience lower responses. This is as expected from the study in Chapter 2. When the secondary stiffness increases for a two degree of freedom model with friction more displacement reduction of the primary mass could be achieved. However, an intermediate secondary stiffness is preferred to avoid any discontinuity in the acceleration response of the primary mass.

5.8 Conclusions

A T beam configuration was used to achieve the objective of reproducing the behaviour of a two degree of freedom system at low frequencies. From the finite element model and its validation, it is possible to demonstrate that this objective is achieved. Using the estimated two degree of freedom model parameters from the curve fitting and estimated friction obtained by measuring the free decay of the system, it is possible to get the shock response of the system close to that obtained by measurements.

Only a few issues arise, especially whether the simplicity of Coulomb friction model is sufficient to model the complicated behaviour of real friction especially at very low input displacement. Since the shaker used does not have a long stroke, the shaker is unable to produce large displacements. From the findings of the past studies and the experimental results obtained, there would be other friction models that are better at representing the behaviour of the system at very low displacement. The difference between the experimental results and simulation is explained in terms of the suitability of Coulomb friction to represent the behaviour of the system in this case.

Otherwise, the experimental results and the simulations are very close. The smallest displacement response was achieved when intermediate friction was used. It is exactly as explained by chapter 2, where the smallest peak displacement response is achieved for levels of intermediate friction. All of the results from this chapter support and validate the earlier theoretical aspects of chapter 2. The comparison between the response of the system with thin and thick secondary beams show that more reduction in the displacement response could be obtained by using the thick secondary beam.

Beams	Dimensions
Primary beam	150×15×3.3 mm
Thin secondary beam	160×15×0.9 mm
Thick secondary beam	160×15×3 mm

Table 5.1: Beam system component dimensions.

Modes	Thin secondary beam (Hz)	Thick secondary beam (Hz)
First mode (flexural mode of the primary beam)	59.4	48.8
Second mode (torsional mode of the secondary beam)	81.2	106.1
Third mode (flexural mode of the secondary beam)	112.9	430.9

Table 5.2: The comparison between the natural frequencies of the first three modes of vibration for a thin and thick secondary beam coupled T beam configuration respectively.

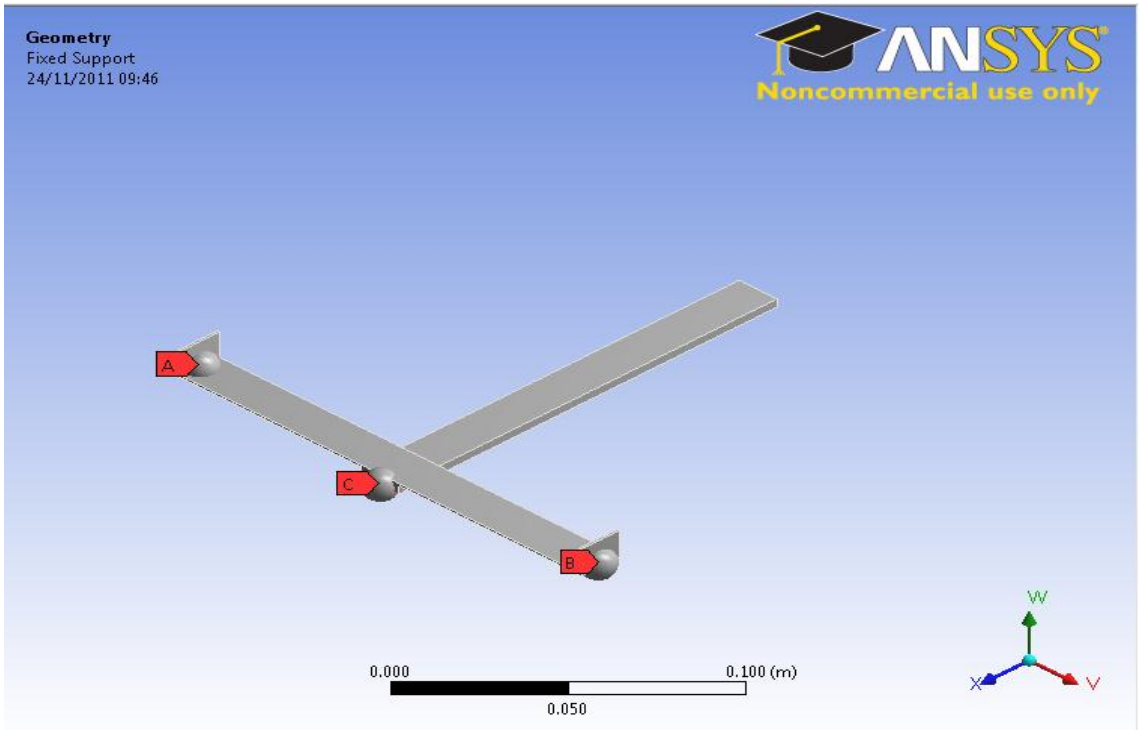

Figure 5.1: An example of the T beam configuration finite element model. A, B and C are point masses representing the accelerometers and bolted connection. A=B=0.6 g (accelerometer and wax). C=5.6 g (bolted connection, accelerometer, and wax).

(a)

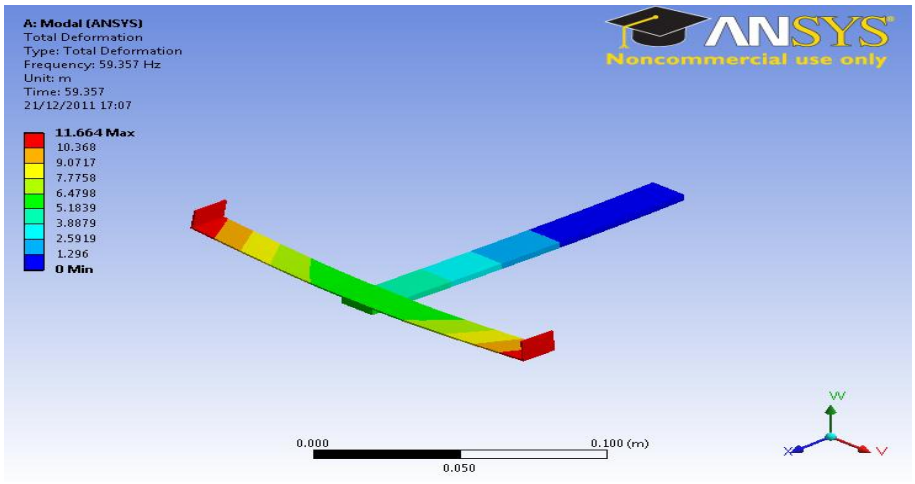

(b)

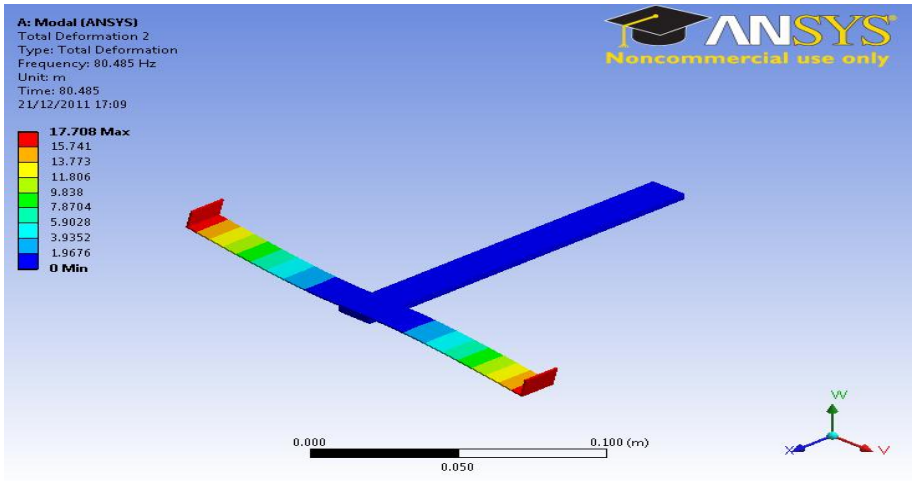

(c)

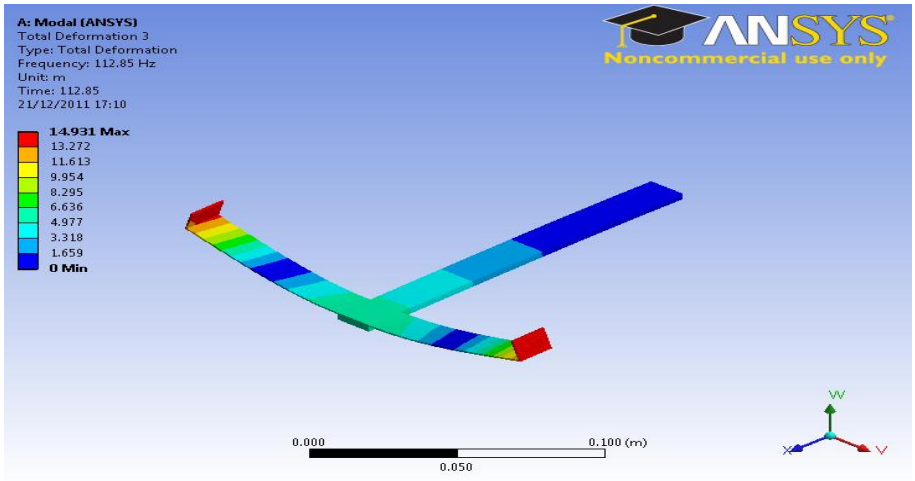

Figure 5.2:The first three modes of the T beam configuration extracted from Ansys when a thin beam secondary beam was used. (a) First mode, flexural mode of the primary beam. (b) Second mode, torsional mode of the primary beam.(c) Third mode, flexural mode of the secondary beam.

(a)

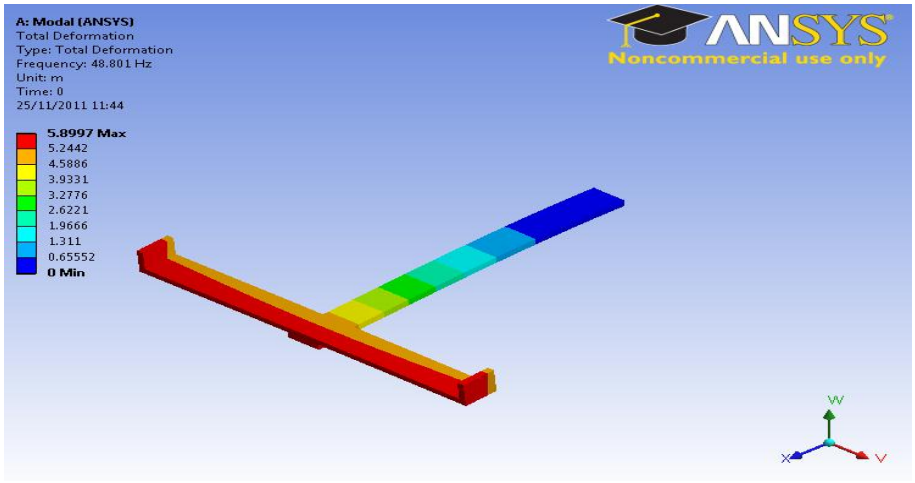

(b)

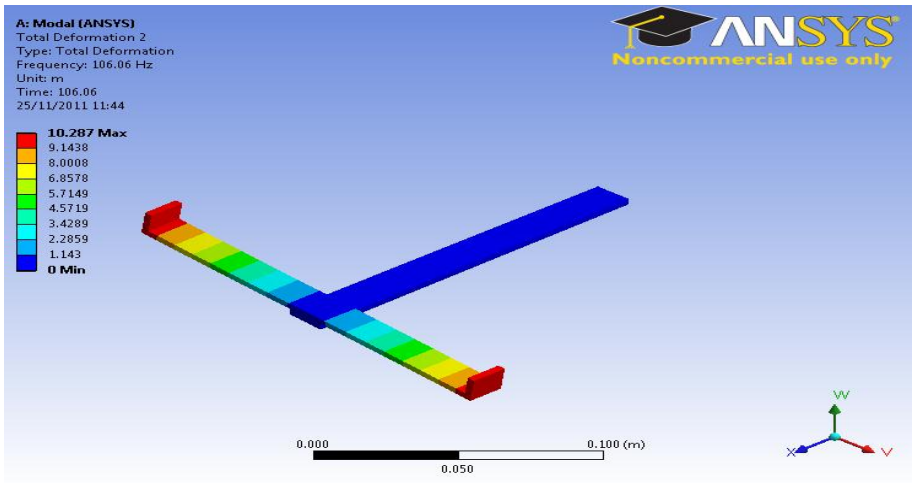

(c)

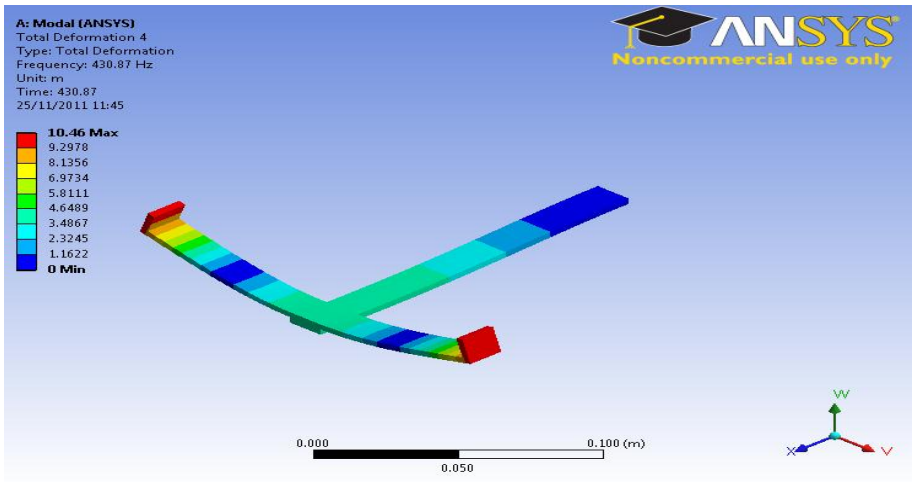

Figure 5.3: The first three modes of the T beam configuration extracted from Ansys when a thick beam secondary beam was used. (a) First mode, flexural mode of the primary beam. (b) Second mode, torsional mode of the primary beam.(c) Third mode, flexural mode of the secondary beam.

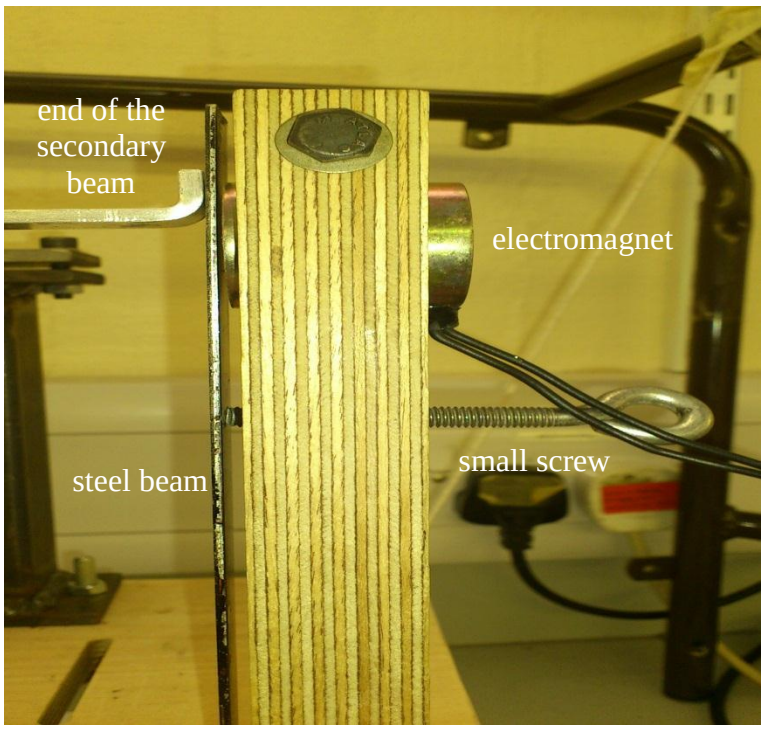

Figure 5.4: Practical implementation of the passive and switchable friction to the two degree of freedom system.

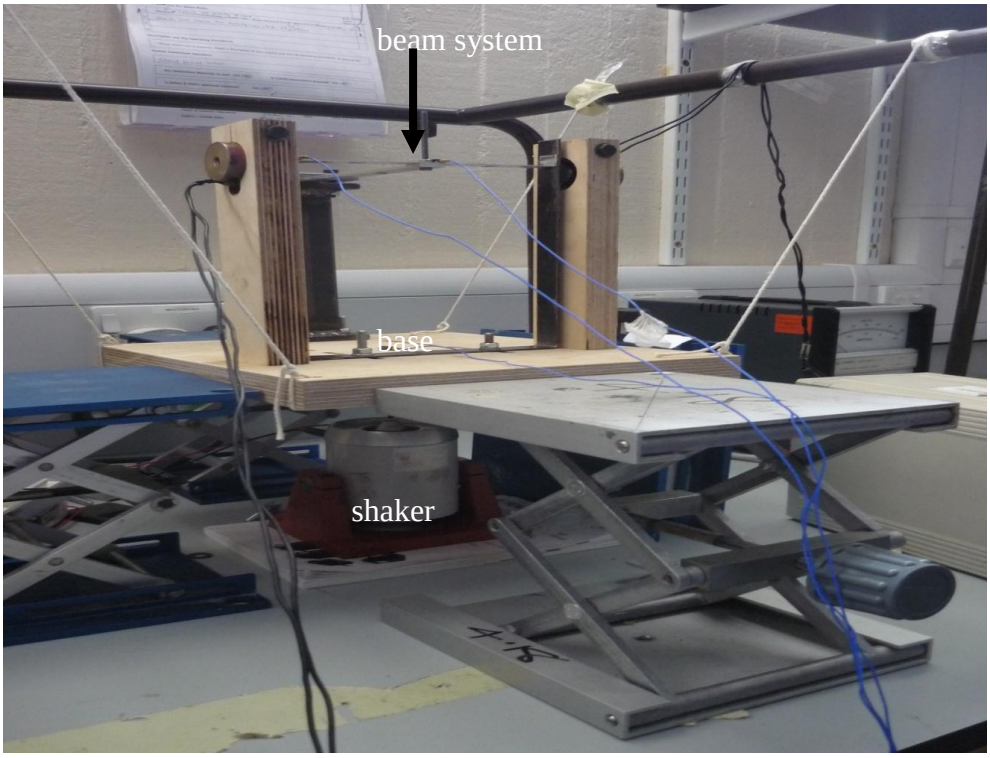

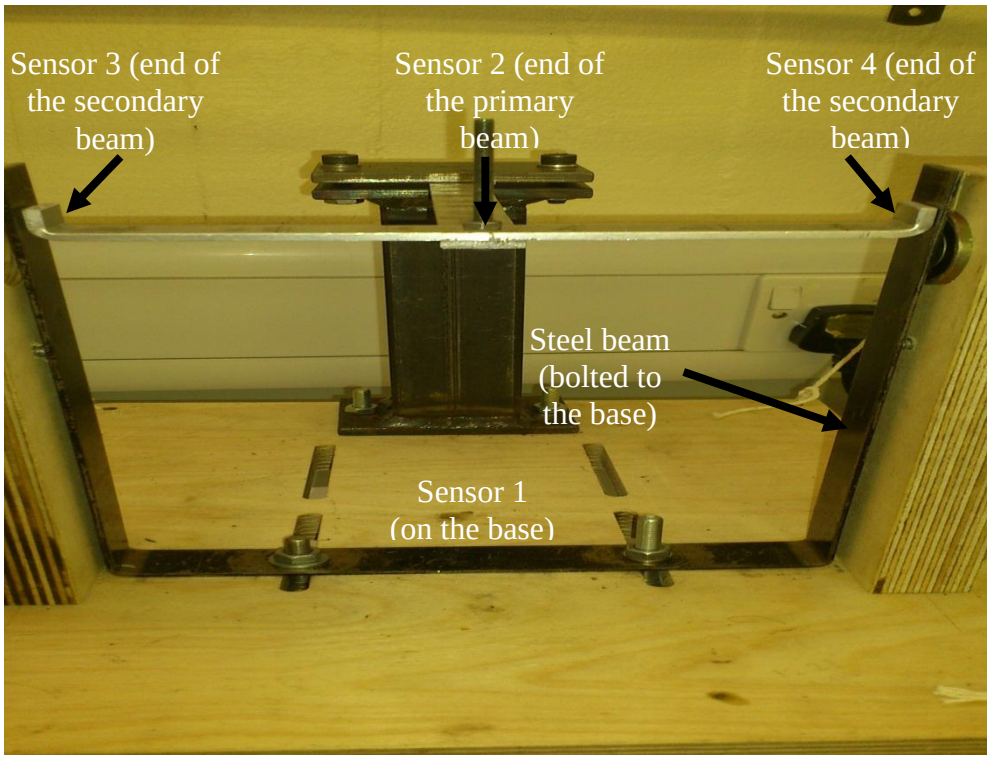

Figure 5.5: Test rig for the experiment to validate response of a two degree of freedom system with Coulomb friction for base displacement.

Modes	FE predicted natural frequency (Hz)	Measured natural frequency (Hz)	Percentage difference
First mode (flexural mode of the primary beam)	59.4	58.0	2.4
Second mode (torsional mode of the primary beam)	80.5	75.3	6.9
Third mode (flexural mode of the secondary beam)	112.9	111.8	0.98

Table 5.3: The comparison between predicted (FE) and measured natural frequencies of the first three modes of vibration for a thin secondary beam configuration.

(a)

(b)

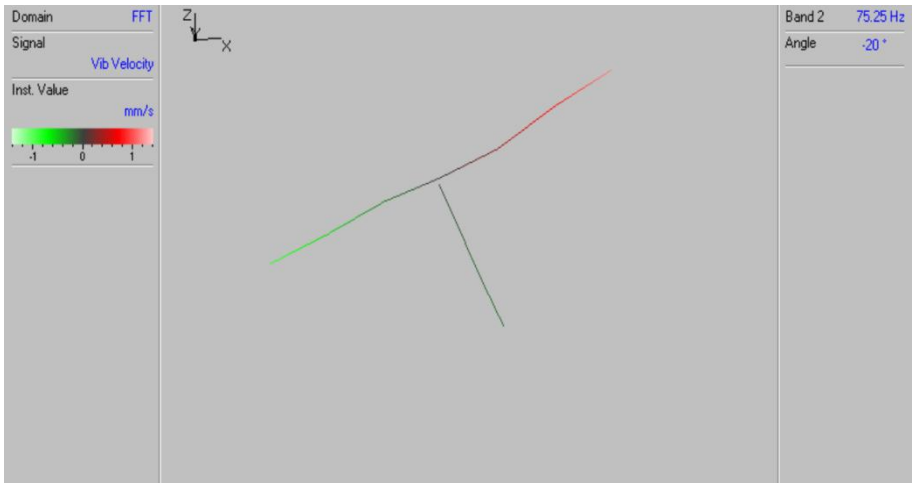

(c)

Figure 5.6: The first three operational deflection shapes (ODS) of the T beam configuration from laser vibrometer measurement when thin beam secondary beam was used. (a) First mode, flexural of the primary beam. (b) Second mode, twisted of the secondary beam.(c) Third mode, flexural of the secondary beam.

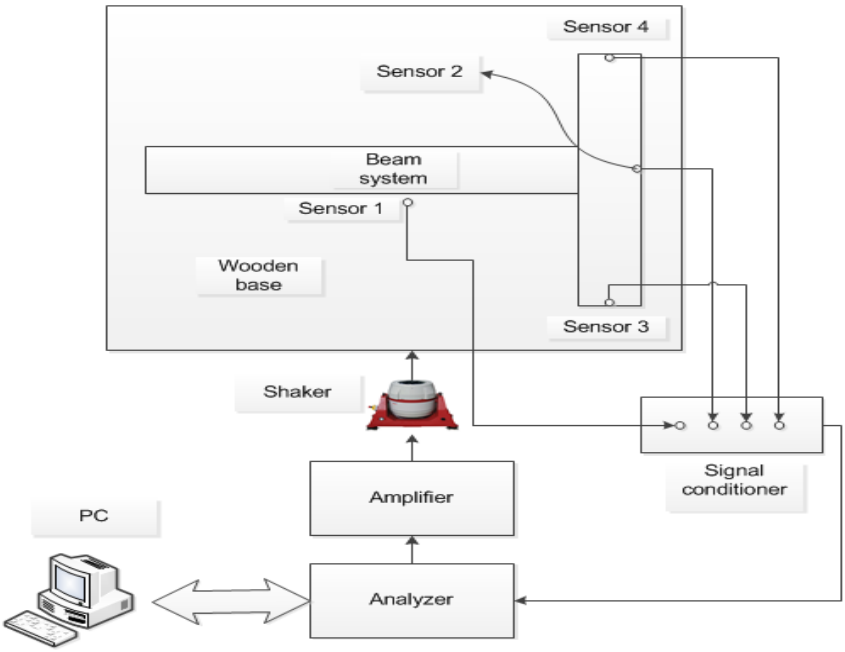

Figure 5.7: Schematic diagram of the setup used for the experiment for base displacement.

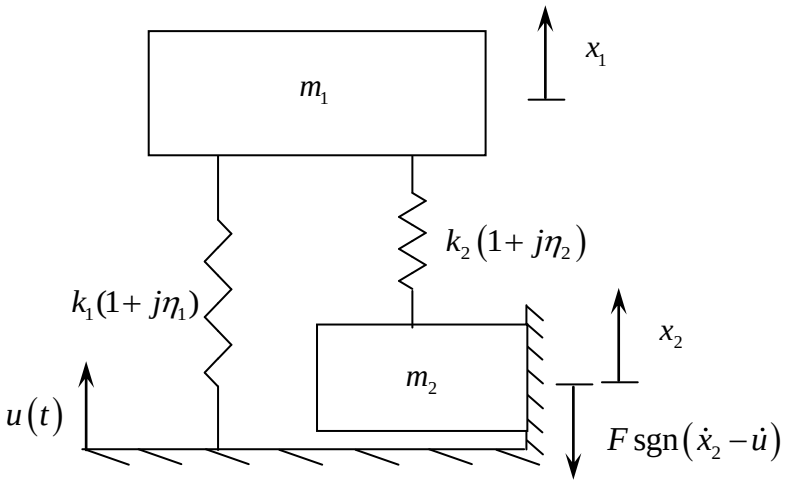

Figure 5.8: Two degree of freedom model with Coulomb friction under base displacement.

(a)

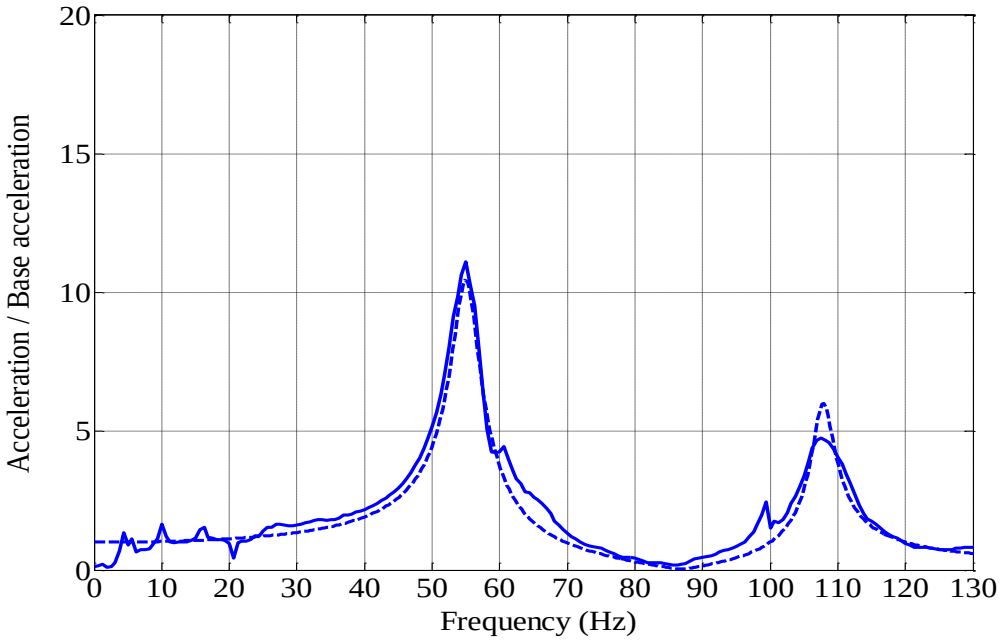

(b)

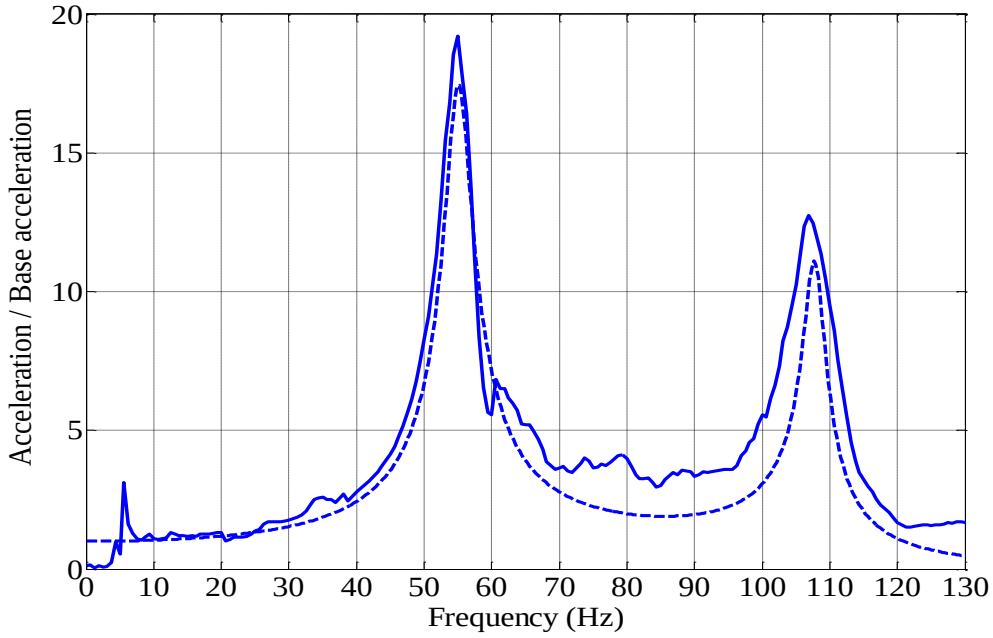

Figure 5.9: Comparison between the acceleration transmissibility measured from the experiment for the case of no friction and thin secondary beam. The acceleration transmissibility was constructed from fitted parameters. (a) The primary system response. Solid line: Acceleration at the end of the first beam (sensor 2). Dash line: Acceleration of the primary mass using fitted parameters. (b) The secondary system response. Solid line: Acceleration at the end of the secondary beam (sensor 3). Dash line: Acceleration of the secondary mass using fitted parameters.

Parameters	Estimated values
k_1	4350.5 N/m
k_2	2279.1 N/m
m_1	0.024 kg
m_2	0.008 kg
η_1	0.09
η_2	0.02
Stiffness ratio, $\hat{k} = \frac{k_2}{k_1}$	0.52
Mass ratio, $\mu = \frac{m_2}{m_1}$	0.32
First natural frequency of a coupled system, ω_1	429.1 rad/s (68.28 Hz)
Frequency ratio, $\hat{\omega} = \frac{\omega_2}{\omega_1}$	1.27

Table 5.4: Two degree of freedom system parameters determined by fitting the two degree of freedom model to the measured acceleration transmissibility from the experiment when friction is zero.

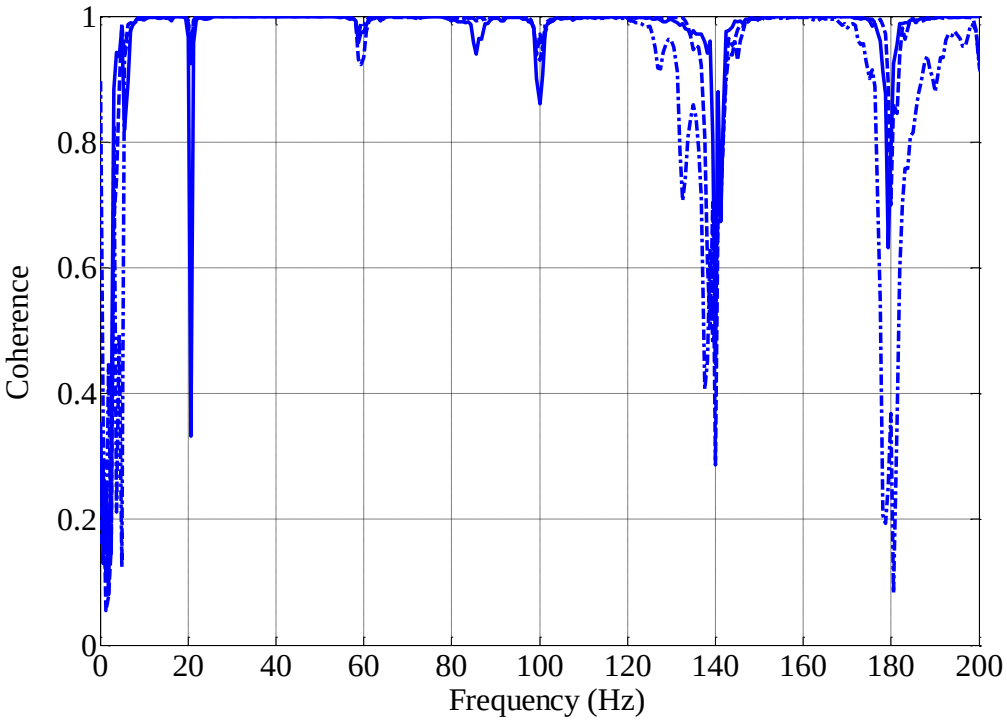

Figure 5.10: Coherence function of the beam system with no friction and thin secondary beam (Response signals of the beam relative to the base response). Solid line: End of the primary beam (sensor 2). Dash line: End of the secondary beam (sensor 3). Dash dot line: Response of the end of the secondary beam (sensor 4).

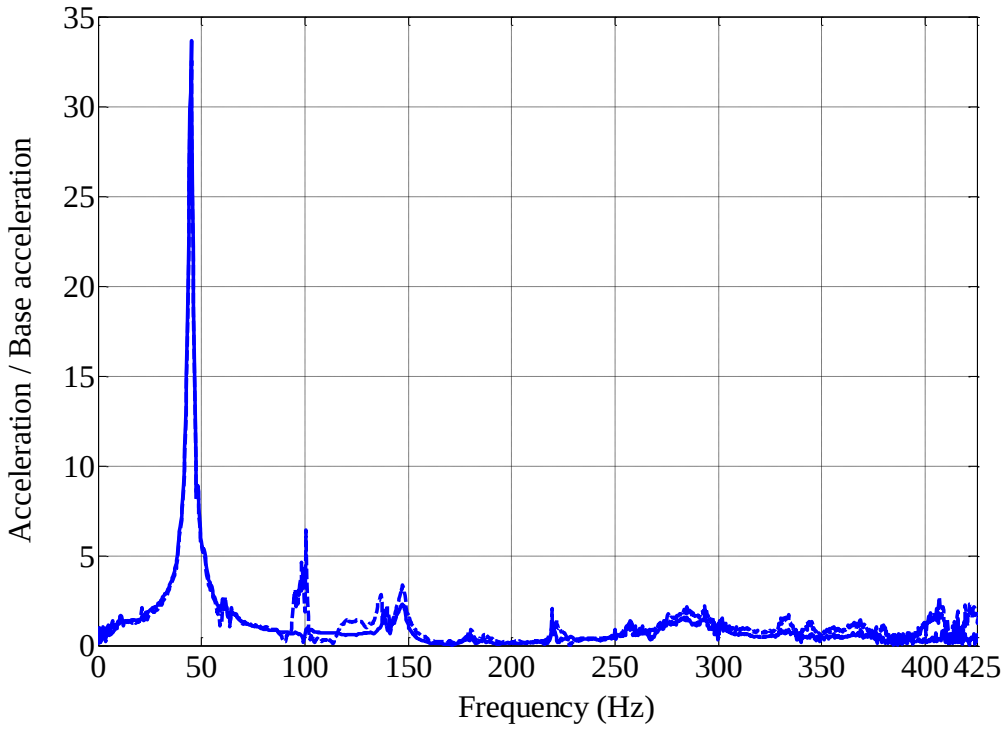

Figure 5.11: The acceleration transmissibility measured from the experiment for the case of no friction and thick secondary beam. Solid line: Acceleration at the end of the first beam (sensor 2). Dash line: Acceleration at the end of the secondary beam (sensor 3).

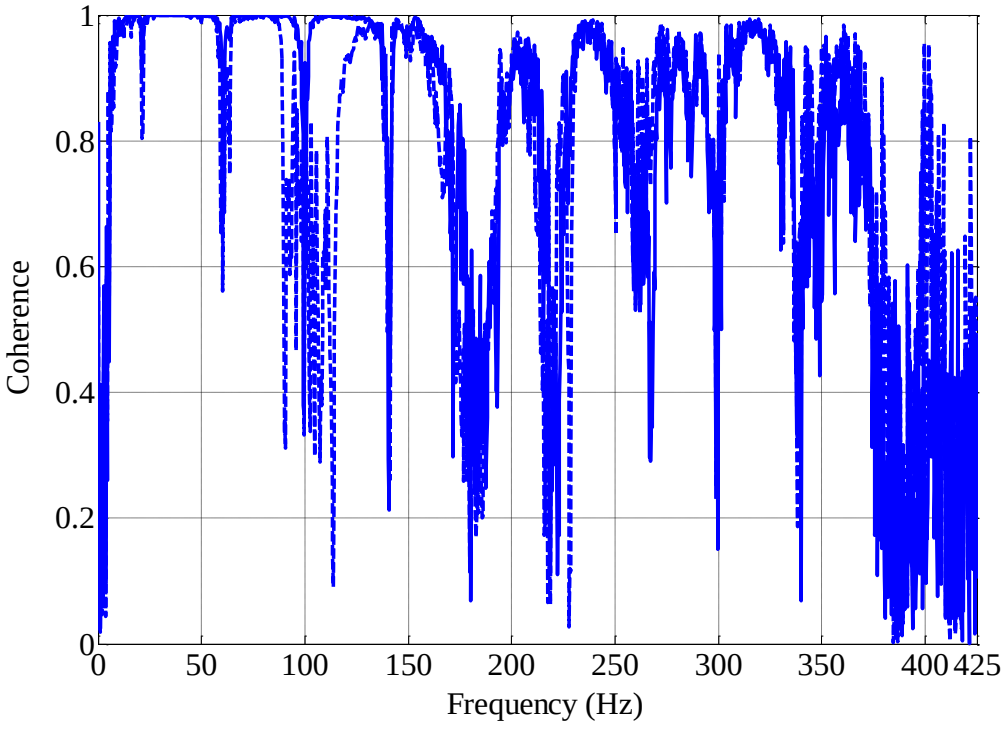

Figure 5.12: Coherence function of the beam system with no friction and thick secondary beam (Response signals of the beam relative to the base response). Solid line: End of the primary beam (sensor 2). Dash line: End of the secondary beam (sensor 3).

(a)

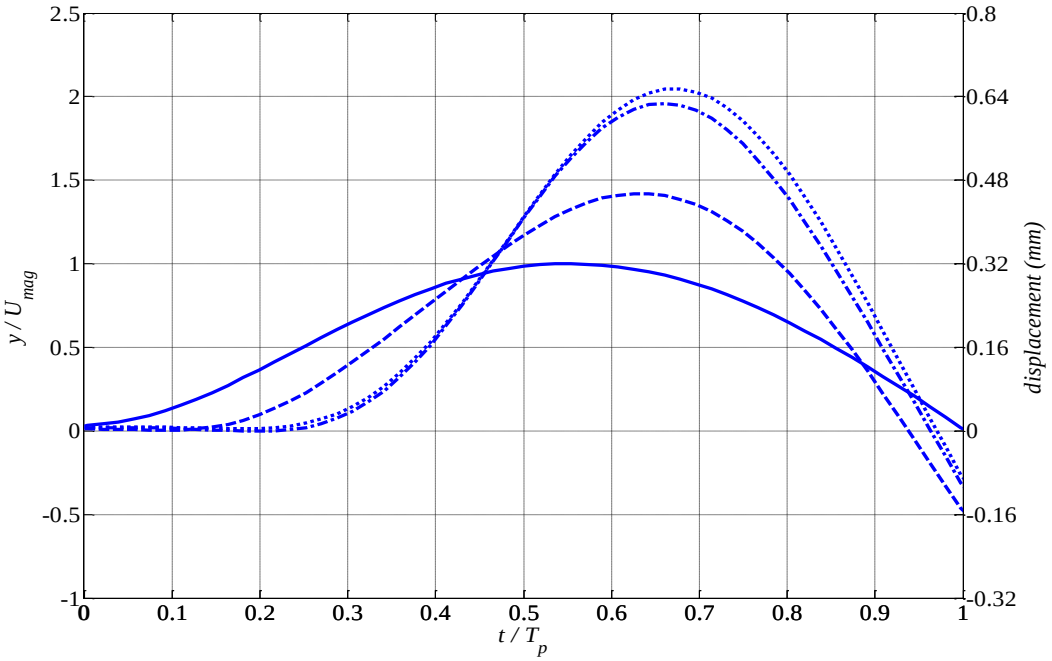

(b)

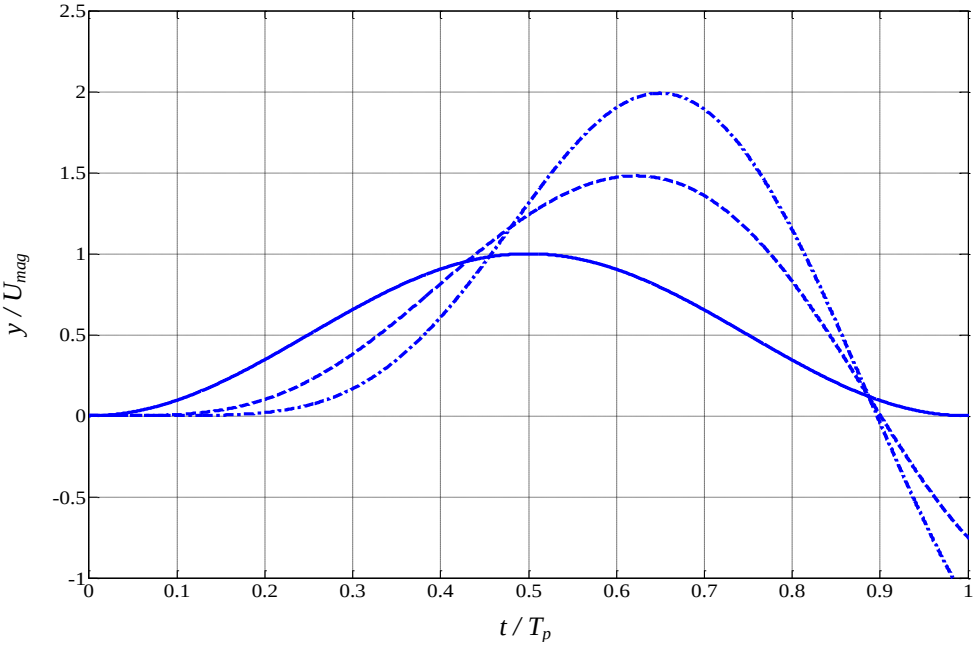

Figure 5.13: Displacement response of the thin secondary beam system with no friction. (a) Measured. Solid line: Base input. Dash line: Response at the end of the primary beam (sensor 2). Dash dot line: Response at the end of the secondary beam (sensor 3). Dot line: Response at the end of the secondary beam (sensor 4). (b) ODE simulation. Solid line: Base input. Dash line: Response of the primary mass. Dash dot line: Response at the secondary mass. Non-dimensional displacement, $y = \frac{\omega_1^2 x}{g}$ .Non-dimensional base input magnitude, $U_{mag} = \frac{\omega_1^2 u_{mag}}{g}$.

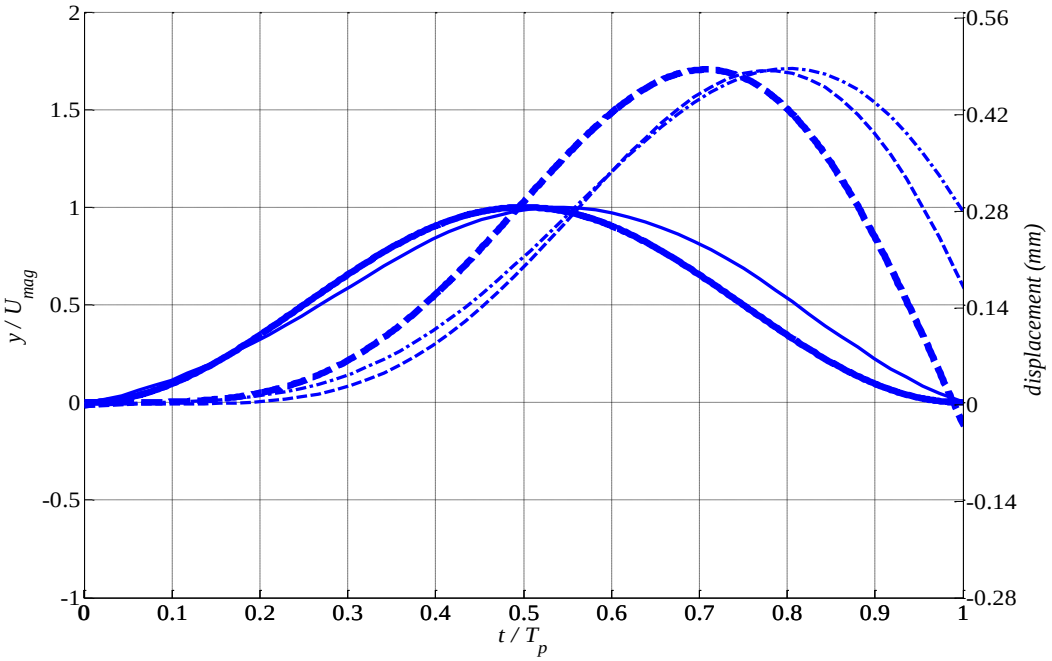

Figure 5.14: Displacement response of the thick secondary beam system with no friction. Thick solid line: Simulation base input. Thick dash line: Response of a single degree of freedom system. Thin solid line: Experimental base input. Thin dash line: Response at the end of the primary beam. Thin dash dot line: Response at the end of the secondary beam.

Non-dimensional displacement, $y = \frac{\omega_1^2 x}{g}$. Non-dimensional base input magnitude, $U_{mag} = \frac{\omega_1^2 u_{mag}}{g}$.

(a)

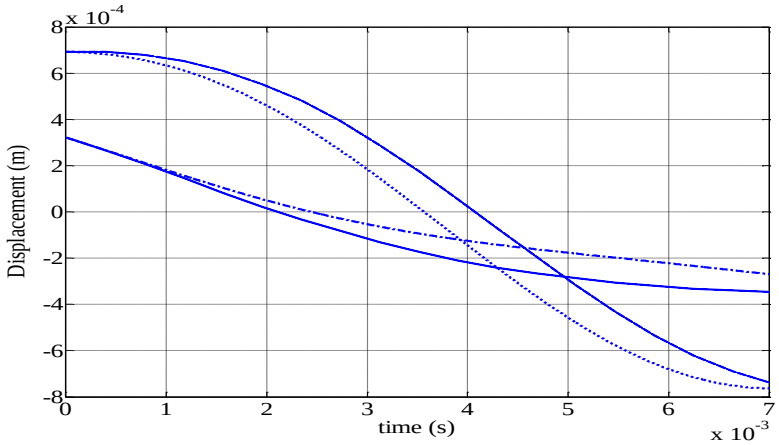

$\hat{F} = 0.39$

(b)

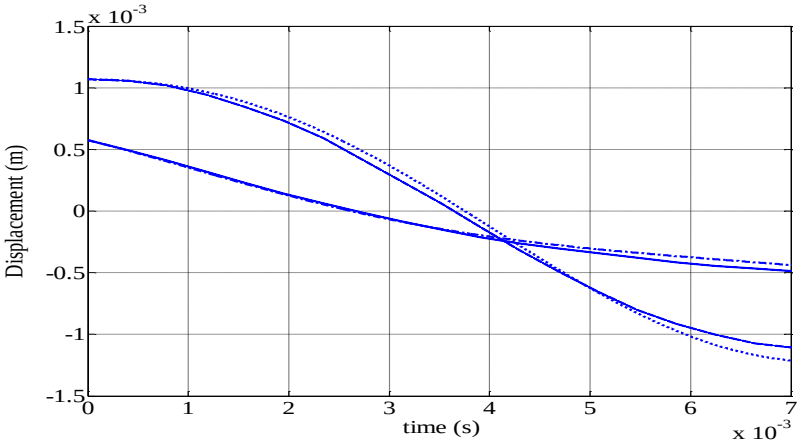

$\hat{F} = 0.6$

(c)

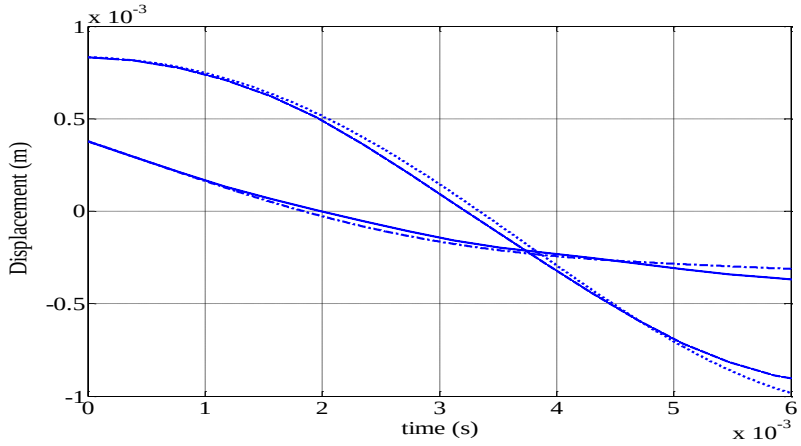

$\hat{F} = 0.48$

Figure 5.15: Comparison of the free vibration response of the beam system with the analytical solutions to estimate the value of friction. Solid line: Response at the end of the primary beam (sensor 2). Dash line: Response at the end of the secondary beam (sensor 3). Dash dot line: Free vibration response of the primary mass response with friction estimated. Dot line: Free vibration response of the secondary mass response with friction estimated.

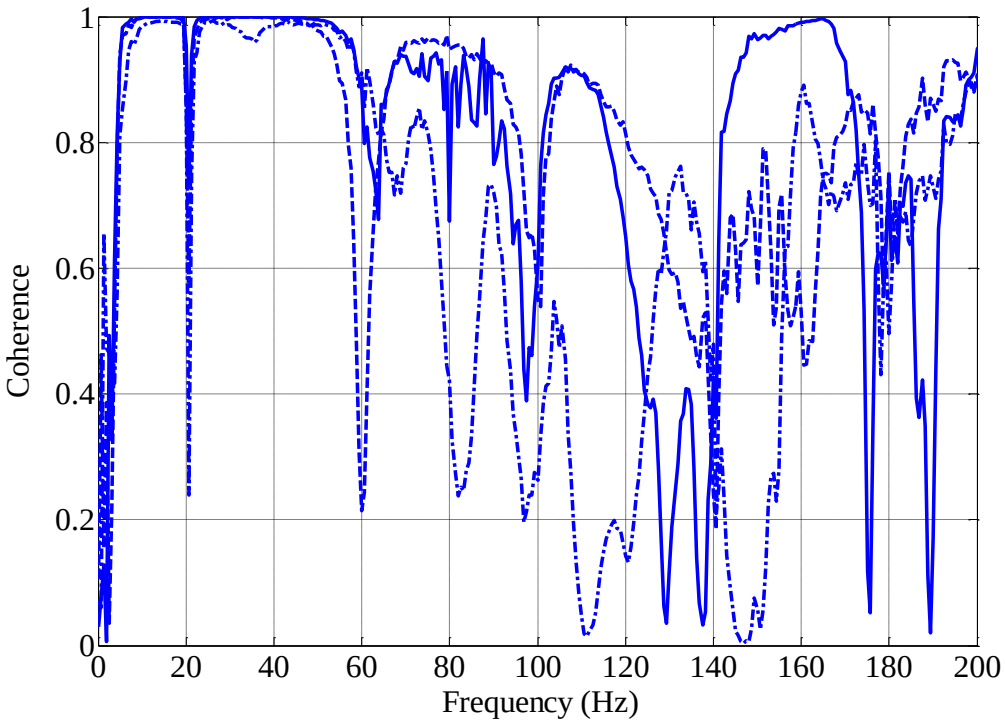

Figure 5.16: Coherence function of the thin secondary beam system with intermediate friction (Response signals of the beam relative to the base response). Solid line: End of the primary beam (sensor 2). Dash line: End of the secondary beam (sensor 3). Dash dot line: End of the secondary beam (sensor 4).

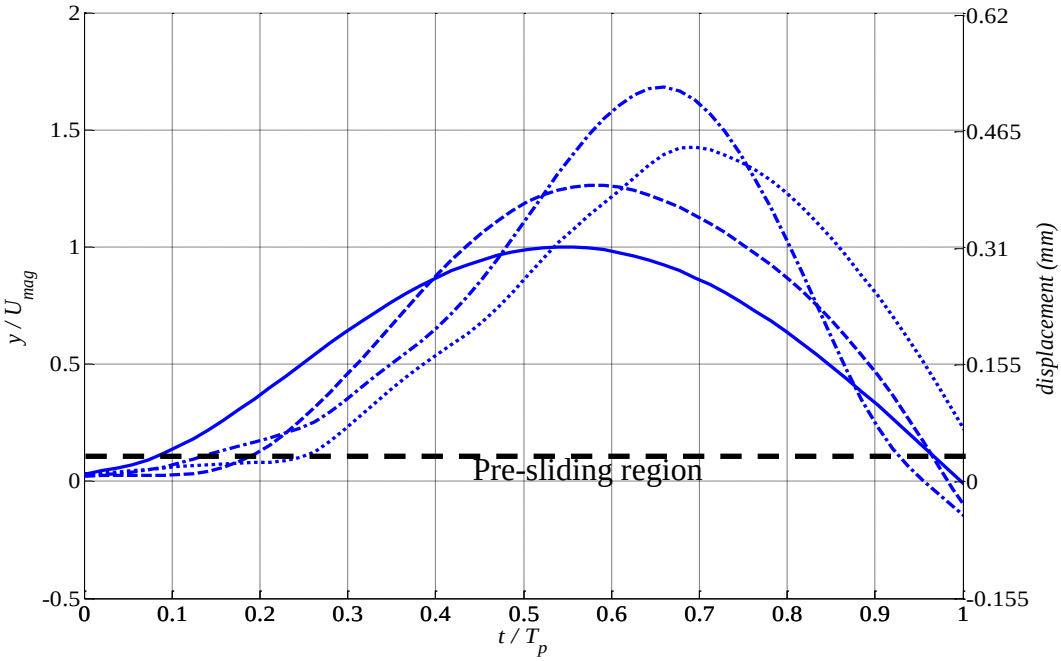

(a)

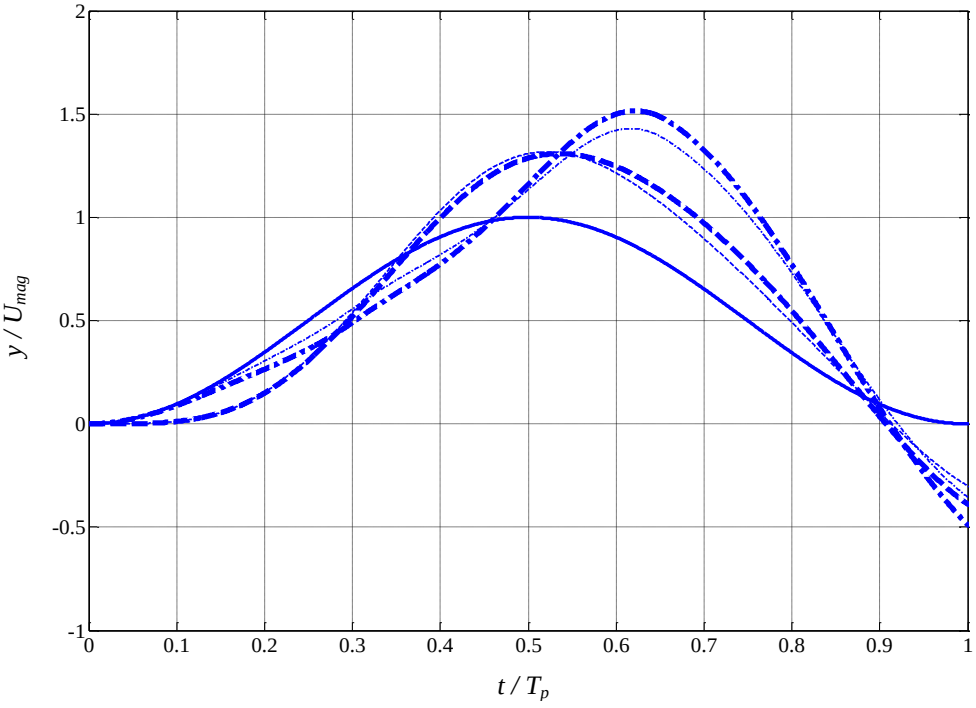

(b)

Figure 5.17: Displacement response of the thin secondary beam system with intermediate friction. (a) Measured. Solid line: Base input. Dash line: Response at the end of the primary beam (sensor 2). Dash dot line: Response at the end of the secondary beam (sensor 3). Dot line: Response at the end of the secondary beam (sensor 4). (b) ODE simulation with Coulomb friction. Solid line: Base input. Dash thick line: Primary mass response, $\hat{F} = 0.39$. Dash thin line: Primary mass response, $\hat{F} = 0.48$. Dash dot thick line: Secondary mass response, $\hat{F} = 0.39$. Dash dot thin line: Secondary mass response, $\hat{F} = 0.48$.

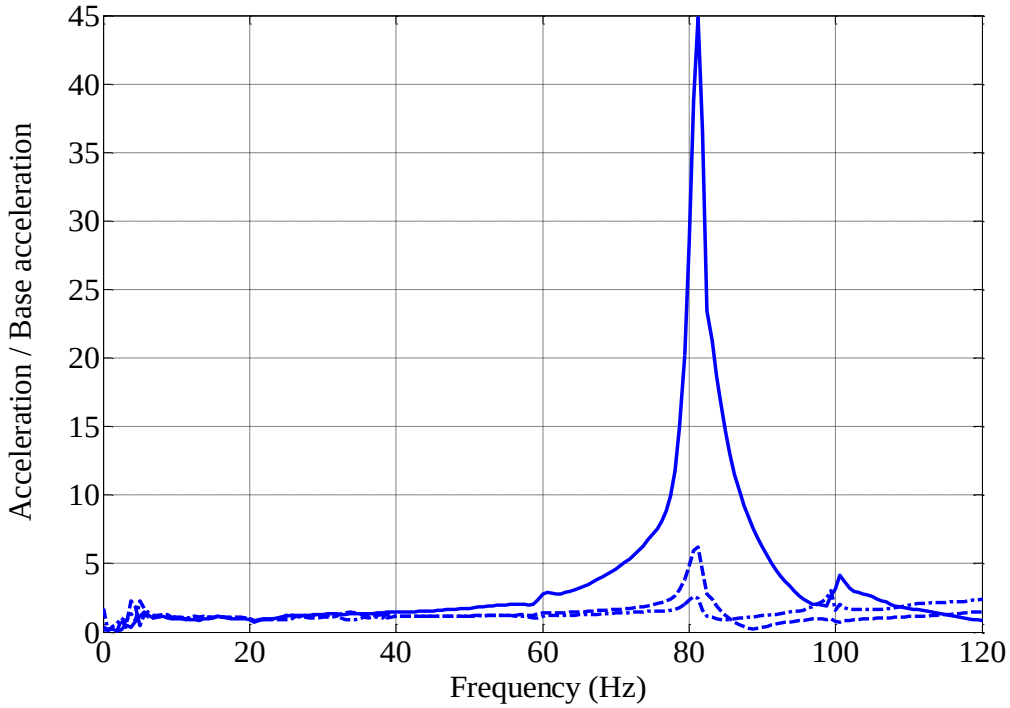

Figure 5.18: The acceleration transmissibility measured from the experiment for the case of high friction and thin secondary beam. Solid line: Acceleration at the end of the first beam (sensor 2). Dash line: Acceleration at the end of the secondary beam (sensor 3). Dash dot line: Acceleration at the end of the secondary beam (sensor 4).

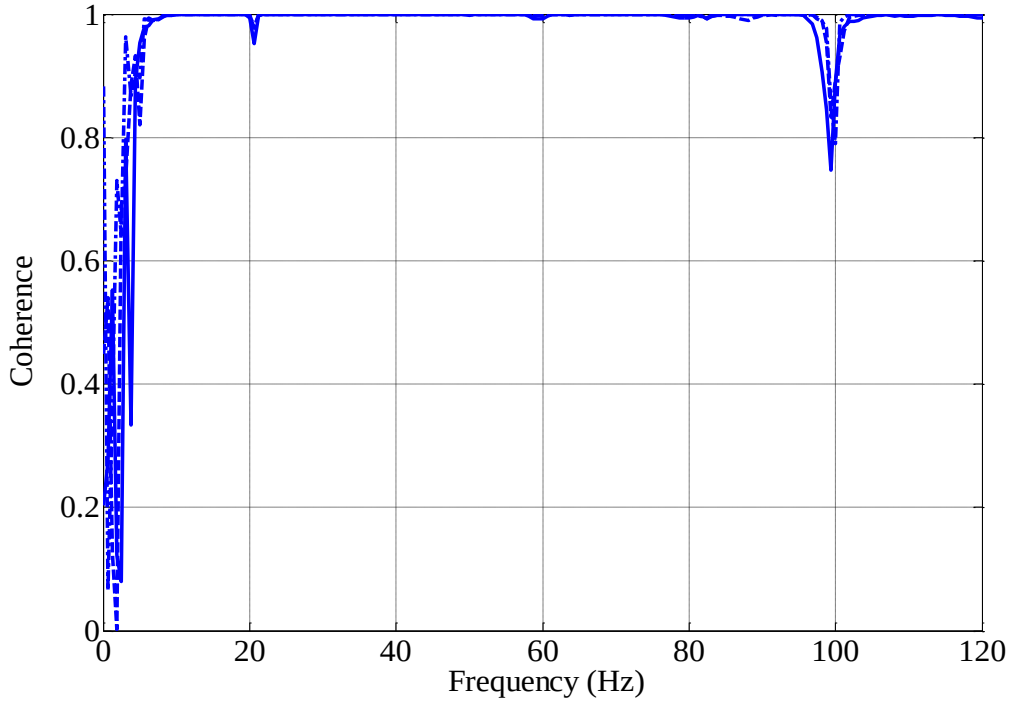

Figure 5.19: Coherence function of the beam system with high friction and thin secondary beam (Response signals of the beam relative to the base response). Solid line: End of the primary beam (sensor 2). Dash line: End of the secondary beam (sensor 3). Dash dot line: End of the secondary beam (sensor 4).

(a)

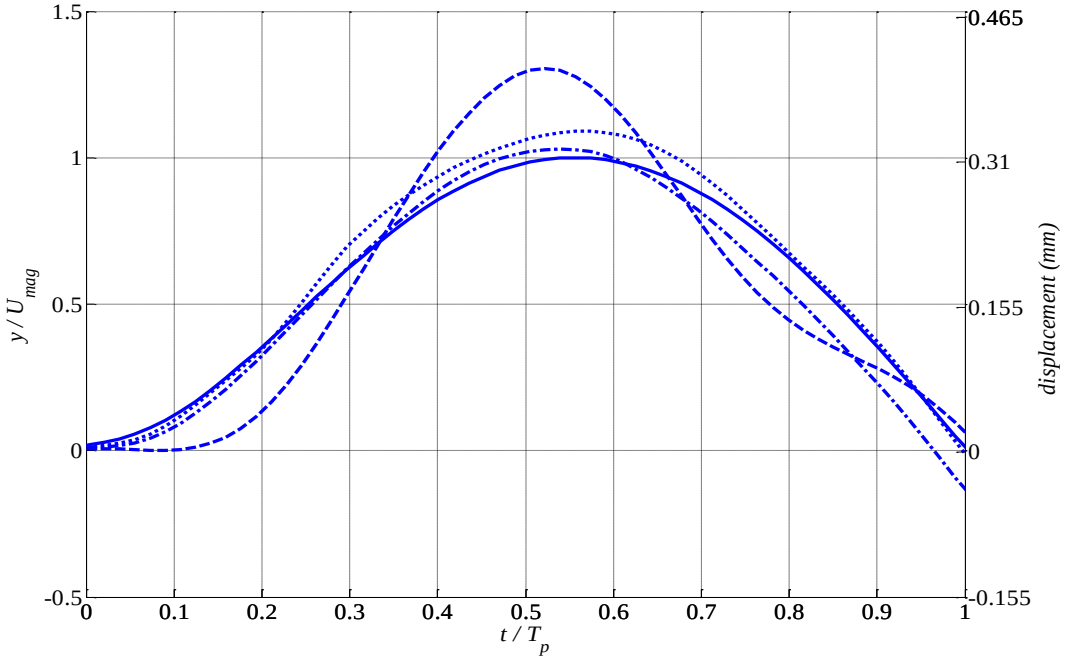

(b)

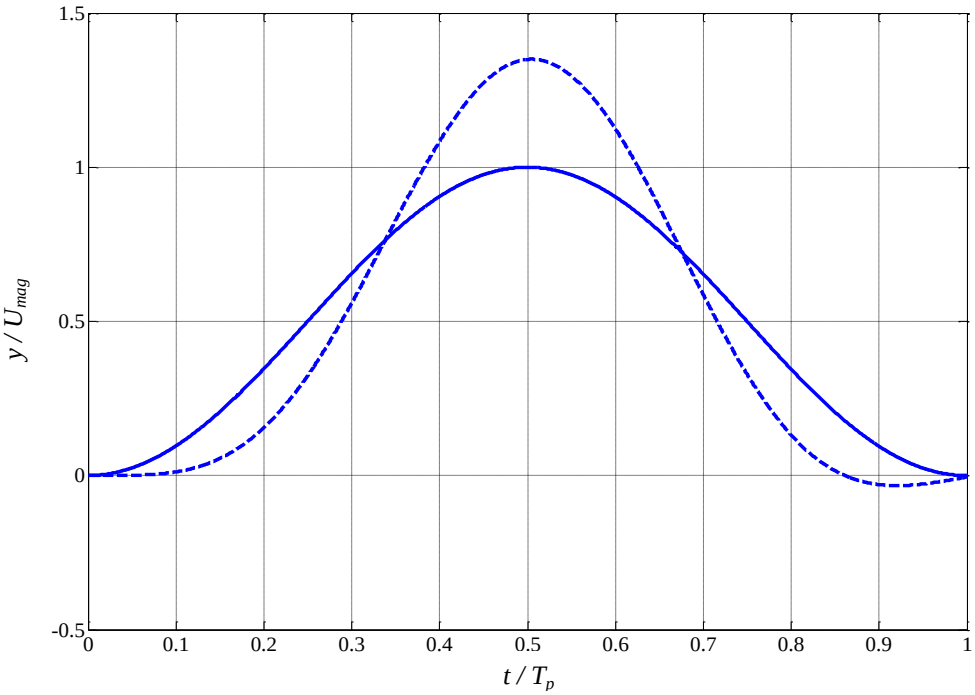

Figure 5.20: Displacement response of the thin secondary beam system with high friction. (a) Measured. Solid line: Base input. Dash line: Response at the end of the primary beam (sensor 2). Dash dot line: Response at the end of the secondary beam (sensor 3). Dot line: Response at the end of the secondary beam (sensor 4). (b) ODE simulation with Coulomb friction. Solid line: Base input and response of the secondary mass. Dash line: Response of the primary mass.

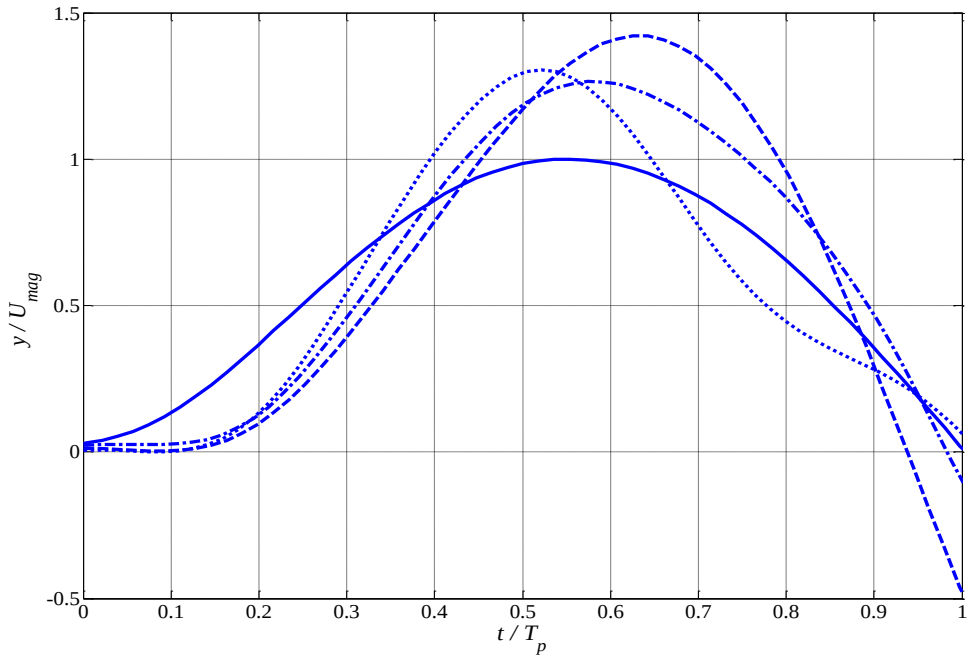

Figure 5.21: Comparison between measured displacement responses at the end of the primary beam with different levels of friction for the case of the thin secondary beam. Solid line: Base input. Dash line: No friction. Dash dot line: Intermediate friction. Dot line: High friction.

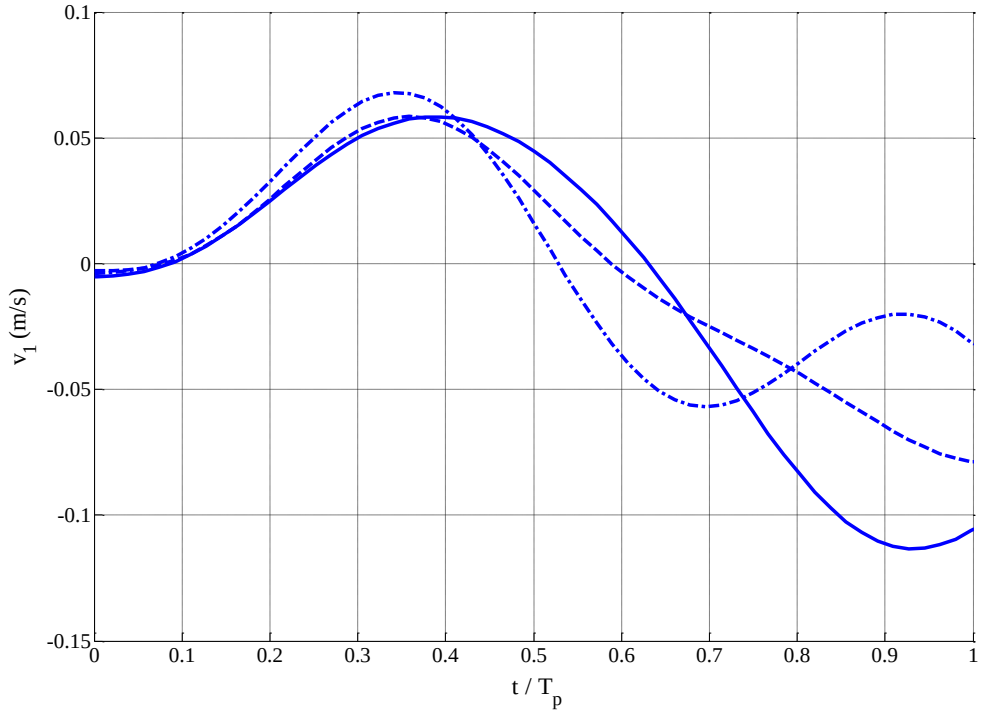

Figure 5.22: Comparison between measured velocity responses at the end of the primary beam with different levels of friction for the case of the thin secondary beam.
Solid line: No friction. Dash line: Intermediate friction. Dash dot line: High friction.

Categories	Experiment			Simulation			
	End of primary beam maximum displacement	End of secondary beam maximum displacement		Primary mass maximum displacement		Secondary mass maximum displacement	
No friction	1.42	Sensor 3	1.96	1.48		1.99	
		Sensor 4	2.05				
Intermediate friction	1.26	Sensor 3	1.68	$\hat{F} = 0.39$	1.31	$\hat{F} = 0.39$	1.52
		Sensor 4	1.43	$\hat{F} = 0.48$	1.32	$\hat{F} = 0.48$	1.43
High friction	1.31	Sensor 3	1.03	1.35		1	
		Sensor 4	1.09				

Table 5.5: Comparison between the measured maximum displacement responses and the predicted responses for three different levels of friction for the case of the thin secondary beam. The maximum displacements are normalized with the maximum base input displacement.

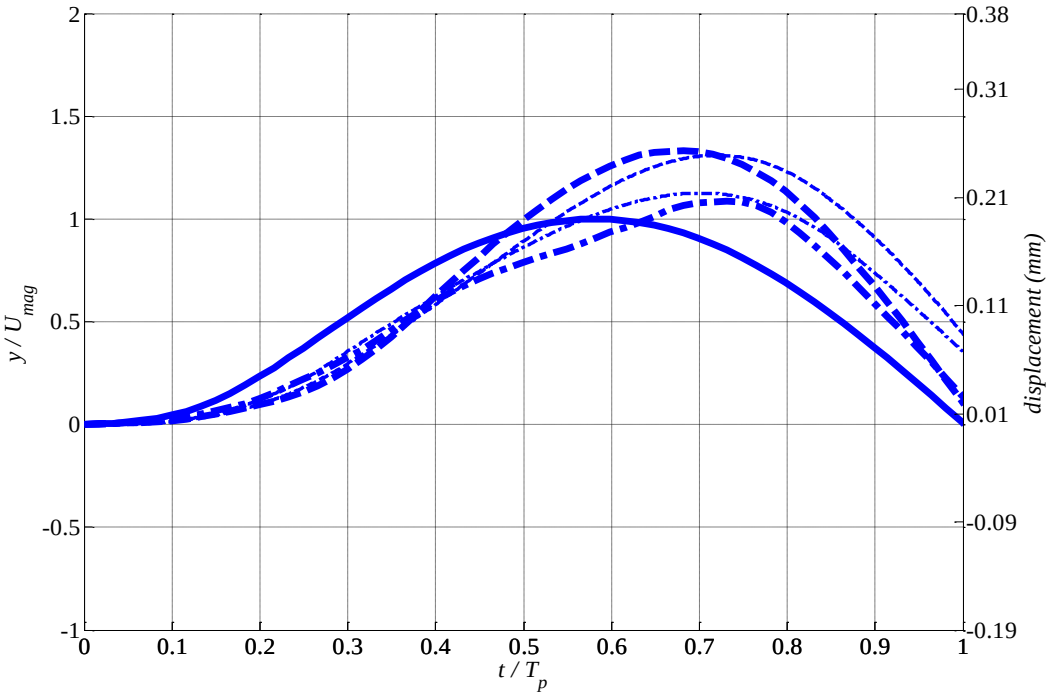

Figure 5.23: Displacement response of the thick secondary beam system with intermediate friction. Thick solid line: Base input. Thick dash line: Measured response at the end of the primary beam. Thick dash dot line: Measured response at the end of the secondary beam. Thin dash line: ODE simulation mass response, $\hat{F} = 0.2$. Thin dash dot line: ODE simulation mass response, $\hat{F} = 0.3$.

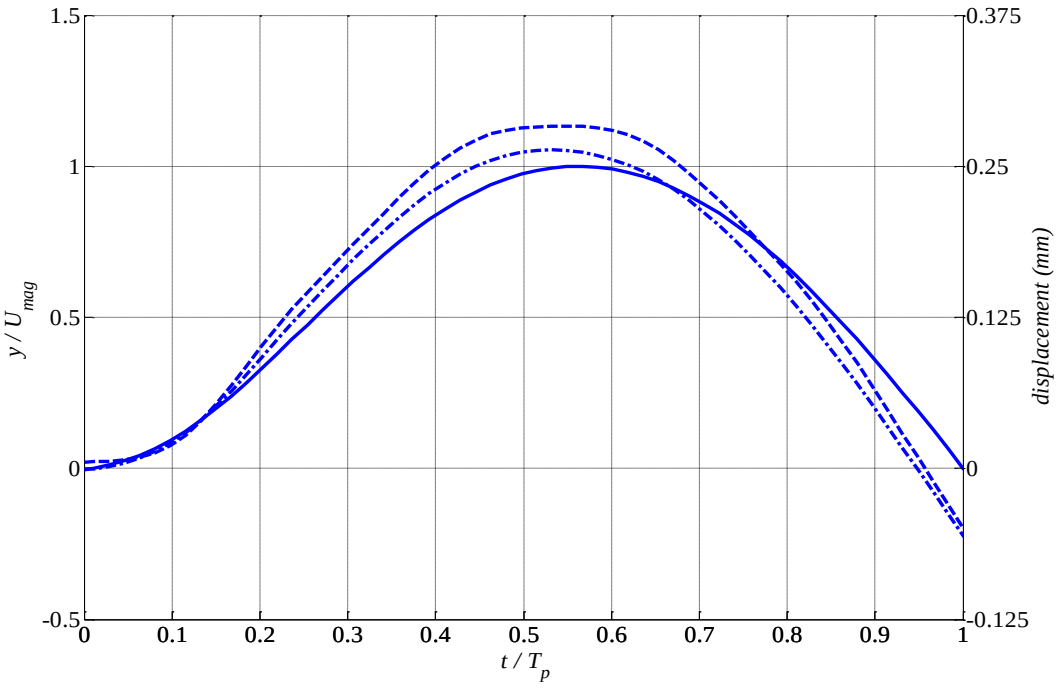

Figure 5.24: Displacement response of the thick secondary beam system with high friction. Solid line: Base input. Dash line: Response at the end of the primary beam. Dash dot line: Response at the end of the secondary beam.

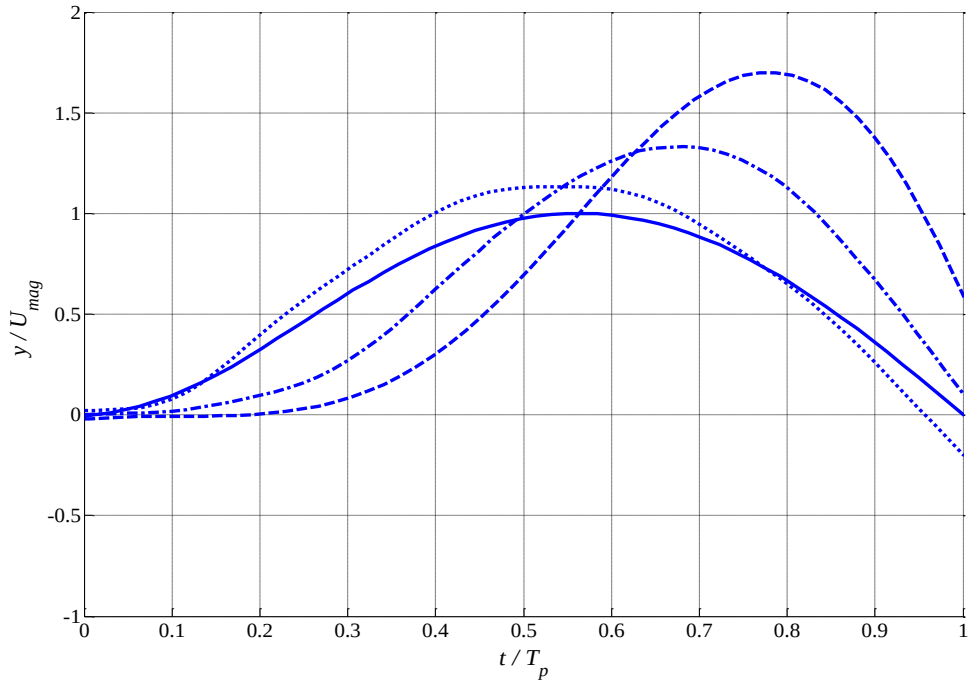

Figure 5.25: Comparison between measured displacement responses at the end of the primary beam with different levels of friction for the case of the thick secondary beam. Solid line: Base input. Dash line: No friction. Dash dot line: Intermediate friction. Dot line: High friction.

Categories	Experiment		Simulation	
	End of primary beam maximum displacement	End of secondary beam maximum displacement		
No friction	1.7	1.71	1.71	
Intermediate friction	1.33	1.09	$\hat{F} = 0.2$	1.31
			$\hat{F} = 0.3$	1.13
High friction	1.13	1.06	1	

Table 5.6: Comparison between the maximum displacements for the responses measured from the experiment and simulation responses for three different levels of friction for the case of the thick secondary beam. The maximum displacements are normalized with the maximum base input displacement.

Categories	Thin secondary beam			Thick secondary beam	
	End of primary beam maximum displacement	End of secondary beam maximum displacement		End of primary beam maximum displacement	End of secondary beam maximum displacement
No friction	1.42	Sensor 3	1.96	1.7	1.71
		Sensor 4	2.05		
Intermediate friction	1.26	Sensor 3	1.68	1.33	1.09
		Sensor 4	1.43		
High friction	1.31	Sensor 3	1.03	1.13	1.06
		Sensor 4	1.09		

Table 5.7: Comparison between the maximum displacement responses of the system s with thin and thick secondary beams. The maximum displacements are normalized with respect to the maximum base input displacement.

6. IMPLEMENTATION AND VALIDATION OF A SWITCHABLE FRICTION SYSTEM

6.1 Introduction

The main objective of this chapter is to implement the practical control of friction by switching on and off the normal forces which are provided experimentally by an electromagnet. The decision logic was performed using a D Space Real Time Interface [72] so that the friction could be changed in real time. The purpose of the implementation is to validate the theoretical response prediction of a two degree of freedom system with the switchable friction given in Chapter 3. The same test rig as previously was used during the experiment, with an electromagnet at each end of the secondary beam. The time histories of the switchable system are compared to the respective passive system, to see the effect of switching friction especially in terms of the displacement response of the primary targeted mass. It is expected, from chapter 3, that the switchable system will give a smaller peak displacement than the passive system. As a two degree of freedom model is used, it is also expected that the acceleration response at the end of the primary beam would be very smooth.

6.2 Implementation of switchable friction

In order to successfully replicate and validate the theoretical concepts presented in chapter 3, an experimental switchable friction system must be able to switch on-off very quickly, essentially instantaneously without significant time delay. The design incorporates an electromagnet near to each end of the secondary beam. An electromagnet has been used by Agrawal *et al* [73, 74] for base-isolated buildings by regulating the normal force and hence the friction. They introduced the electromagnetic semi active friction damper which consists of a friction pad installed between two steel plates. The normal force is varied by changing the electric current in solenoids located at the outer surface. This has advantages over a hydraulic actuator in terms of its instantaneous response and its ability to provide a force in the order of 20 kN [75]. Also, Ramirez [3] used an electromagnet in his experiment to achieve switchable stiffness and he showed that an electromagnet can be switched on and off almost instantaneously.

For this validation experiment, the steel beam applies a normal load to both ends of the secondary beam and hence, friction is applied when the electromagnet is switched off. On the other hand, when the electromagnet is switched on, the electromagnet attracts the steel beam and both ends of the secondary beam are free to move without friction. In order to implement the switching, the proposed control strategy from chapter 3 is used. There three parameters are used to implement the model control strategy, namely the relative displacement across the primary spring, relative velocity between the base and secondary mass (friction direction) and the absolute velocity of the primary mass. As the beam system is used for the validation, the three parameters are the relative displacement between the end of the primary beam and the base, the relative velocity between the end of the secondary beam and the base (friction direction) and the absolute velocity at the end of the primary beam. Four accelerometers are used to obtain the responses of the base, the end of the primary beam and both ends of the secondary beam to calculate the parameters. The friction is turned off by switching the electromagnet on when the relative velocity (the end of the secondary beam and the base) has the same sign as the relative displacement (the end of the primary beam and the base) but the opposite sign to the absolute velocity (the end of the primary beam). In any other case, the friction is turned on. The decision logic to implement the proposed control strategy is outlined in Figure 6.1.

This logic was implemented in the Simulink environment which runs on the D Space RTI 1005 platform. Jalili *et al* [76] also used a D Space platform in their experiment to achieve

a switchable stiffness. Because the parameters involve velocity and displacement, the acceleration signal has to be numerically integrated before the decision process. The absolute or relative acceleration is fed into a series of 'Discrete Time Integrator' blocks in Simulink which is used to perform the integration to obtain both velocity and displacement. In order to obtain displacement two integrator blocks are needed, while only one is needed to obtain velocity. Before a signal is fed into the integrator block it has to be filtered with a high pass filter to eliminate the low frequencies. Subsequently, the decision logic outlined in Figure 6.1 is performed. This sequence of processes is shown in the Simulink model in Figure 6.2 with a green rectangle. The trigger function is included in the Simulink model to ensure the model is evaluated only after the acceleration response reaches certain level. The Simulink model is marked with a blue rectangle in Figure 6.2.

In order to drive the electromagnet, this control action operates a relay which turns on and off the current from the power source. The electromagnet cannot be directly operated by the D Space system due to output current limitations [76]. A metal–oxide–semiconductor field-effect transistor (MOSFET) was used to implement this requirement. It is a transistor used for amplifying and switching electronic signals. It is connected to the D Space system and a power source so that the switching process performed by D Space can turn on and off the supplied current from the current source to drive the electromagnet. The configuration of the MOSFET circuit is shown in Figure 6.3. The whole schematic diagram of the setup used for the experiment to validate the response of the system with switchable friction is shown in Figure 6.4.

6.3 Time response validation for the system with switchable friction

6.3.1 Background information

From chapter 3, theoretically a switchable friction system produces a smaller response than a passive system. The reduction of the response of the switchable system is increased significantly if the stiffness ratio of the two degree of freedom is increased, typically by increasing the secondary spring stiffness. Based on the estimated two degree of freedom parameters determined from the previous chapter, the system with the thin secondary beam can serve as the comparison to a two degree of freedom model with a soft secondary spring and a low stiffness ratio. Therefore, it is expected that it is possible to have a reduction in the displacement response at the end of the primary beam during the experiment but the

reduction will be small. It is also expected that the primary mass will have smooth acceleration response.

From chapter 3, it is discussed that the system with an intermediate spring stiffness can produce larger displacement reduction and at the same time produce smooth acceleration response at the primary mass. If more reduction is needed, the beam dimensions have to be changed to serve as the comparison to the two degree of freedom model with a stiffer secondary spring. One way to do this is to increase the thickness of the secondary beam. However, it was decided to perform the experiment only with the thin secondary beam. The reason of this decision is because the system with the thick secondary beam mentioned in the previous chapter is not expected to produce the behaviour of the two degree of freedom system with intermediate spring if the pulse length used is about 0.02 s. In this case, the system behaves more or less like a single degree of freedom system or a two degree of freedom system with a stiff secondary spring.

6.3.2 Results

The value of the parameters used in the logic, namely the relative displacement (the end of the primary beam and the base), the relative velocity (the end of the secondary beam and the base) and the absolute velocity (the end of the primary beam) are plotted in Figures 6.5, 6.6 and 6.7 respectively. To observe how the electromagnet was switched on and off, the voltage generated by the D Space system is plotted versus time in Figure 6.8. The voltage switches between 0 and 10 V, where 0 V means no voltage generated so friction is on and 10 V means the electromagnet is turned on and attracts the steel beam resulting in zero friction.

The displacement response of the switchable friction system is presented in Figure 6.9 for the case when friction is not high, so that the end of the secondary beam slides with respect to the friction interface. The length of the pulse used was 0.02 s, corresponding to the length of pulse generated with the procedure described in previous chapter. For comparison, the displacement response of the passive system is plotted in the same figure. The displacement amplitudes are normalized with respect to the maximum of the base input. The time axis is normalized with respect to the length of the pulse. Table 6.1 compares the maximum displacement for the system with switchable friction and passive friction. Moreover, the velocity response of the switchable friction system is presented in

Figure 6.10. For comparison, the velocity response of the passive system is also plotted. The velocity amplitudes are presented in m / s.

In order to observe whether the measured displacement response of the beam system agrees with the two degree of freedom model ODE simulation, a comparison between the measured and predicted displacement responses is also presented in Figure 6.11. The level of friction $\hat{F} = 0.48$ is used in the simulations, which corresponds to the value of friction estimated previously. Table 6.2 compares the measured and simulated maximum displacements.

Finally, the acceleration response of the switchable friction system is presented in Figure 6.12. The acceleration amplitudes are presented in m / s^2.

6.3.3 Discussion

The differences between the switchable and passive systems are caused by how and when the friction is switched on and off. In order to understand what happens, it is important to monitor the change of sign for the three parameters which subsequently cause the switching.

The relative displacement, which is shown in Figure 6.5, changes sign at normalised time about 0.4 and 0.82. The relative velocity, which is shown in Figure 6.6, changes sign at normalised time about 0.36 and 0.73. Finally, the absolute velocity at the end of the primary beam, which is shown in Figure 6.7, changes sign at normalised time about 0.57. However, bear in mind that both the relative velocity and absolute velocity change sign several times at the start of the motion until normalized time about 0.1 because of the high frequency oscillations of small magnitude.

Based on these parameters, it can be seen that the friction is switched on and off several times during the experiment as shown in Figure 6.8. Following the discussion presented in Chapter 3, friction is supposed to be switched off from the start of the shock base input. This is because, during the start of the motion, all of the parameters act in the same direction. However, during the experiment, at the start of motion from normalised time 0 to 0.1, the friction switches on and off several times within a short period of time. This is because the absolute velocity at the end of the primary beam and the relative velocity

between the end of the secondary beam and the base change sign very rapidly during that short period; see Figures 6.6 and 6.7. This behaviour might be avoided in the future by using a low pass filter to filter the high frequency content of the relative and absolute velocities before performing the logic or setting some thresholds on the signal levels required for the switching. The high frequency vibration is possibly caused by the base input which excites the higher order modes of the beam system. It could also be caused by the response of the steel beam which subsequently imposes the vibration to the T beam system.

As the velocity response increases when the normalised time reaches 0.1, the process of friction switching gets better and works as expected. Immediately after that, the friction is turned off until about 0.36 when the relative velocity turns positive. When the relative velocity turns positive, the friction is switched on because now friction is in the opposite direction to both the relative displacement and absolute velocity. Then, the friction is turned off again at about 0.57, because the absolute velocity turns negative. The elastic restoring force and friction act in the same direction as the absolute velocity, so it is better to have zero friction. Finally, the friction is turned on again at 0.73 because the relative velocity turns negative and now friction once more acts in the opposite direction to both the relative displacement and absolute velocity.

From Figure 6.9, there is not much difference between the switchable and passive system response at the start of the shock input because the friction is not turned off completely. Then, after the friction is switched off completely at normalised time about 0.1, the response of both ends of the primary beam and the secondary beam begin to deviate from the passive system. The response at the end of the secondary beam deviates from the passive system right after time equal to 0.1, because friction is applied directly at the end of the secondary beam. Then, the displacement response at the end of the secondary beam for the system with the switchable friction starts to become smaller compared to the passive system, until normalized time about 0.63. It then reaches a higher peak compared to the passive system at normalized time about 0.7. The response at the end of the primary beam deviates a little later, after normalised time about 0.36. When the friction is turned on at the normalised time about 0.36, the displacement response at the end of the primary beam tends to be smaller than the passive system before reaching the peak response at the normalized time about 0.57. These patterns can also be observed from the velocity response of the system shown in Figure 6.10.

It can be seen that the maximum displacement response at the end of the primary beam for switchable friction is reduced compared to the passive case. From Table 6.1, the normalised response reduces from 1.59 to 1.33, which is about 16.4 % smaller. On the other hand, the displacement response at the end of the secondary beam is slightly higher for the case of switchable friction. The normalised response for the case of switchable friction is 1.35 compared to 1.25 for the passive system. However, the motive of using switchable friction is to reduce the displacement response at the end of the primary beam and the slight increase in the response at the end of the secondary beam is not of concern. The most important thing is that a significant reduction is achieved in the response at the end of the primary beam.

Examination of Figure 6.11 shows that the measured and predicted displacement responses are slightly different. The difference is small especially for the first half of the pulse length. After the midpoint of the pulse, the difference is bigger at the time the base is moving downward in the negative direction. This is because the base input is not following the exact versed sine curve. As there is gravity, the base moves faster towards the negative direction, which causes a significant deviation between measurements and predictions. Otherwise, the deviation is quite small and it is mainly caused by the process of rapid friction switching at the beginning of the base shock input. The deviation could also be caused by uneven friction as the surface moves. The comparison between the maximum displacements in Table 6.2 shows a good agreement except for one case, the displacement response at the end of the secondary beam for the case of switchable friction is about 18% lower than the prediction. From earlier discussions, for a two degree of freedom model with a soft secondary spring, a very small change in friction produces a change in the response of secondary mass which could be significant. Therefore, a difference of 18% is considered acceptable since there could exist some small changes in the level of friction as sliding occurs. Moreover, the measured response at the end of the primary beam is very close to the predicted response, within 4% of the value.

From the discussion in Chapter 3, one expects to have discontinuity and unsmooth acceleration response when switching occurs. In practice, there are four switching points not including the switching points between normalised time between 0 and 0.1 when the switching process occurs very rapidly. The four switching points are at normalised time 0.1, 0.36, 0.57 and 0.73. In Figure 6.12 the switching points are marked as the dashed black lines. From comparison of Figures 6.12(a) and (b), it can be observed that the acceleration

response at the end of the primary beam is much smoother than at the end of the secondary beam especially in the region of switching; the acceleration response for the latter is not very smooth. This is as expected, as friction causes unsmooth and discontinuous acceleration at the point where it is applied. If it is applied directly to the primary targeted mass, as in the case of a single degree of freedom system, it would cause an unsmooth acceleration on it. This was the main reason why the two degree of freedom model with friction applied to the secondary mass was introduced in this study. It is proven that applying friction at the end of the secondary mass can produce a relatively smooth acceleration response on the primary mass whilst still producing some reduction in the maximum response.

6.4 Conclusions

The practical control of friction by switching on and off the normal forces can easily be provided by an electromagnet. This actuator works almost instantaneously in providing a force to switch on and off an electromagnet in real time. The existence of the D Space Real Time Interface platform makes it much easier to perform the decision logic. The system behaved as expected, from Chapter 3, with only slight explainable differences. The switchable system gives a smaller peak displacement response than the passive system at the end of primary beam, which serves as a comparison to the primary mass in a two degree of freedom model. This shows that the switchable system provides an improvement to the shock response in comparison to a passive system. Furthermore, the acceleration response at the end of the primary beam is very smooth. This proves that the two degree of freedom model, with friction applied to the secondary mass, provides a better acceleration response of the primary targeted mass. By using switchable friction in the two degree of freedom model, it is possible to obtain a better displacement response compared to the passive system and a better acceleration response compared to a single degree of freedom model.

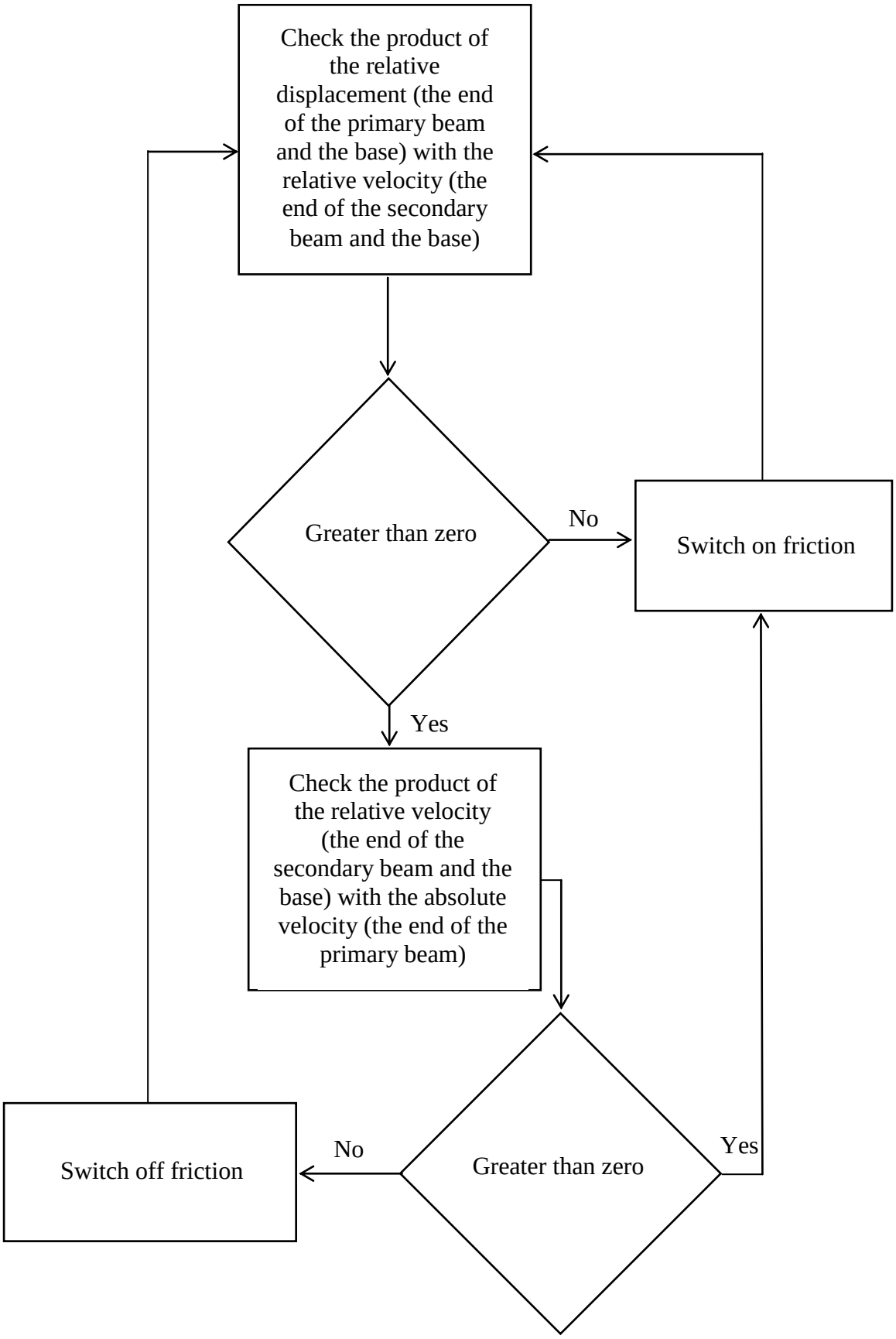

Figure 6.1: The decision logic to switch on and off friction depending on three measured parameters.

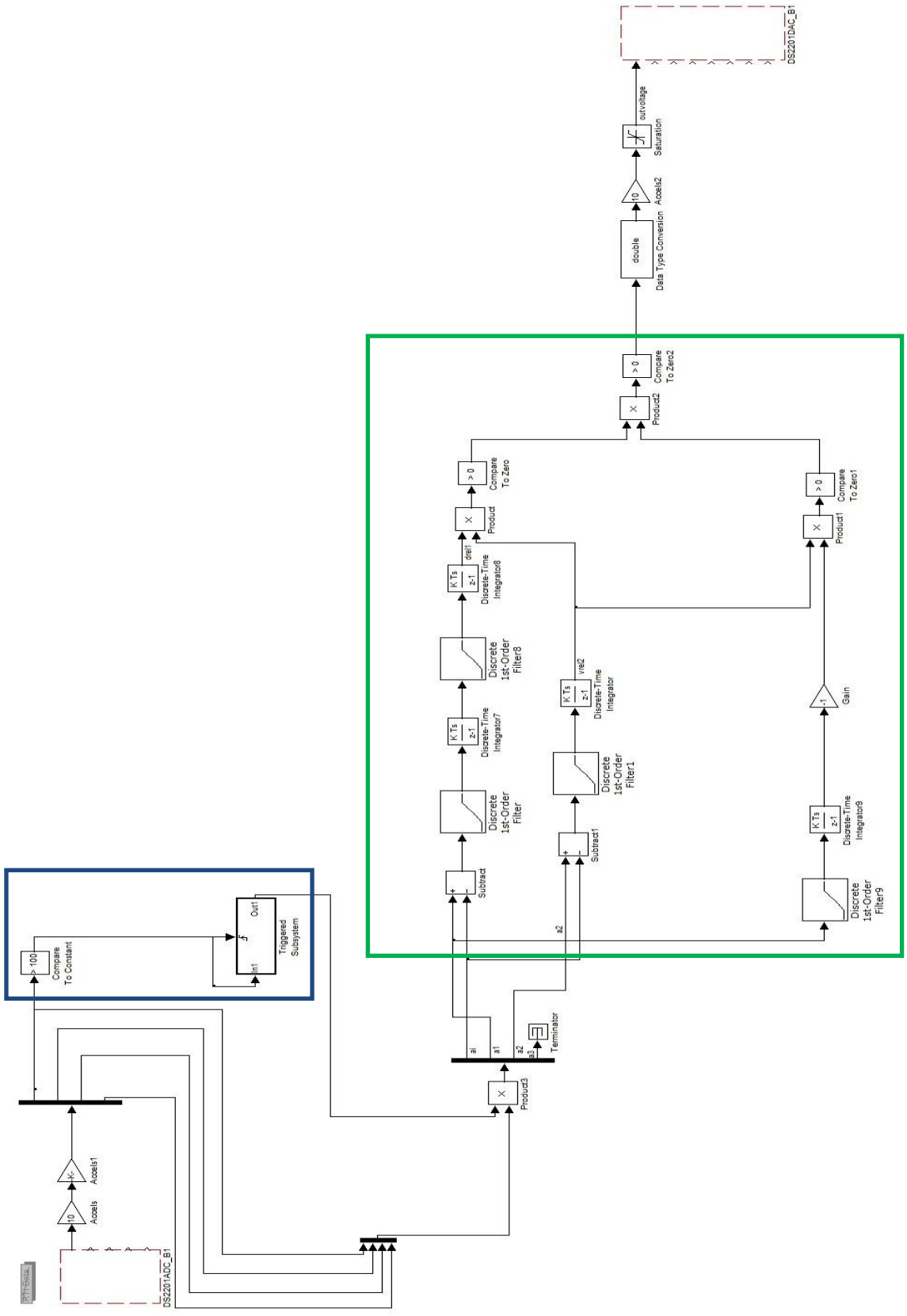

Figure 6.2: Simulink model to perform the decision logic which runs on the DSpace RTI Platform 1005. Green rectangle: Numerical integration and decision logic sequences. Blue rectangle: Trigger function.

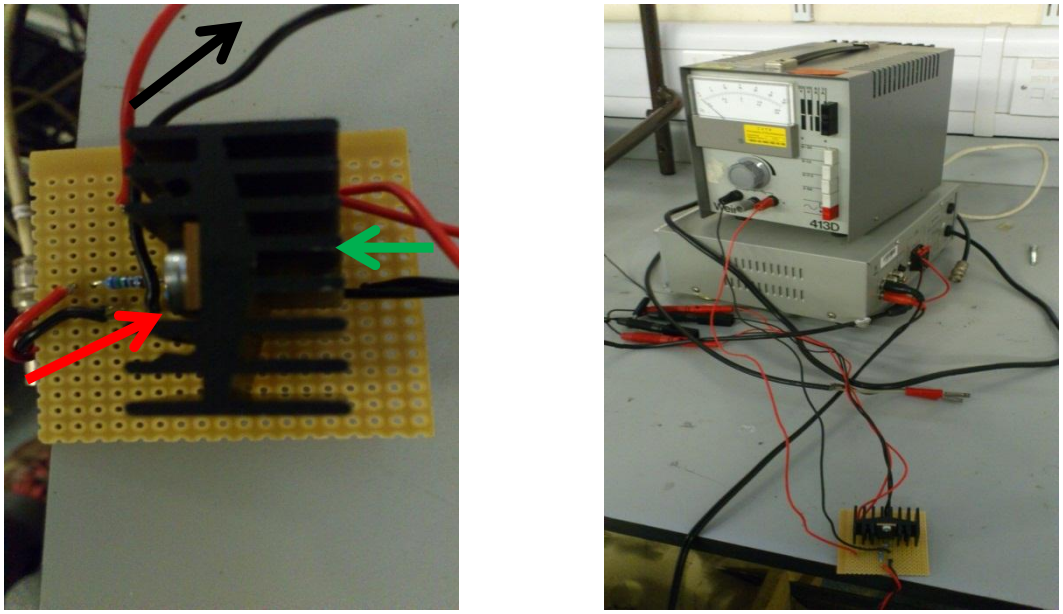

Figure 6.3: The configuration of the MOSFET circuit. Red arrow: Voltage from the DSpace system to switch on and off the current from a power supply to electromagnet. Green arrow: Current from power supply. Black arrow: Current to electromagnet.

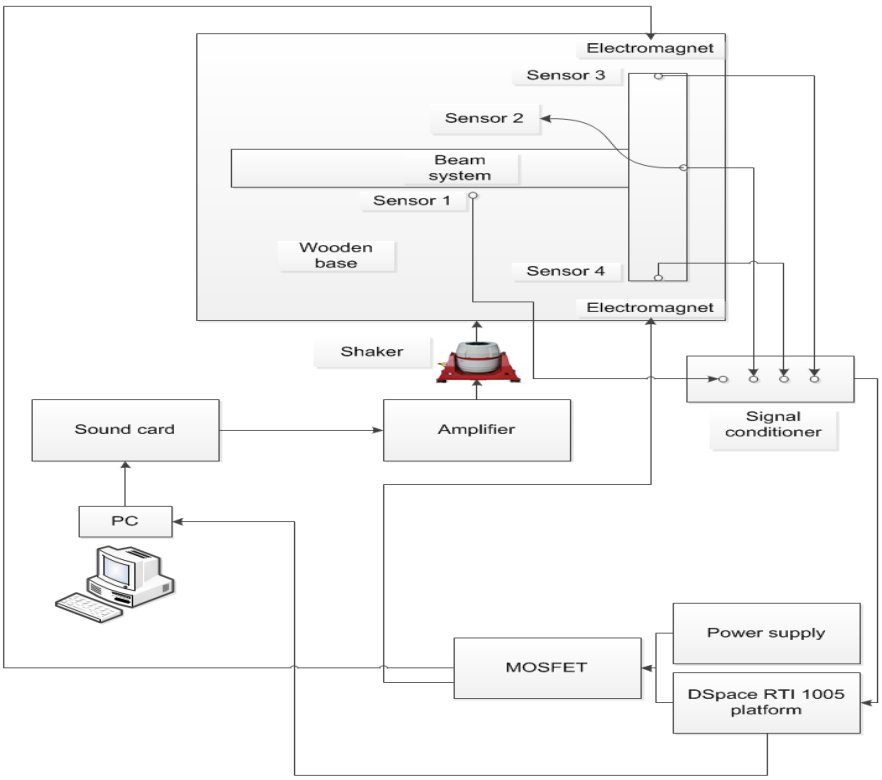

Figure 6.4: Schematic diagram of the setup used for the experiment to validate the response of the system with switchable friction.

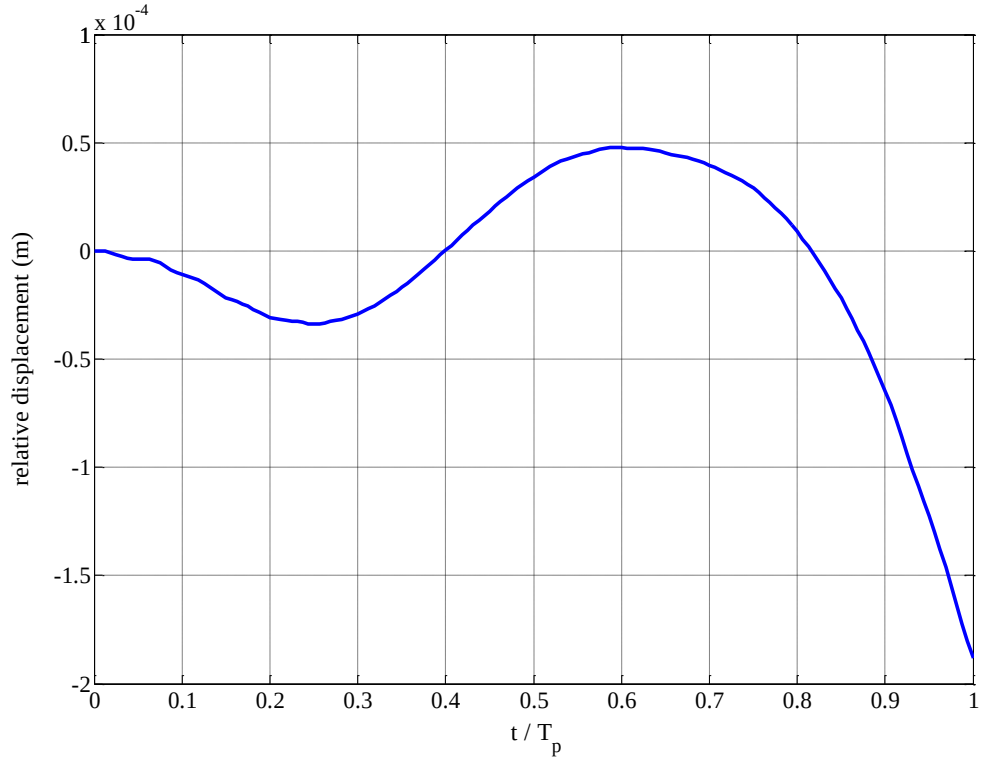

Figure 6.5: Measured relative displacement between the end of the primary mass and the base for the system with switchable friction.

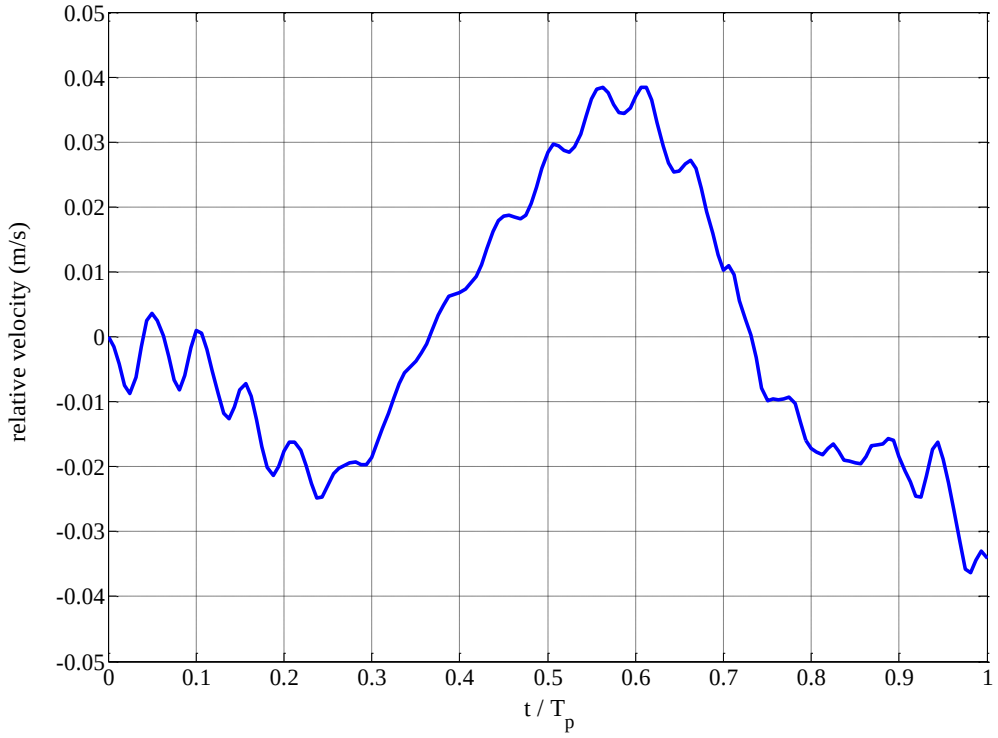

Figure 6.6: Measured relative velocity between the end of the secondary beam and the base for the system with switchable friction.

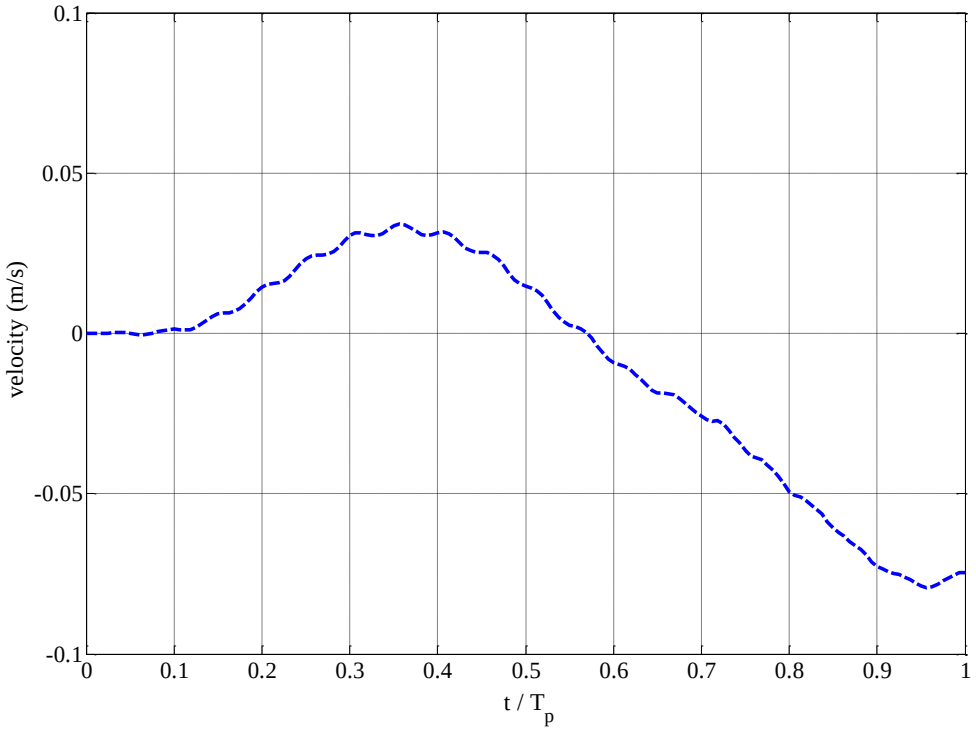

Figure 6.7: Measured absolute velocity at the end of the primary beam for the system with switchable friction.

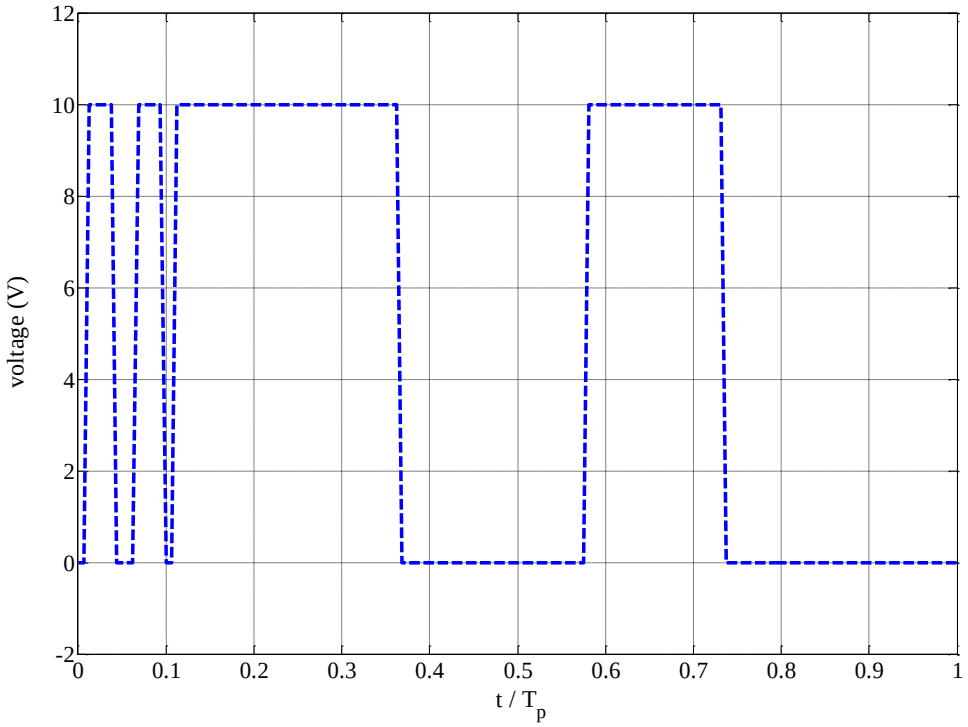

Figure 6.8: Output voltage versus time as the base input is applied to the beam system with switchable friction. When voltage=10 V (the electromagnet attracts the steel beam and friction is off). When voltage = 0 V (the electromagnet is off, the steel beam applies friction at the end of the secondary beam).

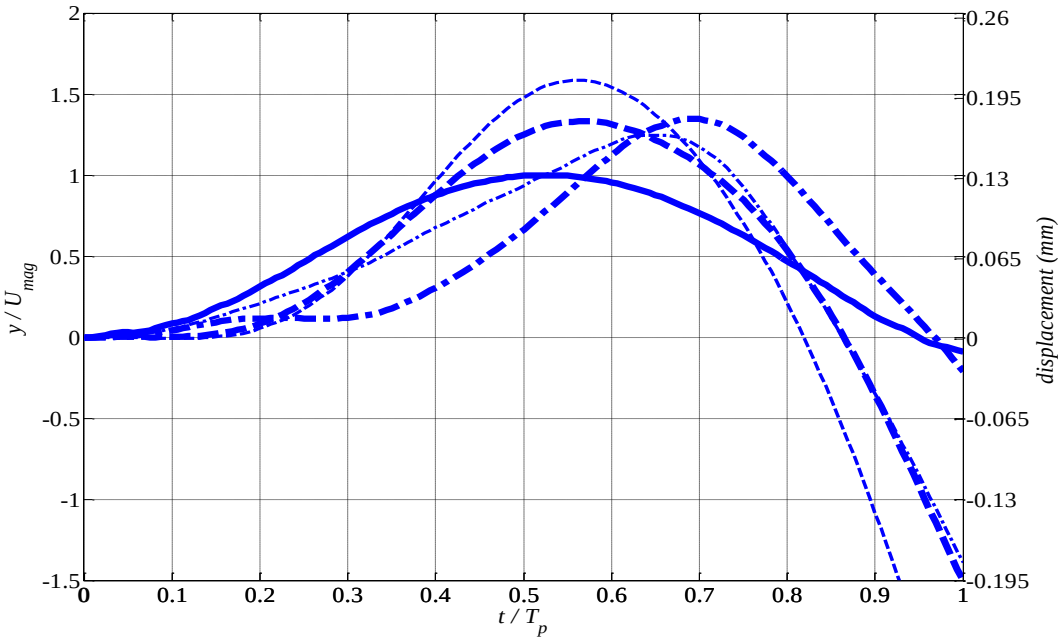

Figure 6.9: Comparison between measured displacement responses of the beam system with switchable and passive friction. Solid thick line: Base input. Dash thick line: End of primary beam, switchable friction. Dash thin line: End of primary beam, passive friction. Dash dot thick line: End of secondary beam, switchable friction. Dash dot thin line: End of secondary beam, passive friction. Non-dimensional displacement, $y = \frac{\omega_1^2 x}{g}$.

Non-dimensional base input magnitude, $U_{mag} = \frac{\omega_1^2 u_{mag}}{g}$.

Categories	Experiment	
	End of primary beam	End of secondary beam
Switchable friction	1.33	1.35
Passive friction	1.59	1.25

Table 6.1: Comparison between the measured maximum displacements for the system with switchable friction and passive friction. The maximum displacements are normalized with respect to the maximum base input displacement.

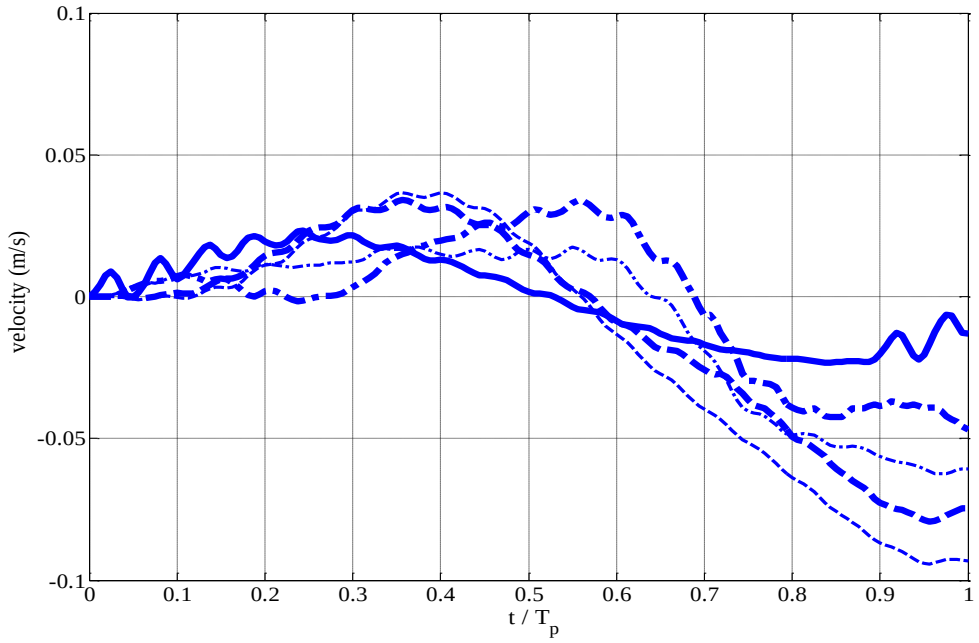

Figure 6.10: Comparison between measured velocity responses of the beam system with switchable and passive friction. Solid thick line: Base input. Dash thick line: End of primary beam, switchable friction. Dash thin line: End of primary beam, passive friction. Dash dot thick line: End of secondary beam, switchable friction. Dash dot thin line: End of secondary beam, passive friction.

(a)

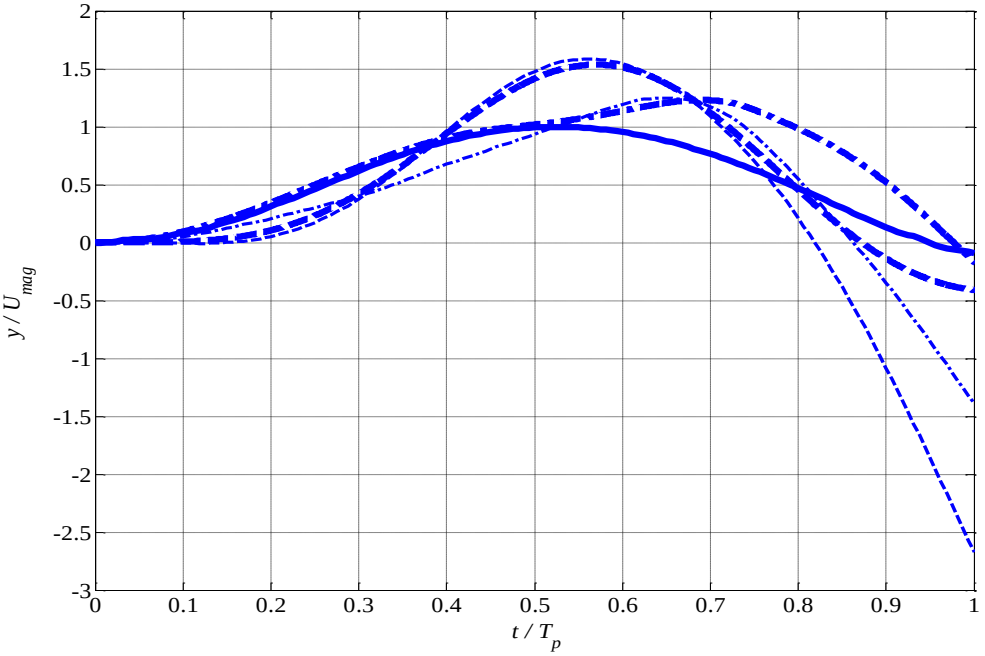

(b)

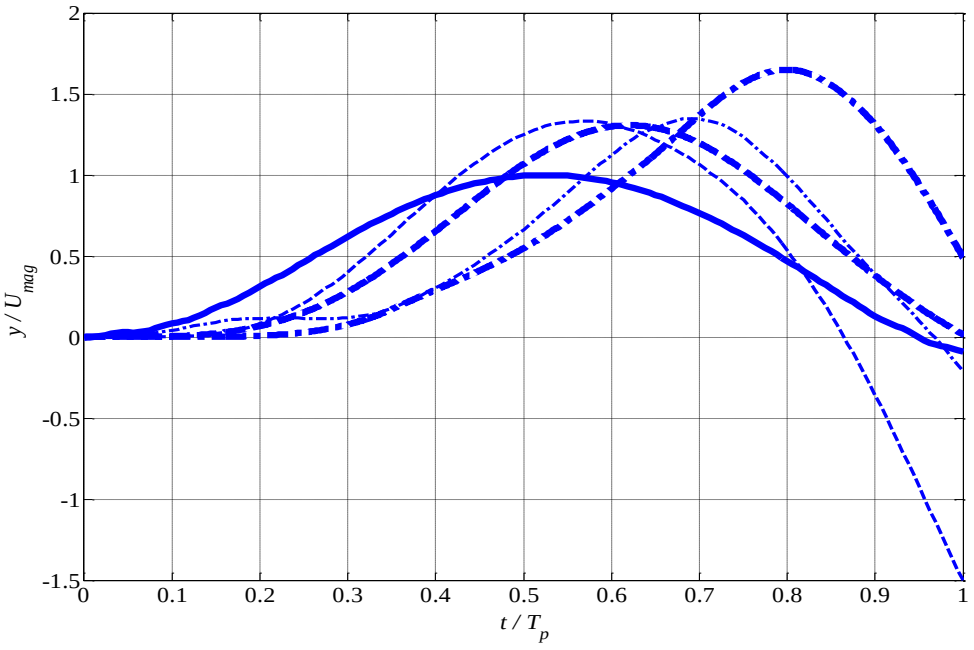

Figure 6.11: Comparison between measured displacement responses of the beam system with ODE simulation. Solid thick line: Base input. Dash thick line: ODE simulation, primary mass. Dash thin line: Measured, end of primary beam. Dash dot thick line: ODE simulation, secondary mass. Dash dot thin line: Measured, end of secondary beam. (a) Passive friction. (b) Switchable friction. Non-dimensional displacement, $y = \frac{\omega_1^2 x}{g}$.Non-dimensional base input magnitude, $U_{mag} = \frac{\omega_1^2 u_{mag}}{g}$. Non-dimensional friction, $\hat{F} = 0.48$.

Categories		Experiment	
		End of primary beam	End of secondary beam
Switchable friction	Measured	1.33	1.35
	ODE simulation	1.31	1.65
Passive friction	Measured	1.59	1.25
	ODE simulation	1.54	1.23

Table 6.2: Comparison between the measured and ODE simulation maximum displacements. The maximum displacements are normalized with the maximum base input displacement. Non-dimensional friction, $\hat{F} = 0.48$.

(a)

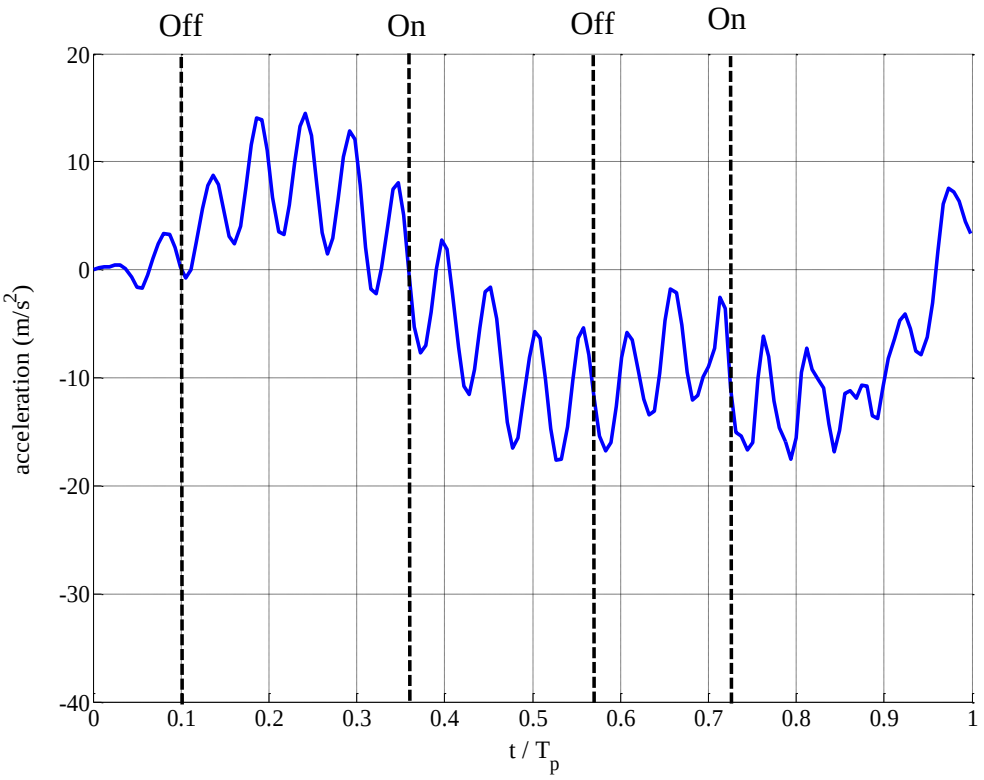

(b)

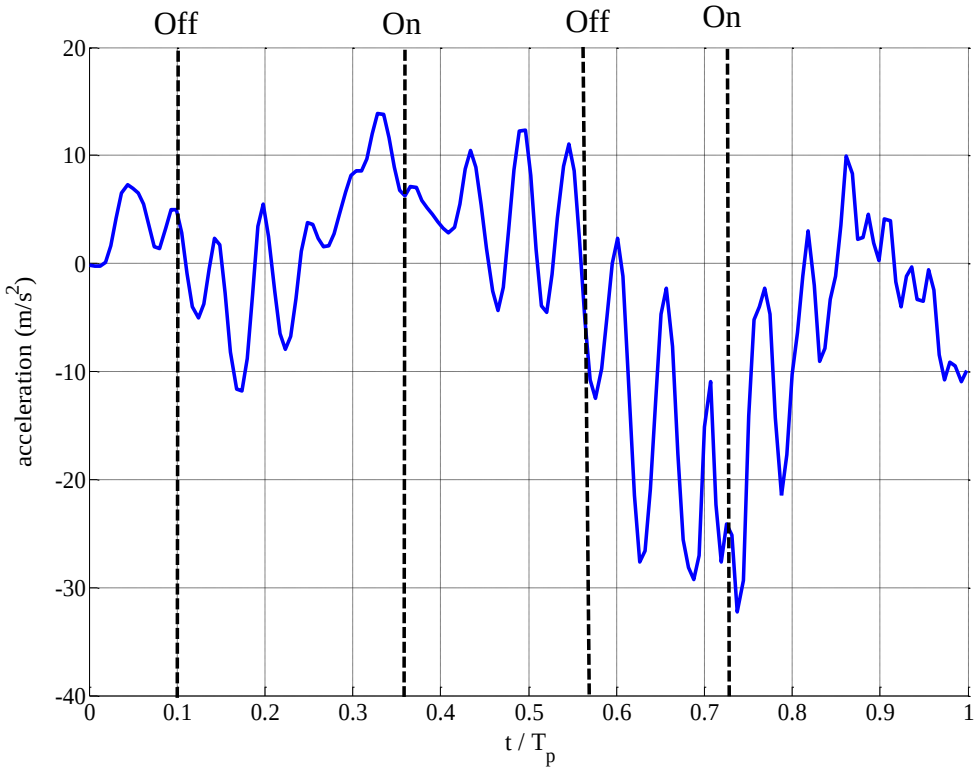

Figure 6.12: Measured acceleration response of the beam system with switchable friction. (a) End of the primary beam. (b) End of the secondary beam. The thick dashed lines mark the point of switching friction on and off.

7. CONCLUSIONS AND RECOMMENDATIONS FOR FURTHER WORK

An investigation of a novel approach for shock isolation and residual vibration control using Coulomb friction has been presented in this thesis. This chapter gives overall conclusions of the study and presents recommendations for future work.

7.1 General conclusions

Good isolation is needed to protect a system from a mechanical shock. The application of the shock input generally involves high accelerations, stresses and deformations, thus the design of good isolators is essential. Typically, passive isolators consist of elastic elements and dissipative elements, and/ or viscoelastic elements. The simplest passive isolation of a system is modelled as a single degree of freedom system with an elastic element, a viscous damper and an isolated mass, which is subjected to transient excitation in the form of a symmetric pulse. The analysis is normally made in the time domain, where the Shock Response Spectra (SRS) plays an important role. The problem is divided in two stages, the response during and after the shock. The incorporation of a viscous damper in the model is expected to produce a high response during the shock, although it is needed for the suppression of the residual vibration after the shock. This is because the force transmission across the viscous damper is dependent upon the magnitude of the relative velocity across it, which is typically high for the case of the shock input.

To overcome this problem it is suggested to use a friction element to replace the viscous damper. The force transmission across the friction element is only dependent upon the direction of the relative velocity across it, which could significantly improve the response of the system during the shock. At the same time, it has the quality of being able to suppress the residual vibration after the shock. Because a friction element is used, a proper way to model friction was sought. For this reason, Coulomb friction was chosen since it is very simple and could model with sufficient accuracy a system with stiff localized contacts and large relative displacements within the contact. The use of Coulomb friction causes unsmooth acceleration response at the point where the friction is applied every time the friction changes its direction. For this reason, a two degree of freedom model, where

friction is applied to a secondary mass is introduced, where the primary mass becomes the isolated mass.

In order to gain a physical insight into the model, a single degree of freedom model was analysed first and acts as a benchmark to the desired two degree of freedom model. It was found that the differences between the models are governed by the secondary elastic element which connects the two masses. If the secondary elastic element is very stiff, the system behaves like a single degree of freedom system with the possibility of a large maximum displacement reduction but unsmooth acceleration response. On the other hand, if the secondary elastic element is of low stiffness, the primary mass experiences a small maximum displacement reduction but relatively smooth acceleration response. For intermediate values of secondary stiffness there is the possibility of significant maximum displacement reduction but with smooth acceleration response for the primary isolated mass.

In order to further improve the response of the system, a control strategy is presented for both models. This is based on the knowledge that the maximum displacement of the passive system could not be smaller than the base input magnitude for the case of the pulse length equal to the natural period of the system. The control strategy is designed such that the net force acting on the primary mass can be reduced at every time step by switching friction on and off, depending upon the direction of the absolute velocity of the primary isolated mass, the force across the elastic element and friction. It was found that the control strategy produces a better response than the passive system for most of the cases, and works well in producing a maximum displacement response that is smaller than the magnitude of the base input.

For the second stage, to suppress the residual vibration after the shock, it was found that the single degree of freedom model has the quality of suppressing the vibration after the shock. There is an issue related to the ability of the two degree of freedom model in suppressing the residual vibration, where the secondary mass stops moving before the system energy is fully dissipated leaving the primary mass to continue oscillating without further dissipation. However, this can be improved by stiffening the secondary elastic element so that more energy can be transferred from the primary mass to the secondary mass to be dissipated by friction.

The theoretical predictions have been experimentally validated with a test rig designed only for the first stage when the shock is applied. A T-beam configuration system which closely replicates the response of a two degree of freedom model at low frequencies was used. The T-beam configuration consists of two beams, namely a primary and a secondary beam connected together with a bolted connection. A steel beam attached to the base is used to apply friction at both ends of the secondary beam. In order to implement switchable friction, an electromagnet is attached at both ends of the secondary beam.

Validation of both the passive and switchable systems gave good results with explainable differences. The switchable system gives a smaller displacement response, especially for the end of the primary beam which serves as the comparison to the primary isolated mass in the model. Moreover, the acceleration response at the end of the primary beam is also relatively smooth compared to the end of the secondary beam where friction is applied, which validates the theoretical predictions. The differences between the experiments and the predictions are caused by a few reasons, such as a slight difference between the experimental and theoretical versed sine input, the suitability of the Coulomb friction to model a system with small displacements, the possibility of friction changes as the surface moves and the possibility of friction differences between the two ends of the secondary beam.

Overall, the thesis has presented a novel approach for shock isolation theoretically using Coulomb friction in two stages, improving the response during the shock and suppressing the residual vibration after the shock. The approach is developed from a passive single and two degree of freedom system and then uses the switchable system for the first stage. For the second stage, the advantages and disadvantages of the single and two degree of freedom systems are presented. Finally, the validity of the theoretical predictions have been tested experimentally only for the first stage, the response during the shock, and a very good agreement has been found between theory and practice. No experiments are conducted on the residual vibration control since there is a limitation on the existing electrodynamic shaker system. For an ideal case, the base is supposed to stop vibrating after a shock in order to investigate the response of the beam system after the shock. However, the base still oscillates after the shock and applies a significant input to the beam system (see Appendix E). This is because the rig itself is essentially a single degree of freedom system which experiences damped oscillation and stops vibrating dependent on the amount of damping present in the rig-shaker system.

7.2 Recommendations for further work

Throughout the thesis, the theoretical and practical insight into the use and application of a friction element for shock isolation has been presented. There are some aspects found during the investigation that might be worthy of further study as mentioned below:

- In the simulation, only a symmetric verse sine pulse was considered. It will be more interesting to investigate further the analysis for more complex shock situation such as non-symmetic pulses or other pulses approaching situations like explosions, waves or earthquakes. It is also interesting to further the analysis to other types of excitation such as harmonic or random excitations.
- During the experiment the value of friction force was not measured. For the analysis, the value of friction was estimated by measuring the free vibration of the beam system. It might be worth trying to measure the value of friction force using alternative approaches.
- The experiment for the case of switchable friction was performed with only a thin secondary beam. It might be worth performing another experiment with a thicker secondary beam to see more reduction in the displacement response at the end of the primary beam, so that the maximum displacement is smaller than the base input magnitude. It is suggested to use a slightly thinner beam than the thick secondary beam used in the experiment of the passive system or a shorter pulse to see significant displacement reduction and smooth acceleration response at the primary mass.
- The experiment was performed only for the case of the shock input equal to the fundamental natural frequency of the beam system. It might be worth conducting the experiment with an input which is short compared to the fundamental natural period.
- No experiment was performed for the case of the residual vibration after the shock. It might be interesting to set the right value of friction that could bring the mass back to its equilibrium in the shortest possible of time as expected in the theoretical predictions. Because of the limitation on the electrodynamic shaker for the case of the residual vibration, it is suggested to do an experiment with an impact hammer.
- In this thesis an electromagnet is used to switch on and off friction. However, it is expected that the electromagnet could also act as a dissipative element that provides

a variable magnetic force at the end of the secondary beam. This might be an interesting area to explore.

7.3 Practical applications

Based on the study throughout the thesis, there are many advantages using either passive or switchable friction. Here are the possible future applications of the system:

- Building foundation: There are some papers on the application of the passive and switchable friction for base-isolated buildings [73, 74, 77]. The shock isolation system developed in this thesis could be used to improve the isolation of the building from earthquake etc if developed further.

- Automotive: The shock isolation system presented in this thesis could be a good fit in the automotive industries. It can be used to isolate the equipments in the engine, for example engine block, radiator or battery from the road excitations.

- Sensitive electronic equipment: The shock isolation system presented in this thesis could become a good alternative in the electronic industries. The friction interface can be fitted into small space such as in the typical electronic equipments. This makes the shock isolation system with friction among the best solution for the problem of shock excitation.

- Machineries: There exists some machineries used to manufacture sensitive equipments which needs proper isolation from the ground excitation. The shock isolation system with friction could be a solution for this problem.

Above are among the possible future applications of the system. The shock isolation system might need further development to suit each particular application. However, it has a high potential to go far especially in solving the problem related to the shock and transient excitations.

REFERENCES

1. M.I.Ismail, M.J.Brennnan, and N.S.Ferguson, *The effect of Coulomb friction on the residual vibration of a shock isolation system*, in *Recent Advanced in Structural Dynamics (RASD)*. 2010: Southampton. p. 12.
2. C.M.Harris and C.E.Crede, *Shock and Vibration Handbook*. 4 ed, ed. C.M.Harris and C.E.Crede. 1995, New York: McGraw-Hill.
3. D.F.L.Ramirez, *Shock isolation using switchable stiffness*, PhD thesis *Institute of Sound and Vibration Research*. 2008, University of Southampton: Southampton. p. 205.
4. R.D.Mindlin, *Dynamics of package cushioning.* Bell Systems Journal, 1945. **24**: p. 109.
5. L.S.Jacobsen and R.S.Ayre, *Engineering Vibrations with Applications to Structures and Machinery*. 1958: McGraw Hill.
6. C.T.Morrow, *Shock and Vibration Engineering*. 1963, New York: John Wiley and Sons.
7. J.C.Snowdon, *Response of nonlinear shock mountings to transient foundation displacements.* Journal of Acoustical Society of America, 1961. **33**(Number 10): p. 1295-1304.
8. G.G.Parfitt and J.C.Snowdon, *Incidence and prevention of damage due to mechanical shock.* Journal of Acoustical Society of America, 1960. **34**(4): p. 462-468.
9. J.C.Snowdon, *Transient response of nonlinear isolation mountings to pulselike displacements.* Journal of Acoustical Society of America, 1962. **35**(Number 3): p. 389-396.
10. J.C.Snowdon, *Steady state and transient behavior of two and three element isolation mountings.* Journal of Acoustical Society of America, 1963. **35**(Number 3): p. 397-403.
11. E.Suhir, *Shock excited vibrations of a conservative duffing oscillator with application to shock protection in portable electronics.* International Journal Solid Structures, 1996. **33**(24): p. 3627-3642.
12. D.W.Shu, et al., *The pulse width effect of single half sine acceleration pulse on the peak response of an actuator arm of hard disk drive.* Material Science and Engineering, 2006. **A 423** p. 199-203.
13. T.Y.Tsai, et al., *Response spectra analysis for undamped structural systems subjected to half-sine impact acceleration pulses.* Microelectronics Reliability, 2007. **47**: p. 1239-1245.
14. C.Y.Zhou and T.X.Yu, *Analytical models for shock isolation of typical components in portable electronics.* Journal of Impact Engineering 2009. **36**: p. 1377-1384.
15. P.Grootenhuis, *The anti-shock mounting of testing machines.* Proceedings of Institution of Mechanical Engineers, 1965. **180**: p. 388-398.
16. M.Novak and L.E.Hifnawy, *Vibration of hammer foundations.* Soil dynamics and earthquake engineering, 1983. **2**(1): p. 43-53.
17. A.G.Chehab and M.Hesham, *Response of block foundations to impact loads.* Journal of Sound and Vibration, 2004. **276**: p. 293-310.
18. T.D.Gillespie, *Fundamentals of Vehicle Dynamics*. 1992, Warrendale, PA: Society of Automotive Engineers.
19. T.P.Waters, Y.Hyun, and M.J.Brennan, *The effect of dual rate suspension damping on vehicle response to transient road inputs.* Journal of Vibration and Acoustics, 2009. **131**: p. 8.
20. Z.Zong and K.Y.Lam, *Biodynamic response of shipboard sitting subject to ship shock motion.* Journal of Biomechanic, 2002. **35**: p. 35-43.

21. C.Liam, *Testing and modeling of shock mitigating seats for high speed craft*. 2011, Virginia Polytechnic Institute and State University: Blacksburg,VA. p. 147.
22. Y.Hyun, *The effect of suspension damping on vehicle response to transient road inputs*, MPhil thesis *Institute of Sound and Vibration Research*. 2005, University of Southampton: Southampton. p. 123.
23. J.P.D.Hartog, *Mechanical Vibrations*. 4 ed. 1985, New York: Dover Publications, INC.
24. J.P.D.Hartog, *Forced vibrations with combined viscous and Coulomb damping.* Philosophical Magazine, 1930. **9**(59): p. 801-817.
25. M.S.Hundal, *Response of a base excited system with Coulomb and viscous friction.* Journal of Sound and Vibration, 1979. **64**(3): p. 371-378.
26. A.A.Ferri, *Friction damping and isolation systems.* Journal of Vibration and Acoustics, 1995. **117(B)**: p. 196-206.
27. X.Tan and R.J.Rogers, *Equivalent viscous damping models of Coulomb friction in multi degree of freedom vibration systems.* Journal of Sound and Vibration, 1995. **185**(1): p. 33-50.
28. H.K.Hong and C.S.Liu, *Coulomb friction oscillator:modelling and responses to harmonic loads and base excitations.* Journal of Sound and Vibration, 2000. **229**(5): p. 1171-1192.
29. H.K.Hong and C.S.Liu, *Non sticking oscillation formulae for Coulomb friction under harmonic loading.* Journal of Sound and Vibration, 2001. **244**(5): p. 883-898.
30. U.Andreaus and P.Casini, *Dynamics of friction oscillators excited by a moving base and/or driving force.* Journal of Sound and Vibration, 2001. **245**(4): p. 685-699.
31. C.S.Liu and W.T.Chang, *Frictional behaviour of a belt driven and periodically excited oscillator.* Journal of Sound and Vibration, 2002. **258**(2): p. 247-268.
32. I.Lopez, J.M.Busturia, and H.Nijmeijer, *Energy dissipation of a friction damper.* Journal of Sound and Vibration, 2004. **278**: p. 539-561.
33. J.H.Lee, E.Berger, and J.H.Kim, *Feasibility study of a tunable friction damper.* Journal of Sound and Vibration, 2005. **283**: p. 707-722.
34. I.Lopez and H.Nijmeijer, *Prediction and validation of the energy dissipation of a friction damper.* Journal of Sound and Vibration, 2009. **328**: p. 396-410.
35. Y.T.Choi and N.M.Wereley. *Shock isolation systems using magnetorheological dampers*. in *Smart Structures and Materials 2004: Damping and Isolation*. 2004. San Diego,CA.
36. S.Timoshenko, D.H.Young, and W.Weaver, *Vibration Problems in Engineering*. 1974: John, Wiley and Sons Inc.
37. C.A.Mercer and P.L.Rees, *An optimum shock isolator.* Journal of Sound and Vibration, 1971. **18**(4): p. 511-520.
38. L.Y.Lu, et al., *Experiment and analysis of a fuzzy controlled piezoelectric seismic isolation system.* Journal of Sound and Vibration, 2010. **329**: p. 1992-2014.
39. J.A.Inaudi, *Modulated homogeneous friction: a semi active damping strategy.* Earthquake Engineering and Structural Dynamics, 1997. **26**: p. 361-376.
40. C.L.Ng and Y.L.Xu, *Semi active control of a building complex with variable friction dampers.* Engineering Structures, 2007. **29**: p. 1209-1225.
41. L.Y.Lu, *Predictive control of seismic structures with semi active friction dampers.* Earthquake Engineering and Structural Dynamics, 2004. **33**: p. 647-668.
42. L.Y.Lu, L.L.Chung, and G.L.Lin, *A general method for semi active feedback control of variable friction dampers.* Journal of Intelligent Material Systems and Structures, 2004. **15**: p. 393-412.
43. L.Y.Lu and G.L.Lin, *Predictive control of smart isolation system for precision equipment subjected to near fault earthquakes.* Engineering Structures, 2008. **30**: p. 3045-3064.

44. Y.Liu, T.P.Waters, and M.J.Brennan, *A comparison of semi active damping control strategies for vibration isolation of harmonic disturbances.* Journal of Sound and Vibration, 2005. **280** p. 21-39.
45. N.Jalili, *A comparative study and analysis of semi active vibration control systems.* Journal of Vibration and Acoustics, 2002. **124**: p. 593-605.
46. P.Dupont, P.Kasturi, and A.Stokes, *Semi active control of friction dampers.* Journal of Sound and Vibration, 1997. **202(2)**: p. 203-218.
47. A.A.Ferri and B.S.Heck, *Semi active suspension using dry friction energy dissipation*, in *American Control Conference*. 1992: Chicago, IL. p. 31-35.
48. D.C.Karnopp, M.J.Crosby, and R.A.Harwood, *Vibration control using semi active force generators.* Journal of Engineering for Industry, 1974. **96**: p. 619-626.
49. H.Yamaguchi and M.Yashima, *Vibration reduction and isolation performance for on off control of a friction force at a spring support* Journal of Sound and Vibration, 1997. **208**(5): p. 729-743.
50. S.Andersson, A.Soderberg, and S.Bjorklund, *Friction models for sliding dry, boundary and mixed lubricated contacts.* Tribology International, 2007. **40**: p. 580-587.
51. E.J.Berger, *Friction modeling for dynamic system simulation.* Applied Mechanics Reviews, 2002. **55**: p. 535-577.
52. B.Fenny, et al., *A historical review on dry-friction and stick-slip phenomena.* Applied Mechanics Reviews, 1998. **51**: p. 321-341.
53. G.J.Stein, R.Zahoransky, and P.Mucka, *On dry friction modelling and simulation in kinematically excited oscillatory systems.* Journal of Sound and Vibration, 2008. **311**: p. 74-96.
54. N.Andreaus and P.Casini, *Dynamics of friction oscillators excited by a moving base and/or driving force.* Journal of Sound and Vibration, 2001. **245**: p. 685-699.
55. N.C.Shekhar, H.Hatwal, and A.K.Mallik, *Performance of non linear isolators and absorbers to shock excitations.* Journal of Sound and Vibration, 1999. **227(2)**: p. 293-307.
56. D.W.Shu, et al., *Shock analysis of a head actuator assembly subjected to half sine acceleration pulses.* International Journal of Impact Engineering 2007. **34** p. 253-263.
57. E.P.Petrov and D.J.Ewins, *Models of friction damping with variable normal load for time-domain analysis of vibrations*, in *Proceedings of the ISMA* 2002: Leuven, Belgium. p. 421-430.
58. N.Mostaghel and T.Davis, *Representations of Coulomb friction for dynamic analysis.* Earthquake Engineering and Structural Dynamics, 1997. **26**: p. 541-548.
59. C.W.Stammers and T.Sireteanu, *Vibration control of machines by use of semi active dry friction damping.* Journal of Sound and Vibration, 1998. **209(4)**: p. 671-684.
60. E.Guglielmino, A.E.Kevin, and R.Ghigliazza, *On the control of the friction force.* Meccanica, 2004. **39**: p. 395-406.
61. M.Ahmadian, R.Brian, and X.Song, *No jerk semi active skyhook control method and apparatus*. 2000: United States Patent.
62. L.N.Virgin, *Introduction to Experimental Nonlinear Dynamics*. 2000, Cambridge: Cambridge University Press.
63. K.Shin and J.Hammond, *Fundamentals of Signal Processing for Sound and Vibration Engineers*. 2008: Wiley-Blackwell
64. R.C.Hilborn, *Chaos and Nonlinear Dynamics*. 1994: Oxford University Press, Inc.
65. A.Kozmin, Y.Mikhlin, and C.Pierre, *Transient in a two DOF nonlinear system.* Nonlinear Dyn 2008. **51**: p. 141-154.

66. R.J.Allemang and D.L.Brown, *A correlation coefficient for modal vector analysis*, in *Proceedings of the 1st International Modal Analysis conference (IMAC)*. 1982: Orlando, Florida.
67. M.I.Friswell and J.E.Mottershead, *Finite Element Model Updating in Structural Dynamics*. 1995, Dordrecht: Kluwer Academic Publishers.
68. J.F.Ferrero and J.J.Barrau, *Study of dry friction under small displacements and near zero sliding velocity.* Wear, 1997. **209**: p. 322-327.
69. L.A.Hagman, *Measurement and modeling of microslip for engineering surfaces in contact*, in *Dept.of Machine Design*. 1997, KTH: Stockholm.
70. J.F.Ferrero, et al., *Analysis of a dry friction problem under small displacements: application to a bolted joint* Wear, 2004. **256** p. 1135-1143.
71. E.Rabinowicz, *The intrinsic variables affecting the stick-slip process.* Proc.Phys Soc., 1958. **71**: p. 668-675.
72. N.Quijano and K.Passino. *A Tutorial Introduction to Control Systems Development and Implementation with dSPACE*. 2002 [cited 2012; Available from: www.dspace.com/files/pdf1/dSPACEtutorial.pdf.
73. A.K.Agrawal and J.N.Yang, *Semi active control strategies for buildings subject to near-field earthquakes*, in *Smart Structures and Materials 2000: Smart Systems for Bridges, Structures and Highways*. 2000: Newport Beach, Calif. p. 359-370.
74. A.K.Agrawal, J.N.Yang, and W.L.He, *Applications of some semiactive control systems to benchmark cable-stayed bridge.* Journal of Structural Engineering, 2003. **129**: p. 884-894.
75. S.Laflamme, et al., *Modified friction device for control of large-scale systems.* Structural control and health monitoring, 2011. **19**: p. 548-564.
76. N.Jalili and A.Ramaratnam, *A switched stiffness approach for structural vibration control: theory and real time implementation.* Journal of Sound and Vibration, 2006. **291**: p. 258-274.
77. S.T.Cruz, F.Lopez-Almansa, and S.Oller, *Numerical simulation of the seismic behaviour of building structures equipped with friction energy dissipators.* Computers and Structures, 2007. **85**: p. 30-42.

Appendix A

Acceleration response of a viscously damped single degree of freedom system.

Consider a viscously damped single degree of freedom system subjected to a base input shown in Figure A1. The objective is to investigate the effect of pulse duration and damping to the acceleration response of the system.

From Figure A2 (a), as the pulse length gets shorter, the acceleration response increases significantly for a viscously damped single degree of freedom system. It is expected since the force transmitted from the base is dependent on the magnitude of the relative velocity across the viscous damper and the shorter duration pulse consists of high frequency contents which cause high relative velocity across the damper. Small damping is used in Figure A2 (a).

In order to see the effect of damping to the acceleration response of the system, Figure A2 (b) is also plotted for the case of large damping. If the large damping is used, the increment is higher for the case of a short duration pulse; see comparison between Figure A2 (a) and (b). The large damping suppress the maximum response when the pulse length equal to the natural period of the system $T_p = T$. However, there is an increment in the response for all of the short duration pulse. The increment is the largest when $T_p = 0.01T$, the shortest duration used in the simulation. This shows that as the pulse length gets shorter, the situation is much worst.

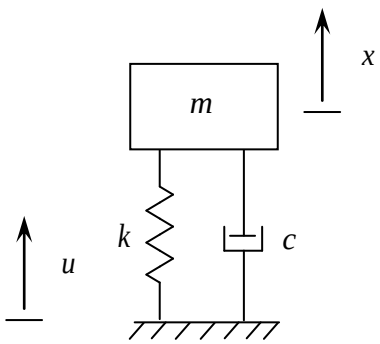

Figure A1: A viscously damped single degree of freedom system subjected to a base input.

(a)

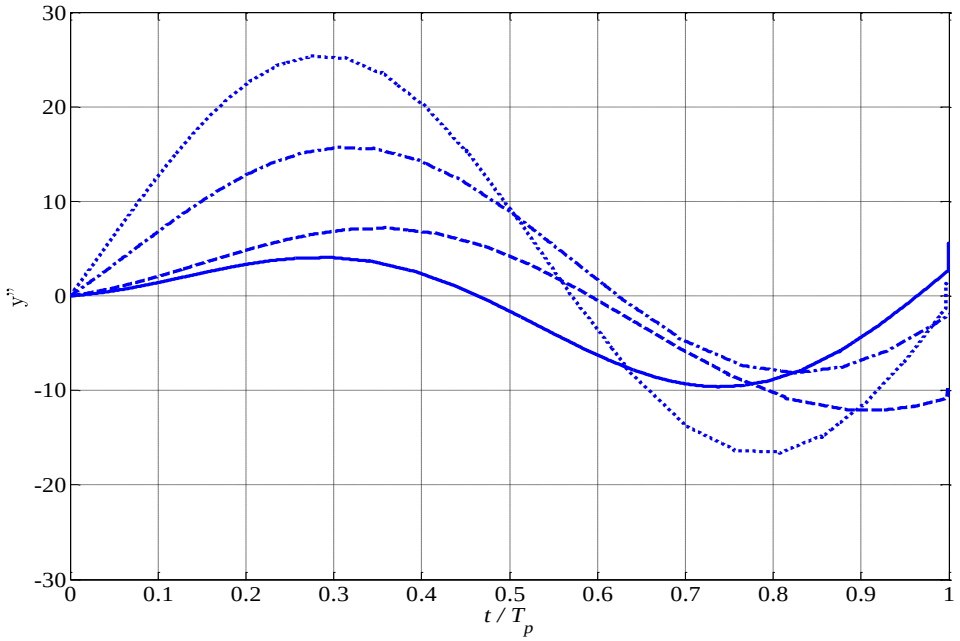

(b)

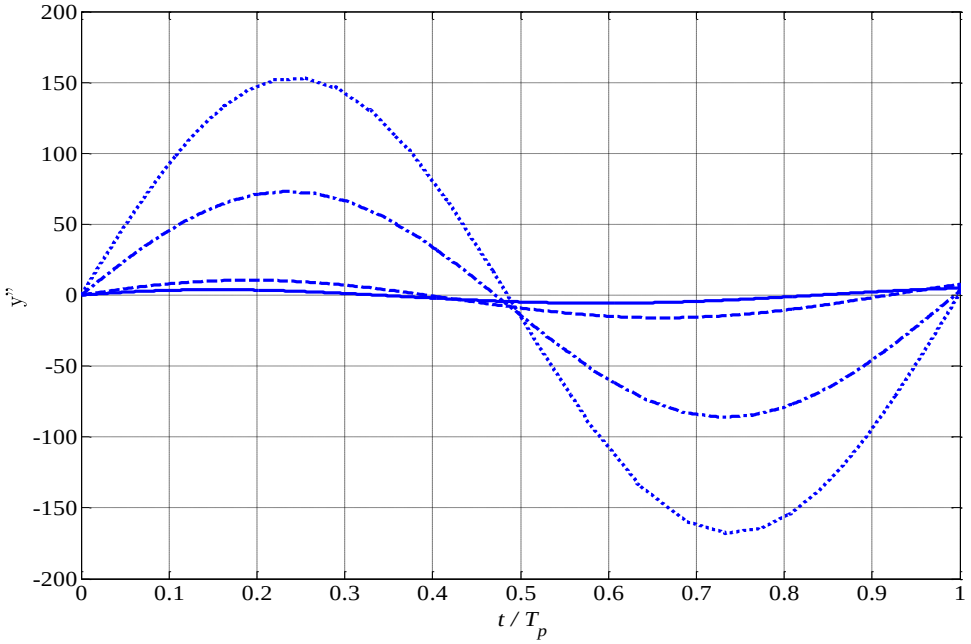

Figure A2: Acceleration response of a viscously damped single degree of freedom system under a versed sine base input. Non-dimensional base input magnitude $U_{mag} = 10$.
(a) Small damping ratio $\varsigma = 0.1$, Large damping ratio $\varsigma = 0.8$. Solid line: Pulse length $T_p = T$. Dash line: Pulse length $T_p = 0.5T$. Dash dot line: Pulse length $T_p = 0.1T$. Dot line: Pulse length $T_p = 0.01T$. T is the natural period of the system. Non-dimensional acceleration $y'' = \frac{\omega_n^2 x''}{g}$. $x'' = \frac{d^2 x}{d\tau^2}$, non-dimensional time $\tau = \omega_n t$.

Appendix B

Displacement shock response spectrum (SRS) for an undamped single degree of freedom system

The SRS [6] is an establish measure of the damaging severity of a shock disturbance. To select a damage criterion (acceleration or displacement), the duration of the pulse with respect to the natural period of the system $\frac{T_p}{T}$ is of great importance (considering a single degree of freedom system). In this section, displacement is the quantity of interest and the SRS for the displacement response of an undamped single degree of freedom system is shown in Figure B1for three types of pulse.

If $T_p \gg T$, the motion of the mass follows the motion of the base during the shock input (Figure B1 for values of $\frac{T_p}{T}$ greater than 2). When $T_p \ll T$, the mass is substantially at rest until motion of the base has ceased (Figure B1 for values of $\frac{T_p}{T}$ smaller than 0.5), and the maximum displacement for this case is very small. Finally, when the length of the pulse T_p is equal or close to the natural period the system T, the displacement response is very large for any type of pulse.

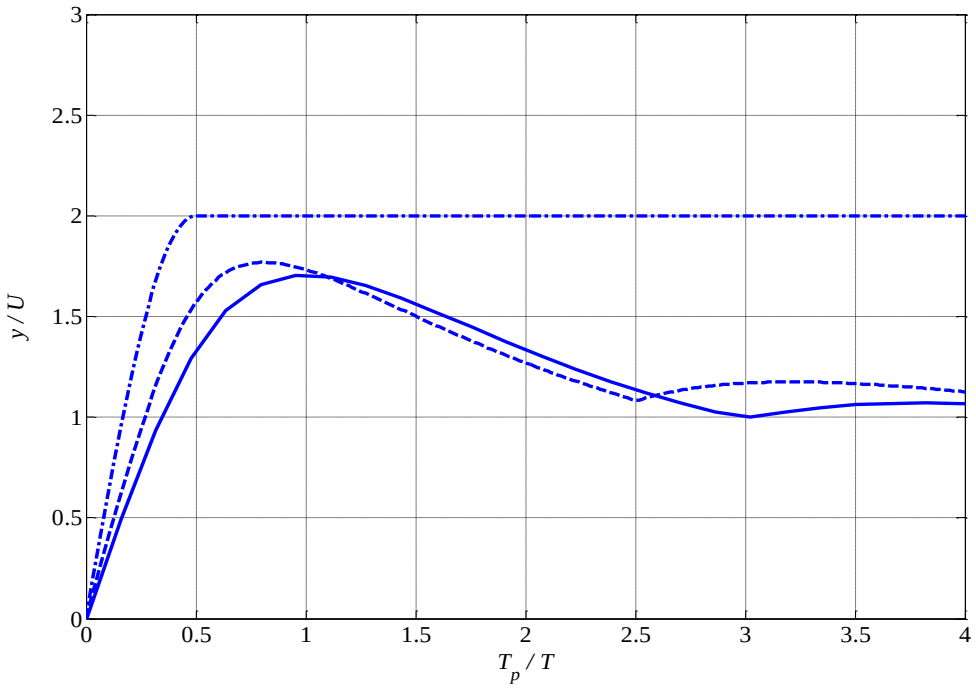

Figure B1: Displacement shock response spectrum (SRS) for an undamped single degree of freedom system. Solid line: Versed sine base input. Dash line: Half sine base input. Dash dot line: Rectangular base input.

Appendix C

A single degree of freedom system under half sine input at the base and on the supported mass

A half sine input with pulse duration close to the natural period of the system is chosen. It is impossible for the mass to follow the exact motion of the input from the start if a half sine input is applied. This is because it requires a finite time for the velocity of the mass to increase and to be equal to the input velocity. It is different compared to a versed sine input, where both input and mass velocity start from zero. In the versed sine case, if friction is large enough to hold the mass from sliding with respect to the friction interface, the mass will follow the exact motion of the input from the start.

The results shown in Figure C1 and C2 are the displacement and relative velocity response of a single degree of freedom system as friction is varied. When the friction is small, for example $\hat{F} = 2.5$, there is stick slip motion of the mass with respect to the friction interface. As friction increases, finally the mass will follow the motion of the input after the mass velocity reaches the same level as the input velocity. The time taken for this to occur is shorter as friction is increased. Friction helps to accelerate the mass until its velocity equals the input velocity. Therefore, as the friction increases, the response of the system will be closer to the exact motion of the input although not exactly the same.

On the other hand, the smallest maximum response of the system as friction is varied is achieved when the friction is just enough to hold the mass from sliding after the moment it sticks. In the case of the parameters values tested, from Figure 2.7, it can be seen that a minimum response is achieved when $\hat{F}$ is slightly smaller than 5. When $\hat{F} = 5$, it takes a longer time for the velocity of the mass to be equal to the input velocity compared to higher friction. Therefore, the displacement response is smaller than the input and the displacement response for higher friction. Then, after the mass reaches the input velocity, it will stick to the friction interface and not slide anymore. Again, the smallest maximum response is obtained when the mass still slides instead of fully sticking.

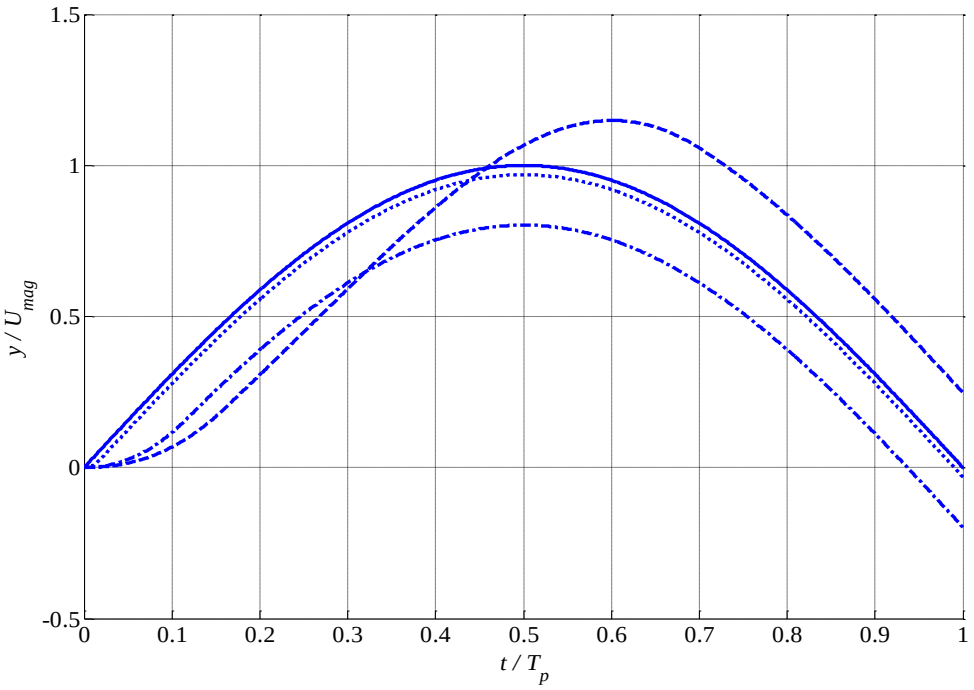

Figure C1: Displacement response of a single degree of freedom system under a half sine base input. Non-dimensional base input magnitude $U_{mag} = 10$ and pulse length $T_p = T$. Solid line: base input. Dash line: $\hat{F} = 2.5$. Dash dot line: $\hat{F} = 5$. Dot line: $\hat{F} = 40$.

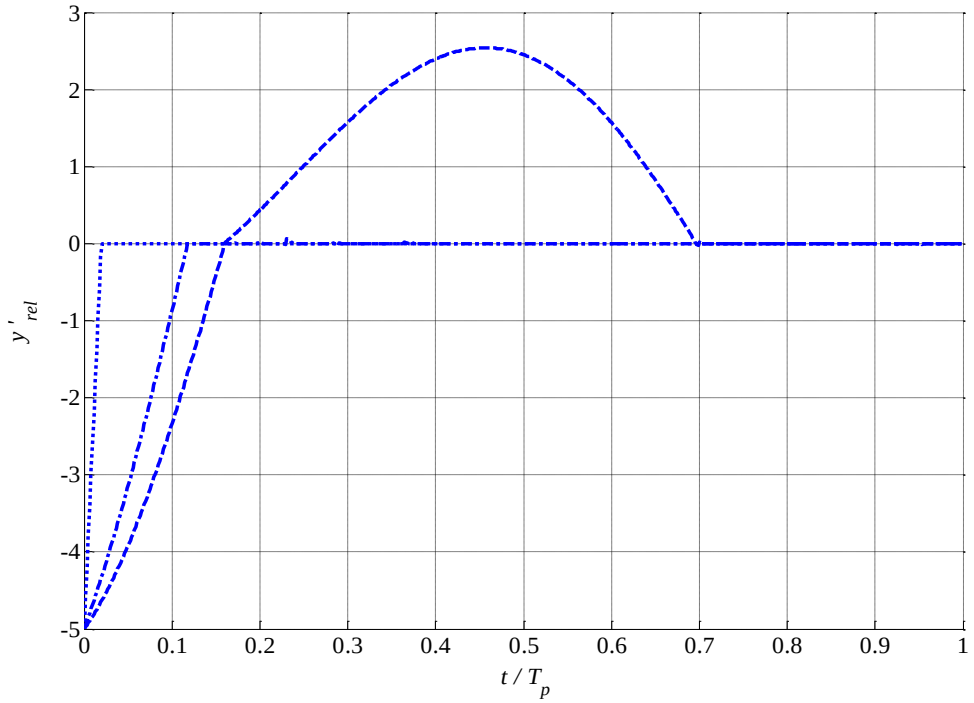

Figure C2: Relative velocity of a single degree of freedom system under a half sine base input. $y'_{rel} = y' - U', y' = \frac{dy}{d\tau}, U' = \frac{dU}{d\tau}, \tau = \omega t$. Non-dimensional base input magnitude $U_{mag} = 10$ and pulse length $T_p = T$. Dash line: $\hat{F} = 2.5$. Dash dot line: $\hat{F} = 5$. Dot line: $\hat{F} = 40$.

Appendix D

A single degree of freedom system under rectangular input at the base and on the supported mass

A rectangular input with pulse duration close to the natural period of the system is chosen. If a rectangular base input is used, equation of motion D1 can be reduced to equation D2.

$$m\ddot{x} + kx + F\,\mathrm{sgn}(\dot{x} - \dot{u}) = ku \tag{D1}$$

$$m\ddot{x} + kx + F\,\mathrm{sgn}(\dot{x}) = ku \tag{D2}$$

This is because the base input velocity $\dot{u}$ will be zero for all time except at $t = 0$ and $t = T_p$ where the velocity is infinite to cause an instantaneous displacement change. Therefore, in this case, the friction only depends upon the direction of the velocity of the mass and friction always opposes the direction of motion. It is possible to have the mass remaining stationary for high friction, whereas for a half sine or a versed sine base input the mass will stick and follow the base input motion for high friction. Refer back to Figure 2.7 to see the maximum displacement of a single degree of freedom system with a rectangular base input as friction is varied.

The displacement, velocity, acceleration and relative displacement of a single degree of freedom system with a rectangular base input are shown in Figures D1 to D4. As friction increases, the magnitude of displacement, velocity and acceleration decrease. For very high friction, i.e. $F \geq 10$, the mass will not move at any instant of time. For friction in the range of $0 < \hat{F} < 10$ the mass will either slide until the end of the shock or stick during the second half of the shock. Based on the parameters used, for $\hat{F} \geq 5$ the mass will stick during the second half of the shock. This is because the acceleration and velocity are both reduced to zero at half of the pulse length if $\hat{F} \geq 5$. Otherwise, the mass will slide until the end of the shock.

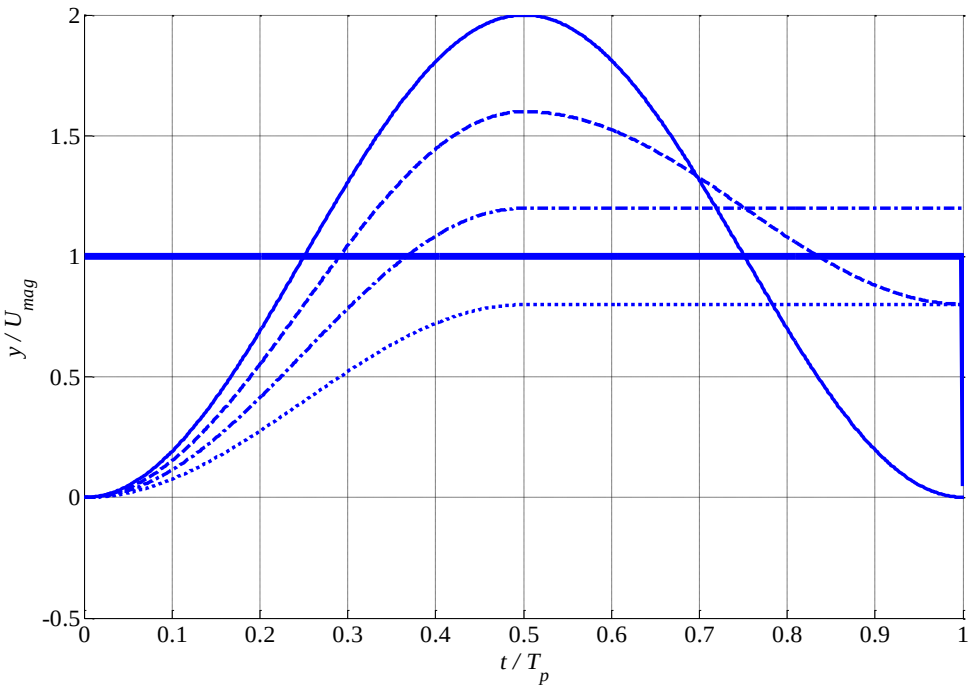

Figure D1: Displacement response of a single degree of freedom system second model for a rectangular base input. Non-dimensional base input magnitude $U_{mag} = 10$ and pulse length $T_p = T$. Bold line: base input. Solid line: $\hat{F} = 0$ .Dash line: $\hat{F} = 2$, Dash dot line: $\hat{F} = 4$ Dot line: $\hat{F} = 6$.

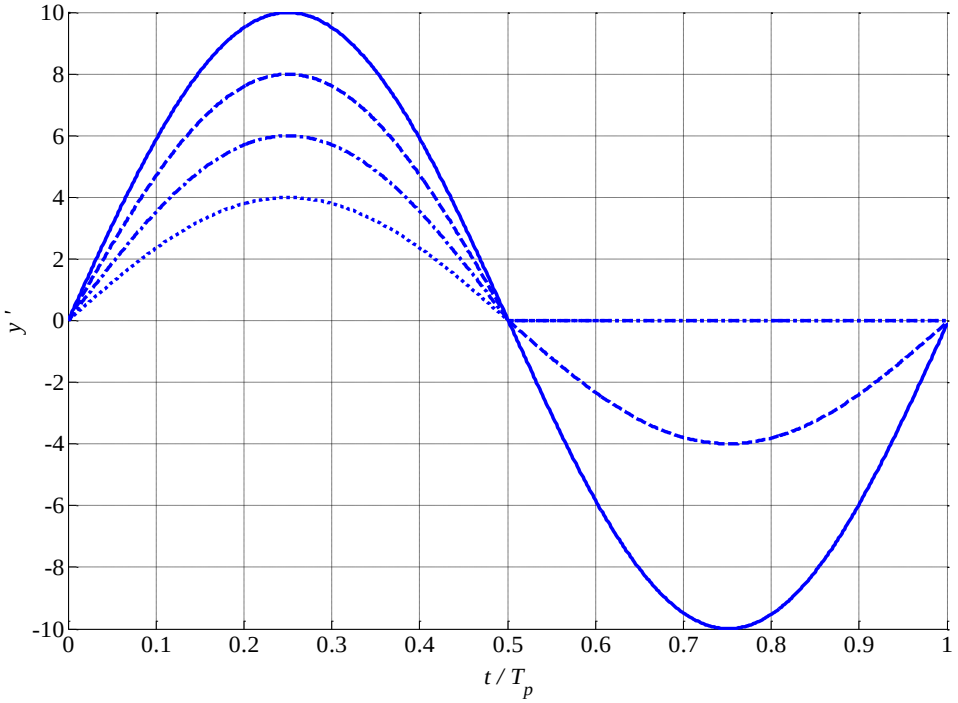

Figure D2: Velocity response of a single degree of freedom system second model for a rectangular base input. Non-dimensional base input magnitude $U_{mag} = 10$ and pulse length $T_p = T$. Solid line: $\hat{F} = 0$ .Dash line: $\hat{F} = 2$, Dash dot line: $\hat{F} = 4$ Dot line: $\hat{F} = 6$.

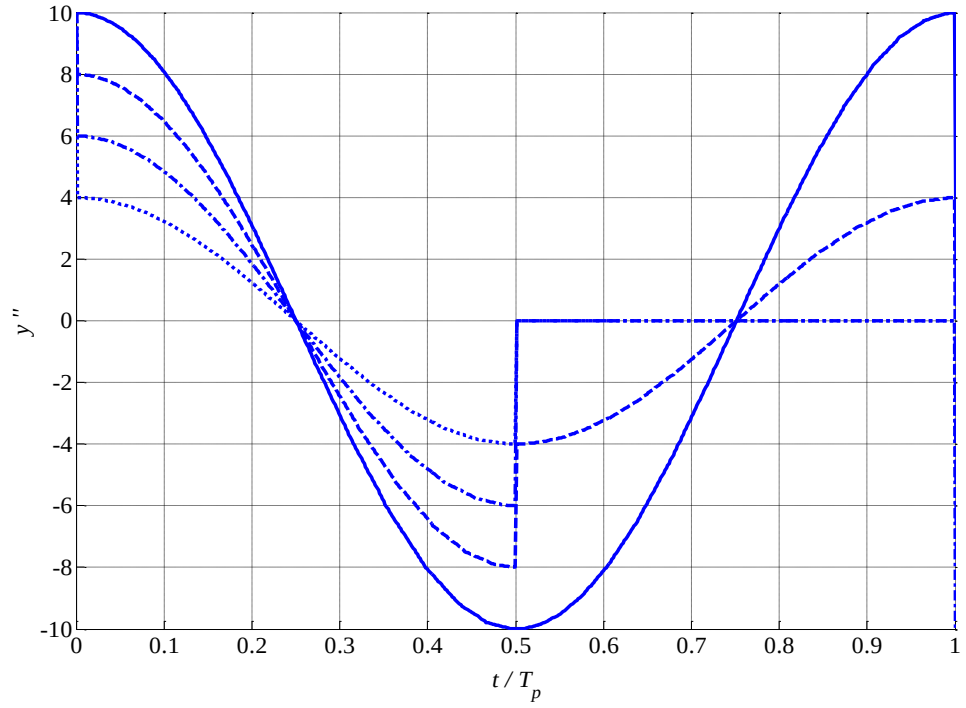

Figure D3: Acceleration response of a single degree of freedom system second model for a rectangular base input. Non-dimensional base input magnitude $U_{mag} = 10$ and pulse length $T_p = T$. Solid line: $\hat{F} = 0$ .Dash line: $\hat{F} = 2$, Dash dot line: $\hat{F} = 4$ Dot line: $\hat{F} = 6$.

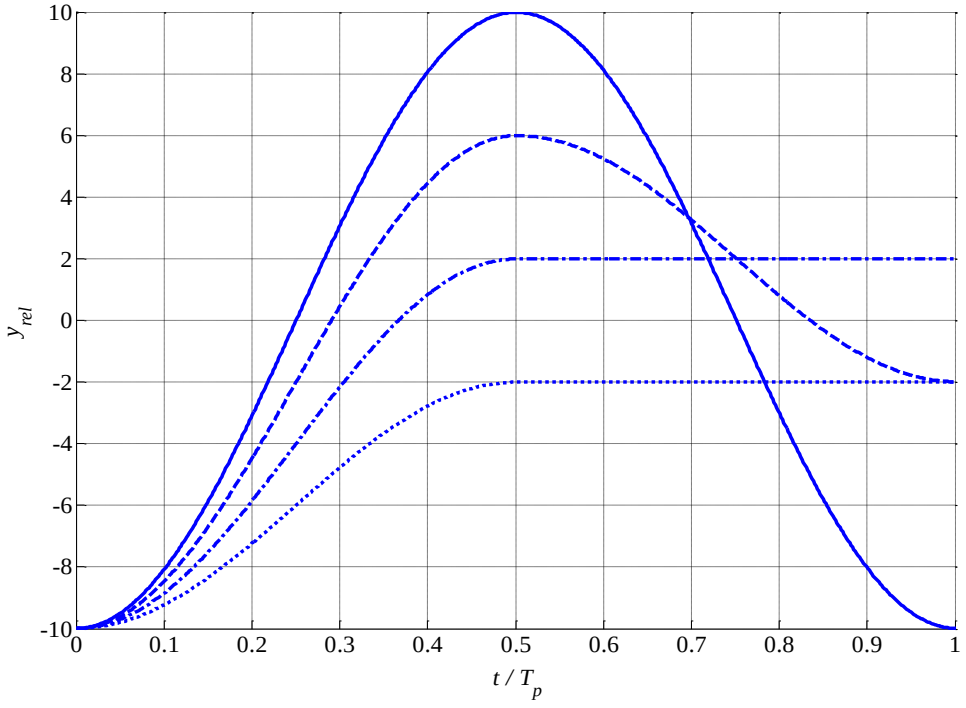

Figure D4: Relative displacement of a single degree of freedom system for a rectangular base input. Non-dimensional base input magnitude $U_{mag} = 10$ and pulse length $T_p = T$. Solid line: $\hat{F} = 0$ .Dash line: $\hat{F} = 2$, Dash dot line: $\hat{F} = 4$ Dot line: $\hat{F} = 6$. $y_{rel} = y - U$.

Appendix E

Generation of an experimental versed sine input

This approach was used by Ramirez to suppress the residual vibration of the rig base. The suppression of the residual vibration is very important if there is a need to conduct an experiment on the system response after the shock. In this study, the decision is only to focus on the experiment for the response during the shock. But, it is still worthwhile to implement this technique to suppress or at least minimize the residual response of the rig base.

If a pulse of very short duration is applied to a shaker, it will oscillate at its natural frequency. If another pulse of the same characteristics is applied exactly after half of the cycle with the right amplitude, then it is expected the response to the second pulse will cancel the response to the first pulse. This idea is represented in Figure E1 considering two impulses and the response of the base due to these impulses. The amplitude of the second pulse needs to be scaled such that

$$\frac{A}{B} = e^{\zeta \omega_n t_o} \tag{E1}$$

where A is the amplitude of the first pulse, B is the amplitude of the second pulse, ω_n is the natural frequency of the rig-shaker system, ς is the damping ratio of the rig-shaker system and t_o is the time when pulse B is applied, in this case half the natural period of the rig-shaker system. For details of this technique please refer to Ramirez thesis [3].

During the experiment, the residual response of the rig's base cannot completely be eliminated as shown in Figure E2. It is possibly caused by the gravity since the rig is arranged in the vertical direction and the delay in the reaction of the shaker system towards the applied impulse.

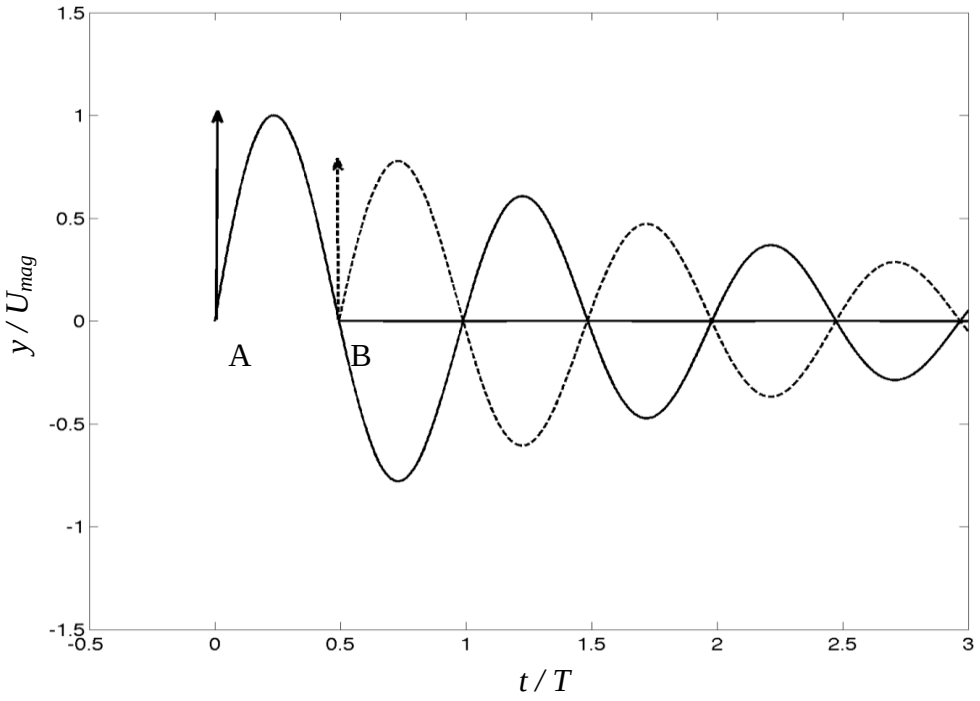

Figure E1: The technique to suppress the residual vibration of the rig base using two impulses, A and B. The second impulse is applied at $t = t_o = 0.5T$ to cancel the response of the first impulse.

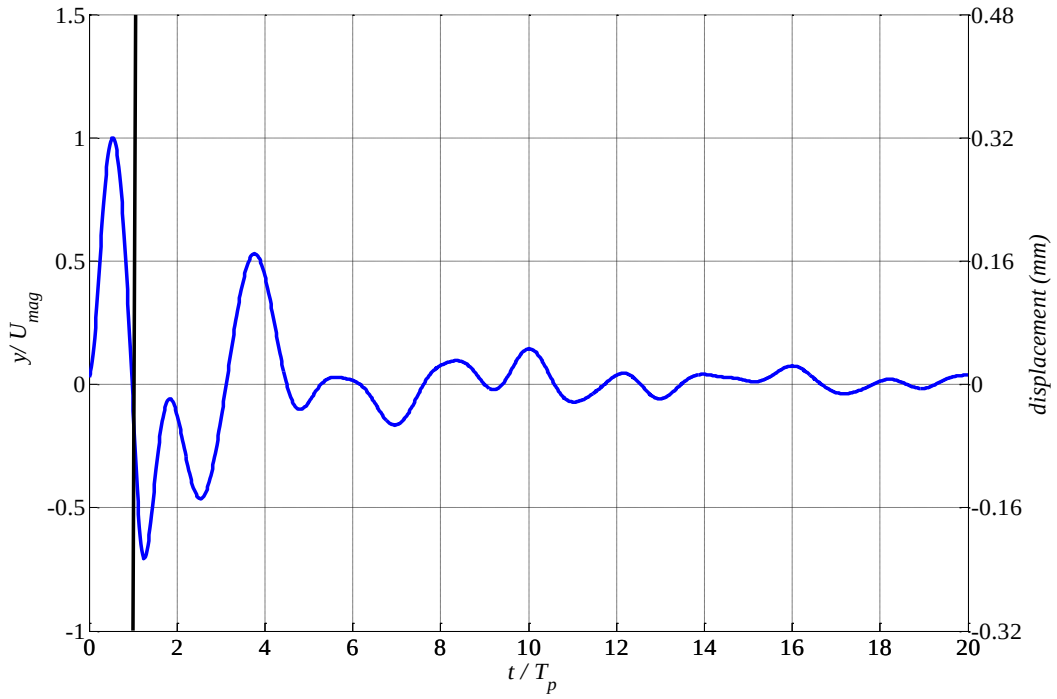

Figure E2: The displacement response of the base when the technique to suppress the residual vibration of the shaker is used. Solid black line: The point where the base supposed to stop moving to allow for the free vibration state to begin.